



UNIVERSIDAD NACIONAL DE COLOMBIA



VNIVERSITAT
DE VALÈNCIA

**MECHANOBIOLOGICAL COMPUTATIONAL
MODEL FOR THE DEVELOPMENT AND
FORMATION OF SYNOVIAL JOINTS**

Kalenia María Márquez Flórez

Universidad Nacional de Colombia, Faculty of Engineering,
Department of Mechanics and Mechatronic Engineering
Bogotá D.C., Colombia

Universitat de València, Faculty of Medicine and Odontology
Department of Pathology
Valencia, Spain

June 2019

MECHANOBIOLOGICAL COMPUTATIONAL MODEL FOR THE DEVELOPMENT AND FORMATION OF SYNOVIAL JOINTS

*This Dissertation is submitted in partial fulfillment of the
requirements for the Degree of Philosophiae Doctor (PhD):*

Kalenia Márquez-Flórez



Advisors:

María Sancho-Tello Valls

Carmen Carda Batalla

Diego Garzón Alvarado

Investigation Line:

Computational Mechanics and Tissular Engineering

Research Groups:

Grupo Modelado y Métodos Numéricos en Ingeniería-GNUM

Universidad Nacional de Colombia, Faculty of Engineering
Department of Mechanics and Mechatronic Engineering
Bogotá D.C., Colombia

Universitat de València, Faculty of Medicine and Odontology
Department of Pathology
Valencia, Spain

June 2019

Kalenia Márquez-Flórez

Mechanobiological computational model for the development and formation of synovial joints, © 2019

Advised by: María Sancho-Tello Valls, Carmen Carda Batalla, Diego Garzón Alvarado

Cover illustration: Kalenia Márquez Flórez

Universidad Nacional de Colombia
Universitat de València



VNIVERSITAT DE VALÈNCIA

Maria Sancho-Tello Valls, Doctora en Medicina i Cirurgia, Professora Titular del Departament de Patologia de la Universitat de València;

Carmen Carda Batalla, Doctora en Medicina i Cirurgia, Doctora en Odontologia, Catedràtica del Departament de Patologia de la Universitat de València;
i

Diego Alexander Garzón Alvarado, Doctor en Mecànica Computacional, *Full Professor* del Departament d'Enginyeria Mecànica i Mecatrònica de la Universidad Nacional de Colombia,

FAN CONSTAR QUÈ:

dins del Programa de Doctorat en Medicina, Kalenia María Márquez Flórez ha realitzat, sota la seua direcció, del treball titulat *Mechanobiological computational model for the development and formation of synovial joints*, que es presenta en aquesta memòria per optar al grau de Doctor per la Universitat de València en cotutela amb la Universidad Nacional de Colombia.

I per tal què així conste a efectes oportuns, i donant el vistiplau per a la presentació d'aquest treball davant el Tribunal de tesi que corresponga, signen el present certificat a València, Març de 2019.

Maria Sancho-Tello Valls
Professora Titular - Universitat de València

Carmen Carda Batalla
Catedràtica - Universitat de València

Diego Alexander Garzón Alvarado
Full professor - Universidad Nacional de Colombia

A mi familia.

*“Pero ustedes saben señores muy bien cómo es esto.
No nos falló la intención, pero sí el presupuesto...”*

Dos colores: Blanco y negro, Jorge Drexler

AGRADECIMIENTOS

Por medio de esta nota quiero agradecer a todos los que, directa o indirectamente, aportaron en el desarrollo de mi tesis. Principalmente, quiero agradecer a mis directores, empezando por el Prof. Diego Garzón, quien me ha acogido e introducido en este mundo de la investigación desde que dejé mis estudios de pregrado, pasando por la maestría y ahora en doctorado (seguro tiene mucha paciencia). Quisiera agradecer a mis directoras, Dra. Carmen Carda y Dra. María Sancho-Tello, por acogerme en su casa, su universidad, y permitirme la oportunidad de trabajar en un tema totalmente nuevo y desafiante para mí. Sí, a ellos tres les agradezco por su guía durante el curso de mi doctorado, como estudiante, como persona y como una investigadora inexperta. También quiero agradecerles por la posibilidad que me dieron de hacer mi doctorado en cotutela entre la Universidad Nacional de Colombia y la *Universitat de València*.

A mis padres, Francisco Márquez e Iveth Flórez, a mi hermano, Blake Márquez, y al resto de mi familia, que con su paciencia, apoyo y ánimos me sostuvieron durante los buenos momentos y las dificultades. Gracias a ellos he llegado a este importante momento de mi vida.

A mis amigos, a Saúl M. a Nataly G., y en especial a Yesid Suárez, gracias por su apoyo constante en todo lo que se me ocurre. Al equipo de Taekwondo de la U. Nacional de Colombia. por permitirme disfrutar de su compañía y campeonatos. A mis compañeros de doctorado, especialmente a Héctor C. y Juan V., sus consejos y apoyo moral y académico fue, y seguirá siendo, invaluable para mí. A Yesid V., por ayudarme desde la distancia y por sus charlas ñoñas interesantes que me subían el ánimo.

A los que me han adoptado durante mi estancia en Valencia; al grupo de Taekwondo de la U. de Valencia; a Karina por acogerme en su hogar, a Sergio por subirme el ánimo cada vez, por la ayuda en la corrección de estilo de partes del documento.

Por último, agradezco a la Universidad Nacional de Colombia, *Alma Mater* que me ha cobijado estos años, y a la que le debo lo que soy ahora. A la *Universitat de València*, por acogerme y mostrarme un mundo académico diferente al que conocía.

gracias

TABLE OF CONTENTS

<i>Agradecimientos</i>	<i>i</i>
<i>Table of contents</i>	<i>iii</i>
<i>List of Tables</i>	<i>vii</i>
<i>List of Figures</i>	<i>ix</i>
<i>Abbreviations</i>	<i>xiii</i>
<i>Abstract</i>	<i>xv</i>
<i>Resumen</i>	<i>xvii</i>
<i>Resum</i>	<i>xxi</i>
<i>General Introduction and Aim</i>	<i>1</i>
<i>Chapter 1. Conceptual Background</i>	<i>7</i>
1.1. PRENATAL DEVELOPMENT	<i>7</i>
1.1.1. <i>Limbs</i>	<i>10</i>
1.1.2. <i>Muscles and tendons</i>	<i>13</i>
1.1.3. <i>Bone development</i>	<i>14</i>
1.1.4. <i>Relevant time-line</i>	<i>15</i>
1.2. JOINTS	<i>17</i>
1.2.1. <i>Synovial Joints</i>	<i>19</i>
1.2.2. <i>Synovial joints structure</i>	<i>21</i>
1.2.3. <i>Articular Cartilage</i>	<i>22</i>
1.2.4. <i>Cartilage diseases</i>	<i>24</i>
1.2.5. <i>Subchondral bone</i>	<i>26</i>
1.3. FINITE ELEMENT METHOD (FEM)	<i>28</i>
<i>Chapter 2. Joint Onset</i>	<i>31</i>
2.1. INTRODUCTION	<i>31</i>
2.2. MATERIALS AND METHODS	<i>34</i>
2.2.1. <i>Biological Aspects Considered for the Joint Development Model</i>	<i>34</i>
2.2.2. <i>Tissue Differentiation</i>	<i>37</i>
2.2.3. <i>Mathematical model for joint formation</i>	<i>38</i>
2.2.4. <i>Growing of the tissue (Domain Growth)</i>	<i>43</i>

2.2.5. Numerical solution of PDEs.....	44
2.2.6. Geometry, initial and boundary conditions, and simulated cases.....	45
2.3. RESULTS	47
2.3.1. Case I: interphalangeal joint development	47
2.3.2. Case II: longer initial bud.....	49
2.3.3. Case III: high growth rate.....	50
2.3.4. Case IV: wider rudiment	50
2.3.5. Case V: implantation of beads bearing GDF-5 (lateral)	52
2.3.6. Case VI: implantation of beads bearing GDF-5 (tip).....	52
2.4. DISCUSSION	54
Chapter 3. Joint Morphogenesis	61
3.1. INTRODUCTION	61
3.2. MATERIALS AND METHODS.....	65
3.2.1. Geometry and boundary conditions	66
3.2.2. Mechanical Aspects.....	67
3.2.3. Molecular Aspects.....	68
3.2.4. Tissue Growth	70
3.2.5. Bone Ossification	72
3.2.6. Translation to reference	72
3.2.7. General algorithm.....	73
3.2.8. Modelled cases.....	75
3.3. RESULTS	76
3.4. DISCUSSION	83
Chapter 4. Patella Onset.....	91
4.1. INTRODUCTION	91
4.2. THEORY I: BIOCHEMICAL THEORY	93
4.2.1. Tendon & eminence development.....	95
4.2.2. Computational and mathematical model.....	96
4.2.3. Results and discussion.....	104
4.3. THEORY II: MECHANICAL THEORY	108
4.3.1. Mathematical Model	109
4.3.2. Geometry and boundary conditions	111
4.3.3. Material properties and tissue differentiation.....	112
4.3.4. Results and discussion.....	112
4.4. THEORY III: TOPOLOGICAL OPTIMIZATION (TO).....	115
4.4.1. Geometry and boundary conditions	118
4.4.2. Material properties	119
4.4.3. Results and discussion.....	119
4.5. NUMERICAL SOLUTION FOR THE THREE THEORIES	120

4.6. GENERAL DISCUSSION.....	120
Chapter 5. Cartilage regeneration	127
5.1. INTRODUCTION	127
5.2. MATERIALS AND METHODS.....	131
5.2.1. Geometry and mesh.....	131
5.2.2. Boundary conditions	133
5.2.3. Material Models.....	134
5.2.4. General algorithm.....	144
5.3. RESULTS	147
5.4. DISCUSSION	152
Chapter 6. General conclusions and recommendations.....	157
6.1. GENERAL CONCLUSIONS	157
6.2. RECOMMENDATIONS	160
Summary.....	163
Summary in valencian.....	187
References.....	213
Appendixes.....	233
APPENDIX A – VALUE OF THE PARAMETERS USED ON CHAPTER 2 (JOINT ONSET)	233
APPENDIX B – VALUE OF THE PARAMETERS USED ON CHAPTER 4 (PATELLA ONSET)	235
APPENDIX C – VALUE OF THE PARAMETERS USED ON CHAPTER 5 (CARTILAGE REGENERATION)	237
APPENDIX D – PUBLISHED AND SUBMITTED WORKS.....	239
APPENDIX E – JOURNALS’ PERMISSIONS.....	241

LIST OF TABLES

<i>Table 2-1 Tissue transformation criteria.</i>	<i>38</i>
<i>Table 3-1 Conditions for the normal and pathological settings.</i>	<i>75</i>
<i>Table 4-1 Relation between molecules and tissue or cell type for the model developed for theory I.....</i>	<i>101</i>
<i>Table 4-2 Molecule and threshold (Th) levels involved in the tissue differentiation.</i>	<i>102</i>
<i>Table 4-3 Tissue properties.....</i>	<i>112</i>

LIST OF FIGURES

<i>Fig. 1-1 Timeline of the human prenatal development</i>	7
<i>Fig. 1-2 Schematic representation of embryo development from the two-cell state to blastocyst</i>	9
<i>Fig. 1-3 Schematic representation of the human blastocyst components at second week</i>	10
<i>Fig. 1-4 Schematic representation of the development of the limb</i>	11
<i>Fig. 1-5 Scheme of human hand development</i>	12
<i>Fig. 1-6 Schematic representation of the muscle development in a 7-week embryo</i>	13
<i>Fig. 1-7 Schematic representation of the endochondral ossification of long bones</i>	15
<i>Fig. 1-8 Relevant timeline for human limb development</i>	16
<i>Fig. 1-9 Schematic representation of the parts of a synovial joint</i>	21
<i>Fig. 1-10 3D schematic representation of the hyaline (articular) cartilage</i>	23
<i>Fig. 1-11 Schematic representation of a finite element mesh</i>	30
<i>Fig. 2-1 Scheme of the stages of the synovial joints during the interphalangeal joint development</i>	33
<i>Fig. 2-2 Molecule concentration for each element</i>	38
<i>Fig. 2-3 Relationship between enzyme (u) and substrate (v) for the Schnakenberg model (enzyme-substrate)</i>	39
<i>Fig. 2-4 Schematic of the boundary conditions employed for the joint onset model</i>	46
<i>Fig. 2-5 Results obtained by the simulation for case I</i>	48
<i>Fig. 2-6 Results obtained by simulation for cases II, III and IV</i>	51
<i>Fig. 2-7 Results obtained by simulation for cases V and VI</i>	53
<i>Fig. 2-8 Comparison of the molecular distribution between the obtained results for case I with those reported in former experimental studies</i>	56
<i>Fig. 3-1 Schematic representation of the boundary conditions implemented on the model</i> ...	66
<i>Fig. 3-2 Geometry of the bone anlagen and the synovial capsule</i>	68
<i>Fig. 3-3 Schematic definition of the concentration areas</i>	70
<i>Fig. 3-4 Translation process from a rotated state to the reference state at (0°)</i>	73
<i>Fig. 3-5 Algorithm designed for joint morphogenesis</i>	74
<i>Fig. 3-6 Geometry of the pathological kilter model</i>	76
<i>Fig. 3-7 Obtained joint shape at different time-steps for normal conditions</i>	77
<i>Fig. 3-8 Stress distribution at different time-steps</i>	78

<i>Fig. 3-9 Obtained joint shape at different unit time for the pathological condition when the effect of the molecules is not included.</i>	79
<i>Fig. 3-10 Obtained hydrostatic and octahedral stresses at different unit time for the w/o molecular effect pathological setting.</i>	79
<i>Fig. 3-11 Obtained joint shape at different unit time for the simulated pathological environments. Palmar side to the left and dorsal to the right.</i>	81
<i>Fig. 3-12 Obtained hydrostatic and octahedral stresses at different unit time for the pathological models.</i>	82
<i>Fig. 3-13 Molecular distribution at different time-steps.</i>	84
<i>Fig. 3-14 Secondary ossification center (SOC) in a developing bone.</i>	86
<i>Fig. 3-15 Comparison of the obtained geometries for the kilter, the 0° palsy, the 90° palsy and the normal conditions.</i>	87
<i>Fig. 4-1 Sagittal sections of the patella from hind limbs of wild-type mouse embryos stained with Alcian Blue and Fast Red to highlight cartilage cells (I. A-C) and Sox9 and Scx expression (II).</i>	94
<i>Fig. 4-2 Schematic representation of the tendon and eminence development.</i>	95
<i>Fig. 4-3 Schematic representation of the patella development process based on the theory proposed by Eyal et al. [117].</i>	97
<i>Fig. 4-4 General algorithm that developed to model the events occurring according to the Theory I.</i>	99
<i>Fig. 4-5 Knee joint geometry employed for patella development study.</i>	103
<i>Fig. 4-6 Obtained distribution of the molecules (TGF-β, BMP, FGF, GDF-5) and Scx-cells during patella development.</i>	106
<i>Fig. 4-7 Obtained tissue differentiation through the time of patella development.</i>	107
<i>Fig. 4-8 Patella development: tissue differentiation for the biochemical model at different angles (60°, 45° and 30°).</i>	107
<i>Fig. 4-9 Diagram of the mechanoregulatory model proposed by Carter et al., (1998) [7].</i>	109
<i>Fig. 4-10 Schematic representation of the geometry and boundary conditions.</i>	111
<i>Fig. 4-11 Results obtained by the simulation for the different angles: stress, tensile strain and patella shape.</i>	114
<i>Fig. 4-12 Results obtained by the simulation for the average hydrostatic stress and patella shape.</i>	115
<i>Fig. 4-13 Results obtained by the simulation through the TO algorithm.</i>	120
<i>Fig. 5-1 Schematic representation of the 2D finite element geometry of the articular surface and subchondral bone, with the scaffold implanted.</i>	132
<i>Fig. 5-2 Boundary conditions applied to the finite element model.</i>	133

<i>Fig. 5-3 Graphic of the angle of the fibers at each zone.</i>	<i>135</i>
<i>Fig. 5-4 Flow chart of the employed algorithm for cartilage or bone regeneration.</i>	<i>146</i>
<i>Fig. 5-5 Simulation of tissue differentiation after scaffold implantation throughout the simulation.....</i>	<i>149</i>
<i>Fig. 5-6 Simulation of collagen fiber orientation after implantation.</i>	<i>150</i>
<i>Fig. 5-7 Simulation of bones' Young's modulus after scaffold implantation.</i>	<i>151</i>
<i>Fig. 5-8 Comparison of our results with the histological findings of a previous experimental study.....</i>	<i>156</i>
<i>Declaration: Figures without reference were done by the authors.</i>	

ABBREVIATIONS

Abbreviation	Definition
<i>AER</i>	<i>Apical Ectodermal Ridge</i>
<i>BMP</i>	<i>Bone Morphogenetic Protein</i>
<i>CA</i>	<i>Cellular Automaton</i>
<i>DDH</i>	<i>Developmental Dysplasia of the Hip</i>
<i>DZ</i>	<i>Deep Zone</i>
<i>ECM</i>	<i>Extracellular Matrix</i>
<i>FEA</i>	<i>Finite Element Analysis</i>
<i>FEM</i>	<i>Finite Element Method</i>
<i>FGF</i>	<i>Fibroblast Growth Factor</i>
<i>FV</i>	<i>Fluid Velocity</i>
<i>GDF</i>	<i>Growth Differentiation Factor</i>
<i>Ihh</i>	<i>Indian hedgehog signaling molecule</i>
<i>MS</i>	<i>Mechanical stimulation</i>
<i>OA</i>	<i>Osteoarthritis</i>
<i>OI</i>	<i>Osteogenic Index</i>
<i>PDE</i>	<i>Partial Differential Equation</i>
<i>POC</i>	<i>Primary Ossification Center</i>
<i>PTHrP</i>	<i>Parathyroid Hormone-related Protein</i>
<i>PVF</i>	<i>Potential Vascularity Factor</i>
<i>RA</i>	<i>Rheumatoid Arthritis</i>
<i>RZ</i>	<i>Radial Zone</i>
<i>SIMP</i>	<i>Solid Isotropic Material with Penalization</i>
<i>SOC</i>	<i>Secondary Ossification Center</i>
<i>SZ</i>	<i>Superficial Zone</i>
<i>TGF-β</i>	<i>Transforming Growth Factor-β</i>
<i>TO</i>	<i>Topological Optimization</i>
σ	<i>Stress</i>

ABSTRACT

The onset and development of the synovial joints is due to different genetic, biochemical, and mechanical factors. It starts at the limb buds, which have an uninterrupted mass of mesenchymal cells within its core, also known as skeletal blastema. Most of these blastemal cells differentiate into chondrocytes; however, some of these cells remain undifferentiated at the site of the future joint (interzone). The separation of the rudiments occurs with cavitation process within the interzone. After the joint cleavage (cavitation), joint morphogenesis occurs, and the bones take their final shape. Once the embryonic period has finished, the synovial joint and its internal structures has developed completely. Though, once the synovial joints are formed, they might suffer several pathologies, such as the osteoarthritis (OA). There are several treatments that have been proposed to regenerate the articular cartilage, among which scaffolds without cellular sources have shown great results.

Understand the processes that the joint tissue goes through are important to develop new direct and effective treatments for joint related pathologies. Computational models seem a good alternative tool to complement the study of the joint processes. Therefore, it was of our interest to study, through computational models, the biochemical interaction for the interzone onset, the cavitation and morphogenesis processes during the joint development. We analyzed these phenomena within the development of an interphalangeal joint and the patella onset. Moreover, we were also interested on analyzing, through a computational model, the processes happening when a defect in the articular cartilage is treated with the implantation of a polymeric scaffold.

All the computational models developed in this study applied theories about tissue behavior under mechanical and biochemical

stimuli. The obtained results were compared to experimental works found in the literature, all of them showed promising outcomes. Hence, we consider that the procedures and considerations taken for each proposed computational model are not far from what is really happening on the analyzed biological phenomena. Moreover, we were able to evaluate mechanical and biochemical conditions the biological phenomena, that would be hard to test through experimental approaches. We hope that these models become useful to medical and biological researches, helping in the design of prevention and therapy strategies for joint related diseases.

This thesis is structured in eight parts including an introduction which tries to aware the importance of the study and the objectives of the thesis. Afterwards, on the second part, we expose some general concepts related to the topics and methods employed to develop the research. Then, the third part describes a computational model proposed to explain joint development from the interzone onset to the cavitation process. The fourth part is focus on the joint morphogenesis as part of the joint development process. Subsequently, the fifth section is dedicated to explaining the sesamoid bones development through a comparison of three theories of the patella onset, evaluated via computational models. The seventh part of this work is a computational model proposed to understand the processes that surround the cartilage regeneration when a polymeric scaffold is implanted in the articular cartilage. In the last part, we concluded the achievements and discussed the main conclusions of the thesis, as well as the recommended future work and perspectives. As an additional chapter, we added a general overview of the thesis in English and in Valencian.

RESUMEN

El desarrollo de las articulaciones sinoviales se debe a diferentes factores genéticos, bioquímicos y mecánicos. Comienza en el brote de las extremidades, que tienen una masa ininterrumpida de células mesenquimales dentro de su núcleo, el blastema esquelético. La mayoría de estas células blastemales se diferencian en condrocitos; sin embargo, algunas de estas células permanecen, sin diferenciar, en el sitio de la futura articulación (interzona). La separación de los rudimentos ocurre con el proceso de cavitación dentro de la interzona. Después de la cavitación, se produce la morfogénesis articular y el hueso toma su forma final. Una vez finalizado el período embrionario, la articulación sinovial y sus estructuras internas se han desarrollado completamente. Aunque una vez que se forman las articulaciones sinoviales, pueden sufrir, a lo largo de la vida, distintas patologías, como la osteoartritis (OA). Hay varios tratamientos que se han propuesto para regenerar el cartílago articular, entre los cuales, los andamiajes (*scaffolds*) sin fuentes celulares han mostrado grandes resultados.

Comprender los procesos por los que pasa el tejido articular es importante para desarrollar nuevos tratamientos directos y efectivos para las patologías relacionadas con las articulaciones. Los modelos computacionales parecen ser una buena herramienta para complementar el estudio de los procesos articulares. Por lo tanto, fue de nuestro interés estudiar, a través de modelos computacionales, la interacción bioquímica de la aparición de la interzona, la cavitación y la morfogénesis durante el desarrollo de articulaciones. Analizamos estos fenómenos en el desarrollo de una articulación interfalángica y el desarrollo de la rótula. Además, también estábamos interesados en analizar, mediante un modelo computacional, los procesos que ocurren

cuando un defecto en el cartílago articular se trata con la implantación de un andamiaje polimérico.

Todos los modelos computacionales desarrollados en este estudio aplicaron teorías sobre el comportamiento de los tejidos bajo estímulos mecánicos y bioquímicos. Los resultados obtenidos, fueron comparados con los trabajos experimentales encontrados en la literatura, todos los modelos mostraron resultados prometedores. Por lo tanto, consideramos que los procedimientos y las suposiciones tomadas para cada modelo computacional propuesto no están lejos de lo que realmente está sucediendo en los fenómenos biológicos analizados. Además, pudimos evaluar las condiciones mecánicas y bioquímicas de los fenómenos biológicos analizados, difíciles de probar a través de enfoques experimentales. Esperamos que estos modelos sean útiles para las investigaciones médicas y biológicas, ayudando en el diseño de estrategias de prevención y terapia para enfermedades relacionadas con las articulaciones.

Esta tesis está estructurada en ocho partes, incluida una introducción que trata de exponer la importancia del estudio y los objetivos de la tesis. Posteriormente, en la segunda parte exponemos algunos conceptos generales relacionados con los temas y métodos empleados para desarrollar la investigación. Luego, la tercera parte describe un modelo computacional propuesto para explicar el desarrollo de articulaciones desde el inicio de la interzona hasta el proceso de cavitación. La cuarta parte se centra en la morfogénesis de las articulaciones como parte del proceso de desarrollo de las mismas. Posteriormente, la quinta sección está dedicada a explicar el desarrollo de los huesos sesamoideos a través de una comparación de tres teorías del desarrollo de la rótula, evaluadas mediante modelos computacionales. La séptima parte de este trabajo es un modelo computacional propuesto para comprender los procesos que rodean la regeneración del cartílago cuando se implanta un andamiaje polimérico en el cartílago articular. En la última parte, se concluyen los logros y se analizan las principales conclusiones de la tesis, así como el trabajo

futuro recomendado y las perspectivas. Como capítulo adicional, agregamos una descripción general de la tesis en inglés y en valenciano.

El desenvolupament de les articulacions sinovials es deu a diferents factors genètics, bioquímics i mecànics. Comença en el brot de les extremitats, que tenen una massa ininterrompuda de cèl·lules mesenquimals dins del seu nucli, el blastema esquelètic. La majoria d'aquestes cèl·lules blastemals es diferencien en condrocits; però, algunes d'aquestes cèl·lules, sense deferenciar, romanen en el lloc de la futura articulació (interzona). La separació dels rudiments passa amb el procés de cavitació dins de la interzona. Després de la cavitació, es produeix la morfogènesi articular i l'os pren la seva forma final. Un cop finalitzat el període embrionari, l'articulació sinovial i les seves estructures internes s'han desenvolupat completament. Encara que, una vegada que es formen les articulacions sinovials, poden patir diverses patologies, com l'osteoartritis (OA). Hi ha diversos tractaments que s'han proposat per regenerar el cartílag articular, entre els quals, les bastides sense fonts cèl·lules han mostrat grans resultats.

Comprendre els processos pels quals passa el teixit articular és important per desenvolupar nous tractaments directes i efectius per a les patologies relacionades amb les articulacions. Els models computacionals semblen ser una bona eina per complementar l'estudi dels processos articulars. Per tant, va ser del nostre interès estudiar, a través de models computacionals, la interacció bioquímica de l'aparició de la interzona, la cavitació i la morfogènesi durant el desenvolupament d'articulacions. Analitzem aquests fenòmens en el desenvolupament d'una articulació interfalàngica i el desenvolupament de la ròtula. A més, també estàvem interessats en analitzar, mitjançant un model computacional, els processos que ocorren quan un defecte en el cartílag articular es tracta amb la implantació d'una bastida polimèric.

Tots els models computacionals desenvolupats en aquest estudi van aplicar teories sobre el comportament dels teixits sota estímuls

mecànics i bioquímics. Els resultats obtinguts, en comparació amb els treballs experimentals trobats en la literatura, tots ells van mostrar resultats prometedors. Per tant, considerem que els procediments i les consideracions preses per a cada model computacional proposat no estan lluny del que realment està succeint en els fenòmens biològics analitzats. A més, vam poder avaluar les condicions mecàniques i bioquímiques dels fenòmens biològics analitzats, que serien difícils de provar a través d'enfocaments experimentals. Esperem que aquests models siguin útils per a les investigacions mèdiques i biològiques, ajudant en el disseny d'estratègies de prevenció i teràpia per a malalties relacionades amb les articulacions.

Aquesta tesi està estructurat en vuit parts, inclosa una introducció que tracta de conèixer la importància de l'estudi i els objectius de la tesi. Posteriorment, a la segona part exposem alguns conceptes generals relacionats amb els temes i mètodes emprats per a desenvolupar la investigació. Després, la tercera part descriu un model computacional proposat per explicar el desenvolupament d'articulacions des de l'inici de la interzona fins al procés de cavitació. La quarta part se centra en la morfogènesi de les articulacions com a part del procés de desenvolupament de les articulacions. Posteriorment, la cinquena secció està dedicada a explicar el desenvolupament dels ossos sesamoïdeos a través d'una comparació de tres teories del desenvolupament de la ròtula, avaluades mitjançant models computacionals. La setena part d'aquest treball és un model computacional proposat per comprendre els processos que envolten la regeneració del cartílag quan s'implanta una bastida polimèric en el cartílag articular. En l'última part, es conclouen els èxits i s'analitzen les principals conclusions de la tesi, així com el treball futures recomanades i les perspectives. Com capítol addicional, afegim una descripció general de la tesi en anglès i en valencià.

GENERAL INTRODUCTION AND

AIM

Imagine how different human beings would be without the flexibility of movements that their bodies owe to the joints. What would have happened if their wrist would not have evolved to the complex joint that it is now? Or what if the movement the hip had not been as wide ranged as it is now? Would we have been able to walk erect? Certainly, we would have been different, we would not be what we are now. The liberty that our joints give us is priceless, they allow us to move freely, to bend, to jump, to grab, to walk, to express our selves.

Now, wonder what would happen if you lose mobility of one of your joints. Surely you would adapt, however, one can bet that at the beginning you would feel like your freedom is being cutback; from then on, your life wouldn't be the same. But what if you were born with a malformation on one of your joints? You might be used to the limitation; after all, you have been living with it since birth. However, on both mentioned cases, when compared to other human beings, you would feel behind on your capacities, and depending on the malformation or joint pathology, you would have to bear with other health issues such as the degradation of articular cartilage of the joint, or pain in other parts of your body due to a bad posture or movement. Consequently, any joint disease brings a substantial drop in the quality

of life. Therefore, it should be of high interest to study, with all available tools, how to prevent and treat joint-related diseases.

In general, joints are described as the site where two or more bones meet and can be classified according to their structure (how they are connected) and their function (how the movement between its bones is) -on Conceptual Background these classifications are described-. Within these classifications, the synovial joints, which also are classified as diarthrosis joints, offer the wider range of motion between bones. It is because of its range of motion and its structure that synovial joints are susceptible to articular diseases such as OA. Also, because of the complexity of the processes involved in its development, synovial joints are susceptible to developmental diseases and malformations, such as developmental dysplasia of the hip.

Synovial joint development is a complex process that initiates on the fetal stages of the prenatal development. Around five weeks of development, limb buds are noticeable. Initially, these limb buds have an uninterrupted core of mesenchymal cells, skeletal blastema, covered by a layer of ectoderm (future skin). Afterwards, these blastemal cells differentiate into chondrocytes, except on the site of the future joints. This area is known as the interzone, where the cavitation process takes place allowing the separation of the bone rudiments. Then, the two opposing cartilaginous rudiments acquire their reciprocal interlocking shapes through the process known as morphogenesis. If there are abnormal conditions during fetal development, joints can develop incomplete or abnormal, or even they might not develop at all.

By the end of the embryonic period, if there were not any abnormal conditions, the synovial joint has developed completely as well as its internal structures, articular cartilage, ligaments and synovial capsule. Moreover, the primary and secondary ossification centers of the bone appear which let the bone grow and ossify until adulthood.

Once the joint is developed, there might be some pathologies that still might impair the normal function of the joint. Among them, the OA, in which the articular cartilage that covers the bone degenerates. There are many causes, from idiopathic to related to trauma, that might end in this disease. Moreover, morphologic abnormalities (developmental diseases) may cause joint incongruities, which modify the load transmission through the cartilage, generating overloaded points that trigger early degeneration of joints. Different treatments have been proposed ranging from symptomatic, with analgesics and anti-inflammatory medications, to more invasive ones such as endochondral transplantation; being the last resort arthrodesis treatments, or total replacement of the joint. Nevertheless, it is preferable to preserve the original function of the joint through the regeneration of the articular cartilage, especially in young patients.

Among the cartilage regeneration treatments are included the osteochondral grafts, which can be considered as the most effective one [1,2]. However, these grafts have some disadvantages: patients must go through two surgeries, they create new defects, they are not appropriate for large defects, they become unstable with time, and normally the new tissue is fibrocartilage but not hyaline cartilage (as the articular cartilage) [1]. Recently, in the last 2 decades, cartilage regeneration has

been based on the use of scaffolds, which allow rapid filling of joint defects, providing a substrate where cells can anchor while maintaining mechanical integrity [3]. With scaffolds/cell-free implants, hyaline (articular) cartilage is generated in the upper part of the scaffold while it displaces into the subchondral bone [4].

Thanks to the growing literature regarding material properties and mechanics of the human body, the use of computational models in the field of biomechanics is expanding rapidly. This has made computational models a useful tool to understand the biomechanical-biochemical interactions that tissues go through during the regeneration and development processes. Computational models contribute to the evaluation of difficult to reach aspects for experimental models [5]. In this way, computational models provide a quantitative and qualitative evaluation of mechanobiological interactions while being fed with clinical or experimental parameters [6].

The biological computational models have been very useful to simulate biological processes: bone regeneration [7], bone growth [8], pattern formation [9–15], and embryonic development [16]. For cartilage, several computational models have been developed [5,17–19]. However, there are none, to our knowledge, related to cartilage regeneration. Regarding joint development, only two computational studies have been developed, the first one was done by Heegaard *et al.*, [20], in which they explored how motion affected joint morphogenesis; and a second one developed by Giorgi *et al.*, [21], who analyzed the effect of movement range with different initial shapes of the joint.

Computational models might be useful to understand critical factors that must be considered for the design of strategies for the early diagnosis and prevention of joint developmental diseases. Also, it would help to recognize factors that might influence how a joint can be repaired. Moreover, computational models might help identify which processes are involved in joint regeneration, and therefore, they can help with the development of effective and direct treatments for treating degenerative joint diseases, all in behalf of improving life quality.

Therefore, the main aim of this work is to computationally model the mechanical and biological aspects during the development of synovial joints. This main objective is divided in three specific ones. First, to formulate the mathematical description of the mechanobiological phenomena for the development of synovial joints. Second, to computationally evaluate the behavior of the models for the interzone onset. Third, to computationally evaluate the behavior for the cavitation and morphogenesis of synovial joints.

This work is organized into five parts. The first part (Joint Onset) describes a computational model for the first stages of the joint onset. It is explained, computationally, the appearance of the interzone and cavitation processes of an interphalangeal joint. On the second part (Joint Morphogenesis), a computational model for the last step of joint formation, the morphogenesis process of an interphalangeal joint from the sagittal view, is exposed. The third part (Patella Onset) explores three different theories that may explain the development of the patella bone (a sesamoid bone) through computational models. In the fourth part (Cartilage regeneration), a computational model of the regeneration

of the articular cartilage when employing a polymeric scaffold is described. Finally, the fifth part (General conclusions) contains the conclusions extracted from the current study. Each part of the developed work (Chapter 2 to Chapter 5) are structured as follows: an introduction on the chapter's subjects, a description of the employed methods and the obtained results, and a discussion of the results.

Additionally, prior to the description of the work developed here was added a chapter (Conceptual Background) in which we expose a brief portrayal of the fetal development, synovial joint structures articular cartilage and the finite element method (FEM).

Statement: *In this thesis the Chapter 2 (Joint Onset) and Chapter 4 (Patella Onset) are from already published works of my authorship: Permissions were obtained from the journals to include the pre-print articles in this thesis (Appendix E – Journals' permissions). The articles are the following:*

Chapter 2 - Joint Onset:

K.M. Márquez-Flórez, J.R. Monaghan, S.J. Shefelbine, A. Ramirez-Martínez, D.A. Garzón-Alvarado, *A computational model for the joint onset and development*, J. Theor. Biol. 454 (2018) 345–356. doi:10.1016/j.jtbi.2018.04.015.

Chapter 4 - Patella Onset:

K. Márquez-Flórez, S. Shefelbine, A. Ramírez-Martínez, D. Garzón-Alvarado, *Computational model for the patella onset*, PLoS One. 13 (2018) e0207770. doi:10.1371/journal.pone.0207770.

Chapter 1. CONCEPTUAL BACKGROUND

1.1. PRENATAL DEVELOPMENT

Prenatal development can be divided into three stages (Fig. 1-1): 1- Early cell division (first two weeks); 2- Embryonic period (from the 3rd to the 8th week); 3- Fetal period (from the 9th week to birth) [22]. The first stage, early cell division, is when the blastocyst develops and sinks into the mucosal lining of the uterus. During the embryonic period, most of the organ systems develop and the embryo takes a human appearance. From the 3rd month to the end of gestation, the fetus and the already existing organs grow.

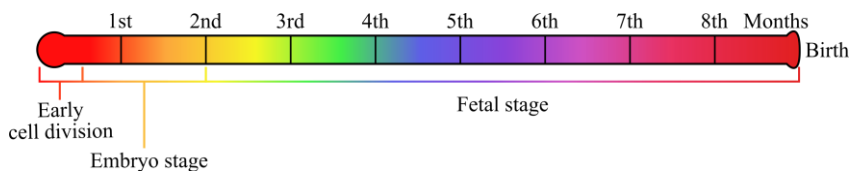


Fig. 1-1 Timeline of the human prenatal development.

On the first stage of development, there is a high chance of lethality, however, the susceptibility to Teratogenesis (congenital malformations) is very low [23]. In the first week, after the penetration of the spermatozoid into the oocyte, the cleavage process takes place.

Conceptual Background

This process is a series of mitotic divisions resulting in an increase number of smaller cells, blastomeres [23] (Fig. 1-2). These blastomeres become a compacted ball of cells, and they group to form a 16-cell morula [23]. When the morula goes into the uterus, a cavity begins to appear (blastocyst cavity). Then the inner mass within the blastocyst becomes the embryoblast (former morula), and the outer mass of the blastocyst will form the trophoblast (Fig. 1-2).

At the beginning of the second week, the blastocyst is partially embedded in the uterine stroma. By the end of the second week, the embryoblast has divided into two layers: the epiblast and the hypoblast, forming the bilaminar disc (Fig. 1-3) [23]. The trophoblast divides into two tissues: the cytotrophoblast and the syncytiotrophoblast (Fig. 1-3). The extraembryonic mesoderm appears, and it is formed by two layers: the somatic and the splanchnic layers (Fig. 1-3). Additionally, two new cavities appear, the amniotic and the yolk cavities [23] (Fig. 1-3).

By the end of the third week, the gastrulation event has occurred, resulting in the rise of the germ layers of the embryo: the ectoderm, the mesoderm, and the endoderm. These layers form all the tissues and organs of the fetus. In fact, as gastrulation takes place, some tissue and organ differentiation has begun in a cephalocaudal direction (head to tail) [23]. The ectodermal layer gives rise to organs and structures that have contact to the exterior such as the central and peripheral nervous systems, the sensory epithelium of the ear, nose and eyes, the skin, hair, nails, enamel of teeth, and the pituitary, mammary and sweat glands. On the other hand, the endodermal germ layer is in charge of the development of the gastrointestinal and respiratory tract,

the urinary bladder, the liver, the pancreas and the epithelial lining of the tympanic cavity and auditory tube. On its part, the mesoderm is in charge of the formation of all the supporting tissues of the body. The mesoderm is divided into 3 layers, the paraxial, intermediate and lateral plate. The paraxial mesoderm forms the somitomeres, which forms the mesenchyme of the head. These mesenchymal cells organize into somites, from which comes the myotomes (muscular tissue), the sclerotome (cartilage and bone), and the dermatome (dermis of the skin) [23].

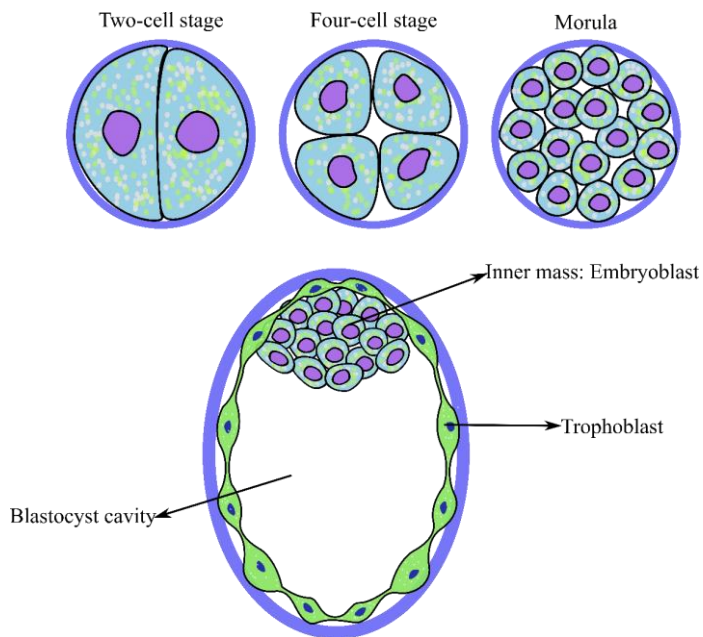


Fig. 1-2 Schematic representation of embryo development from the two-cell state to blastocyst. On top, the development of the embryo from the two-cell stage to the morula stage. On the bottom is shown a schematic representation of a human blastocyst showing the blastocyst cavity, the inner cell mass or embryoblast and the trophoblast.

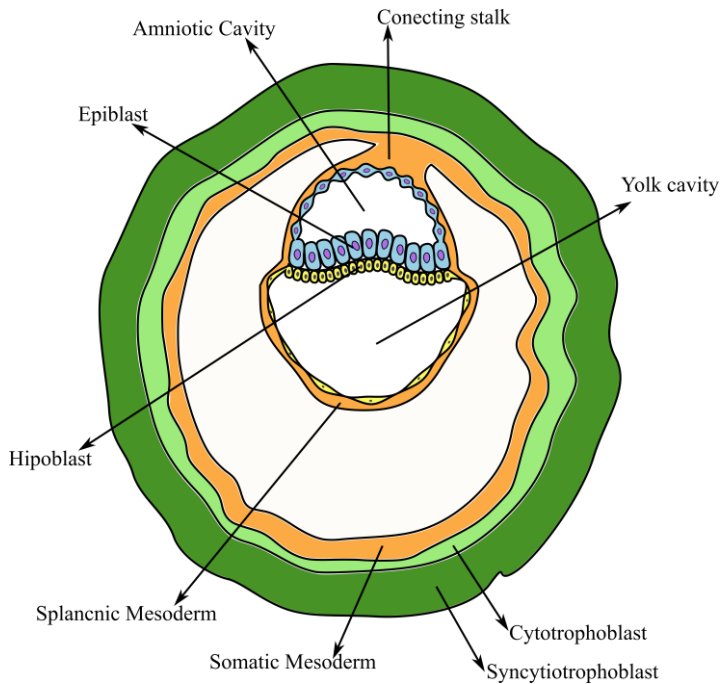


Fig. 1-3 Schematic representation of the human blastocyst components at second week.

Finally, the last stage, fetal stage, is characterized by rapid growth of the fetus and the organ systems. Also, it is worth mentioning that during the fifth month of pregnancy, the fetus movements are recognizable by the mother [23].

1.1.1. LIMBS

At the end of the fourth week, limb buds are noticeable (Fig. 1-4-A). The forelimbs onset occurs first and the hind limbs two days later. Initially, these limb buds are conformed by a core of mesenchymal cells covered by a layer of ectoderm (Fig. 1-4-D).

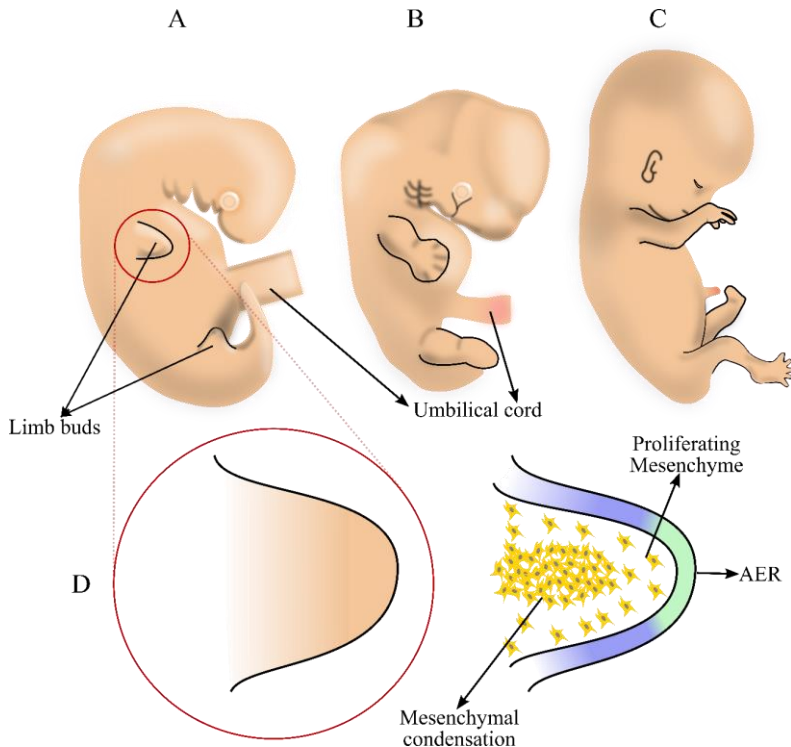


Fig. 1-4 Schematic representation of the development of the limb.

A: limb buds at 5 weeks. **B:** limb buds at 6 weeks. **C:** at 8 weeks the hind limbs are completely developed.

The ectoderm at the distal border of the limb thickens and forms the apical ectodermal ridge (AER) (Fig. 1-4-D), that influences the adjacent mesenchymal cells, causing them to remain undifferentiated and with a rapid proliferation. As limbs grow, cells located at a greater distance from the AER differentiate into cartilage; therefore, the limbs develop in a proximodistal direction.

At six weeks (embryos), the distal part of the limb buds flattens in order to form the hands and feet (Fig. 1-4-B). Fingers and toes start to appear around the seventh week (at 48 days), when cell death in the

Conceptual Background

AER separates the ridge (Fig. 1-5-A). The fingers and toes keep forming due to their continued outgrowth under the influence of AER, the condensation of the mesenchymal cells that form cartilaginous digital rays (future bones), and the death of the tissue between the rays (Fig. 1-5-B). At eight weeks the main parts of the extremities can be recognizable (Fig. 1-5-C).

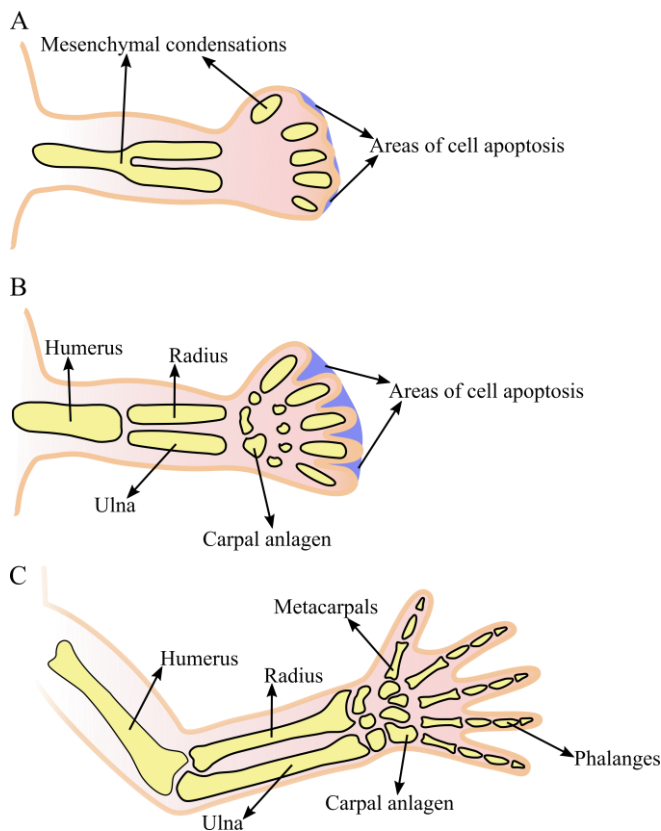


Fig. 1-5 Scheme of human hand development.

A: at 48 days, apoptosis in the AER initiates the digit separation and bone development begins with the condensation of mesenchyme, which later differentiates into chondrocytes. **B:** at 51 days, apoptosis in the interdigital spaces allows the fingers to separate. **C:** at 56 days, the main parts of the extremities can be recognizable and almost all joints are formed.

While the limb bud is shaping, the mesenchymal cells within the buds begin to condense and differentiate into chondrocytes. At six weeks, the shadowing of the first bone anlagen can be seen (Fig. 1-5-A). Later, these bones anlagen separate, forming the joints between them (Fig. 1-5-B and Fig. 1-5-C).

1.1.2. MUSCLES AND TENDONS

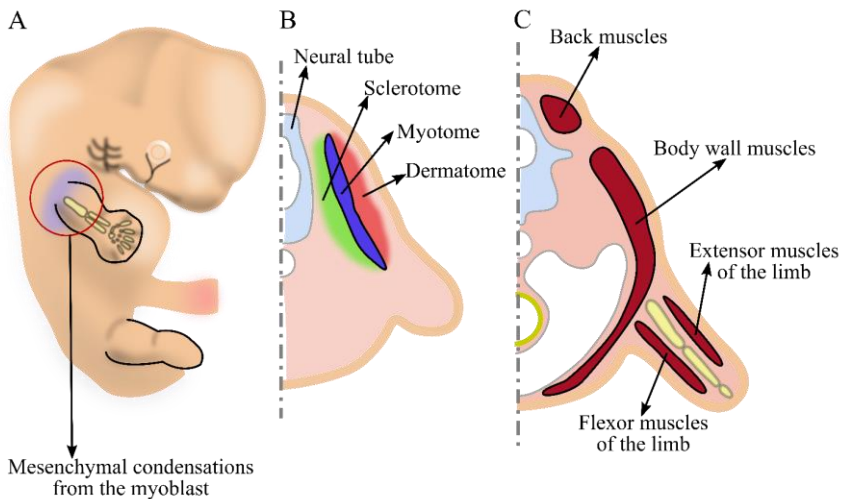


Fig. 1-6 Schematic representation of the muscle development in a 7-week embryo.

A: seventh week, a condensation of mesenchymal cells from the myoblast is located near the base of the limb buds. **B:** the myotome cells contribute to muscles, the dermatome cells form the dermis of the back, and the sclerotome forms the tendons. **C:** cross section through half the embryo, the muscles of the limbs start as a segmented structure that splits into the extensor and flexor muscles as the limb grows.

During development, precursor cells from the myoblast fuse and form long multinucleated muscle fibers. By the end of the third month, myofibrils appear and organize in cross-striations [23]. On the limbs, the first sheds of muscles can be observed after the seventh week as a

condensation of mesenchymal cells near the base of the limb buds (Fig. 1-6). The muscles start as a segmented structure that splits into the extensor (dorsal) and flexor (ventral) muscles as the limb grow (Fig. 1-6); afterwards, additional splitting and fusions occur so that a single muscle could be formed with several original segments. On the other hand, tendons are formed by sclerotome cells. These cells are lying adjacent to the myotomes.

1.1.3. BONE DEVELOPMENT

By the end of the embryonic period, the primary and secondary ossification centers (POC and SOC), which let the bone grow and ossify gradually until adulthood, appear. Around the 8th week, the endochondral ossification process starts, allowing the bone anlage (condensed chondrocyte cells) of the diaphysis (shaft) to ossify (Fig. 1-7-B). The POC appears between the 8th and 9th week when the perichondrium differentiates into periosteum (Fig. 1-7-C). Then, around the 10th week, the cartilage in the center of the diaphysis becomes calcified while blood vessels invade the area allowing osteoblast to deposit bone on the remaining cartilage spicules (Fig. 1-7-C). Bone replaces the cartilage, extending the ossification towards each end of the diaphysis. Thereafter, the same process is repeated in the epiphyses, giving rise to the SOC (Fig. 1-7-C). Bone fills the epiphyses from the SOC out, except for the articular cartilage and the growth plate (cartilage structure between the epiphyses and the diaphysis). At birth, the diaphysis of the bones generally are ossified, and, in some cases, the epiphyses are still entirely cartilaginous, whereas in other cases the

SOC has already arisen (Fig. 1-7-C). The growth plates allow the bone to grow in length until it has reached its full extent. In adulthood, these plates disappear and ossify fusing with the diaphysis of the bone.

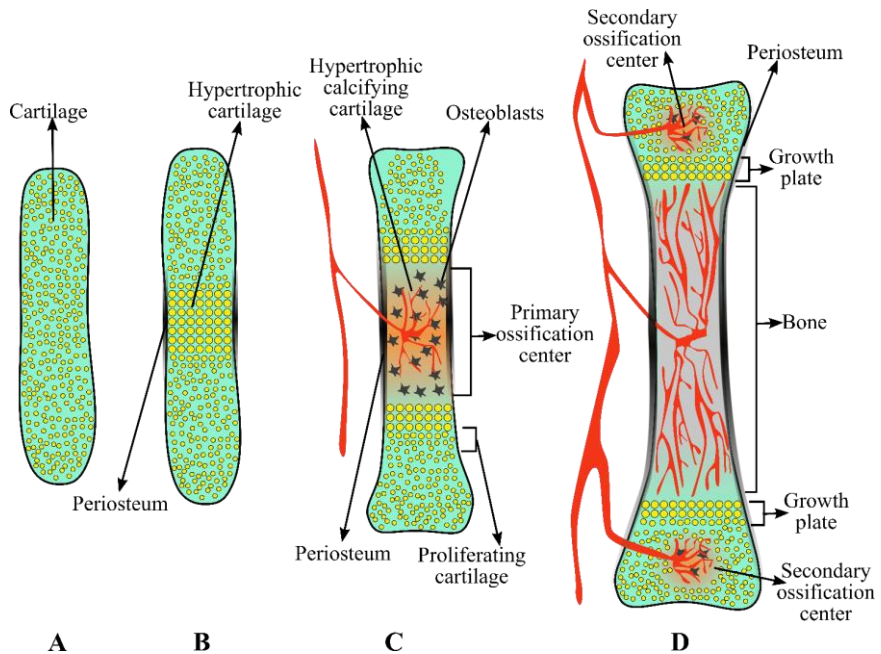


Fig. 1-7 Schematic representation of the endochondral ossification of long bones.

A: chondrocytes forming a cartilage mold of the bone (anlage). **B:** 8 weeks, the chondrocytes in the shaft of the bone (diaphysis) hypertrophy and the periosteum starts to onset **C:** 9 weeks, blood vessels invade the diaphysis bringing osteoblast, and the chondrocytes undergo hypertrophy and apoptosis, mineralizing the diaphysis; then the osteoblast bund to the mineralized matrix and deposit bone matrices. **D:** at birth, blood vessels invade the epiphyses rising the secondary ossification center; growth is maintained due to the proliferation of the chondrocytes in the growth plate.

1.1.4. RELEVANT TIME-LINE

To summarize, in the following figure (Fig. 1-8) is shown the relevant timeline for limb development in which the relevant processes are exposed.

Conceptual Background

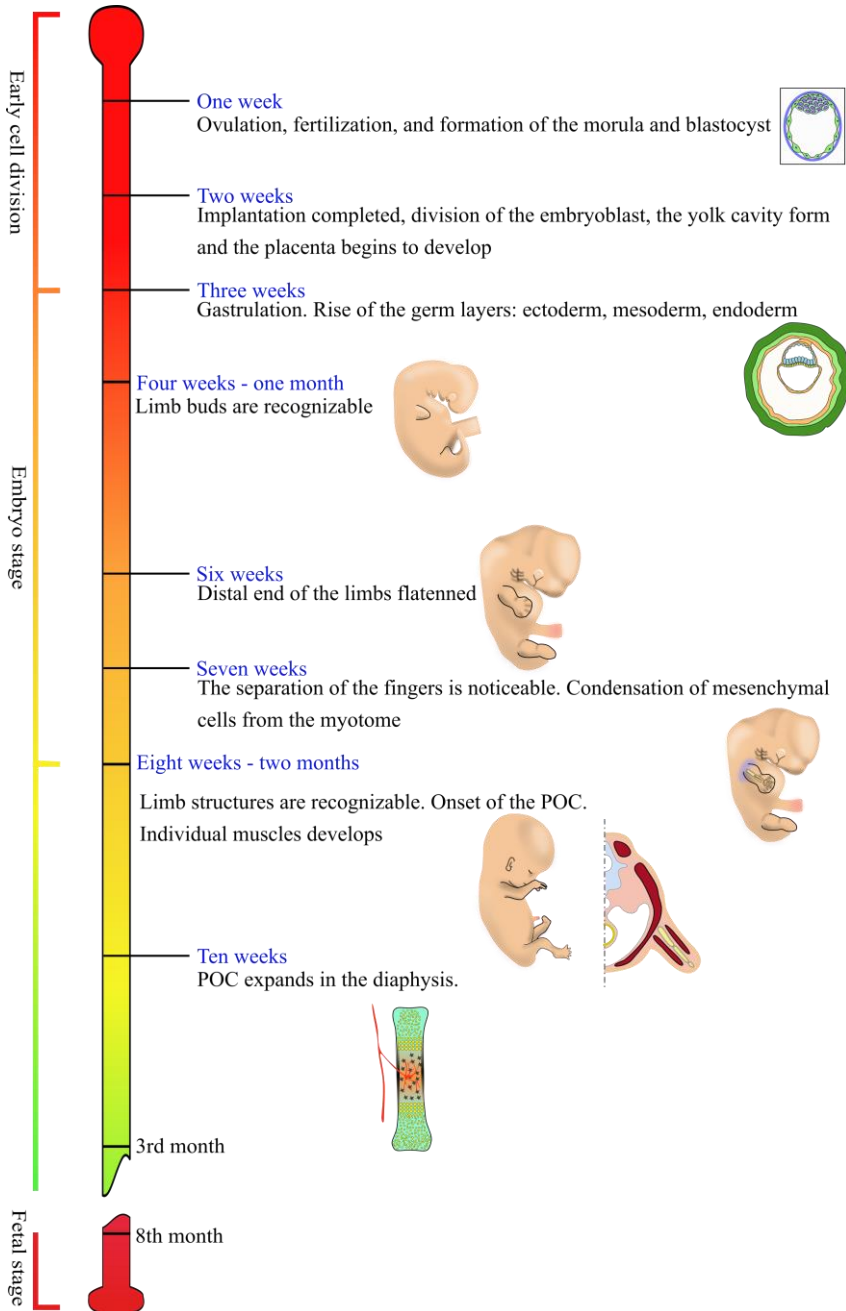


Fig. 1-8 Relevant timeline for human limb development.

1.2. JOINTS

Joints are the anatomical sites where two or more bones meet, and their function is to allow a relative movement between bones without losing the stability of the skeleton [24]. There are about 206 bones in the adult human body, and almost all of them are in contact with at least one other bone. Therefore, the total number of joints can be hundreds.

Joints are classified depending on both its structure and function. Structural classification of joints is related to how the bones are connected, while functional classification is used to describe the relative movement between bones.

There are three main classes of joints when classified based on their structure: the fibrous joints unite adjacent bones by fibrous connective tissue; the cartilaginous joint connects bones through hyaline cartilage or fibrocartilage; and the synovial joints do not completely connect articulating bones, *i.e.*, the articulating bony surfaces are not in continuity as in the other types of joints. Instead, in the synovial joints, the articulating surfaces are covered by hyaline cartilage with limited contact between them and a very low coefficient of friction, making the relative movement between them quite easy. Additionally, in the synovial joints, there is a fibrous capsule that surrounds the linked bones, the synovial capsule, that is filled with a lubricant fluid, the synovial fluid, that helps to smooth the relative movement between the bones.

On the other hand, joints are functionally classified as synarthrosis (low mobility), amphiarthrosis (slight mobility) and diarthrosis (free mobility). Fibrous and cartilaginous joints can be classified to either synarthrosis or amphiarthrosis, whereas synovial joints are always classified as diarthrosis.

The main function of the synarthroses is to provide a strong union between the articulating bones, hence, this kind of joints are mostly located in places where bones should protect internal organs [24]. Among examples of this type of joints are included the bones of the skull (fibrous joints), and the manubriosternal joint (cartilaginous joint).

In amphiarthroses, the bones are connected by either an interosseous ligament (fibrous joint) or by a disk of fibrocartilage (cartilaginous joint) [24]. The function of these joints is both for protection and to bring slight mobility between the involved bones. Examples of these joints are the intervertebral joints (cartilaginous joint), the pubic symphysis of the pelvis (cartilaginous joint), the joints between ribs and sternum (cartilaginous joint), and the syndesmosis joints (fibrous joints).

Diarthroses joints are highly movable joints in which the shapes of the opposing cartilaginous surfaces are relatively congruent and encircled within a synovial capsule filled with synovial fluid (all synovial joints). Examples of these are included the hip, knee, shoulder, elbow, among others.

1.2.1. SYNOVIAL JOINTS

Most synovial or diarthrotic joints are in the appendicular skeleton (limbs), therefore they give the limbs a large range of motion. Moreover, depending on the axis of motion of each joint (degrees of freedom), joints can be classified into three categories: uniaxial, biaxial and multiaxial. A uniaxial joint allows the relative motion between bones only around one axis, such as the elbow. A biaxial joint allows motion in two planes or around two axes, such as the metacarpophalangeal. And finally, joints such as the shoulder or the hip are considered as multiaxial, since they allow movement in several directions (posterior-anterior, lateral-medial and around their long axis).

Further classification of the synovial joints is related to their articulating surfaces shapes. There are six types of joint within this classification: pivot, hinge, condyloid, saddle, plane, and ball-and-socket joints.

Pivot joints allow one bone to rotate on its axis, such as the proximal radioulnar joint, where the head of the radius is largely encircled by a ligament as it articulates with the radial notch of the ulna. Functionally, this type of joint is classified as uniaxial joint.

The hinge joint only allows two kinds of motion (bending and straightening) along a single axis, such as an interphalangeal joint. Thus, hinge joints are functionally classified as uniaxial joints.

The condyloid or ellipsoidal joints have a shallow depression at the end of one of the bones that articulate with a rounded structure from

adjacent bones. They can be found between the radius and carpal bones or between the distal end of a metacarpal bone and the proximal phalanx. Functionally, condyloid joints are biaxial joints that allow for two planes of movement.

In saddle joints, the articulating surfaces present a saddle shape, like a seat on a horse, but convex on one bone and concave in the other. They can be found in the articulation between the trapezium carpal bone and the first metacarpal bone (base of the thumb), providing the thumb with the ability to move in two planes (parallel and perpendicular to the palm). This movement of the joint is what gives the humans their characteristic opposable thumbs [24]. These joints are functionally classified as biaxial joints.

In plane joints, the articulating surfaces are flat so the bones can slide against each other. Plane joints can be found between the carpal bones (intercarpal joints) of the wrist or the tarsal bones (intertarsal joints) of the foot, between the clavicle and acromion of the scapula (acromioclavicular joint), and between the superior and inferior articular processes of adjacent vertebrae (zygapophysial joints). Regarding their functionality classification, because of their shape, these joints can be described as multiaxial joints. However, depending on the ligaments and neighbor bones, their movement could be limited.

Finally, the ball-and-socket joints are the joints that present the highest range of motion. Their main feature is that one bone has a rounded head (ball) that fits into a concave articulation (socket) of the other bone. The only ball-and-socket joints of the body are the hip and

the glenohumeral (shoulder). Ball-and-socket joints are functionally classified as multiaxial joints.

1.2.2. SYNOVIAL JOINTS STRUCTURE

Although different structures can be found in synovial joints, they all present four common features (Fig. 1-9): the enclosed articular capsule containing synovial fluid (lubricant); the articulating cartilage surfaces, which slide against each other; the synovial membrane, which covers the inner side of the capsule; and the ligaments, tendon and muscles, which provide stability to the joint.

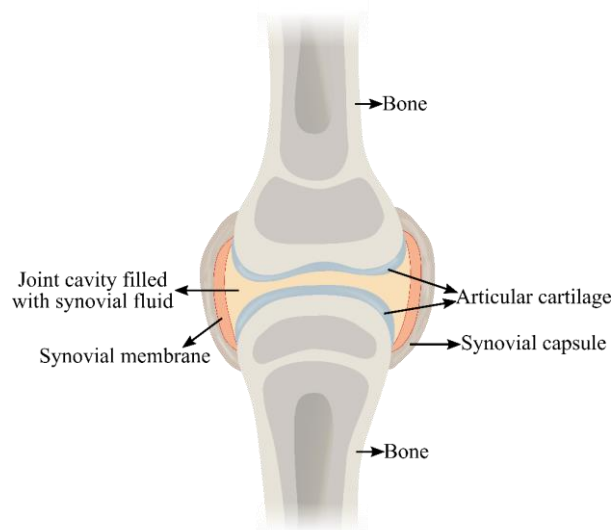


Fig. 1-9 Schematic representation of the parts of a synovial joint.

1.2.3. ARTICULAR CARTILAGE

The cartilage is a specialized form of connective tissue, made-up by chondrocytes. The chondrocytes are cells isolated in small spaces of the extracellular matrix (ECM), composed by type II collagen fibers embedded within a ground substance, *i.e.*, colloidal gel full of water. The cartilage is a non-vascularized tissue so the cells get nutrients from the ground substance and its self-repairing capabilities are very limited [25]. There are three types of cartilage: elastic, fibrous, and hyaline.

The elastic cartilage, as the name describes, is the most elastic of the three. It can be found in the epiglottis, in the external ear and in the walls of the ear conduct and the Eustachian tubes. Its extracellular matrix is rich in both elastic fibers and collagen type II fibers.

The fibrous cartilage can be seen as a transition between dense connective tissue and hyaline cartilage since it is made up of a combination of dense collagen fibers (type I) and chondrocytes within lacunae surrounded by hyaline matrix [25]. This type of cartilage can be found in the intervertebral disks, the meniscus and, sometimes, in the ligaments and tendons insertion sites.

The hyaline cartilage is the most abundant in the human body. It covers the articulating bone ends in synovial joints, forming the articular cartilage, a surface that helps to the force transmission and distribution. The thickness of the articular cartilage varies from joint to joint, but in humans is usually between 2-4 *mm* [26]. It can be described as a poroelastic tissue, in which cells (chondrocytes) are embedded within an ECM composed by a network of collagen fibers and

proteoglycans aggregates and some glycoproteins in abundant water [27]. The biomechanical properties of the articular cartilage (hyaline) depend on its ECM. Approximately 15% of the wet weight of the hyaline cartilage is collagen fibers, mostly collagen type II. These fibers form a 3-dimensional fibrillar network of rope-like molecular aggregates which are arranged depending on the depth of the zone within the cartilage (Fig. 1-10). These collagen fibers stabilize the network of proteoglycans aggregates (macromolecules of glycosaminoglycans polymers, mainly chondroitin sulfate and keratin sulfate) that branch from central protein cores that themselves branch from even larger glycosaminoglycans, hyaluronic acid (Fig. 1-10) [26].

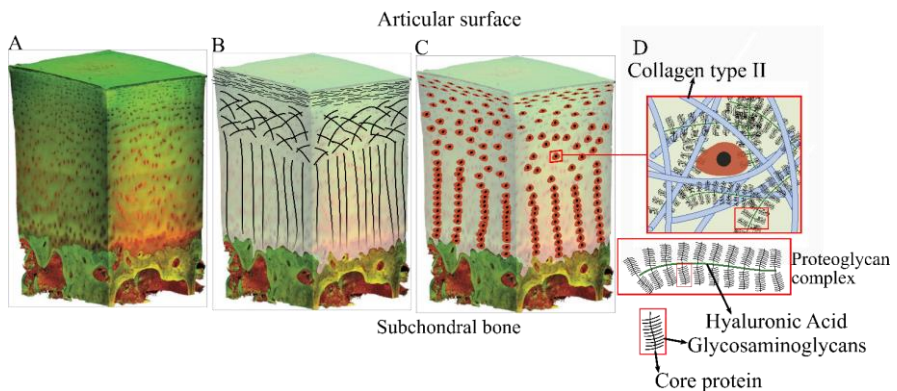


Fig. 1-10 3D schematic representation of the hyaline (articular) cartilage.

A: hyaline cartilage from the anterior region of the lateral femoral condyle of a young adult human female. The changes in size and spatial distribution of the chondrocytes through the cartilage can be appreciated in this 3-D digital volumetric fluorescence imaging of serially sectioned, eosin-Y and acridine orange-stained tissue, which was modified from (28). **B:** collagen fibers orientation through the depth of the hyaline cartilage are perpendicular to the subchondral bone in the deep zone and tangentially oriented on the articular surface. **C:** chondrocytes distribution within the articular cartilage. **D:** macromolecular composition of the extracellular matrix of the articular cartilage.

The hyaline cartilage is maintained by the chondrocytes, which are in charge of the production of the ECM material, so they oversee the growth and repair of cartilage tissue. Moreover, the volume of the chondrocytes in cartilage is less than 10% of the total cartilage volume, and this percentage reduces with age [27].

1.2.4. CARTILAGE DISEASES

There are more than 100 pathologies of synovial joints, specifically for the articular cartilage. What is more discouraging is that all these pathologies do not share common pathways, and furthermore, some of them are still not fully understood [26]. Nevertheless, each arthritic disease usually targets a group of joints so it can be related to a joint function or articular structure. Among all the pathologies the most common diseases are OA, rheumatoid arthritis (RA) and gout [26].

OA is a degenerative joint disease caused by the wearing and degeneration of the hyaline cartilage due to multiple injuries to the joint surface, aging, repeated trauma, surgery, obesity, and hormonal disorders. This degeneration might cause the eventual loss of a portion of the articular cartilage or the entire joint surface, which is worsened by the poor ability of self-regeneration of the hyaline cartilage. In fact, sometimes this cartilage degeneration causes that bones rub against each other, generating pain [27]. Then, the bones thicken and form bony spurs which can break off into the joint irritating soft tissues, producing joint stiffness. Moreover, the synovial capsule becomes inflamed causing more pain and, due to the inflammation, it generates cytokines

and enzymes that may damage the cartilage even more. Usually, the cartilage tends to remodel itself through the replacement of worn cartilage by a tougher tissue (fibrous cartilage), generating an uneven articular surface, which can also cause pain and joint stiffness [26].

OA progresses through four stages [28]. In Grade I, the surface and subsurface damage is minor, only small fissures and pits at points of high stress of the joint. In Grade II, more damage can be seen at the surface of the cartilage, however, still confined at the areas of high stress. In Grade III, there is a complete loss of cartilage at the zones of high stress, and probably there are formations of bony spurs. At this stage is when the patient starts to feel pain. In Grade IV large areas of bone might be exposed and the articular surface becomes irregular.

Currently, OA cannot be fully healed. However, when diagnosed on the first stages, a modification in the lifestyle (weight loss, nutritional supplements, physical therapy, and other strategies) can reduce the disease advance velocity and relieve pain. The problem is that it is difficult to diagnose OA at an early stage because the joint pain and stiffness usually appear in the later stages (Grade III and IV), when can be too late. When nothing else works, surgery (joint replacement) is the last approach for treating OA. Total joint replacement (TJR) or arthroplasty is a surgical procedure that removes affected parts (both articular surfaces) of the joint and replaces them with an artificial equivalent. In the partial joint replacement, only one of the articular surfaces is replaced with a replica.

On the other hand, RA is an autoimmune disorder in which the immune system attacks, mistakenly, the healthy synovium.

Consequently, the production of synovial fluid is retarded and therefore there is an inflammation of the joint cavity and neighbor tissue, which eventually may contribute to damage joint tissue, including the cartilage. The common symptoms, which can come and go, include chronic pain, and joint stiffness and swelling. In contrast to OA, RA affects small joints symmetrically.

Gout is a metabolism disorder in which final metabolite, uric acid, crystallizes and precipitates in the synovial joint and neighbor tissues. The high concentration of uric acid within the joint increases the inflammatory response of the immune system. Among the symptoms of gout are included a red, tender and swollen joint with pain.

1.2.5.SUBCHONDRAL BONE

The subchondral bone is the layer of bone just under the cartilage; chondral refers to cartilage, while the prefix sub means beneath. The subchondral bone remains connected to the articular cartilage through the calcified cartilage and varies its architecture and physiology by region [29]. The subchondral bone is composed by two layers, the subchondral bone plate, under the calcified cartilage, and the subchondral trabecular bone, which is closer to the medullary cavity [29,30]. The subchondral bone plate has similar characteristics of the compact (cortical) bone and its thickness ranges from $10\mu m$ to $3mm$ [29,30]. The subchondral bone is formed via endochondral ossification of the of the cartilaginous structure on the epiphyses of the bone [30]. The function of the subchondral bone is that of shock absorber by attenuating forces generated by locomotion. The compact subchondral

bone plate provides support, and the subchondral trabecular component provides elasticity for shock absorption [29].

The subchondral bone matrix is a biphasic material which includes organic and inorganic matrices. Up to 88% of the organic matrix is collagen type I, the other 12% is made of the dry weight of osteocalcin, osteonectin, phosphoproteins, lipids and proteoglycans [30]. The inorganic component of the subchondral bone is mainly hydroxyapatite crystals, which supply rigidity [29]. This unique composition of the subchondral bone is designed to help with the dispersion of loads across the joint [29].

The subchondral trabecular bone and the inner side of the subchondral bone plate are covered by osteoblasts and osteoclasts which allows the subchondral bone to adapt its morphology in response to stresses. This adaptation follows Wolff's Law, which states that bone will adapt in response to the loading under which it is subjected [29,31]. The osteoblasts and osteoclasts facilitate the adaptive response through apposition and resorption activities, respectively [29].

The rich vascularization and innervation of subchondral bone facilitates the local response to both physiologic and pathologic events [29]. Physiologically, the subchondral trabecular bone might provide an additional source of cartilage nutrition in addition to the synovial fluid [30]. On the other hand, the bone marrow of the subchondral trabecular bone maintains a heterogenous population of multi-potent mesenchymal cells which provide progenitor cells for differentiation of osteochondral or any other cell lineage [30].

The subchondral bone is also affected by the OA, although it is yet unclear if the pathological changes within the subchondral bone precede the changes in the articular cartilage, or if the subchondral bone changes are consequence of the bone adaptation that follows the alterations in the biochemical and mechanical properties of the cartilage [32]. In early stages of OA, it can be noticed an increase in thickness of the subchondral bone plate as well as of the underlying trabeculae. In later stages, the subchondral bone goes through remodeling processes, especially in areas where the overlaying articular cartilage has suffered advanced destruction [32]. In advanced stages of OA, besides the extensive bone sclerosis, the bone can also suffer necrosis, and in areas of total cartilage destruction, the synovial fluid gets access to the bone marrow inducing changes of the mesenchymal cells [32]. This leads to cartilage-nodules within the subchondral bone. These changes in the subchondral bone are responsible for the osteoarthritic joint pain [32].

1.3.FINITE ELEMENT METHOD (FEM)

In general, every phenomenon in nature can be described with the aid of physics through equations relating quantities of interest. That way, mathematics becomes an aid to understand and quantify any physical phenomena such as structural or fluid behavior, stress distribution in complex structures, thermal transport, aerodynamic loads, the concentration of molecules, pollutants and other substances, wave propagation, the growth of biological cells, weather predictions, etc. Engineers and scientists have two major tasks when studying a physical phenomenon: first, the mathematical formulation of the

physical process; and second, numerical analysis. For the development of the mathematical model of a process, some assumptions related to how the process work needs to be made. It might be possible that the formulation of the mathematical model is not that difficult; however, the solution, numerical analysis, within a domain is a gigantic task. It is here where approximate methods of analysis are valuable tools to find approximate solutions to the mathematical model of our interest.

Most processes in nature can be described by using partial differential equations (PDEs). However, to solve these equations for an arbitrary shape through classical methods is nearly impossible. Therefore, computational technics to solve large equations systems have been developed in the last decades, among which the most prominent and used is the FEM.

FEM is a numerical tool used to obtain approximated solutions of a problem, which can be interpreted as a prediction of how the process will develop under given conditions [33]. The base of FEM is: “Divide and conquer!”

In FEM, the area of study (the domain of interest) has to be divided into small finite elements, which can be just called elements, connected by nodes. That way a finite element mesh of the analyzed structure is obtained (Fig. 1-11). Thereafter, the PDEs are calculated in every single element [33]. These calculations are done through polynomial approximations, which are in fact interpolations over the element. This denotes that the exact values at specific points within the element are calculated, but not within the entire element. These specific points are the abovementioned nodes (also called nodal points), which

Conceptual Background

often are at the boundary of the element and shared with neighbor elements. All the individual elemental results are then combined to obtain the final result of the entire domain of interest.

The accuracy with which the variable is calculated depends on the type of approximation (interpolation) that is used, which can be linear, quadratic, cubic, etc. Moreover, the accuracy of the solution can also be improved if the number of elements, and therefore nodes, increases [33]. However, the computational cost can escalate a lot with the number of elements and the complexity of the considered approximations. The results are usually presented as contour plots giving information of how the variable is distributed at any given time (Fig. 1-11).

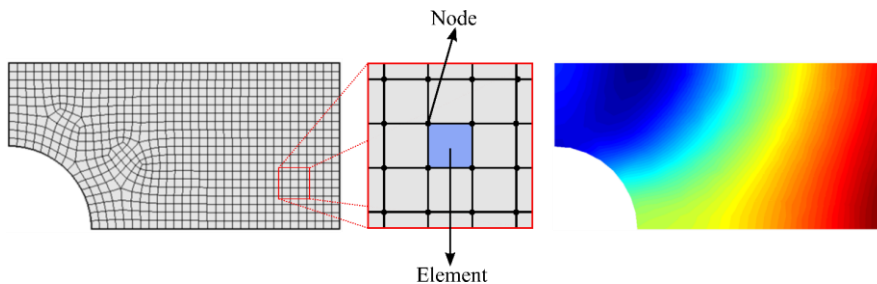


Fig. 1-11 Schematic representation of a finite element mesh.
Left: finite elements of a domain of interest. Center: Zoom of a part of the mesh where an element and surrounding nodes are specified. Right: the contour plot of the result of a variable within the domain of interest.

Chapter 2. JOINT ONSET

2.1. INTRODUCTION

As previously mentioned, the joint formation occurs in the embryonic stages of life and is critical to allow movement between bones. The appendicular skeleton formation initiates with the appearance of the limb bud, which has within it an uninterrupted and uniform condensation of mesenchymal cells (skeletal blastema) [34,35] (Fig. 2-1-A). Most blastemal cells differentiate into chondrocytes; however, some of the blastemal cells remain undifferentiated at the site of the future joint known as interzone (Fig. 2-1-B).

The definitive separation of the future bones of the joint occurs with cavitation, which creates a space between chondrocyte rudiments, that later will be occupied by synovial fluid (Fig. 2-1-C). Some studies (in rats and avian embryos) have shown that cells in the middle of the interzone display necrotic features which induce the separation of the chondrocyte rudiments [36–38]. After cleavage, joint morphogenesis occurs as cells proliferate on either side of the joint, and it takes its shape (Fig. 2-1-D) [34,39]. This shape is influenced by movements and muscle contractions that occur during limb development [21,40], as well as by local and systemic biochemical factors [34].

Experimental models, *in vivo* and *in vitro*, have explored the conditions in which abnormal environments affect the embryo development and have provided insights about the molecules that play

critical roles in joint formation [34,41–47]. In the initial stages of joint development, Wnt is expressed to maintain the mesenchymal nature of cells at the interzone [34,46,48,49]. Simultaneously, Growth Differential Factor-5 (GDF-5) is also expressed playing a pivotal role in joint development by marking the interzone site [50–52]. The GDF-5 antagonists, chordin and noggin, are expressed in chondrocytes in the developing rudiment. HOX genes may also play a role in defining boundaries and the limb patterns in development [46]. After the onset of the interzone, other molecules take lead of bone development; for instance, Indian hedgehog signaling molecule (Ihh) and Parathyroid Hormone-related Protein (PTHrP) control growth and differentiation to regulate ossification and the final shape of the bones [53].

Results from *in vivo* experiments studying joint onset conditions during embryo development are complemented by computational studies. Computational models have analyzed the effect of muscle load on the shape of the developing joint, both in 2D [20] and 3D [21]. However, these models do not describe the initial stages of joint development (interzone onset and cavitation). Moreover, computational models can also be used to understand the biochemical and molecular behavior of the biological phenomenon of development. For instance, the interactions of Ihh, PTHrP and Vascular Endothelial Growth Factor (VEGF) in endochondral ossification have been studied in 1D finite element model for the human-distal-femoral growth plate [54]. The previous model was extended to a 2D simulation of bone growth during the fetal stage and analyzed the shape in later stages [9]. These models have been expanded to simulate cartilage hypertrophy (during bone

growth) and onset of the secondary ossification center [9,55,56]. Also, Garzón-Alvarado *et al.*, presented a mathematical model of chondrocyte hypertrophy, which was able to predict the onset of secondary ossification centers of long bones, regulated by molecular factors [13].

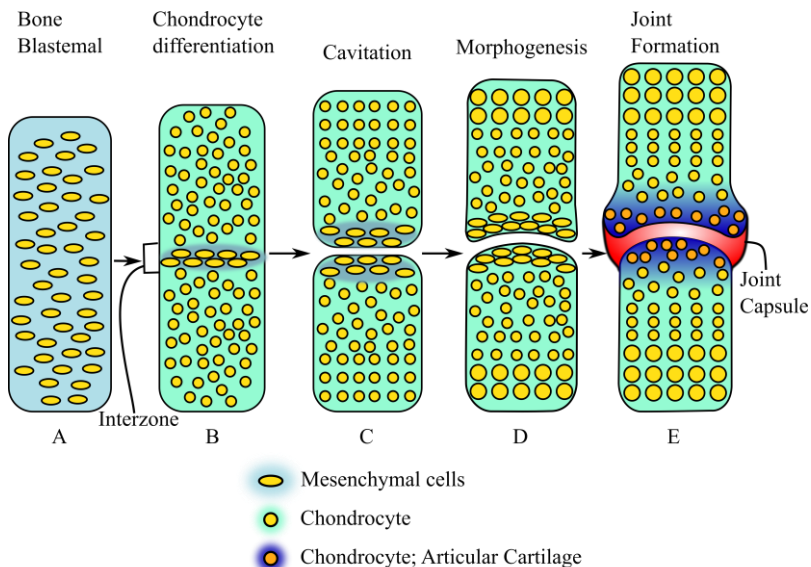


Fig. 2-1 Scheme of the stages of the synovial joints during the interphalangeal joint development. A. Blastemal cells, which are mesenchymal cells condensed in the first stages of the limb; no joint formation is observed. B. Interzone formation: it is composed by an aggrupation and condensation of mesenchymal cells. Meanwhile, the mesenchymal cells that will form (future) bones condensate and differentiate into chondrocytes cells, establishing ananlagen bones [34]. C. The cavitation process initiates, and the formation of the synovial cavity takes place. D. Morphogenetic process starts to mold the opposite surfaces of the joint, E. Finally, all joint components are developed, including articular cartilage, joint capsule and synovial cavity.

Reaction-diffusion systems are often used as models for pattern formation of a variety of structures during development [13,46,57]. Such tuned systems produce well-organized patterns called Turing patterns, which result in definitive patterns of molecule distribution

[46,57]. In an enzyme-substrate model (or *depletion model* as proposed by Turing [58]), a stable spatial pattern forms after temporal evolution [59]. The patterns of chemical gradients are influenced by the diffusion rates, the growth rates, and the bounding geometry of the system [60]. In this work, we use reaction-diffusion equations and the formation of Turing patterns to simulate the location of joint cleavage, the number of joints formed and the condylar shape of the joint.

The aim of this work was to develop a computational model based on two generic molecular actions (proliferation and growth) and two regulatory loops, expressed as reaction-diffusion equations. The aim was to predict the molecular patterns associated with the joint formation process and the way in which it influences the final shape of the joint. The model was solved in a finite elements' framework. Mathematical equations predicted patterns representing molecular mechanisms that model the structures and shapes of joint development such as interzone onset, cavitation, and condylar shape of the bones ends of the joint.

2.2. MATERIALS AND METHODS

2.2.1. BIOLOGICAL ASPECTS CONSIDERED FOR THE JOINT DEVELOPMENT MODEL

There are many biochemical factors influencing joint development [34,61–64]. Advances in experimental techniques have provided detailed information regarding geometry, processes timing, and regulatory interactions [65]. However, the joint development

process is not entirely clear in the literature. Therefore, based on what is reported, we modeled six generic molecular factors involved in joint onset; each factor may represent multiple molecules achieving the same action. The process in our model was organized into two stages; the first stage marks the interzone onset, where high concentration of a molecule (G) establish where the mesenchymal tissue will not differentiate into chondral tissue (interzone). Afterwards, those zones that differentiate into cartilage secrete (I) and (P) which establish a regulatory loop that governs cell proliferation and hypertrophy, commencing bone growth and ossification processes (second stage). Meanwhile, the domain keeps growing and other molecules, (H) and (W), regulated the joint separation and related structures.

We modeled two factors in demarcating the position of the joint: a factor (G) which is in charge of locating the cleavage position and its antagonist (N) is everywhere else. The factor (G) could represent GDF-5, which belongs to the Bone Morphogenetic Protein (BMP) family and promotes interzone tissue function, preventing the differentiation of the mesenchymal tissue into cartilage [50–52]. Its antagonist could be the BMP antagonist Noggin (N). Also, it is considered a factor regulating cellular proliferation, termed growth (H), this molecule controls the differential amount of growth in the tissue from proximal to distal. This molecule could be relate to HOX genes [62–64], or any other molecule related to bone limb bud growth. Mathematically, there is a gradient in H, which affected the growth rate by promoting the longitudinal growth of the limb and bone anlagen.

Many studies have shown that after formation of the interzone, cartilage behavior is governed by a negative feedback loop involving *Ihh* and PTHrP [66]. We introduce a factor (I) that could represent *Ihh*, which regulates chondrocyte proliferation, maturation, and hypertrophy [66–69], and a factor (P), which could represent PTHrP and inhibits chondrocyte hypertrophy [67]. Additionally, factor (W) was expressed in the interzone, inducing cell death and allowing the creation of a joint space. This factor represents Wnt/ β -catenin signaling that leads to separation of the rudiments [34,36,37,70] and is also observed in parts of the fibrous capsule and the synovial lining of the joint capsule in later stages of development [46,57].

The variables in our model represented concentrations of each mentioned molecular factor ($S_G, S_N, S_H, S_I, S_P, S_W$) and their diffusion coefficients, D_i . Variables also included the growth rates based upon the concentration S of each molecule. All these variables will feed a finite element model with Partial Differential Equation integrated with a Cellular Automaton-like system (PDE+CA-like), CA-like because it was not based on any of the traditional CA models but can be explained as one. The PDE describes the molecular diffusion and established the biochemical concentrations, which enable the CA-like part to determine whether the tissue differentiated or not. For this last part, each element started with a tissue state (mesenchymal, pre-cartilaginous, cartilaginous, interzone) and the CA-like system allowed the element to “jump” (differentiate) from one tissue state to another, according to the molecular concentration within each element. Additionally, each tissue state was associated with a cell type and cell concentration.

In general terms, our model worked as follows on each time-step: first, the PDE solver determined the concentration of each molecule throughout the domain. According to the computed concentrations and gradients, the expansion or growth of the tissue was determined. Thereafter, the CA-like system, based on the new concentration within each element determined whether the element should change its tissue state. This process loop until the stop criteria was reached.

2.2.2. TISSUE DIFFERENTIATION

In this model, we assumed that a tissue differentiation was defined through a CA-like system, regulated by the concentration of a certain molecule within each element (Eq. 2-1). The differentiation of each element (lattice), took place once the concentration of a specific molecule reached a threshold (Table 2-1), this transition was evaluated at the end of each time-step. The inner concentration of each element was computed as the average of the molecule concentration on each of its nodes (Fig. 2-2). Thus, that concentration produces local differentiation which determines the physiological structures in a generic joint. Table 2-1 shows the original tissue, the new tissue and the concentration threshold that regulated the differentiation. For instance, high concentration of (G) indicated that those elements (the tissue state within the element), will be interzone. On the other hand, a high concentration of (W), which diffused from the interzone to the anlagen at a low rate, produced a differentiation of the chondrocytes of the joint surface into articular cartilage tissue. After the tissue was assigned as

articular cartilage, it will not change its category, no matter what internal variations occurred. Hence, dedifferentiation or future stages in the ossification process was not considered in the model.

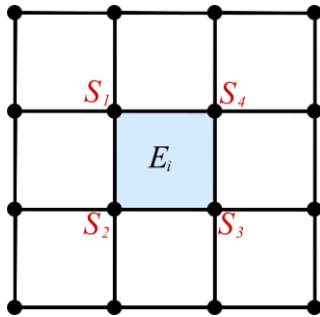


Fig. 2-2 Molecule concentration for each element.

$$\bar{S}_{E_i} = \frac{S_1 + S_2 + S_3 + S_4}{4} \geq S^{Th} \tag{Eq. 2-1}$$

For the joint capsule, the tissue on each element, externally located to the interzone and adjacent to the future bones, differentiated into fibrous tissue, in the presence of a high concentration of (W).

Table 2-1 Tissue transformation criteria.

Transformation from the original tissue to the new one regulated by a certain molecule.

Original Tissue	Molecule	New Tissue	Concentration Threshold Parameter
Mesenchyme-Bone Blastema	G	Interzone	S_G^{Th}
Mesenchyme -Bone Blastema	I	Chondrogenic	S_I^{Th}
Chondrogenic	W	Articular Cartilage	$1S_W^{Th}$
Mesenchyme	W	Joint Capsule	$2S_W^{Th}$

2.2.3. MATHEMATICAL MODEL FOR JOINT FORMATION

In our model we had two Turing reaction-diffusion systems, both of them following an enzyme (S_u)-substrate (S_v) model (Fig. 2-3):

1) between the protein that marks the onset of the interzone (G) and its antagonist (N); and 2) between (P), which at low concentrations allow chondrocyte hypertrophy and its antagonist (I).

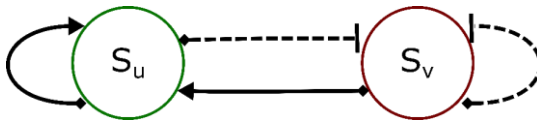


Fig. 2-3 Relationship between enzyme (u) and substrate (v) for the Schnakenberg model (enzyme-substrate). The continuous line shows activation; the dashed line, inhibition.

In order to represent the differential equations, we use the suffix u and v to represent the enzyme molecule and the substrate, respectively, for each loop (G-N and I-P). The regulatory reaction diffusion loop between the molecules was modeled as follows (Eq. 2-2):

$$\frac{\partial S_u}{\partial t} + \nabla \cdot (S_u \mathbf{v}) = D_u \nabla^2 S_u + f(S_u, S_v) \tag{a}$$

$$\frac{\partial S_v}{\partial t} + \nabla \cdot (S_v \mathbf{v}) = D_v \nabla^2 S_v + g(S_u, S_v) \tag{b} \quad \text{Eq. 2-2}$$

where S_u and S_v are the concentrations of the interacting molecules; \mathbf{v} is the tissue growth velocity (defined as the growth velocity of each point of the tissue induced by the local growth rate, see section 2.2.4), D_u and D_v are the diffusion coefficients for each molecule; and $f(S_u, S_v)$ and $g(S_u, S_v)$ are the reaction functions between the two molecules. These functions can be developed following a generic reaction mechanism known as Schnakenberg equation, which have been used before in the modeling of development

process and can produce several patterns similar to those found in nature [9,71–73] (Eq. 2-3 and Eq. 2-4):

$$f(S_u, S_v) = \gamma C_{cell}(a - S_u + S_u^2 S_v) \quad \text{Eq. 2-3}$$

$$g(S_u, S_v) = \gamma C_{cell}(b - S_u^2 S_v) \quad \text{Eq. 2-4}$$

where γ is a factor that takes into account the expression rate of each molecule; C_{cell} is the concentration of cells that express molecules. In our model, mesenchymal cells (C_M), which are associated with mesenchymal tissue, express the factors G and N, and pre-cartilage cells (C_C) which are associated with cartilage tissue, express factor I and P. C_{cell} had a value of one or zero, depending on the cell type, therefore this term acted as switch depending on the tissue type; for instance, ($C_C = 0$) if the tissue was mesenchymal, and ($C_C = 1$) if the tissue was pre-cartilage, whereas ($C_M = 0$) if the cells are pre-cartilaginous, and ($C_M = 1$) if the cells are mesenchymal. The constants a and b are source terms of each molecule involved in the loop. These equations establish a nonlinear interaction between the molecules u and v : in presence of v , u is upregulated, while in presence of u , v is downregulated [46,57] (Fig. 2-3). The reaction term interacts with the diffusion and produces patterns that emerge when certain requirements are fulfilled. Turing considered an interacting system which steady state would be driven unstable by diffusion [46,57]. Each reaction-diffusion system, in order to guarantee the Turing instability to occur, should satisfy the following statements (Eq. 2-5, Eq. 2-6 and Eq. 2-7). The conditions for instability could give us information about the presence (or not) of the Turing patterns [74]:

$$\frac{\partial f}{\partial S_u} + \frac{\partial g}{\partial S_v} < 0 \quad \text{Eq. 2-5}$$

$$\frac{\partial f}{\partial S_u} \cdot \frac{\partial g}{\partial S_v} - \frac{\partial f}{\partial S_v} \cdot \frac{\partial g}{\partial S_u} > 0 \quad \text{Eq. 2-6}$$

$$D_u \frac{\partial g}{\partial S_v} + D_v \frac{\partial f}{\partial S_u} > 2\sqrt{D_u D_v} \sqrt{\frac{\partial f}{\partial S_u} \cdot \frac{\partial g}{\partial S_v} - \frac{\partial f}{\partial S_v} \cdot \frac{\partial g}{\partial S_u}} > 0 \quad \text{Eq. 2-7}$$

where all the functions are evaluated in the homogeneous steady state solution (S_u^*, S_v^*) , which is given by $f(S_u^*, S_v^*) = 0$ and $g(S_u^*, S_v^*) = 0$. If the parameters of Eq. 2-3 and Eq. 2-4 satisfy the inequalities Eq. 2-5, Eq. 2-6 and Eq. 2-7, then they are in the Turing space. The inequalities Eq. 2-5 and Eq. 2-6 should be accomplished to assure the stability of the temporal evolution (when the concentration of the molecules reaches a stable value that would no change in time). The inequality Eq. 2-7, is necessary to reach the spatial instability of Turing (Pattern formation).

In order to develop the model, we adopted a few simplifications. First, since initial molecular distributions are unknown, we assumed all molecules (G), (N), (I), and (P), were distributed around the steady-state concentrations, (G) and (N) before the interzone onset, and (P) and (I) right after the onset of the interzone (at the second stage). The steady-state is obtained when there are no temporal changes in absence of diffusion, which means that equations Eq. 2-3 and Eq. 2-4 are both equal to zero $f(S_u^*, S_v^*) = 0$ and $g(S_u^*, S_v^*) = 0$.

After the formation of the interzone, on the second stage of the process, the cells within it will release a molecule (W) which leads to

separation of the rudiments (cleavage) and cavitation. Subsequently, the development of the surface cartilage and other joint structures begin. The concentration W was dependent on the concentration of the molecule (G) and modeled as follows (Eq. 2-8):

$$\frac{\partial S_W}{\partial t} + \nabla \cdot (S_W \mathbf{v}) = D_W \nabla^2 S_W + p(S_W) \quad \text{Eq. 2-8}$$

where S_W is the concentration of (W); \mathbf{v} is the tissue growth velocity (defined as growth velocity of each point of the tissue induced by the local growth rate, see section 2.2.4), D_W is the diffusion coefficient for the (W) molecule; and $p(S_W)$ was the function that determines whether the concentration of (W) should be activated or not depending on the concentration of (G). In this case, we have used (Eq. 2-9):

$$p(S_W) = \vartheta C_{INT} \quad \text{Eq. 2-9}$$

where ϑ is a constant that has considered the expression rate of W by the interzone cells, the latter given by the concentration of cells as C_{INT} , this term would take the value of one if the tissue is interzone and zero otherwise.

We considered that differential growth factor (H) was always present in the simulation of the joint formation and that together with (I), promotes anlage growth. The concentration equation for (H) was modeled using the equation given by Eq. 2-10:

$$\frac{\partial S_H}{\partial t} + \nabla \cdot (S_H \mathbf{v}) = D_H \nabla^2 S_H \quad \text{Eq. 2-10}$$

2.2.4. GROWING OF THE TISSUE (DOMAIN GROWTH)

Proliferation and growth is not uniform within the tissues [65]. The tissue growth rate depends on how each cell detects the concentrations and gradients of molecules around; (I), (P), and (H) in this case. The concentration of the molecules promotes isotropic growth; whereas, the gradient of molecules influences the direction of the growth [75]. In a general form (Eq. 2-11):

$$\mathbf{d}^{growth} = \underbrace{\left(\alpha_i \frac{\partial S_I}{\partial x_j} \mathbf{e}_i \otimes \mathbf{e}_j + \beta_i \frac{\partial S_P}{\partial x_j} \mathbf{e}_i \otimes \mathbf{e}_j + \mu_i \frac{\partial S_H}{\partial x_j} \mathbf{e}_i \otimes \mathbf{e}_j \right)}_{\text{Growth on the direction of the concentration gradient}} + \underbrace{\left(\alpha_{iso} S_I \delta_{ij} \mathbf{e}_i \otimes \mathbf{e}_j + \beta_{iso} S_P \delta_{ij} \mathbf{e}_i \otimes \mathbf{e}_j + \mu_{iso} S_H \delta_{ij} \mathbf{e}_i \otimes \mathbf{e}_j \right)}_{\text{Isometric (volumetric) growth due to the concentration of each molecule}} \quad \text{Eq. 2-11}$$

where \mathbf{d}^{growth} is the strain tensor of the growth rate; S_I, S_P and S_H are the concentrations of the molecules (I), (P), and (H) respectively; α_i, β_i, μ_i are constants which determine how much the gradient of the concentration of each molecule influences on the directional growth; and $\alpha_{iso}, \beta_{iso},$ and μ_{iso} are constants that indicate the influence of the concentration of each molecule on the isometric growth; \mathbf{e}_k are the unitary directional vector in a Cartesian coordinate system; $\frac{\partial S_r}{\partial x_k}$ is the partial derivate in the k th direction of the r th molecule concentration; δ_{ij} is the Delta-Kronecker tensor; and i, j take values of 1 or 2 (x-direction an y-direction). Also, the following statement should be

satisfied so that the growth is only in the direction of the molecular gradients (Eq. 2-12):

$$\theta_i \frac{\partial S_K}{\partial x_j} = \begin{cases} \theta_i \frac{\partial S_K}{\partial x_i} & \text{if } i = j \\ 0 & \text{Other case} \end{cases} \quad \text{Eq. 2-12}$$

with $\theta_i = \alpha_i, \beta_i, \mu_i$; $S_K = S_I, S_P, S_H$ which are the concentrations of the molecules (I), (P), and (H) respectively.

In the growth equation, the concentration of each molecule has a volumetric effect due to an increase in cell quantity, without increasing cell concentration [cell/unit volume] [46,57]. A molecular gradient increases cell quantity in the direction of the gradient, without increasing the cell concentration; which means that there is cell proliferation in the direction of gradient. The parameters of the equations are listed in Appendix A.

From the deformation and growth given by Eq. 2-11 the growth velocity on each point of the domain can be calculated. The relation between this velocity and the growth tensor is given by Eq. 2-13 [76].

$$tr(\mathbf{d}^{growth}) = \nabla \cdot \mathbf{v} \quad \text{Eq. 2-13}$$

2.2.5. NUMERICAL SOLUTION OF PDES.

PDES were solved with FEM and implemented in a user Subroutine in Fortran and solved with ABAQUS 6.10 (Dassault Systèmes USA, Waltham, MA). Both mesh and time-step were refined until further refinement, no longer yielded noticeable improvements. The system was solved employing a Lagrangian actualized method, so

that for each instant of time the mesh and the domain moved as consequence of the growth.

2.2.6. GEOMETRY, INITIAL AND BOUNDARY CONDITIONS, AND SIMULATED CASES

In order to evaluate the feasibility and versatility of this computational model, we considered six cases. Every case had different conditions either in geometry or slight changes in one or more of the equation constants, such as growth rate (Appendix A). For the geometric domain, we considered that the process started with a condensation of mesenchymal cells and a random distribution of factors (G) and (N). A detailed description of the employed boundary conditions for most of the analyzed cases are shown (Fig. 2-4).

As we do not know the exact initial condition, we have used a random spatial distribution with fluctuations around the fixed point (10 % of the homogeneous steady state) for (G) and (N) (S_G^* , S_N^*), and (P), and (I) (S_p^* , S_i^*) systems. The fixed point was found by setting equations (Eq. 2-3) and (Eq. 2-4) to zero, so there were no temporal changes in absence of diffusion ($f(S_u^*, S_v^*) = 0$ and $g(S_u^*, S_v^*) = 0$). As for (W) and (H), we used a zero-initial condition in the entire domain.

For all stages of the simulation, the flux was null at the boundary (no molecules entering or leaving) (Fig. 2-4). The (H) molecule had high concentration ($S_H = 1.0$) in the proximal side and low concentration ($S_H = 0.0$) in the distal part (Fig. 2-4), which resulted in an increased growth at the proximal part compared to the distal end.

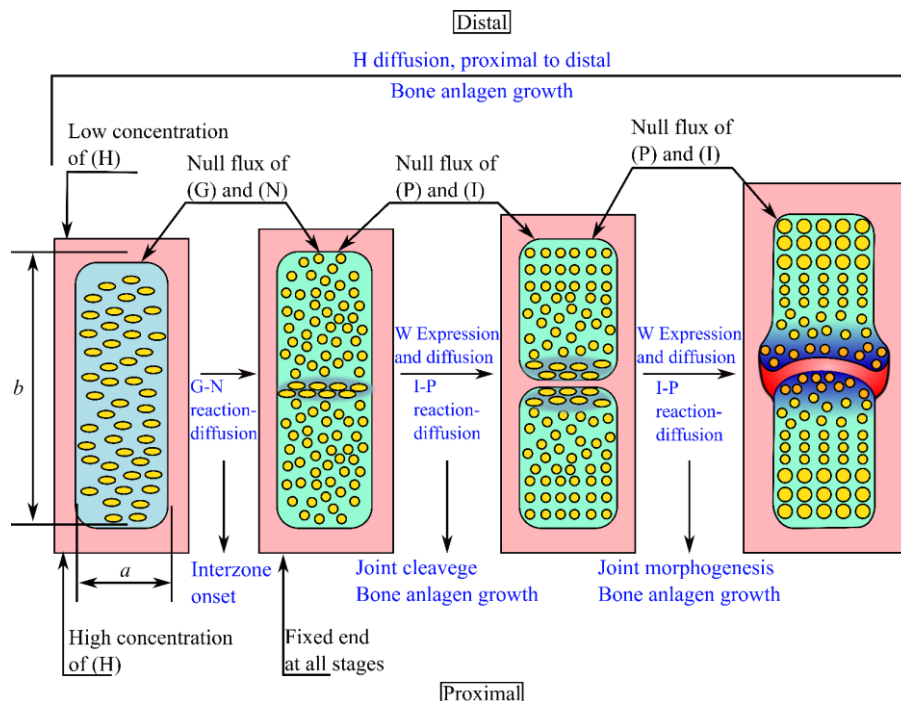


Fig. 2-4 Schematic of the boundary conditions employed for the joint onset model. The entire domain was fixed in the lower contour to solve the growth equations. The flux of all the molecules was null on the outer boundary. The molecule (H) diffused through the entire domain and had a high concentration on the proximal part, in contrast with a low concentration on the distal one. On their part, (P) and (I) only diffused inside of each bone anlagen, after the onset of the interzone and each set of equations were solved for each of these areas. Finally, (W) diffuses outside the bone anlagen after the onset of the interzone.

We explored four cases. In the first one we create the conditions for the development of an interphalangeal joint. The following three cases are modifications of the first one, where we tested how changing the dimensions of the initial domain affects the joint development (*cases II* and *IV*); also, how the growth rates of the domain modified the final outcome (*case IV*). On the other hand, we replicated an experimental procedure [77], where beads of GDF-5 were implanted on the side and tip of a developing chick autopod.

2.3. RESULTS

2.3.1. CASE I: INTERPHALANGEAL JOINT DEVELOPMENT

In the *case I*, the limb bud had a length/width ratio of 3, based on histology of the phalange anlage [78]. In the first stage (G-N reaction-diffusion), we obtained the spatial distributions of (G) and (N) over time, that indicated the formation of a stable Turing pattern (Fig. 2-5). The region where (G) was high indicated the interzone onset (shown with an ‘*’) and location for cavitation.

In the second stage (P-I reaction), (P) accumulated in the distal part of the bones, where it kept the proliferative state of the chondrocyte cells (Fig. 2-5). (I) was inhibited when there was a high concentration of (P), and in the zones of high (I) the hypertrophy was accelerated. Also, the growth of the tissue was influenced by the concentration and gradient of the molecules (I), (P), and (H) according to the equation (Eq. 2-11). In regions with a high concentration of (I) and low concentration of (P), which caused hypertrophy of the cells, an epiphysis-like structure was obtained, wider than the rest of the bone (Fig. 2-5). After the onset of the interzone, (W) started diffusing. (W) was expressed in the interzone and where the fibrous capsule and the synovial lining of the joint capsule will form (Fig. 2-5). Thus, we obtained a hinge-like joint structure, which was similar in shape to an interphalangeal joint. The distal bone had a wider proximal end and the proximal one was uniform in width (Fig. 2-5).

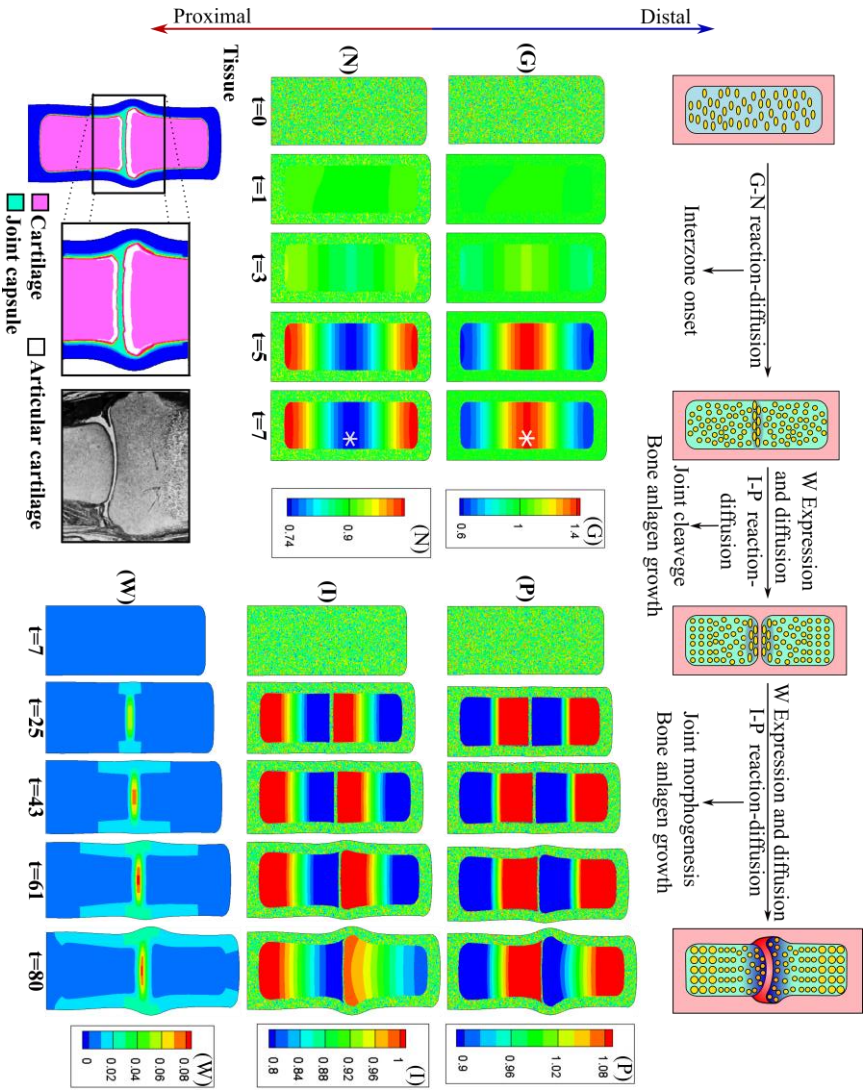


Fig. 2-5 Results obtained by the simulation for case I.

Distribution of the factors (G), (N), (P), (D), and (W) over time and the final tissue. High concentration of (G) marks the interzone, which occurs on early stages of the joint development (time unit=7). The molecule (D) is concentrated in the lower part of the bone molds, whereas (P) is in the opposite regions. The molecule (W) starts acting after (G) reaches higher concentration in the interzone, marking the separation of the two bones and the differentiation of cells into diverse joint structures. Additionally, in the bottom left the formation of the joint structures can be seen, such as the articular cartilage and the joint capsule. This result is compared with a histological image of an interphalangeal joint, which is modified from [79].

2.3.2. CASE II: LONGER INITIAL BUD

We considered the case of a longer limb bud with length/width ratio of 5 (Fig. 2-4). As the domain was longer, the Turing pattern formed 3 high concentration regions of (G). One in the proximal tip and the other two spaced along the domain (Fig. 2-6). Therefore, the model was able to predict the formation of 3 joint surfaces, similar to a finger with three phalanges.

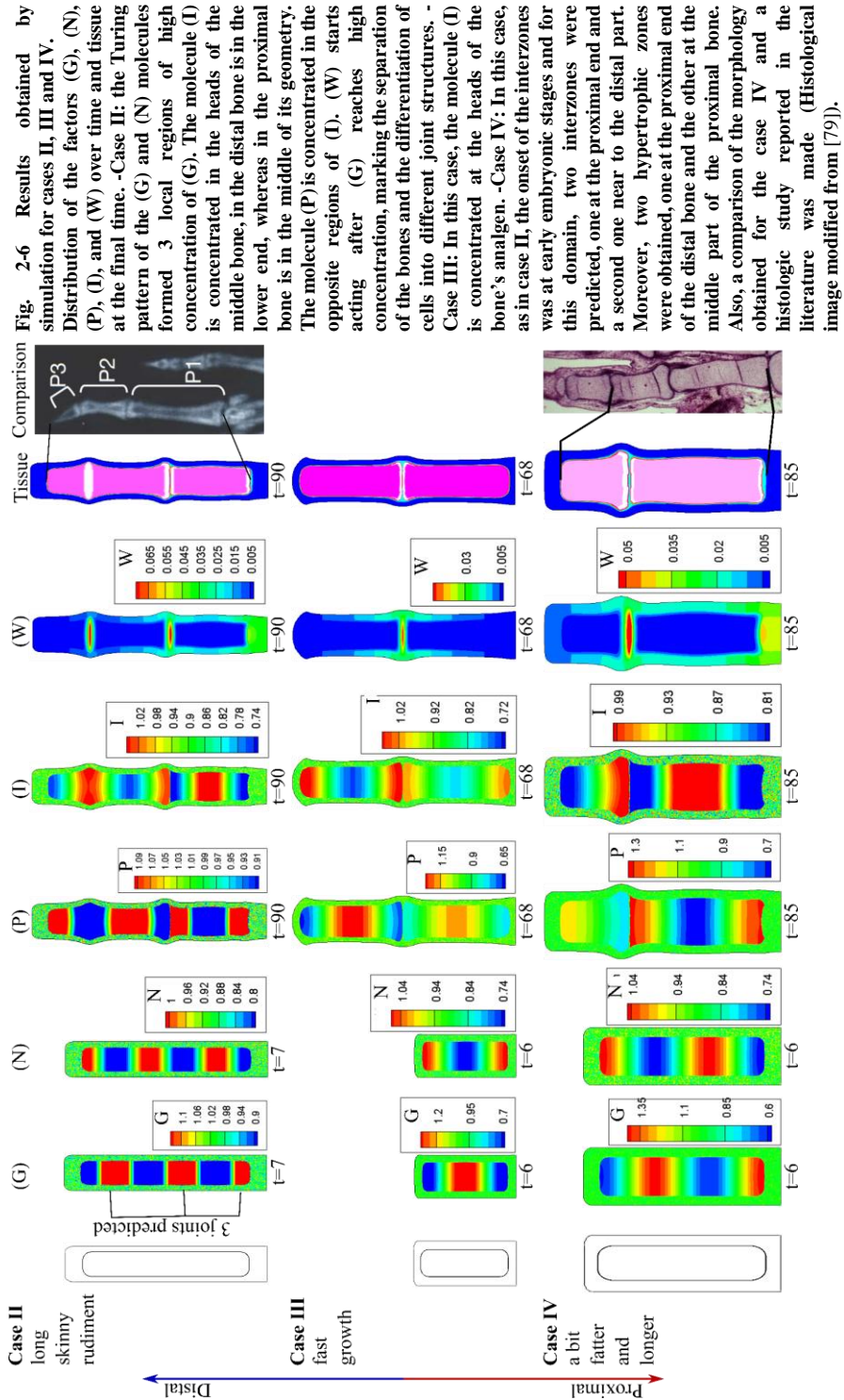
In the second stage, we obtained that (P) had high concentration at different areas on each bone. For instance, in the distal bone the concentration of (P) was high on the distal end; for the middle bone, the concentration of (P) was high in the middle part; and for the proximal bone, (P) had high concentration on both ends (Fig. 2-6). (I) had the opposite distribution of (P) (Fig. 2-6) hence, the distal bone had one large epiphysis (the proximal tip), the middle bone had both ends as large epiphyses, and the proximal bone had almost uniform width. The pattern, on the proximal bone, was characteristic of long bones [53], where a hypertrophic (Ihh) molecule was on the middle of the bone and its antagonist (PTHrP) were on the tips of the bone [9]. Regarding (W), it was expressed after the onset of the interzone. Both, the fibrous capsule and the synovial lining of the joint capsule, formed as in *case I*. However, we observed (W) in three locations (in the bottom, the middle and near the top) (Fig. 2-6 *case II*).

2.3.3. CASE III: HIGH GROWTH RATE

In *Case III*, the growth rates (expressed as α_i, β_i, μ_i) were greater than in other cases. As a result, an accelerated growth of the segments was produced. As in *Case I*, a single joint was predicted. However, since the growth velocity was greater, the final rudiments were much larger compared to the case I (Fig. 2-5 and Fig. 2-6). Additionally, the distributions of (P) and (I) that were obtained were different than *case I*; in this case, molecule (I) had high concentrations on both ends of the rudiments, whereas for *Case I* only on one end of the rudiments. This indicates that growth rate may determine whether the rudiment will have an epiphysis on one end or at both ends.

2.3.4. CASE IV: WIDER RUDIMENT

For this case, we considered a length/width ratio of 2.5 and obtained a joint between a large bone and a shorter one. Furthermore, two joint regions were obtained, one in the proximal end and a second one close to the distal end (Fig. 2-6). The distal bone had a high concentration of (I) at the proximal end. As a result, the cells on this zone would hypertrophy and the proximal head of the distal bone would have volumetric expansion, similar to *Case I*. Even though, the proximal bone was larger, its molecular patterns of (P) and (I) are similar to those seen clinically on a long bone [53], where PTHrP had a high concentration in the ends of the bone and Ihh was high close to the mineralization zone (in the hypertrophic zone of the growth plate).



2.3.5. CASE V: IMPLANTATION OF BEADS BEARING GDF-5 (LATERAL)

For this case, we considered that the length/width ratio was 3, as in *Case I*. A bead of GDF-5 (Concentration $S_G = 1.5$) was placed in the distal and lateral part of the rudiment to simulate the experimental scenario according to [77], where a GDF-5 bead was placed on the side of a developing chick autopod.

On this model, the (I) molecule started to accumulate near the zone of the bead of GDF-5 and then it formed an intercalated stripe-like pattern. (P) was inhibited when there is a high concentration of (I); the latter promoted cell hypertrophy, making the tissue to grow at a greater rate than the surrounding area (Fig. 2-7). Moreover, the diffusion of the (W) molecule was expressed in the zone where the (G) molecule was seeded. Therefore, the shape of the future bone was affected, due to the modified molecular pattern which altered bone growth. Also, no joint was formed inside the domain as consequence of the abnormal growth and molecular patterns, matching the experimental results.

2.3.6. CASE VI: IMPLANTATION OF BEADS BEARING GDF-5 (TIP)

A seed of high concentration of GDF-5 (concentration, $S_G = 1.5$) was planted on the tip of the phalanx as it was previously reported [77]. Since there was a high concentration of (G) on the tip of the rudiment, the (G-N) patterns were disturbed and no interzone was formed, therefore there was an absence of joint.

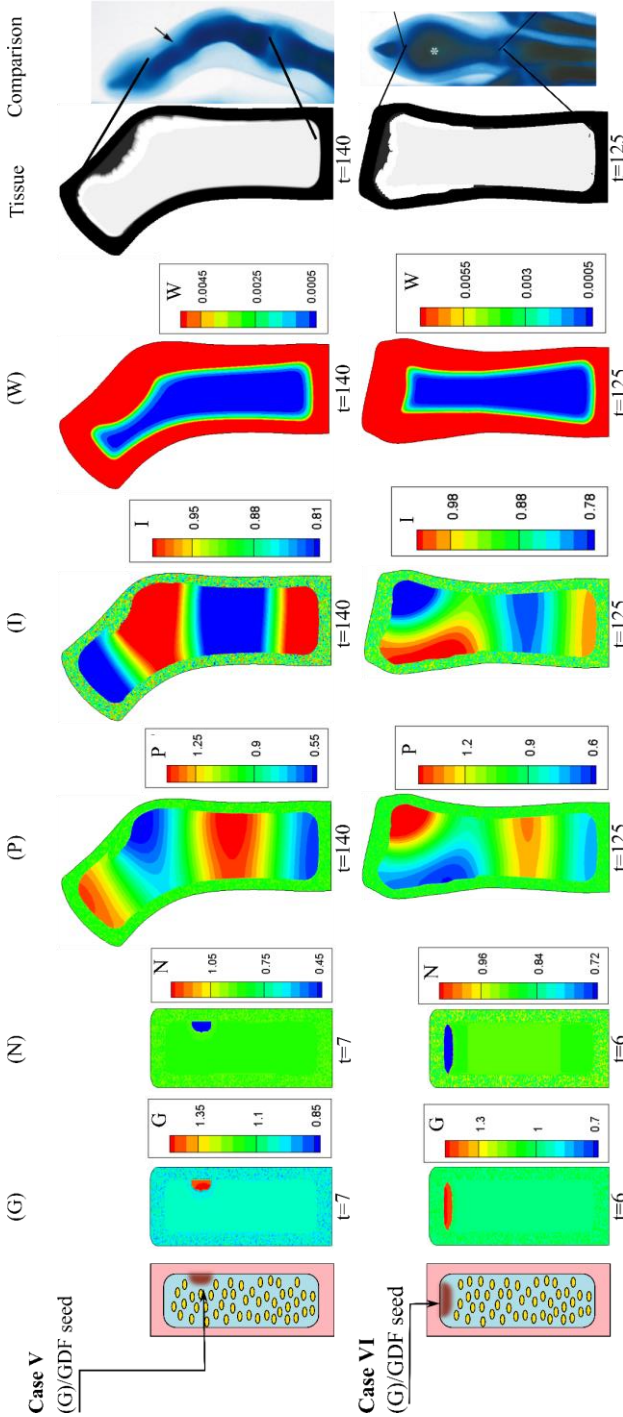


Fig. 2-7 Results obtained by simulation for cases V and VI.

A high concentration of (G) was obtained where the seed was implanted, and almost null in other parts of the domain. Molecules (P) and (I) distribute in a stripe-like way and as a result a deformed bone was obtained. The molecule (W), at the beginning, was only located where the seed bearing was placed, then it diffused on the contour of the bone mold, contributing to the abnormal growth of the bone. Additionally, a comparison of the morphology between the bone obtained with the simulation, and the one reported by Merino *et al.* [77] was made. For the Case V the right figure shows of the autopod following the implantation of a GDF bead in the third interdigit at stage 28 (modified from [77]). The digit started curving due to the absence of the interphalangeal (arrow) and can be detailed that this finger only had three phalanges instead of five. The arrow shows a zone of incomplete joint formation. On our case VI, where the molecule (G) related with GDF-5, was implanted on one side of the mesenchymal condensation, no joint formed and the finger also curved. For the Case VI, the right image shows the morphology of the autopod after implantation of a GDF-5 bead (*) at the tip of digit 28 (modified from [77]). Our results for this Case VI, also show the final bulb-like shaped bone and again, no joint was formed, which agrees with previous literature reports [77].

The (P) molecule started to accumulate in the center of the bone anlage and then became more concentrated in the extreme where the seed was planted. However, its distribution was shapeless (Fig. 2-7). As in the previous case, there was a high accumulation of (W) where the (G) seed was planted.

2.4. DISCUSSION

Previous works have shown the molecule interactions for the digit patterning onset. On the work of Raspopovic *et al.* [80], they propose that the digit patterning is controlled by a BMP-Sox9-Wnt Turing network, which is also controlled by two morphogens (Hox genes and Fibroblast Growth Factor (FGF) signaling)[80]. Wnt concentration is high in the interdigital zone, which repress the chondrogenesis and the expression of Sox9, limited to the digits, whereas BMP, is out of phase with Sox9, and it is also found on the digits [80]. Hox gens are in charge of limiting the Turing instability in the interdigital region, then the digit patterning is independent from the rest of the skeleton. Finally, FGF, which have not shown a periodic pattern but only a proximo-distal gradient, being highest in the apical ectodermal ridge (AER), controls the wavelength and prevent bifurcations [80].

In this study, we have developed a reaction-diffusion model to simulate the biochemical system that regulates joint formation, starting from the last stage analyzed by Raspopovic *et al.* [80], right after the digit patterning. We assumed that inside the phalanges anlagen is an enzyme substrate process between the proteins (N) and (G), a BMP

molecule which determines where joint cleavage occurs. This first loop of proteins is essential to the formation of the interzone. (G) demarks the interzone and (N) establishes a regulatory loop to avoid other zones from reaching this condition. After cleavage, a negative feedback loop of proteins (P) and (I) determine where cartilage hypertrophy occurs. (I) establishes the growth of the articular and hyaline cartilage. In those areas, where the level of (P) is low, the potential zones for hypertrophy and mineralization are established. All these four molecules had a random initial condition. A gradient in molecule (H) was represented from proximal to distal, during the entire simulation, which was in charge of increasing domain length. Finally, molecule (W) diffused from the interzone joint cells to promote the differentiation from mesenchymal to capsule tissue.

We analyzed six different cases, which showed slight differences between them, either in geometry or in growth rates. For *Case I* we can compare the results obtained for the molecule (G) with expression of GDF-5 obtained through histological studies, to demonstrate similar distributions (Fig. 2-8). Additionally, the (I) and (P) loop resulted in a distribution where (P) is near the distal ends and (I) is at the proximal ends of the rudiment, as seen histologically for Ihh and PTHrP (Fig. 2-8).

The (W) molecule established the formation of the articular cartilage on each joint surface and was consistent with distribution of Wnt in the literature (Fig. 2-8) [81,82]. When we evaluated morphology changes in the joint (Fig. 2-5), we observed that the shape of the joint is comparable with the histologic findings [79]; both sides of the joint

had articular cartilage, however, on one side there was a epiphysis-like structure, due to the chondrocyte hypertrophy caused by the low concentration of (P). This led to the formation of a larger epiphysis-like on the distal side, and a not so wide on the proximal end. From this point on, the morphology of the joint is likely influenced by mechanical conditions [81].

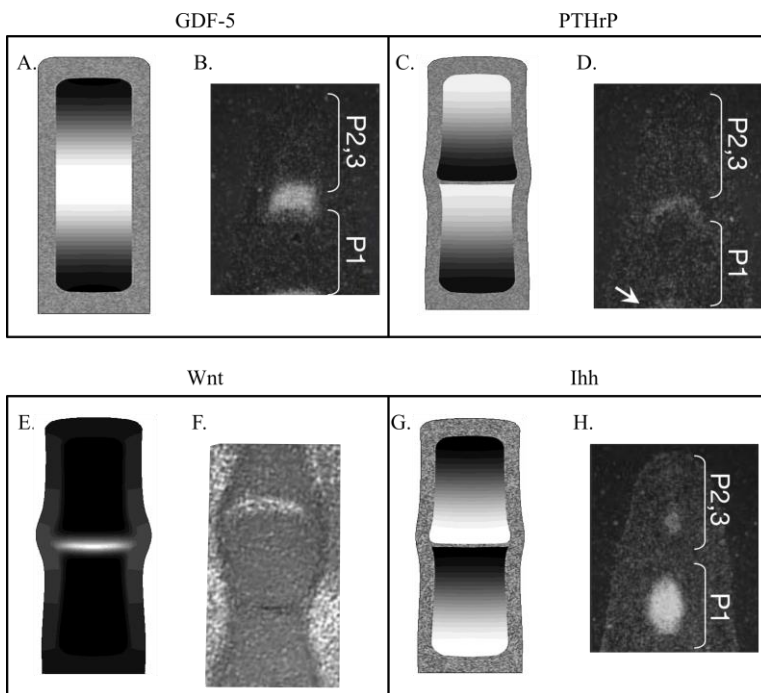


Fig. 2-8 Comparison of the molecular distribution between the obtained results for case I with those reported in former experimental studies.

A. Obtained result for the concentration of GDF-5 during the process of interzone onset; **B.** GDF-5 expression in the digit formation at E13.5, modified from [81]; **C.** Obtained result for the concentration of PTHrP during the process of joint formation; **D.** PTHrP expression in the digit formation at E13.5, modified from [81]; **E.** Obtained result for the concentration of Wnt during the process joint morphogenesis; Wnt expression in the digit regions of the foot at day 7.5; **F.** Modified from [82]; **G.** Obtained result for the concentration of Ihh during the process of joint formation; **H.** Ihh expression in the digit formation at E13.5, modified from [81]. High concentrations are showed in white.

Our results suggest that the size of the initial domain during development may have an influence on the number of joints formed. When the length/width ratio was 3, one joint was obtained, but when this ratio was increased to 5, three joints were acquired in the simulation. This result is related to the fact that Turing patterns depend on the domain ratio, therefore the number of joints will be subject to the initial ratio. However, literature show that one joint form at a time [83,84], therefore, it could be possible that each time that the distal blastema reach a ratio of 3 (approx.), a joint is formed.

At the beginning of the process, growth is not as volumetric (isotropic) as it is directional (by gradient), with time the growth becomes mainly volumetric in some zones and in others mostly directional [46,57]. For instance, for the articular cartilage, growth is mostly volumetric (due to the concentration of the molecules) and will define the epiphysis. Whereas for pre-cartilaginous and mesenchymal tissue, growth is influenced by both, the concentration and the directional growth.

For a faster growth velocity (*case III*), we obtain a single joint with two growing regions, located at both ends of the rudiments (high concentration of (I) at the ends of the bones). Regarding *case IV*, we started with a domain with a length/width ratio of 2.5 and with constant values specified in Appendix A. In this case, the goal was to simulate the onset of a joint located between a large bone and a shorter one. This configuration is similar to a joint between a metatarsal or metacarpal bone and a phalanx (Fig. 2-6), where we have a large bone on the proximal side and a shorter one on the distal side. For the proximal

anlage, the molecular distribution (P-I) was similar to that of a large bone, where the PTHrP molecule is established on the heads of the bone and Ihh on the middle part [53].

In *case V* and *case VI*, we simulated a study performed by Merino *et al.*, [77]. They analyzed the effects of GDF-5 local administration in the developing autopod of embryonic chicks. They implanted GDF-5 beads at the tip of the digits that promoted intense cartilage growth and failed to induce morphological or molecular signs of joint formation [77]. Additionally, they implanted GDF-5 beads in the interdigit joints, which resulted in an inhibition of the formation of joints in the adjacent digits. This suggests that the role of GDF-5 is to control growth and differentiate the cartilage of the epiphyseal regions from the phalanges, rather than accounting for the differentiation of the synovial joint tissues [77].

When we compare the results obtained in this study for *case V* and *case VI* with those reported in Merino *et al.* [77] (Fig. 2-7), the morphology achieved in both studies were similar. We did not obtain any joint due to the effect of the implantation of the molecule (G), which modified the Turing patterns, whereas on the Merino *et al.* [77] experimentation the GDF-5 beds were added shortly after joints were formed (Fig. 2-7). Moreover, when we simulated the implantation of the molecule on one side of the mesenchymal condensation, the resulting rudiment was curved, as reported in Merino *et al.*, [77] (Fig. 2-7). Similarly, when we simulated the implantation of the molecule (G) on the tip of the mold, a bulb was formed, as well as in Merino *et al.*, [77] (Fig. 2-7). These effects could be due to the fact that high

concentrations of (G) implies, after the cavitation process, high concentrations of (W), which differentiate the tissue into articular cartilage. This abnormal location of articular cartilage impacts on the Turing pattern between (I) and (P), hence abnormal growth of the tissue is obtained.

In this work, a simplified model to study development of joints was proposed. This model considered 6 generic factors, which predicted location of the joint, cavitation, and morphology. There was good agreement between the obtained results from our simulation model and those reported in the literature from experimental works, where histological analyses were performed.

However, during prenatal development, there are additional factors such as mechanical, genetic, and environmental aspects. We modeled generic molecules, as there are often multiple molecules that influence the same biological process. Nonetheless, we showed that simple pattern formation between enzyme-substrate molecules predicts many events related to the joint formation. In this model, we used simplified initial geometry and demonstrated that the initial length/width relation is crucial to pattern formation. We assumed null flux at the boundaries of our rudiment, which may not sufficiently represent communication of the rudiment with surrounding tissues. However, it was a necessary approximation given the lack of data that demonstrate flux out of the rudiment. We also assumed random initial molecular distribution and demonstrated the influence of altering the initial conditions (with beads of molecule G). The random distribution is a necessary assumption of the initial state of the limb bud.

In conclusion, this work proposes a simplified computational model of the regulatory mechanisms that influence the formation of joints. All the results obtained were compared with those reported on former studies, which were qualitatively similar. Then, the proposed computational model may be the first, and a good approximation, of the phenomenon of joint formation. The model shows a good response with interphalangeal and metacarpal/metatarsal-phalanx joint development. This work will be useful for researchers focused on pathologies associated with embryo and joint development. Furthermore, this model could provide new insight and guidelines of experimentation, and of course, new mathematical and computational models as well.

Chapter 3. JOINT MORPHOGENESIS

3.1. INTRODUCTION

As it was said on the previous chapter, joint development is characterized by 3 steps: interzone onset, cavitation, and morphogenesis. The interzone determines the joint place within the bone blastema and it is characterized by cells that stopped their differentiation to chondrocytes [34,85]. The interzone gives place to the cavitation process, which leads to the physical separation of the anlagen [34]. Afterwards, comes the last step of the joint development, its morphogenesis, within this process the joint molds to its final shape finishing the joint development process, although some studies have shown that the morphogenesis of the joints might initiate before the cavitation process [21,40,86]. During cavitation and morphogenesis chondrocytes proliferate within the bone rudiments allowing their growth and shaping [39].

The consequences of an abnormal joint morphogenesis can be debilitating and jeopardize the life quality of the individual, as for the case of the developmental dysplasia of the hip (DDH), which has a frequency of 5 out of 1000 hips [21,87], or in arthrogryposis multiplex congenita (AMC), which due to an abnormal fibrosis of the muscles the individual develops multiple joint contractures [88]. Although it is an important health issue to address, there are still imprecisions

understanding on how and which factors guide the morphogenesis process [44].

In fact, experimental and computational studies have shown that there is a relationship between mechanical stress and the skeletal morphogenesis, growth, regeneration, maintenance and degeneration [89–97]. Moreover, in the past, it was assumed that the fetal movement is one of the factors that affects the joint morphogenesis [21]. Researchers have found malformations at the knee joint when chicks embryos have been immobilize through neuromuscular blocking agents [98,99]. Also, it was found that other joints develop fused or with non-interlocking joint shapes [100]. This aspect has also been explored in mice genetically modified to have “muscle-less limb”, in which the joints also developed with malformations, in particular the elbow and shoulder [101,102]. From those studies, there is no doubt that motion and loading could affect the morphogenesis process during joint development. However, there are very few studies that have deeply explored this issue.

From a computational perspective, two models have been developed to evaluate the relationship between joint morphogenesis and mechanical stresses [20,21]. Heegaard *et al.* (1999) developed an idealized proximal interphalangeal model, including the mechanical load provided by the muscles through the tendons, to evaluate the epiphyseal growth through a modified version of Carter’s ossification theory [103]. In that study, Heegaard *et al.* evaluated how the joint morphogenesis is influenced by the contraction of the muscles, resulting in a congruent development of the joint’s surfaces. That model

was the first mechanobiological model that simulated the joint mechanical environment in the prenatal phase.

On the other hand, experimental studies have found that static compressive and cyclic compression loads inhibits and promote cartilage growth, respectively [21,104,105] [106–108]. Using that experimental results, Giorgi *et al.* [21] developed a 3D computational model of the joint morphogenesis, including the joint capsule. They also analyzed the effect of movement range with different initial shapes of the joint. In addition, they employed idealized shapes for generic joints such as ball and socket and hinge and applied typical movements for each type of joint.

Both aforementioned computational works, the one developed by Heegaard *et al.* and the one done by Giorgi *et al.*, used the hydrostatic stress distribution for describing the growth and joint morphogenesis [20,21]. Although, those seminal works obtained important results about the morphogenesis process, the final shapes of the two opposite rudiments do not match entirely to a real interphalangeal joint shape; strengthening the fact that biochemical interactions during bone morphogenesis might be necessary to achieve congruent joint shapes.

From the biochemical perspective, some experimental works have identified the biochemical factors that might influence the entire process of joint development. These works have found that Hox genes, Bone Morphogenetic Proteins (BMPs), Growth and Differentiation Factors (GDFs), Wnt, chordin and noggin all influence the interzone onset and the cavitation process [85,95,109]. Based on these literatures,

we designed a computational model with the aim of explaining the interaction of these molecules during the joint onset, as described in the previous chapter (Joint Onset). The previous chapter explained how self-regulatory loops of biochemical factors may influence the interzone onset, cell differentiation, tissue growth, cavitation process and synovial capsule development. In the previous chapter we explained how biochemical factors influence the joint development, from the interzone onset to the cavitation process, in which the joint took its initial shape due to cell proliferation, however, we did not model how the joint achieves its definitive shape, the final morphogenesis.

As it was described, the morphogenesis is regulated by biochemical and mechanical stimuli. Nevertheless, to date, there is no experimental or computational model able to accurately explain how a synovial joint is shaped. Moreover, none of the existing computational models have integrated the biochemical stimulus as a factor for joint shaping. Understanding how these biochemical and mechanical stimuli influence the joint morphogenesis process might be useful for the prevention and treatment of developmental diseases.

Here, a 2D finite element model of the interphalangeal joint was developed, which included the synovial capsule as domain surrounding the bone rudiments. This model considers the biochemical and mechanical effects on the joint morphogenesis, from the cavitation stage to the appearance of primary and secondary ossification centers (POC and SOC). Furthermore, the model was tested to replicate different conditions that might be present in a pathological context, as

when there is a muscular abnormality or joint malalignment. This model provides a steppingstone to establish an understanding on the mechanisms that influence the joint morphogenesis. This study could be useful for physicians and researchers interested in the design of new joint's treatments and skeletal development.

3.2. MATERIALS AND METHODS

In this work a finite element model of a synovial joint morphogenesis was developed. The model includes the effect of possible molecules and mechanical factors involved in the joint morphogenesis process. The model initiates with an approximate geometry of a synovial joint, interphalangeal joint, after the cavitation. The initial reference geometry was adapted from the result of a previous work of the authors [96]. The computational process is as follows: The distal bone anlage was rotated to simulate the movement of the finger, only four steps of the movement were evaluated: when the distal phalanx was at 0° , 30° , 60° and 90° . Stresses were computed elementally on each position and then were translated into a reference state (at 0°) and averaged at each element. Once all data was translated to the reference state, cartilage growth and ossification parameters were computed. Then, the geometry of the reference state was updated considering by the stresses and biochemical factors. Thus, this process continued until the shape of the joint agrees with the shape of an interphalangeal joint.

3.2.1. GEOMETRY AND BOUNDARY CONDITIONS

For this model, it was assumed that the finger, viewed on a sagittal plane, had a cyclic extension-flexion movement, where the distal phalanx rotated around the proximal phalanx. Four steps of the movement were evaluated: when the distal phalanx was at 90° , 60° , 30° and 0° with respect to the vertical line y (Fig. 3-1). The geometry of the model was approximated and adapted from the last step of the previous chapter's result (see Joint Onset).

The domain was meshed employing linear quadrilateral elements, the size of which was refined until further refinement no longer yielded noticeable improvements. All the equations were solved with FEM and implemented in a user element Subroutine in FORTRAN and solved with ABAQUS v6.13 (Dassault Systèmes).

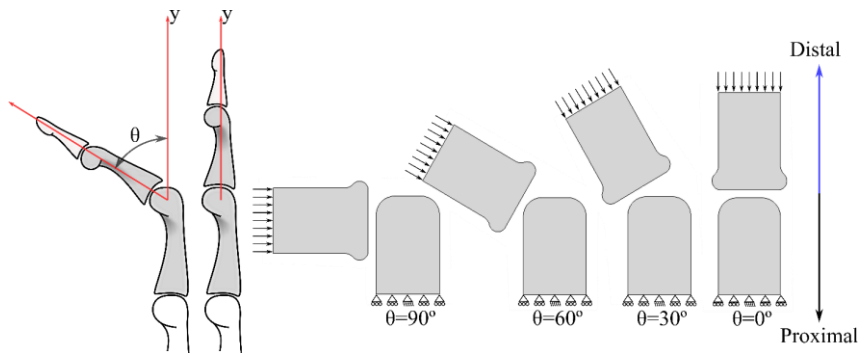


Fig. 3-1 Schematic representation of the boundary conditions implemented on the model. The inferior boundary of the proximal phalanx has the central node fixed; the other nodes of the boundary are allowed to move laterally. Palmar side to the left and dorsal to the right.

3.2.2. MECHANICAL ASPECTS

Regarding the mechanical part of the model, a displacement of $1\mu\text{m}$ was to the top surface of the distal rudiment towards the proximal element at each motion stage (Fig. 3-1) [20]. The displacement had distal to proximal direction related to the distal phalanx (Fig. 3-1). The proximal phalanx was fixed on its bottom central node, the other bottom nodes could move on the lateral direction. For simplicity's sake, some considerations were made, i.e., the modelling of contact between the phalanges was avoided by including the synovial capsule, as a circumference surrounding the joint, with a maximal diameter of 6 mm and large enough to contain the joint throughout movement sequences (Fig. 3-2), previous studies have proven that the inclusion of the synovial capsule does not affect the results of the simulation [21], instead, it saves computational time.

The bones were initially considered as fully cartilaginous, as they are at this stage of human development. Additionally, all tissues were modelled as linear-elastic, isotropic and homogeneous materials; the cartilage of the anlagen bones was assumed as nearly incompressible (Poisson's ratio of 0.49). Each cartilage rudiment section had a Young's modulus of 1000 kPa, while the synovial capsule had a Young's modulus of 1 kPa; establishing a relation 1000:1 between the cartilage and the capsule tissues. These material properties were assumed by the authors as they act as symbolic and are easy scalable to recreate any other real or unreal conditions. In each iteration, it was computed stresses (octahedral, hydrostatic and shear) and strains. The model was developed with a plane strain approach.

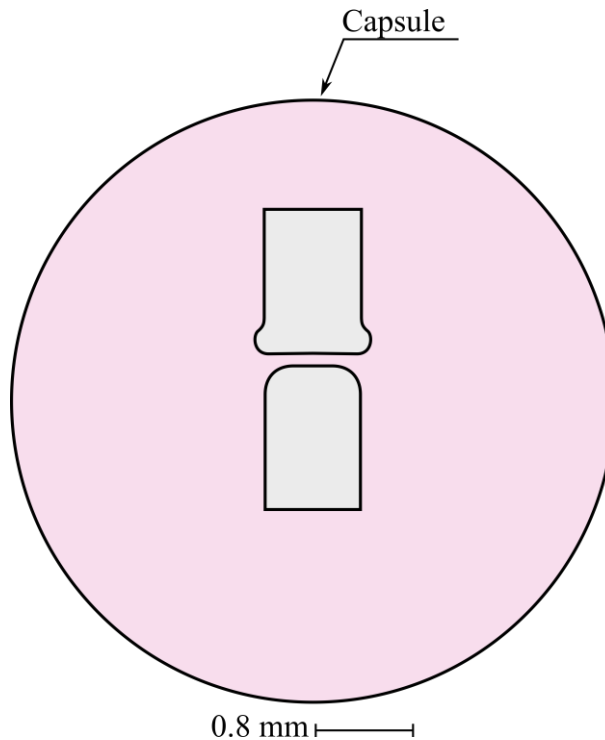


Fig. 3-2 Geometry of the bone anlagen and the synovial capsule.

3.2.3. MOLECULAR ASPECTS

There are many molecules that have a role during joint development which might influence bone growth, ossification and shaping. For instance, VEGF is involved in bone angiogenesis, and in various aspects of bone development, including chondrocyte osteoblast differentiation, and osteoclast recruitment [110]. Moreover, several studies have suggested a potential role of $TGF\alpha$ in early bone development, growth and ossification [111]. During embryonic stages, $TGF\alpha$ regulates the endochondral ossification, the osteoclast recruitment, and the vascularization at the primary and secondary

ossification center [111]. On the other hand, studies have shown that the chondrocyte hypertrophy and maturation is determined by PTHrP and Ihh autoregulatory loop that interacts with the chondrocytes population [9]; Ihh is said to control chondrocyte proliferation, maturation, and hypertrophy [66–69], whereas PTHrP inhibits chondrocyte hypertrophy, keeping chondrocytes in proliferative state [67]. Also, the literature show that although the strong canonical Wnt signaling pathway inhibits chondrocyte cell fate determination and maintenance (which induce the cavitation process [34,36,37,70,96]), the weaker Wnt signaling promotes chondrocyte hypertrophy [112].

Among the wide range of molecules that might influence in some way the bone shaping, we narrowed them to only three (Ihh-PTHrP and Wnt). This simplification was made since the authors had already considered them in a previous work in which the joint onset from interzone to the cavitation process was modeled [96]. Nevertheless, these molecules are the ones that have been reported in the literature have the more influence in bone growth, hence shaping. The molecules were included in the model as constants within the domain, it was considered molecular distribution after a reaction-diffusion system (Ihh-PTHrP) and diffusion (Wnt) unchanged after the joint onset. The initial distribution of the aforementioned molecules was taken from the last step of the previous chapter results (Joint Onset).

In each time-step, the bone anlage was divided in four regions (A1 to A4) of constant concentration. The length of the regions (l) was proportional to the length of the anlage (L) and was calculated as the quotient of L /number of regions (Fig. 3-3). Since the growth rate was

small compared to the time length, the change of the domain did not affect the molecular distribution.

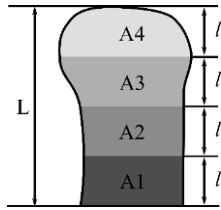


Fig. 3-3 Schematic definition of the concentration areas. Each area has a length proportional to length of the bone anlage, the proportion was kept throughout the simulation.

3.2.4. TISSUE GROWTH

For the tissue growth modeling, it was supposed that the tissue response to the mechanical stimuli had a positive relationship between cartilage growth and cyclic hydrostatic stress, and it was inhibited by the octahedral shear stress [113]. Additionally, it was considered that high concentrations of PTHrP and Wnt promote chondrocyte proliferation, therefore, cartilage growth. Hence, if a cartilage element had PTHrP and Wnt concentrations above a threshold (TH_{PTHrP} as 1.1 and TH_{Wnt} as 0.01) the cartilage could grow.

Concerning the cell (chondrocyte) concentration, C_c , it was assumed that these cells do not migrate within the domain; they only proliferated within the bone anlage keeping a constant cell concentration. Then, the cell (chondrocyte) concentration, C_c , is related with the growth velocity as follows (Eq. 3-1):

$$\frac{dC_c}{dt} + C_c \nabla \cdot \mathbf{v} = \alpha(PTHrP, Wnt)S_{Hyd}$$

With

Eq. 3-1

$$\alpha = \begin{cases} \alpha = 0 & \text{if } PTHrP < 1.1 \text{ and } Wnt < 0.01 \\ \alpha = 2.0 & \text{if } PTHrP > 1.1 \text{ and } Wnt > 0.01 \end{cases}$$

where S_{Hyd} is the hydrostatic stress of the element; \mathbf{v} is the growth velocity on each point of the domain; α , is a constant that indicate the influence of the hydrostatic stress on the element's isometric growth; S_{PTHrP} and S_{Wnt} are the concentrations of PTHrP and Wnt within the element. However, since the cellular concentration was kept constant the first term of the equation is equal to zero ($\frac{dC_c}{dt} = 0$). Moreover, the growth velocity \mathbf{v} can be related to the strain tensor (\mathbf{d}^{growth}) following the Eq. 3-2.

$$tr(\mathbf{d}^{growth}) = \nabla \cdot \mathbf{v} = \frac{\alpha(PTHrP, Wnt)}{C_c} S_{Hyd} \quad \text{Eq. 3-2}$$

Then, the strain tensor can be computed as:

$$\mathbf{d}^{growth} = \frac{\alpha(PTHrP, Wnt)}{C_c} S_{Hyd} \delta_{ij} \mathbf{e}_i \otimes \mathbf{e}_j \quad \text{Eq. 3-3}$$

where \mathbf{e}_k are the unitary directional vector in a Cartesian coordinate system; δ_{ij} is the Delta-Kronecker tensor; and i, j take values of 1 or 2 (x -direction and y -direction). In the growth equation, the hydrostatic stress S_{Hyd} had a volumetric effect by increasing cell quantity, without increasing cell concentration [cell/unit volume].

3.2.5. BONE OSSIFICATION

For the bone ossification it was considered the osteogenic index (OI). OI was calculated and used to predict the appearance of the POC and SOC within the anlagen [114–116]. The OI is a scalar parameter which considers the effect of the hydrostatic stress and the octahedral shear stress [8]. This parameter, OI, can be used to predict which regions of the cartilaginous anlage are likely to ossify first (high OI) [93]. Therefore, the cartilage on the diaphysis was considered to ossify under high OI (Eq. 3-4) and low PTHrP and Wnt, whereas for the SOC, only the OI was considered.

$$OI = k_1 S_{Hyd} + k_2 S_{Oct} \quad \text{Eq. 3-4}$$

S_{Hyd} is the hydrostatic stress; S_{Oct} is the octahedral shear stress; k_1 and k_2 are the constants weighting the contribution of S_{Hyd} and S_{Oct} , respectively. k_1 took the value of 0.7 and k_2 of 1 for the proximal phalanx, and for the distal of -0.35 and 1 for k_1 and k_2 , respectively. The ossification process of the tissue, POC and SOC, was assumed as a mineralization of the tissue which increased the Young's modulus of the element until it reached 20000 kPa.

3.2.6. TRANSLATION TO REFERENCE

At each time-step, a static implicit FEM analysis was done at each flexion position (90°, 60°, 30° and 0°), then, the results were translated to a reference position (which is at 0°). Once all the results were at the reference position, they could be averaged in a unique

geometry where the cartilage growth and ossification were calculated. This was done by calculating the centroid of each element of the rotated state (red) and pivot them to the coordinates on the reference state (0°) (blue), these centroids carry the information about the stresses of the each element (Fig. 3-4). Afterwards, each element of the reference state (blue) assumes the value of the closest centroid of the rotated state. With the obtained quantities at reference state, the calculations of OI and cartilage growth were done, and the geometry of the reference state was updated. Then, the distal phalanx of this new reference state was rotate at each analyzed position and process begins again.

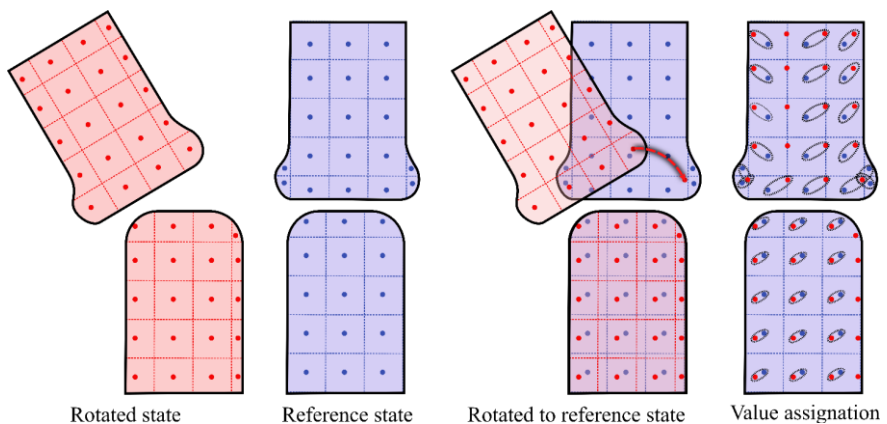


Fig. 3-4 Translation process from a rotated state to the reference state at (0°). Palmar side to the left and dorsal to the right.

3.2.7. GENERAL ALGORITHM

The algorithm proposed for the morphogenesis model is shown in Fig. 3-5. The computational model initiated with the drawing and meshing of the geometry at its position (90° , 60° , 30° and 0°), then, the

mechanical conditions were applied, and the stresses were calculated through FEM. Afterwards, the centroids of the elements at each rotated position were spun to a reference state (which is at 0° and also meshed with linear quadrilateral elements); to each element of the reference position was assigned the values of stresses of the nearest centroid of the rotated states.

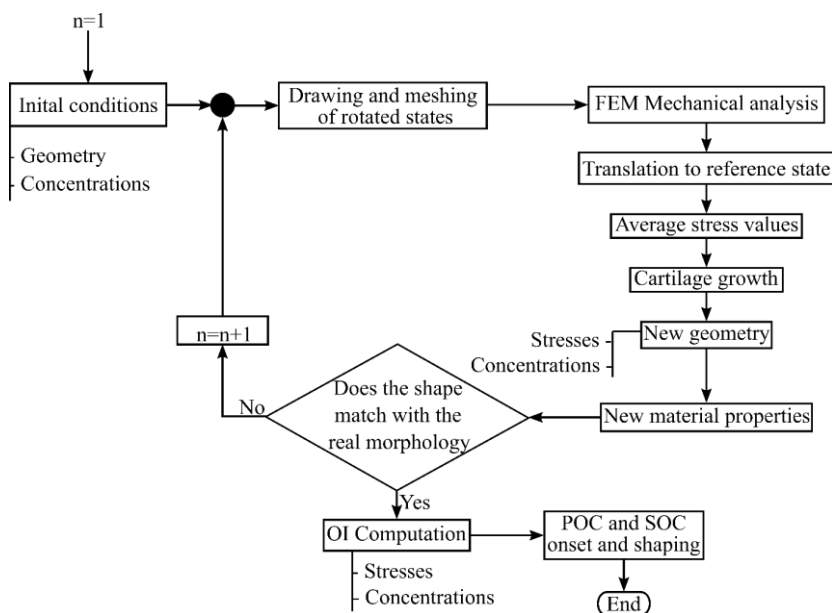


Fig. 3-5 Algorithm designed for joint morphogenesis.

Once all the data from the rotated positions were at 0°, the stresses from all rotated positions were averaged within each element of the reference state. With the averaged stresses and the molecular concentrations (determined as mentioned in Molecular Aspects) the cartilage growth was determined producing a new reference geometry of the bone rudiments. This new geometry was then subjectively

evaluated, and if it resembled that of an interphalangeal joint, then the POC and SOC were determined through the OI, if not, the reference geometry was rotated again to the analyzed positions (90°, 60°, 30° and 0°).

3.2.8. MODELLED CASES

The model was tested in five different cases (Table 3-1). The first one replicate normal conditions and the following four simulated pathological settings. In first pathological setting, the effect of the molecules was not considered; the growth depended only on the hydrostatic and octahedral stresses. In the second one, a dislocation of 0.3 μm between the two phalanges was included (Fig. 3-6). Moreover, two palsy environments were simulated in which only one rotated position was considered; the distal phalanx was at 0° or 90° flexion angle.

Table 3-1 Conditions for the normal and pathological settings.

		Angles	Averaged	Dislocation
<i>Normal</i>		90° 60° 30° 0°	Yes	0 μm
<i>Pathological</i>	Kilter	90° 60° 30° 0°	Yes	0.3 μm
	w/o molecular	90° 60° 30° 0°	Yes	0 μm
	0° palsy	0°	No	0 μm
	90° palsy	90°	No	0 μm

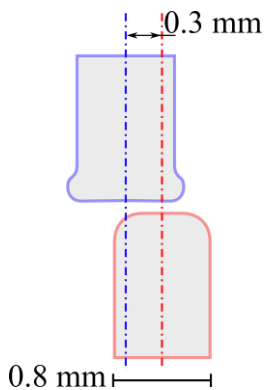


Fig. 3-6 Geometry of the pathological kilter model.
Blue, the distal phalanx and red the proximal phalanx. Palmar side to the left and dorsal to the right.

3.3. RESULTS

The final stage of the joint development process, in which the joints achieve their final shape, was simulated through a computational model. For this model it was considered the distribution of molecular factors that influence in the chondrocyte hypertrophy and proliferation, and the hydrostatic stress loading which promotes cartilage grow. An average result was calculated considering each finger flexion angle and translated to the reference position (0° flexion angle); all finger positions were given the same weight. The results show the morphogenesis process of an interphalangeal joint (Fig. 3-7). The upper surface of the proximal bone evolves into a concave shape, whereas the bottom surface of the distal phalanx sculpts into a convex form. The obtained shape of the joint was similar to that of an interphalangeal joint observed in the sagittal plane (Fig. 3-7).

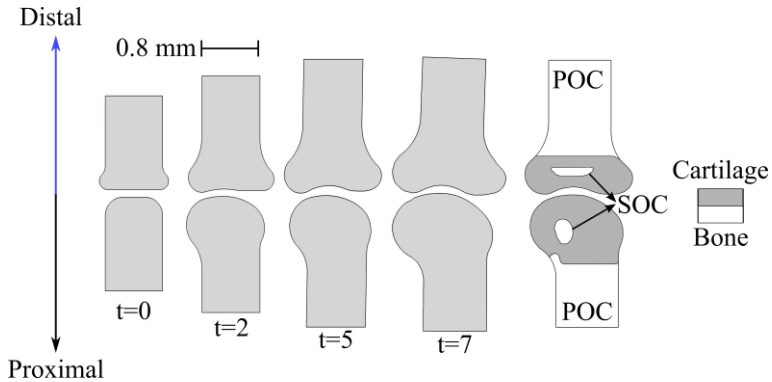
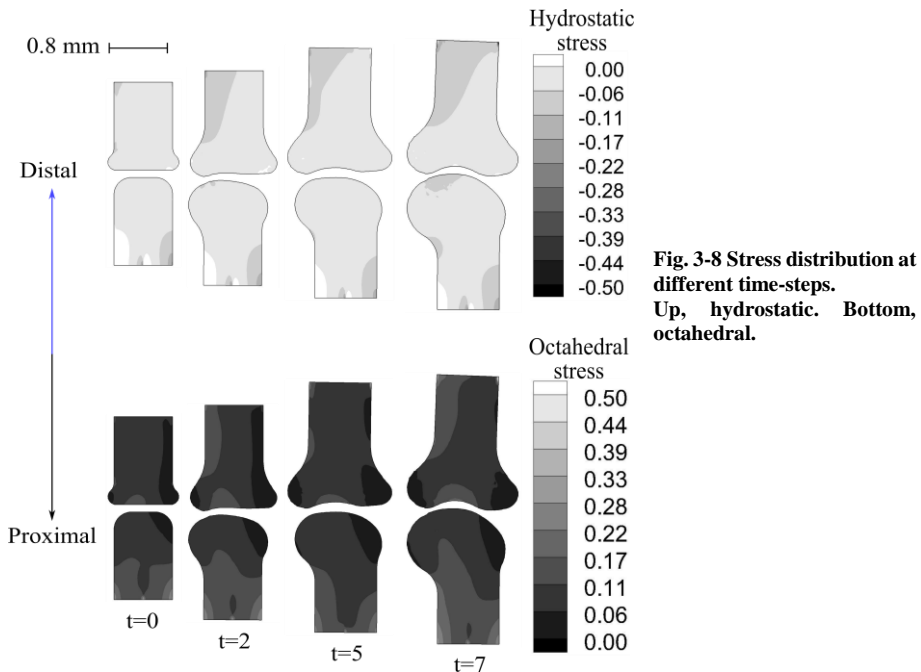


Fig. 3-7 Obtained joint shape at different time-steps for normal conditions. Palmar side to the left and dorsal to the right.

On the other hand, the octahedral shear stress, the hydrostatic and the shear stresses distributions were obtained for different time-steps (Fig. 3-8). The proximal phalanx had high compressive hydrostatic stress on the anterior part of the joint surface, the main zone in contact with the distal rudiment (Fig. 3-8). As for the distal rudiment, it also had high compressive hydrostatic stress on its anterior side, but along the whole anlage, especially for the first steps (Fig. 3-8).

On the last steps, the hydrostatic stress distribution remains almost the same for the proximal anlage. However, for the distal one, it tends to become more uniform on the bone diaphysis (Fig. 3-8). Also, hydrostatic compressive stress on the head of the distal bone is smaller compared to the rest of the bone (Fig. 3-8). In addition, the octahedral stress was high at the bottom of the proximal rudiment, as well as in the contact surface of the distal (Fig. 3-8).



Additionally, some pathological environments were simulated to evaluate some conditions that might be present during development which can affect the joint morphogenesis. The first one tested the conditions when the molecular effect is neglected which produced an abnormal growth of the rudiments. The distal one grew much more than in normal conditions and there was absence of the head of the bone anlagen, while in the proximal rudiment the head developed but in an abnormal shape. Furthermore, the hydrostatic and octahedral stress distributions were similar to normal conditions (Fig. 3-10); the proximal phalanx had high compressive hydrostatic stress on the palmar part of the joint surface and the distal rudiment had high compressive hydrostatic stress on its palmar side, but along the length of the anlage.

As for the octahedral stress distribution it was high ant the bottom of the proximal rudiment and in the contact surface of the distal, like in normal conditions.

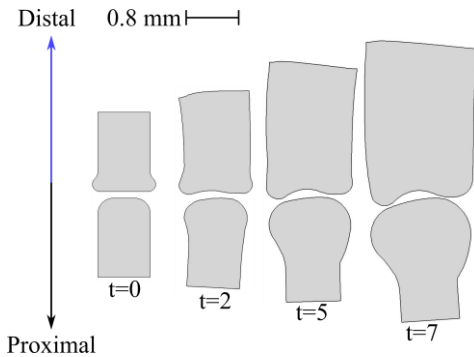


Fig. 3-9 Obtained joint shape at different unit time for the pathological condition when the effect of the molecules is not included. Palmar side to the left and dorsal to the right.

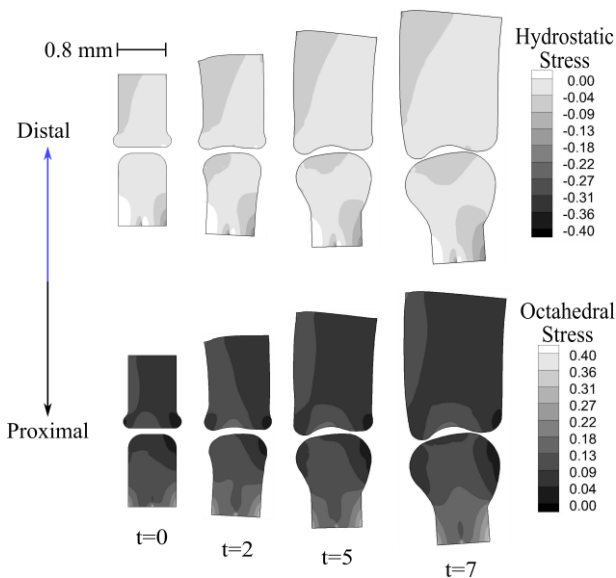


Fig. 3-10 Obtained hydrostatic and octahedral stresses at different unit time for the w/o molecular effect pathological setting. Palmar side to the left and dorsal to the right. Units [kPa].

The second pathological setting (Kilter) tested the conditions when there was an offset; the distal phalanx was moved 0.3 *mm* to the palmar side. For the kilter model all the positions (90°, 60°, 30° and 0°) were considered to influence the joint morphogenesis. In the end, an abnormal form of the joint was obtained in which the distal phalanx appears to have the concave shape on its dorsal side, while the proximal phalanx is shaped like a concave geometry, similar to that of normal conditions (Fig. 3-11).

Additionally, two paralysis environments were tested in which the phalanges were kept at a fixed angle throughout the simulation, 0° and 90° palsy were modeled. Undoubtedly, the paralysis environment affects the joint shape, since no coherent joint shape was obtained in neither case of paralysis (Fig. 3-11). For the 90° palsy model, the distal phalanx did not obtain a convex shape, while for the 0° palsy model the distal phalanx had a shallow convex shape.

The joint shape is affected due to the changes in the hydrostatic and octahedral stresses distribution (Fig. 3-12). In the kilter model the stress distribution within the proximal phalanx was similar to the one in normal conditions, however, for the distal phalanx the hydrostatic stress was not as high in the palmar side, and the octahedral stress had high concentrations at the zone of contact.

In the paralysis model at 0° the hydrostatic and octahedral stresses for both phalanges were mostly concentrated at the center of the geometries at all time-steps. However, for the 90° palsy model the hydrostatic stress was almost uniform for the distal phalanx, and the proximal had higher hydrostatic compression stress at the dorsal side.

As for the for the octahedral stress of the 90° palsy, it banded in a similar way of normal conditions for both, distal and proximal phalanx. However, the distal phalanx did not have a zone of high concentration of octahedral stress at the contact surface.

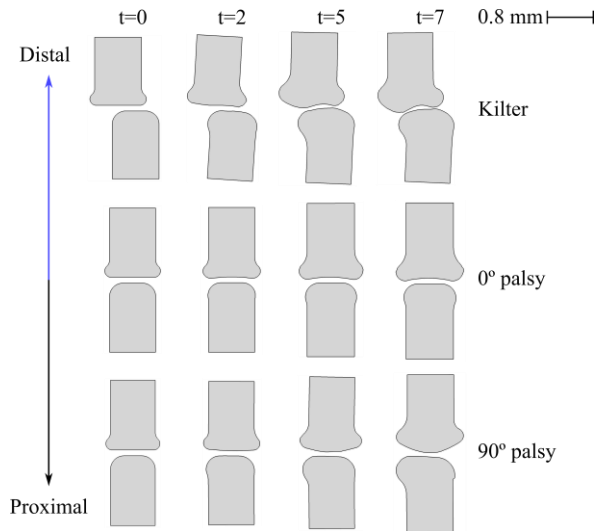


Fig. 3-11 Obtained joint shape at different unit time for the simulated pathological environments. Palmar side to the left and dorsal to the right.

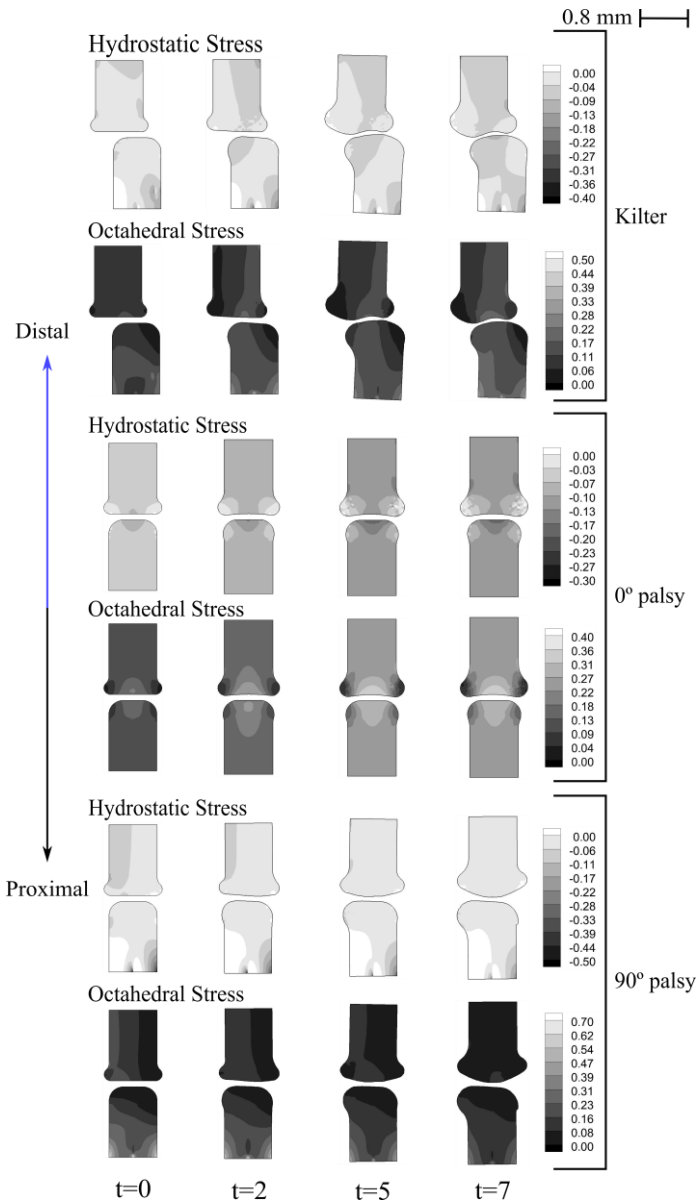


Fig. 3-12 Obtained hydrostatic and octahedral stresses at different unit time for the pathological models. Palmar side to the left and dorsal to the right. Units [kPa].

3.4. DISCUSSION

Previous works have tried to describe the joint morphogenesis as a result of cartilage tissue response to hydrostatic stress distribution [20,21]. They showed how both ends of the bone rudiments changed their shape according to the hydrostatic stress distribution, however, the final shapes of the two opposite rudiments do not agree to the morphology of the joint. Therefore, it confirms that not only the mechanical environment affects the morphogenesis of the heads of the bones, but also there are biochemical aspects that should be considered.

From a biochemical point of view, in our previous chapter (Joint Onset) we analyzed the biochemical interaction of the joint onset, from the appearance of the interzone to the cavitation process. During these stages, only the interaction of molecules is responsible to regulate the joint development. However, during the morphogenesis process it is also necessary to include the effect of mechanical loading.

In this study, the molecular and mechanical factors, influence joint morphogenesis. It was assumed that the molecules involved on the previous steps of joint development, interzone onset and cavitation, also have influence during the morphogenesis. The distribution of the molecular factors was kept constant within each time-step of the domain (Fig. 3-13). The concentration of the molecules in conjunction with the stresses influenced the growth of the cartilage. As hydrostatic compression stress, PTHrP and Wnt promote cartilage growth and chondrocyte proliferation, respectively, in the zones where we have a high concentration of both, cartilage growth is promoted. For instance,

the top and palmar part of the proximal phalanx has a high concentration of hydrostatic stress and PTHrP or Wnt, therefore, this zone of the proximal phalanx mold into a concave shape.

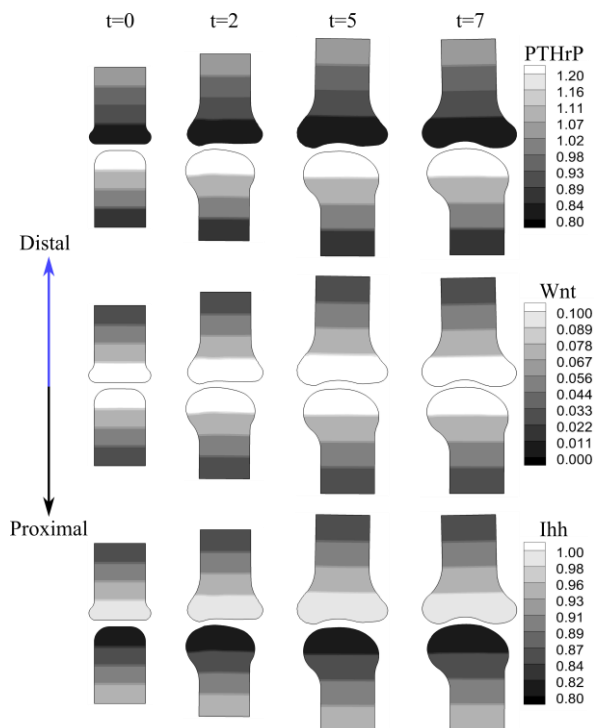


Fig. 3-13 Molecular distribution at different time-steps. Palmar side to the left and dorsal to the right.

Four different positions of the interphalangeal joint were analyzed. The stresses values obtained at each position were averaged and translated to a reference system (0° flexion). The same weight was given to each position since there are no reports in the literature about how the finger movements of the fetus are during the morphogenesis stage. Hydrostatic stress and the concentrations PTHrP-Ihh and Wnt

were considered to play a role during joint morphogenesis, therefore, in the zones where we have a high concentration of these molecules and hydrostatic stress, cartilage growth is promoted. For instance, the top and anterior part of the proximal phalanx has a high concentration of hydrostatic stress and PTHrP, therefore, this zone of the proximal phalanx evolved into a concave shape. Additionally, the distal phalanx joint surface shaped into a convex structure due to high concentrations of octahedral shear stress on the center of the joint surface, which inhibited cartilage growth. The obtained final shapes of the bones' diaphysis were coherent with those of an interphalangeal joint (Fig. 3-14).

As part of the endochondral ossification, if the effect of the OI is included, the shapes of SOC and POC can be also explained as seen in our results (Fig. 3-14). The model showed how the OI predict the areas of high ossification on the diaphysis. The OI computation was based on the one proposed by Carter and Wong (1988) [93]. They established that the OI is calculated based on the octahedral shear stress and the hydrostatic stress multiplied by an empirical constant k_i . In this study, the values of the multipliers k_i were different for each stress and phalanx, condition which we considered was necessary for a coherent ossification process. The obtained results are comparable with those from former studies, where only the endochondral ossification and OI distribution was analyzed [56,93,116]. On the proximal phalanx the SOC was shaped as a circular structure. On the distal anlage, the SOC took an elliptical shape, most likely due to how the convex surface distributed the octahedral shear stress and hydrostatic stresses (OI).

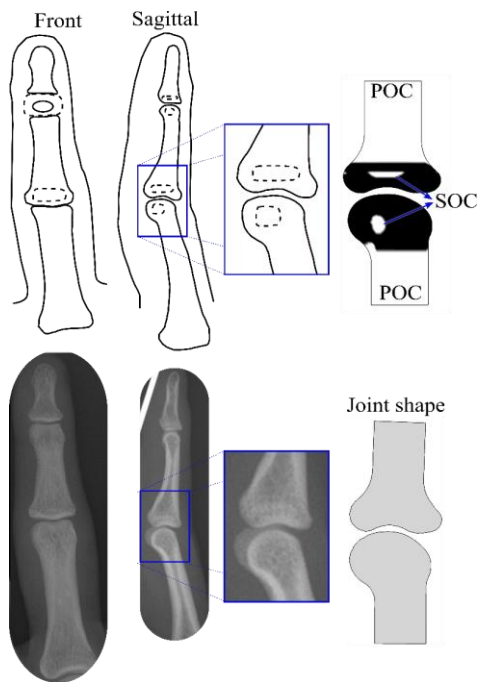


Fig. 3-14 Secondary ossification center (SOC) in a developing bone.
Top: schematic drawing of SOC in a developing bone, and the SOC obtained with the model. Bottom: comparison between an x-ray phalanx and the result from the joint morphogenesis computational model.

When pathological conditions were simulated it affected the joint development, resulting in an abnormal geometry for all cases (Fig. 3-15). In the pathological setting where the effect of the molecules was retired from the model, the obtained geometry was much larger than normal conditions, this abnormal growth might be since the effect of the stresses is not limited by the molecular concentrations.

In the pathological setting where the phalanges were dislocated (kilter) the hydrostatic stress was almost similar for the proximal phalanx, but for the distal it had lower values than in normal conditions (Fig. 3-12). Also, the octahedral stress was higher than in normal

conditions, which in combination with the lower hydrostatic stress provoked a lower overall growth.

As for when the finger was kept straight (0° palsy), the hydrostatic stress and the octahedral stress were higher than in normal conditions, which also influenced on the overall growth of the phalanges (Fig. 3-12). Moreover, when the paralysis model was kept with a 90° flexion, the hydrostatic stress was smaller than in normal conditions, as well as the octahedral stress; in fact, for the distal phalanx there was no zone of high octahedral stress, therefore, nothing inhibited the cartilage to grow which resulted in the absence of the convex shape in the distal phalanx articular surface (Fig. 3-12).

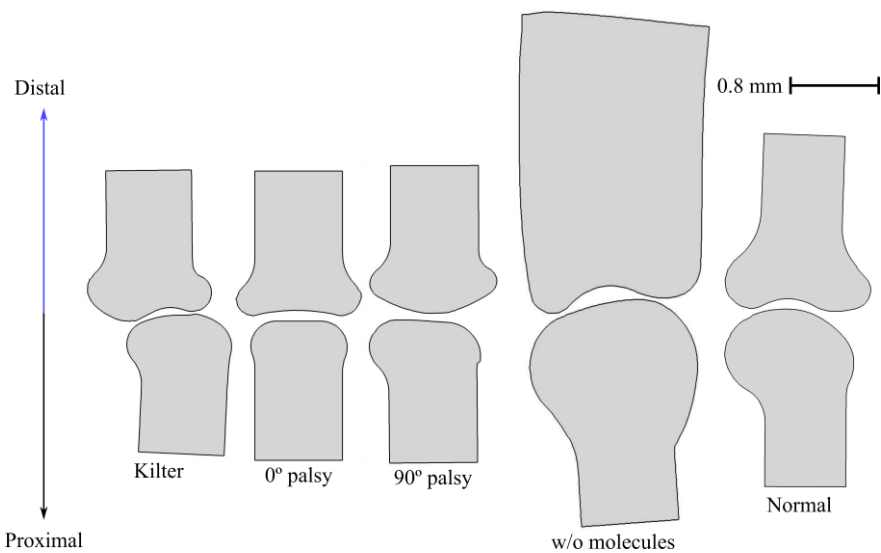


Fig. 3-15 Comparison of the obtained geometries for the kilter, the 0° palsy, the 90° palsy and the normal conditions

The final shape of the normal condition model was compared to x-ray images of interphalangeal joints (Fig. 3-14). The obtained joint shape agrees remarkably with the ones observed in the *x-rays*. Therefore, this work sheds some light on how the mechanical environment combined with biochemical factors influence the morphogenesis of a synovial joint. It is worth mentioning that hydrostatic stress, as it promotes cartilage growth, is key for joint morphogenesis. However, for a joint to achieve complex shapes, it is necessary to include the cell/tissue responses to the biochemical and mechanical stimuli. The combined response to these stimuli produces the necessary chondrocyte proliferation and cartilage ECM productions on specific zones, which molds the bones epiphyses to their final congruent joint surfaces' shapes.

To our knowledge, this is the first computational model able to include several aspects of joint development, such as the main molecular and mechanical stimuli, and predict, successfully, the final shape of a synovial joint, like an interphalangeal joint. Moreover, the model also predicts, thoroughly, the molecular distribution of the principal biochemical within the developing bone, as well as the onset of POC and SOC.

The obtained results are remarkable despite the assumptions that had to be made for simplicity's sake and computational savings. As limitations for this model is included the fact that this is only a 2D model, therefore only one plane of motion was included. Additionally, some simplifications were made regarding the material behavior and properties. Likewise, since there is no information related to embryo

movement during development, and much less in relation to the fetus finger motion, all the analyzed positions were considered to have the same weight and influence on the morphogenesis process. Nevertheless, the presented model gives an excellent approximation of what is happening during joint development and morphogenesis and brings a new understanding of these processes, which, eventually, may lead to the development of new treatments for developmental diseases, or even prevent malformations of the fetus.

Chapter 4. PATELLA ONSET

4.1. INTRODUCTION

Although the development of the skeletal system has been studied over the past centuries, the development of a group of bones known as sesamoid bones is still unknown [117]. Sesamoid bones, such as the patella, are bones embedded superficially within tendons; these tendons are usually around joints. The name sesamoid comes from the Latin word *sesamum* (sesame seed), due to the small size of most of these bones, and the morphological resemblance of this bone to the seed [117]. Sesamoid bones can be found in several joints throughout the body, including hand, wrist, foot, neck, ear and knee. The patella, or kneecap, is the largest, most recognized and studied sesamoid bone in the human body.

The patella has an important role in the stability of the knee, facilitating the function and locomotion of the lower limb [118]. It is believed that its main purpose is to increase the moment arm of the quadriceps muscle, by augmenting the distance between this muscle and the center of rotation of the knee joint [119]. The patella contributes to the compressive force distribution of the patella-femoral joint by increasing the contact area during flexion of the knee [119]. In addition, the patella protects the quadriceps tendon from high stress [120], while centralizing the pull of the quadriceps muscle complex, protecting the knee from dislocating [119].

The accepted theory about the development of the patella is that it develops inside the tendon in response to mechanical stimuli evoked when the muscles contract [114,117,121]. This theory is based on the idea that mechanical stimuli play a crucial role in tissue differentiation [7]. Therefore, while the tendon is immature, a zone of the tendon is subjected to high hydrostatic stress and low tensile strain. This leads to the differentiation of the fibrous tissue into cartilage and then to the ossification of the cartilage to form the patella.

According to the aforementioned tissue adaptation theory, Topological Optimization (TO) may also be suitable to explain the development of the patella. TO distributes the material in a design domain through the minimization of the strain energy; as a result, this material redistribution produces an optimal configuration for low energy consumption [122]. This theory has been widely used in many engineering and biology fields, such as the architecture of the proximal femur [123–126] as well as in the design of scaffolds, implants, bone replacements, and prostheses [127–130].

On the other hand, a recent study [117] proposed that the patella initially develops as part of the femur, similar to the way in which a bone eminence is developed. This eminence is initially formed by progenitor cells that express both Sox9 and Scx. This mechanism is controlled by Transforming Growth Factor-Beta (TGF- β) and Bone Morphogenetic Protein-4 (BMP-4), which determine the differentiation of chondrogenic cells. According to this theory, the eminence is separated from the preexisting cartilaginous femur under different environmental conditions, but they consider more plausible that the

patella may be separated from the femur because of the presence of a remaining joint inducer molecule on the epiphysis. As a result of this process, a new bone embedded within the tendon is formed, thus creating a sesamoid bone, which will be the patella [117].

Currently, to the best of the authors' knowledge, there is not an accepted (or unified) mechanism in the literature that explains the formation of sesamoid bones. In fact, the development of the patella could result from the combination of the above-mentioned theories. The aim of this work is to evaluate, separately, the outcome of three conceptual computational models for the development of the kneecap. The first model considers the biochemical aspects present on the onset of the quadriceps and patellar tendon. The second model examines the cell behavior under the mechanical stimuli present during the formation of this sesamoid bone. The last model optimizes the mechanical environment of the tissues based on minimizing strain energy (TO).

The computational models allow a comparison of the three theories of patellar development, demonstrating the strengths and the plausibility of each theory. These models provide a steppingstone to establish a unified theory about the onset of this bone, which might be able to predict patellar-associated diseases.

4.2. THEORY I: BIOCHEMICAL THEORY

This biochemical theory was first proposed by Eyal *et al.* [117], as a molecular model for the development of the patella. According to this theory, the patella develops as a bone eminence attached to the

distal femur head, where new sox9-positive chondrogenic cells attach to the formed femur distal head (Fig. 4-1-II and Fig. 4-1-IC) [117]. This new aggregation of chondrogenic cells separates from the preexisting cartilage because of the effect of a remaining joint inducer on the femur articular surface (Fig. 4-1-IA). Thus, a new bone embedded within the tendon is formed.

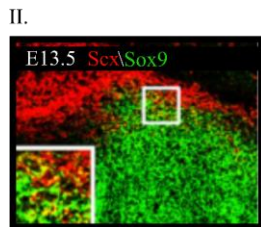
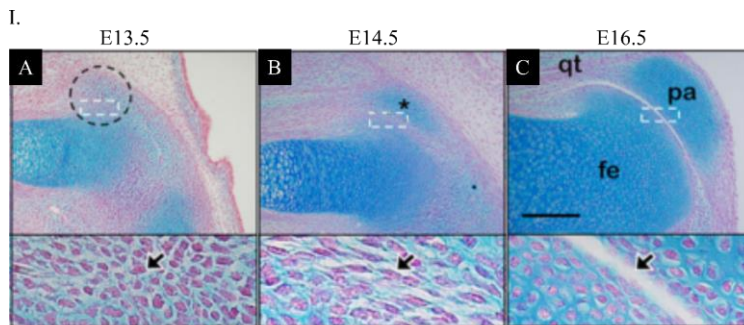


Fig. 4-1 Sagittal sections of the patella from hind limbs of wild-type mouse embryos stained with Alcian Blue and Fast Red to highlight cartilage cells (I. A-C) and Sox9 and Scx expression (II).

(I. A) At E13.5 embryonic days, an aggregation of chondrogenic cells is seen at the presumable location of the patella (dashed circles) that appears to be part of the femur, as the boundary cells are absent (arrows). (I. B) At E14.5, although the patella (*) and femur are distinguishable, the patellofemoral joint is missing. The boundary between the two cartilaginous elements is occupied by cells with distinct flat and elongated morphology (arrow). (I. C) At E16.5, the patella (pa) appears as a distinct cartilaginous structure embedded within the quadriceps tendon (qt) and separated from the femur (fe) by the patellofemoral joint (arrows). (II) Fluorescence labelling using digoxigenin- and fluorescein-labelled antisense RNA probes for Sox9 and Scx. At E13.5, cells that express both Sox9 and Scx are observed at the presumable patella location. Scale bars: 200 μ m. Modified from [117].

To develop this model, it is necessary to explore both phenomena: the development of the tendon and the eminence formation. The following section describes some of the key events involved in the development of the tendon and bone eminence.

4.2.1. TENDON & EMINENCE DEVELOPMENT

Early events of tendon formation involve the presence of Scx-positive cells (tendon progenitor cells) on the syndetome, a subdomain of the sclerotome (ventromedial compartment of the somite that gives rise to skeletal tissue) [131]. Furthermore, the cells located on the bone heads and muscle ends release TGF- β . This molecule attracts Scx-expressing cells towards the bone head and muscle end; therefore, the region of this type of cells increases [131] (Fig. 4-2-A and Fig. 4-2-B).

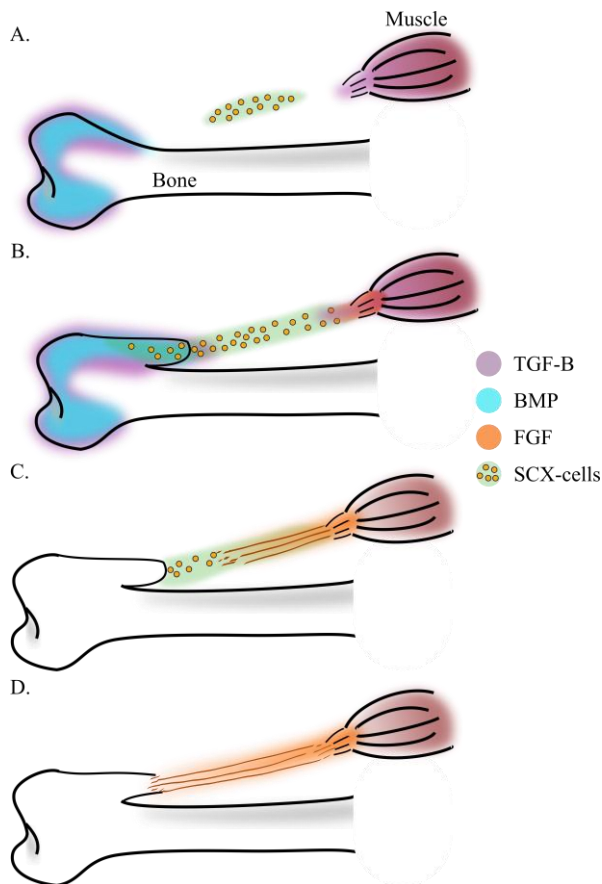


Fig. 4-2 Schematic representation of the tendon and eminence development.

A. The process starts with the expression of BMP on the bone epiphyses, the bone is still a cartilaginous mould. Also, the muscle and the epiphyses of the bone express TGF- β . **B.** The expression of TGF- β attracts and recruits Scx-cells. Those cells that express Scx and BMP start differentiating into chondrocytes. **C.** The muscle express FGF because its front detects the presence of Scx-cell. FGF induce the differentiation of Scx-cells into tenocytes. **D.** The formation of the eminence and tendon is complete.

On the muscle end, the muscle cells perceive the presence of Scx-expressing cells and deliver the FGF [132,133]. FGF (that diffuses from the muscle through the Scx-cells domain) promotes the differentiation of Scx-expressing cells into tendon cells (tenocytes). The direction of the FGF gradient determines the direction of the tendon fibers [132,133] (Fig. 4-2-C).

Simultaneously from the bone side, BMPs, which regulate the differentiation of Scx-expressing cells into chondrocytes, diffuse from the bone head [134]. BMP stimulates the Scx-cells to differentiate into chondrocytes. These chondrocytes will later shape the bone eminence where the tendon is attached (Fig. 4-2-B and Fig. 4-2-C) [134]. Thus, a fully formed tendon is obtained between the bone and the muscle (Fig. 4-2-D).

4.2.2. COMPUTATIONAL AND MATHEMATICAL MODEL

The biochemical model simulates the expression and diffusion of molecular signals during patellar development as proposed by Eyal *et al.* [117]. It is based on the formation of the quadriceps and patellar tendons (Fig. 4-3) and assumes that some molecules are remnants of the femur-tibia joint formation process [117], such as GDF-5 (Fig. 4-3-a) [50–52], which later will induce the joint onset between the patella and the femur.

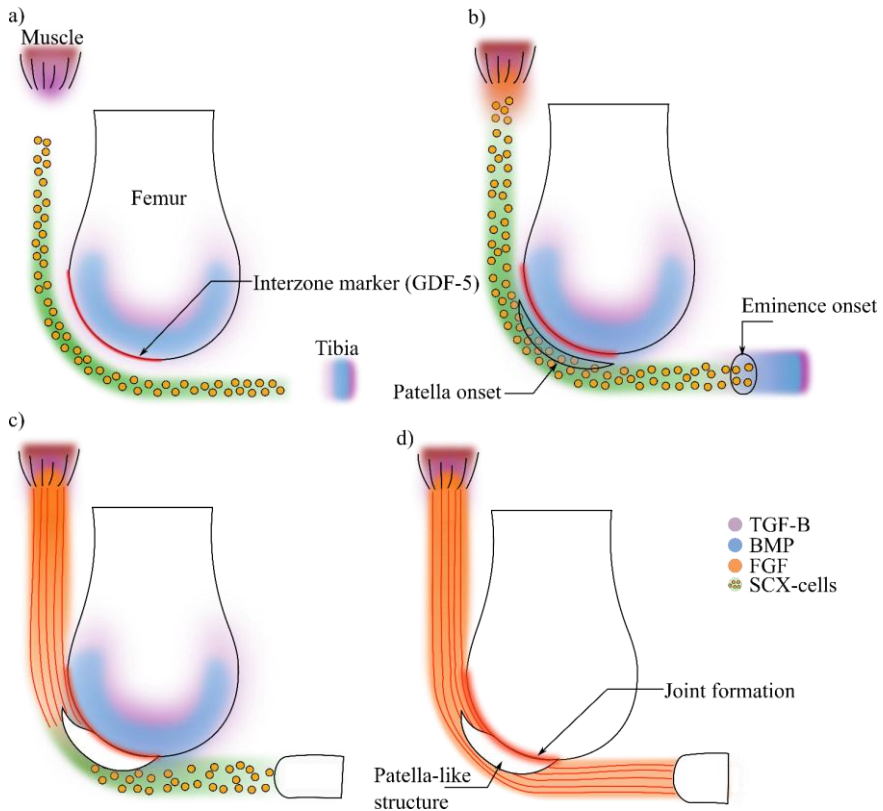


Fig. 4-3 Schematic representation of the patella development process based on the theory proposed by Eyal *et al.* [117].

A. The process initiates with the Scx-cells necessary for tendon development. The muscle and the bones epiphyses (which in this stage are cartilaginous) express TGF- β which recruit Scx-cells towards the muscle and the bones. Moreover, the bone epiphyses also express BMP factors and some of the remaining interzone marker molecules. **B.** Those Scx-cells exposed to a concentration of BMP start differentiating into chondrocytes. Also, when the muscle front detects Scx-cells, starts expressing FGF. **C.** FGF molecule induces the differentiation of the Scx-cells into tenocytes, whereas the Scx-cells exposed to BMP keep the chondrocyte differentiation, forming the future patella and the tibia eminence. **D.** The patella forms attached to the cartilaginous femur epiphysis, so a joint formation process starts due to the interzone markers left from earlier processes.

A general algorithm of this model is shown in Fig. 4-4. The model starts with the initial conditions given by the concentrations of the molecules and the initial domain of Scx-cells (Fig. 4-3-A) [131]. Then, TGF- β and BMP diffuse from the muscle and the bone [132,133] and consequently, the Scx-cells are attracted towards high

concentration of TGF- β (Fig. 4-3-B). Once the muscle detects the presence of Scx-cells, it expresses FGF (Fig. 4-3-B) [132,133]. The differentiation process involves the Scx-cells and the concentrations of FGF and BMP. If there is enough concentration of Scx-cells and BMP, the cells in the tissue differentiate into chondrocytes [134], whereas if there is enough concentration of Scx-cells and FGF, the cells differentiate into tenocytes (tendon tissue) (Fig. 4-3-B) [132,133]. At the same time, the remaining interzone marker (in this model named GDF-5) diffuses inside the newly formed cartilage structure (Fig. 4-3-C), which will induce later the joint formation between the patella and the femur (Fig. 4-3-D) [50–52].

Additionally, it is considered that the flexion of the leg during embryonic stages could influence the patella onset; therefore, this methodology was applied for different leg angles (30°, 45°, 60°, 90°) without the modification of any other parameter.

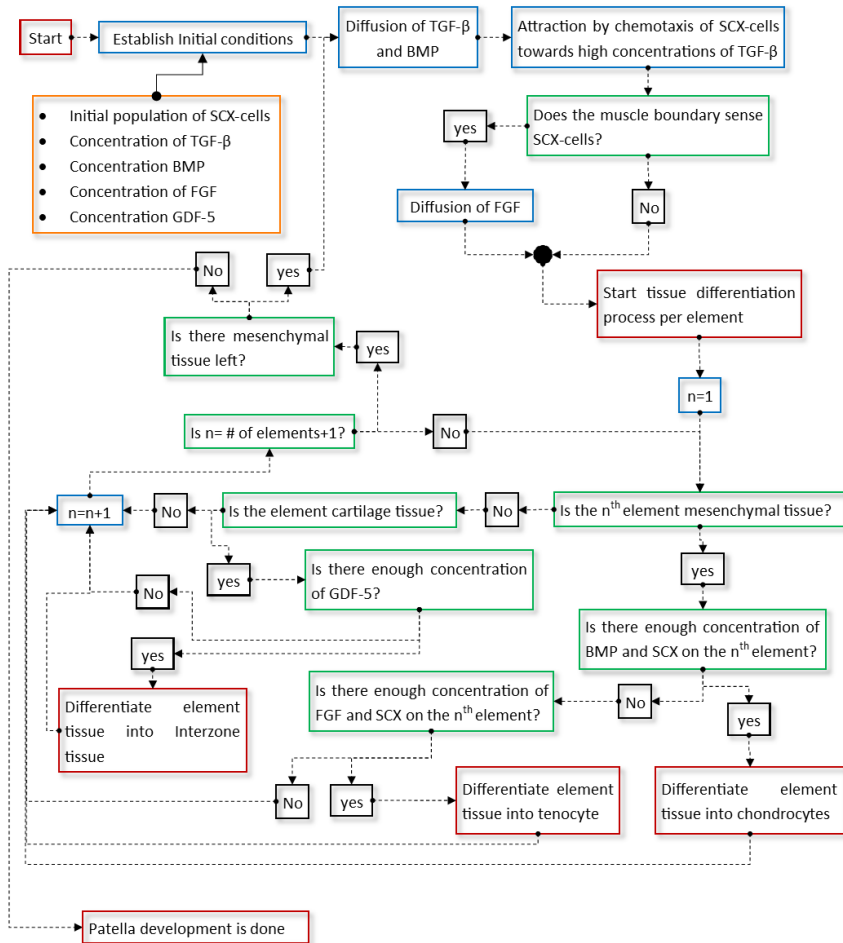


Fig. 4-4 General algorithm that developed to model the events occurring according to the Theory I.

4.2.2.1. Mathematical model: Molecules

4.2.2.1.1. Scx-cells

Initially, a domain with Scx-expressing cells is defined where the tendon will be formed [131] (Fig. 4-3). Then, these cells will be attracted towards high concentration of TGF-β by a chemotaxis process.

Therefore, the Scx-cells will migrate toward the bone and the muscle ends (Fig. 4-2 and Fig. 4-3). The concentration of cells (per volume unit) follow a chemotactic model that will depend on the concentration of the chemoattractant (TGF- β). Eq. 4-1 describes the temporal evolution of Scx-cell density as a function of a diffusion and chemotaxis process.

$$\frac{\partial b}{\partial t} = \nabla \cdot [(\mu(s_{at}(x, t))\nabla b(x, t)) - (\chi(s_{at}(x, t))b(x, t)\nabla s_{at}(x, t))] + g(b(x, t), s_{at}(x, t)) \quad \text{Eq. 4-1}$$

where $b(x, t)$ is the Scx-cell density population; $s_{at}(x, t)$ is the concentration of the chemical attractor (TGF- β); $\mu(s_{at}(x, t))$ is the diffusion coefficient of the Scx-cells; $\chi(s_{at}(x, t))$ is the chemotactic coefficient; and $g(b(x, t), s_{at}(x, t))$ is the cell proliferation and death rates.

4.2.2.1.2. TGF- β , BMP, FGF & GDF-5

The attractant chemical (TGF- β) and the other molecules (BMP, FGF and GDF-5) followed a diffusion model as described in (Eq. 4-2).

$$\frac{\partial s}{\partial t} = D_i \nabla^2 s(x, t) \quad \text{Eq. 4-2}$$

In this case, $s(x, t)$ is the concentration of the molecule in question (TGF- β , FGF, BMP and GDF-5); D_i is the diffusion coefficient for the molecule i within the developing tendon or cartilage, with $i =$ TGF- β , FGF, BMP and GDF-5. A summary of the diffusion rates is in (Appendix B). It must be remarked that these values were

obtained by trial and error to match the molecular behavior reported in the literature. Additionally, Table 4-1 summarizes the relationship between molecules, cells and tissues.

Table 4-1 Relation between molecules and tissue or cell type for the model developed for theory I.

	<i>Scx-cells</i>	<i>Cartilage-patella</i>	<i>Cartilage-bone</i>	<i>Tendon</i>	<i>Muscle</i>
<i>TGF-B</i>	Attraction towards high concentration [132,133]	Low diffusion	Expressed by the tissue [132,133]	---	Expressed by the tissue [132,133]
<i>FGF</i>	Differentiation to tenocytes [132,133]	Low diffusion	Low diffusion	Induces the formation of tendon tissue [132,133]	Expressed by the tissue, once the tissue detects Scx-cells [132,133]
<i>BMP</i>	Differentiation to chondrocytes [132,133]	Low diffusion	Expressed by the tissue [132,133]	Induces the formation of cartilage (patella) tissue [134]	---
<i>GDF-5</i>	---	Induces interzone onset [50-52]	Induces interzone onset [50-52]	---	---

TGF- β : Secreted by the bones and the muscle, attracts the Scx-cells towards the bones and the muscle.

FGF: Secreted by the muscle, induces the differentiation of Scx-cells into tenocytes.

BMP: Secreted by the bones, induces the differentiation of Scx-cells into chondrocytes.

GDF-5: Joint marker, induces the split of the forming patella from the femur.

4.2.2.2. Tissue differentiation

The model takes into account that a tissue changes its state when the concentration of a certain molecule achieves a threshold concentration (b_c^{Th} , S_{BMP}^{Th} , S_{FGF}^{Th} and S_{GDF-5}^{Th}) (Table 4-2). The thresholds have been chosen through an iterative process, since they are not reported in the literature. These values are summarized Appendix B. Subsequently, a cellular automaton-like (CA-Like model) was used to regulate the tissue-state based on the concentration of a certain molecule within the tissue.

Concentrations of Scx-cells and BMP molecules induces the differentiation of mesenchymal tissue to chondrocytes (*i.e.*, cartilage tissue), whereas concentrations of Scx-cells and FGF induces the differentiation of mesenchymal tissue to tenocytes (*i.e.*, tendon tissue). Additionally, high concentration of GDF-5 in cartilage tissue induces the formation of the interzone between the femur and the future patella.

Table 4-2 Molecule and threshold (Th) levels involved in the tissue differentiation. The threshold values are specified in the Appendix B.

Original Tissue	Molecules	New tissue	Concentration threshold parameters
Mesenchymal	Scx-cells & BMP	Cartilage	b_c^{Th} & S_{BMP}^{Th}
Mesenchymal	Scx-cells & FGF	Tendon	b_c^{Th} & S_{FGF}^{Th}
Cartilage	GDF-5	Interzone	S_{GDF-5}^{Th}

4.2.2.3. Geometry and boundary conditions

We developed a simple geometry of the forming knee joint (Fig. 4-5). The geometry is based on the study of Sarin *et al.* [114], where a two-dimensional finite element analysis (FEA) was developed to determine the stress history of a developing sesamoid. The radius of the

condyle was considered as 4 mm and the thickness of the tendon as 1.75 mm (Fig. 4-5) [135]. Quadrilateral elements were used in the finite element model.

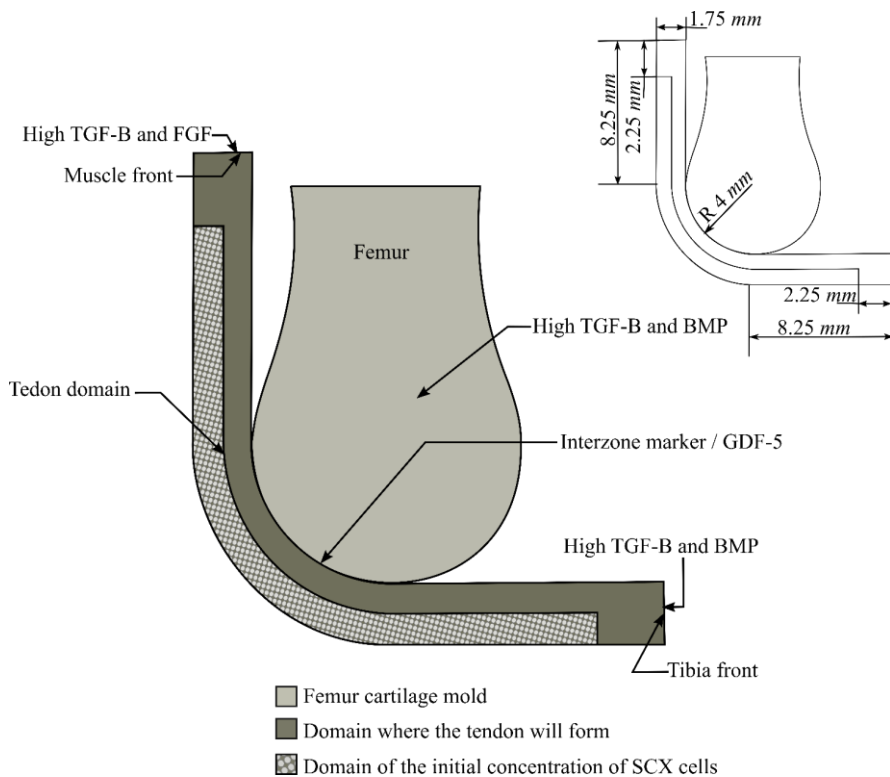


Fig. 4-5 Knee joint geometry employed for patella development study. Initial concentrations domains and mechanical boundary conditions for the model of the theory II.

The model consisted of three regions: the first region represents the femoral cartilage, a second one filled with Scx-cells, and a third one filled of mesenchymal cells. The tendon domain is formed by the second and third regions. The muscle end has a high concentration of TGF- β and FGF, whereas the tibia end and the femur have high

concentrations of TGF- β and BMP [132,133]. In contrast, the interzone marker (GDF-5), that diffuses at a low rate, is on the line shared by the femur cartilage and the domain where the tendon will be (Fig. 4-5).

4.2.3. RESULTS AND DISCUSSION

As shown in Fig. 4-6, the molecules TGF- β and BMP diffused and attracted the Scx-expressing cells towards the bones and muscle end. Once the muscle end detected the Scx-cells, the muscle cells expressed FGF; this molecule promoted the differentiation from mesenchymal cells (Scx-cells) into tenocytes, and the FGF gradient settled the direction of the collagen fibers of the tendon (Fig. 4-7). Simultaneously, BMP (which diffused from the femur bone) produced the differentiation from Scx-cells into chondrocytes (Fig. 4-7).

The tendon is formed from the muscle end and it gradually advanced to the tibia (Fig. 4-7, t=7). Also, a cartilaginous bone eminence developed at a distance from the femoral head, where there was enough concentration of BMP that induced the differentiation from Scx-cells to chondrocytes (Fig. 4-7, t=42): this was the beginning of the formation of the patella. This cartilaginous structure increased in size towards the femur until both cartilaginous structures (femur anlage and forming patella) merged (Fig. 4-7, t=60).

At the same time, the tendon continued developing until it reached and embedded the new cartilaginous formation: the patella (Fig. 4-7, t=50). The result of this process was a developed tendon with a cartilaginous structure, still attached to the femur, and embedded superficially within it (Fig. 4-7, t=60). Due to the presence of GDF-5,

an interzone was formed between the cartilaginous structure (patella-like) and the femur anlage (Fig. 4-7, $t=60$). This interzone allowed the detachment of the cartilaginous patella from the femur while still embedded within the tendon (Fig. 4-7, $t=117$). The final morphology of the femur and the patella would eventually adapt to mechanical loads due to muscle contractions, with matching articular surfaces. This model simulated only formation of the patella and not morphogenesis.

At some distance from the tibia end, a cartilaginous structure also started forming where there was enough concentration of BMP and Scx-cells (tibia eminence) (Fig. 4-7, $t=60$). The patellar tendon attached to the tibia via this structure (Fig. 4-7, $t=117$).

This theory was evaluated with different flexion angles of the leg, without modifying any other parameter. Flexion angles of 30° , 45° , 60° and 90° were considered (Fig. 4-8). The range of the angle changed the coincident area between the zone where the tendon will form and the distal head of the femur. The coincident area was smaller for 30° , 45° , and 60° , and larger for 90° . No patella-like structure was achieved with 30° and 45° ; only a little incipient patella at 60° ; and a complete patella-like structure was obtained with 90° . This outcome was possible since the coincident area is much smaller and proximal with 30° , 45° and 60° . Therefore, there is not enough diffusion of BMP so that the Scx-cells can differentiate into chondrocytes before the tendon develops completely.

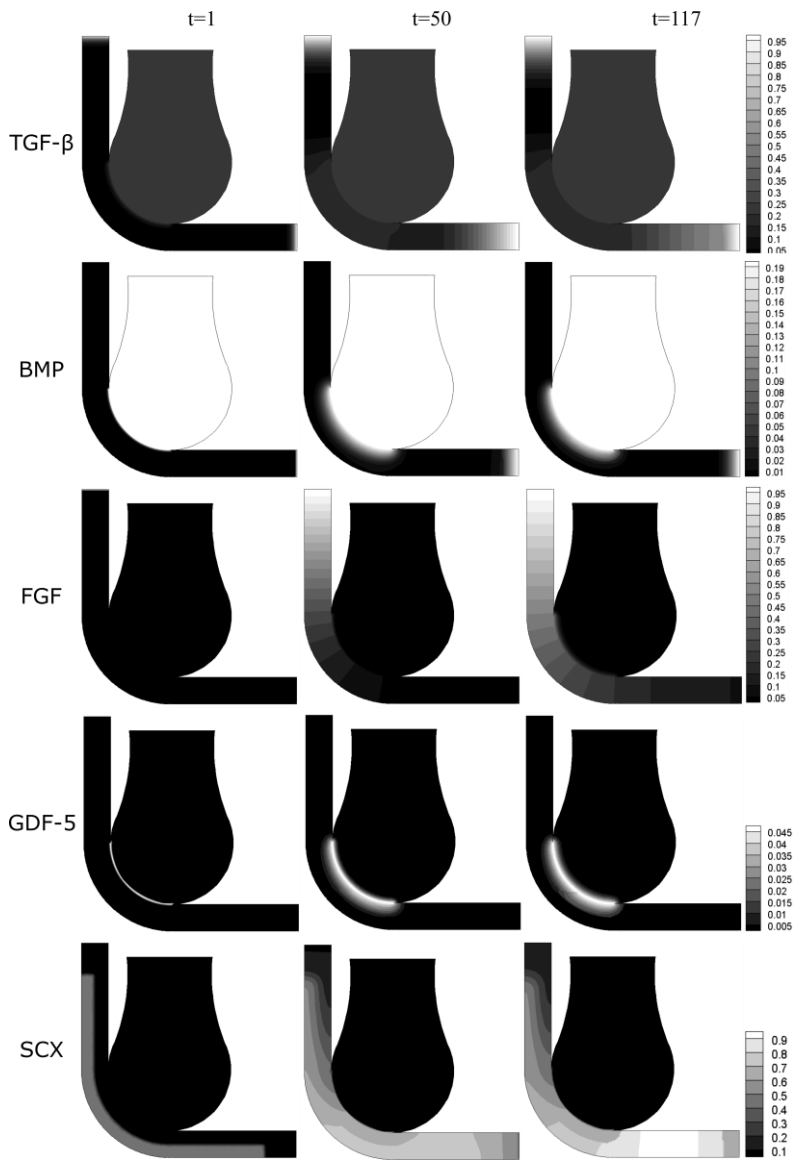


Fig. 4-6 Obtained distribution of the molecules (TGF-β, BMP, FGF, GDF-5) and Scx-cells during patella development.

The bar scale shows the concentration of each molecule (TGF-β, BMP, FGF, GDF-5) in ng/ml, whereas in the bottom of the image is shown the Scx-cells concentration per volume unit (cells/ml) involved in the process of patella development. Time: t=1, 50, 117.

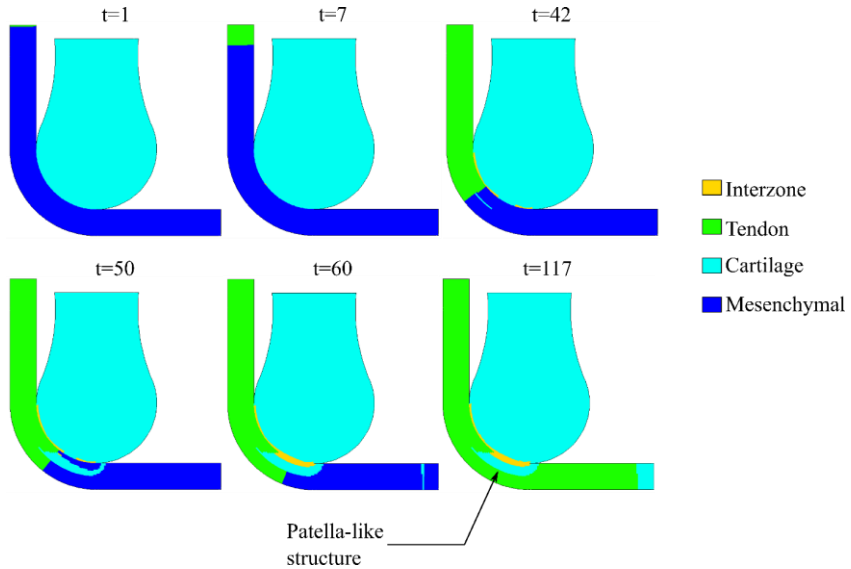


Fig. 4-7 Obtained tissue differentiation through the time of patella development. At t=7 the tendon (green) starts developing from the muscle end. By t=42 an incipient of the developing patella can be noticed. The patella keeps growing from towards the femur head (t=60). By the end of the simulation (t=117) the patella-like structure and tendon are completely formed

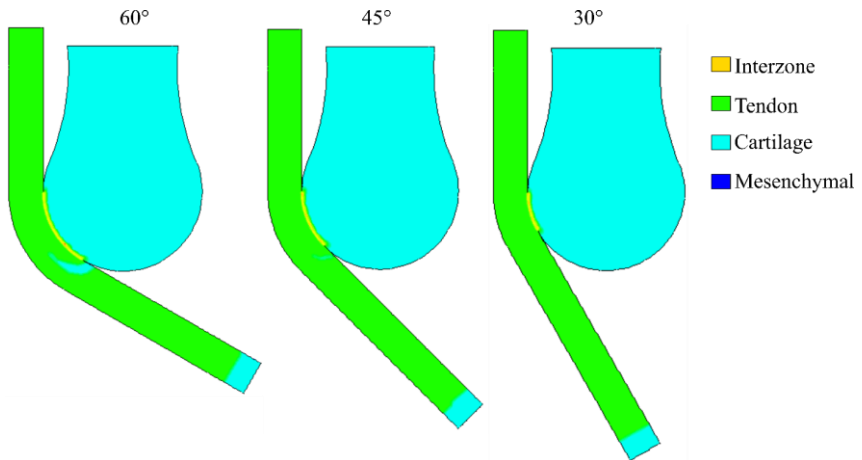


Fig. 4-8 Patella development: tissue differentiation for the biochemical model at different angles (60°, 45° and 30°). For knee flexion angles different than 90°, the patella developed smaller (60°) or did not develop at all.

The results obtained with this theory for the 90° model were coherent with the histological observations made by Eyal *et al.* [117]. Additionally, a patella-like structure embedded superficially within the tendon was obtained just by considering the biochemical factors implicated in the tendon and the eminence development (Fig. 4-7). This indicates that the patella onset might be highly influenced by the phenomenon surrounding tendon development. Hence, it might be possible that the patella onset is a consequence of a biochemical process, without any biomechanical influence. This theory could be supported by the fact that the absence of the patella in the knee joint does not affect its functionality [136].

4.3. THEORY II: MECHANICAL THEORY

The mechanical stimuli play a crucial role in tissue differentiation [7,137]. Although, according to previous studies, when the muscular activity was inhibited in embryos, the patella was smaller than in control animals [138]; therefore, the mechanical conditions of the forming tendons might create a favorable environment for the development of the patella [114,117,121,139].

The tendon is a fibrous or dense connective tissue composed by bundles of parallel fibers of type I collagen, which helps with the role of mediating movement [140]. According to the theory proposed by Carter *et al.*, [7], if we have fibrous tissue (such as tendon) under high compressive hydrostatic stress (with low principal tensile strain), it may differentiate from fibrous tissue to cartilage (Fig. 4-9). This new tissue (within the tendon) will be the sesamoid bone: the patella.

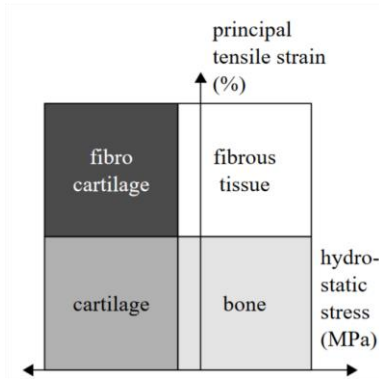


Fig. 4-9 Diagram of the mechanoregulatory model proposed by Carter *et al.*, (1998) [7]. Modified from [141]

4.3.1. MATHEMATICAL MODEL

Initially, a newly formed fibrous tendon wrapped around the distal end of the femur was assumed. The mechanical load was applied on the quadriceps side of the tendon. The tendon was modeled as a composite material: matrix and fibers. The fibers were modeled as an orthotropic material and they were oriented following the longitudinal axis of the tendon.

The model followed the momentum equation that determines the internal stresses of the body (Eq. 4-3):

$$\nabla \cdot \boldsymbol{\sigma} + \mathbf{b} = \mathbf{0} \quad \text{Eq. 4-3}$$

where $\boldsymbol{\sigma}$ is the stress tensor, and \mathbf{b} is the body forces. The stresses and strains were related through the constitutive equation, which in general form is given by (Eq. 4-4):

$$\boldsymbol{\sigma} = \mathbf{D}\boldsymbol{\varepsilon} \quad \text{Eq. 4-4}$$

where \mathbf{D} is the matrix of elastic constants, and $\boldsymbol{\varepsilon}$ is the strain tensor. Since the tendon was composed of a matrix and fibers, then, the relationship between stress and strain is given by (Eq. 4-5):

$$\boldsymbol{\sigma} = \boldsymbol{\sigma}_m + \boldsymbol{\sigma}_f = (\mathbf{D}_m + \mathbf{D}_f)\boldsymbol{\varepsilon} = \mathbf{D}_m\mathbf{B}\mathbf{u} + \mathbf{D}_f\mathbf{B}\mathbf{u} \quad \text{Eq. 4-5}$$

where \mathbf{D}_m and \mathbf{D}_f are the matrix of elastic constants for the matrix and the fibers, respectively. The matrix was considered as an isotropic material; therefore, the term \mathbf{D}_m is defined as (Eq. 4-6)

$$\mathbf{D}_m = \frac{E}{1 - \nu^2} \begin{bmatrix} 1 & \nu & 0 \\ \nu & 1 & 0 \\ 0 & 0 & (1 - \nu)/2 \end{bmatrix} \quad \text{Eq. 4-6}$$

Whereas \mathbf{D}_f , for a link for fiber oriented on the horizontal axis, is defined as (Eq. 4-7):

$$\mathbf{D}_f\mathbf{B} = \begin{bmatrix} 1 & 0 & -1 & 0 \\ 0 & 0 & 0 & 0 \\ -1 & 0 & 1 & 0 \\ 0 & 0 & 0 & 0 \end{bmatrix} \quad \text{Eq. 4-7}$$

The stress inside the tendon was evaluated at different flexion angles: $\theta = 110^\circ, 90^\circ, 60^\circ, 45^\circ$, and 30° (Fig. 4-10). In order to facilitate the comparison of results, each case ($\theta = 110^\circ, 90^\circ, 60^\circ, 45^\circ$, and 30°) had the same number of finite elements; in other words, there was a correspondence of finite elements between cases.

4.3.2. GEOMETRY AND BOUNDARY CONDITIONS

The geometry of this model was a simplified version of a knee joint in formation (Fig. 4-10) based on similar works [114,139]. The geometry considers a tendon wrapped around the femur distal head. The thickness of the tendon was 1.75 mm and the radius of the bone was 4.0 mm [135].

The mechanical load was applied on the tendon as 1 mm displacement, simulating the contraction force of the quadriceps, whereas the other end of the tendon (attachment with the tibia) was fixed (Fig. 4-10). The nodes on the line in contact with the femur could only move through the contact line (Fig. 4-10).

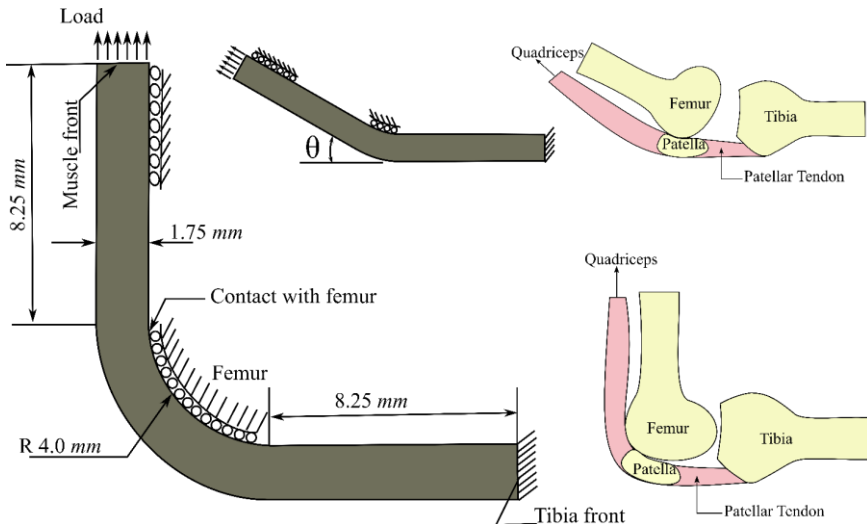


Fig. 4-10 Schematic representation of the geometry and boundary conditions. Mechanical boundary conditions for the model of the theory II.

4.3.3. MATERIAL PROPERTIES AND TISSUE DIFFERENTIATION

The differentiation from tendon tissue to cartilage was assumed as a function of hydrostatic stress and tensile strain following Carter *et al.* [7]. When the hydrostatic stress and the principal tensile strain on the fibrous tissue (tendon) reached a specific threshold $-\sigma_{hyd}^{cart}$ (Appendix B)- the tissue differentiated into cartilage. Table 4-3 summarizes the mechanical properties of the biological tissues used in this work. All the properties were obtained from the literature [114,142]. The properties of the tendon depended on the direction of the tendon collagen fiber.

Table 4-3 Tissue properties

<i>Tissue</i>	<i>Poisson</i>	<i>Young's modulus [MPa]</i>	<i>Reference</i>
<i>Cartilage</i>	0.497	6.1	[8]
<i>Tendon (matrix)</i>	0.4	6.1	[114]
<i>Tendon (fiber)</i>	0.4	800	[114]

4.3.4. RESULTS AND DISCUSSION

This theory postulates that the patella bone is formed due to high hydrostatic stress and low tensile strain on specific regions of a fibrous tissue, such as the tendon. The results of all angles of flexion of the leg were projected on the domain at 90° to facilitate comparison of the stress distributions (Fig. 4-11).

Considering that the understanding of the embryonic movement is limited, three different scenarios were modeled in which the effect of each leg angle was averaged. These scenarios were designed in order to differentially weigh the contribution of each angle to represent the time spent in that angle. The weightings for the angles of 30°, 45°, 60°, 90°

and 110° for the three cases were as follows: 1) 5%, 10%, 15%, 25% and 45% (weighting high flexion), 2) 60%, 25%, 9%, 5%, and 1% (weighting low flexion angles); 3) 1%, 5%, 9%, 25% and 60% (heavily weighting high flexion).

The elements which had a compression stress above $\sigma_{\text{hyd}}^{\text{cart}}$, were differentiated into cartilage (Fig. 4-12). In each case the size and shape of the patella were different; the smallest patella occurred when weighting for the smallest angles.

The results obtained with this model also showed the development of a patella-like structure embedded within the tendon. The size of the structure depended on the flexion angle; in other words, the angle determined the mechanical load (hydrostatic pressure) in the tendon. This may imply that the mechanical conditions that surround the newly formed tendon might influence the patella development. For instance, different studies have noticed that several years after the excision of the patella, some fibrocartilage or even bony islands appear in the former site of the patella [136,143,144]. This could indicate that the wrapping (mechanical environment) of the tendon over the distal femoral head generates the necessary mechanical conditions for the patella onset

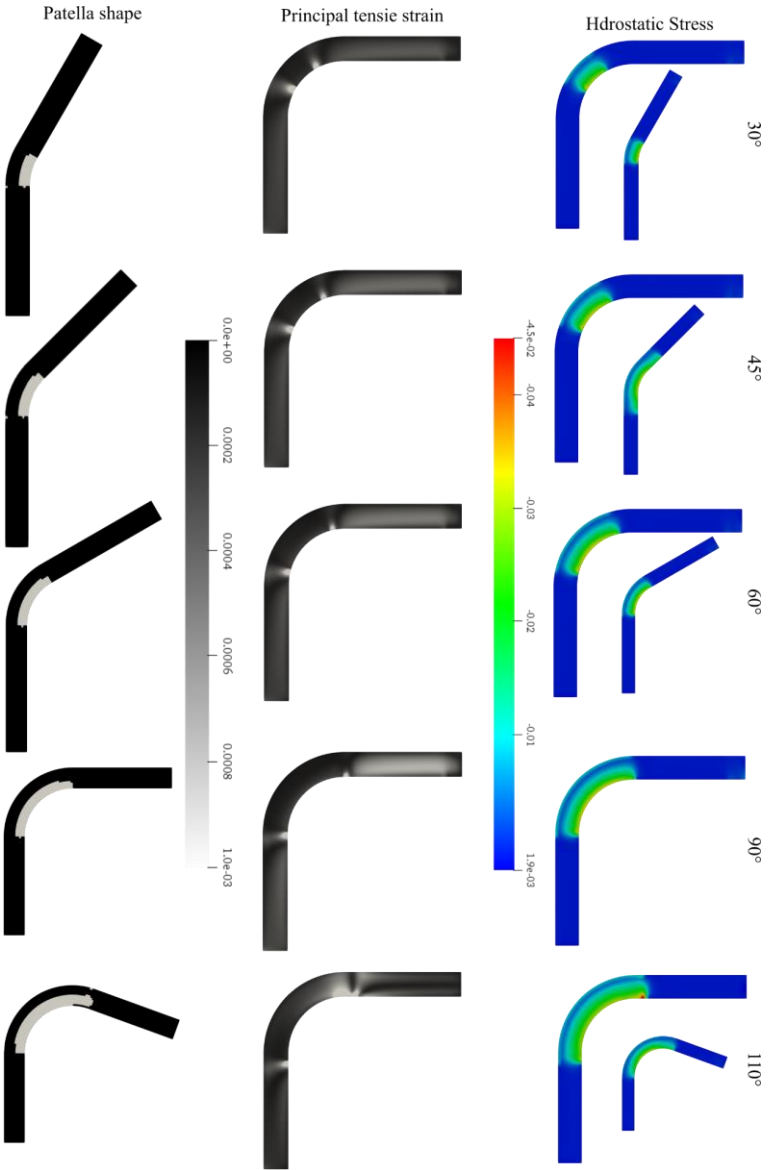


Fig. 4-11 Results obtained by the simulation for the different angles: stress, tensile strain and patella shape.
 Up: Hydrostatic stress distribution on the tendon at different angles 30°, 45°, 60°, 90° and 110°. The value of the hydrostatic pressure was projected on the 90° domain for comparison. Middle: principal tensile strain for 30°, 45°, 60°, 90° and 110°. Bottom: the obtained patella shape, where the elements that have the hydrostatic stress above the tissue differentiation threshold $\sigma_{h^{ydt}}^{crit}$.

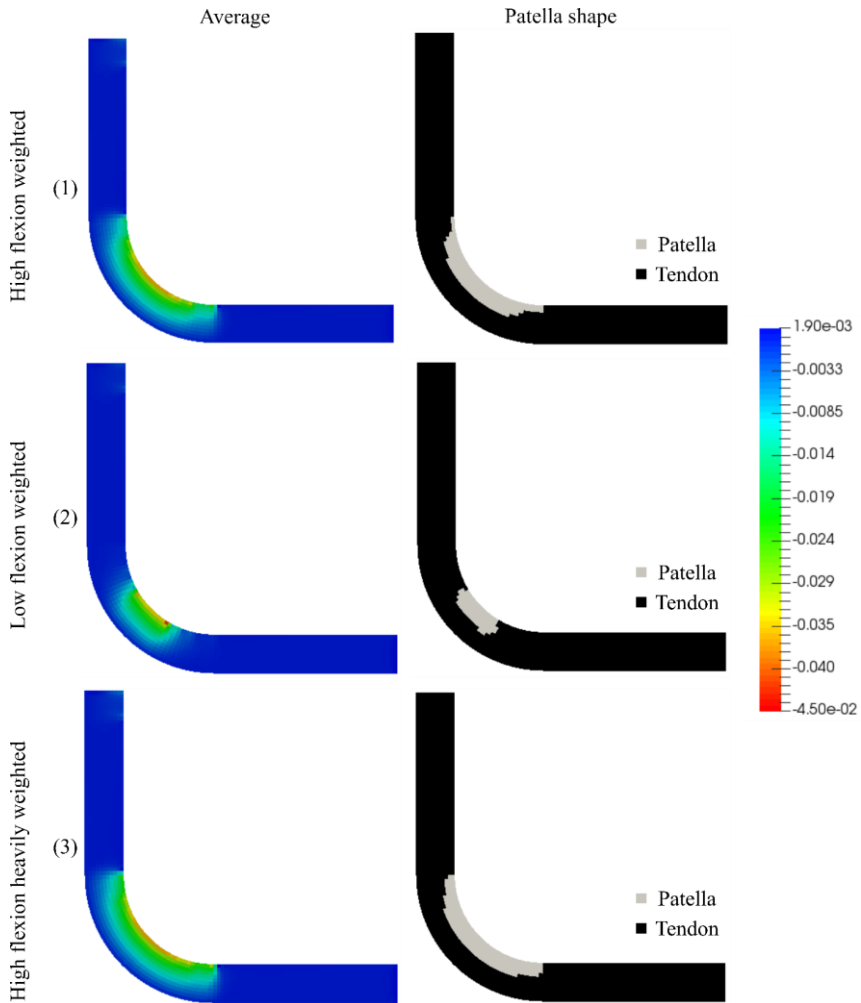


Fig. 4-12 Results obtained by the simulation for the average hydrostatic stress and patella shape. **Left:** Average hydrostatic stress for the three analyzed cases. (1) 5%, 10%, 15%, 25% and 45% (weighting high flexion); (2) 60%, 25%, 9%, 5%, and 1% (weighting low flexion angles); (3) 1%, 5%, 9%, 25% and 60% (heavily weighting high flexion) for the 30°, 45°, 60°, 90° and 110° respectively. **Right:** Patella shape: where the elements that have the hydrostatic stress above the tissue differentiation threshold σ_{hyd}^{cart} .

4.4. THEORY III: TOPOLOGICAL OPTIMIZATION (TO)

This theory is also based on mechanical stimuli and its influence on tissue differentiation. It is based on the fact that tissues adapt to their

stress and strain environment; therefore, TO might be suitable to explain this adaptation. TO can be applied in tissue remodeling, since it iteratively redistributes the material in a design domain determining an optimal material arrangement or tissue type [125]. Specifically, TO allocates denser material (cartilage) to regions under relatively high strain energy and allocates a less dense material (tendon) to zones with a low strain energy. This adaptation process can be characterized as a self-enhancing system [122], with the objective of minimizing tendon strain. Therefore, articular surface wear will be reduced due to the low relative movement between the distal femoral head joint surface and the tendon.

As an initial condition, it was considered that the tendon was already formed and loaded. A two-dimensional FEA analysis based on the algorithm proposed on Sigmund [145], was performed. The algorithm is based on the “power-law approach” or SIMP approach (Solid Isotropic Material with Penalization) [145]. This approach assumes that the material properties are constant within each element of the design domain, whereas the relative material densities of the elements are the variables [145]. The density is usually considered as a design variable, so it could take values between 0 and 1, with 0 representing void and 1 representing solid [146]. Thus, the relation between the elastic modulus and the relative material density is given in Eq. 4-8:

$$E(x) = \rho(x)^p E^o \tag{Eq. 4-8}$$

where E^o is the Young's modulus of the material in solid state, when $\rho = 1$. In addition, the penalization power parameter is $p=3$ as recommended by Sigmund [145].

The aim of this optimization process is to minimize the strain energy in order to find the relative material densities of the elements (in a design domain). Then, the objective function and constraints can be expressed as follows (Eq. 4-9):

$$\begin{aligned} \min_{\rho} C(\rho, \mathbf{u}) &= \mathbf{U}^T \mathbf{F} && \text{Eq. 4-9} \\ \text{s. t.:} & \left. \begin{aligned} \mathbf{K}(\rho) \mathbf{u} &= \mathbf{F} \\ \frac{V(\rho)}{V_o} &= f \\ 0 < \rho_{min} &\leq \rho(x) \leq 1 \end{aligned} \right\} \end{aligned}$$

where C is compliance, ρ is density, \mathbf{F} is the load vector, \mathbf{u} is the global displacement vector, V_o is the initial domain (domain constraint) and f is the volume fraction. The density was relaxed to have any value from 0 to 1, being the lower bound non-zero to avoid singularities.

The global stiffness matrix $\mathbf{K}(\rho)$ in Eq. 4-9 is calculated by summing up the stiffness matrices of all the elements, which depend on the elemental value of the density ρ_e Eq. 4-10:

$$\mathbf{K}(\rho) = \sum_{e=1}^{Nel} \mathbf{K}_e(\rho_e) = \sum_{e=1}^{Nel} \int_{\Omega_e} \mathbf{B}^T \mathbf{D}(\rho_e) \mathbf{B} d\Omega \quad \text{Eq. 4-10}$$

where $\mathbf{K}_e(\rho_e)$ is the stiffness matrix of the element, \mathbf{B} is the shape function derivatives, and $\mathbf{D}(\rho_e)$ is the constitutive matrix which depends on the material density. Sensitivities of the objective function and volume constraint with respect to ρ_e are calculated as follows (Eq. 4-11 and Eq. 4-12):

$$\frac{\partial C}{\partial \rho_e} = -\mathbf{u}_e^T \frac{\partial \mathbf{K}_e}{\partial \rho_e} \mathbf{u}_e = -p \rho_e^{p-1} \mathbf{u}_e^T \mathbf{K}_e^0 \mathbf{u}_e \quad \text{Eq. 4-11}$$

$$\frac{\partial V}{\partial \rho_e} = \int_{\Omega_e} dV \quad \text{Eq. 4-12}$$

A heuristic updating scheme for the design variable is formulated as (Eq. 4-13):

$$\rho_e^{new} = \begin{cases} \max(\rho_{min}, \rho_e - m) & \text{if } \rho_e B_e^\eta \leq \max(\rho_{min}, \rho_e - m), \\ \rho_e B_e^\eta & \text{if } \max(\rho_{min}, \rho_e - m) < \rho_e B_e^\eta < \min(1, \rho_e + m), \\ \min(1, \rho_e + m) & \text{if } \min(1, \rho_e - m) \leq \rho_e B_e^\eta, \end{cases} \quad \text{Eq. 4-13}$$

where m is a positive moving limit, η is the numerical damping coefficient and B_e is the optimality condition which is calculated as (Eq. 4-14):

$$B_e = \frac{\frac{\partial C}{\partial \rho_e}}{\lambda \frac{\partial V}{\partial \rho_e}} \quad \text{Eq. 4-14}$$

4.4.1. GEOMETRY AND BOUNDARY CONDITIONS

The same geometry and boundary conditions of Theory II (Theory II: Geometry and boundary conditions) were used in this model.

4.4.2. MATERIAL PROPERTIES

The tissue properties of the initial domain (tendon and fibers) are summarized in (Table 4-3) (Theory II: Material properties and tissue differentiation). The properties of the tendon depended on the direction of the tendon collagen fibers.

4.4.3. RESULTS AND DISCUSSION

In this third theory, the appearance of the patella is due to a TO process in the recently formed patellar tendon. Different angles were tested for this model; however, we only obtained coherent results (formed patella) with 90° and 110°. For these angles, we observed a high-density zone close to the usual patella position. Specifically, for the 90° case, the shape of the high-density zone is more consistent with reality (Fig. 4-13). This suggests that the mechanical environment that surrounds the tendon may affect the patella and its development.

Some studies have uncovered that quite a long while after the extraction of the patella, islands of fibrocartilage, or even bone show up in the previous site of the patella. [143,144]. These islands might be the result of the optimization process that the human body undergoes due to the abnormal conditions after the patella excision. The strain energy is reduced in this process, which allows the tendon to have small displacements and deformations.

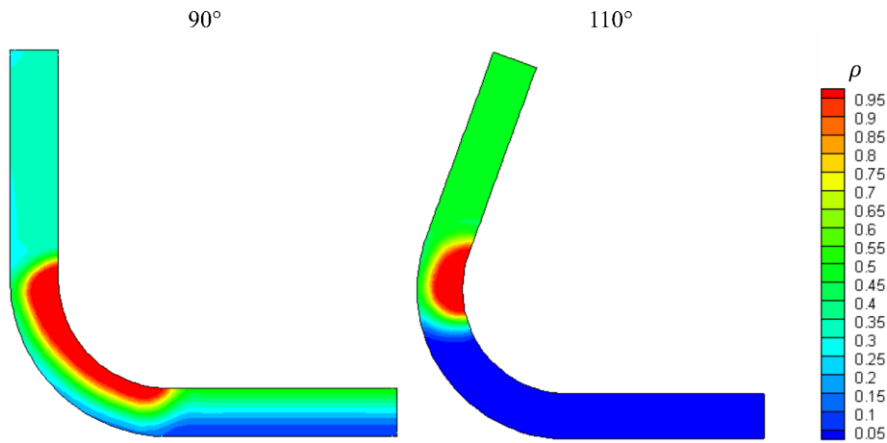


Fig. 4-13 Results obtained by the simulation through the TO algorithm. Density values for the patellar tendon at 90° and 110°.

4.5. NUMERICAL SOLUTION FOR THE THREE THEORIES

All the equations of the three theories were solved with FEM and implemented in a user Subroutine in Fortran and solved with ABAQUS 6.10 (Dassault Systèmes USA, Waltham, MA). Both mesh and time-step were refined until further refinement no longer yielded noticeable improvements in all models.

4.6. GENERAL DISCUSSION

We developed three models to simulate the process of patella formation according to three different theories. The aim was to evaluate, individually, the potential influence of each of these theories in the patella onset. The first theory considers the biochemical interactions that are present during the patellar tendon formation, while the second and third theories are based on the mechanical stimuli that

the newly developed patellar tendon goes through. All three models used a simplified knee geometry, considering both the tendon and the femur for the biochemical-based theory (Fig. 4-5), and only the tendon for the mechanical-based theories; the femur was assumed as a rigid body.

The biochemical model is a conceptual model of the development of the patella based on the theory proposed by Eyal *et al.* [117], where the patella initially forms as a bone eminence, involving Scx-cells whose differentiation is regulated by TGF- β and BMP-4. The separation of the patella from the femur is regulated through the interzone molecule GDF-5. The simulated molecular distribution agrees with that previously shown [117], where at the end a patella-like structure embedded superficially within the tendon was obtained. We assumed the diffusion rates of the molecules based on an iterative process, since they are not reported in the literature and are particularly difficult to measure.

Additionally, we also simulated the biochemical model when the leg was extended at different angles (30°, 45°, 60°, 90°). The latter was to establish how the position of the leg affected the development of the patella, in the case that only biochemical factors influenced the formation of this sesamoid bone. When the angles of the leg were modified to 30°, 45° or 60°, the region through which BMP diffused from the femur distal end to the tendon region was smaller. Consequently, the patella obtained was either not significant or null (Fig. 4-8). This may be evidence, according to this theory, that having an angle close to 90° is necessary to form the patella.

On the other hand, the first mechanical model is based on the theories which state that mechanical stimuli play a crucial role in tissue differentiation. Particularly, this model is built upon Carter's theory [7], in which hydrostatic compression and low principal strain are stimuli that induce fibrous tissue differentiation into cartilage. It was assumed that the constant movements of the fetus (distinct knee angles) stimulate the concentration of high compression loads on some areas of the newly formed tendon. The latter induces the differentiation of the tendon cells into cartilage, on those high hydrostatic stress zones. Therefore, a cartilage structure is formed embedded within the tendon, which later will ossify and become the patella bone.

Following this last theory (the mechano-differentiation model), a patella-like structure was obtained. When different flexion angles of the leg were evaluated, we observed an influence on the size of the patella (Fig. 4-11). Additionally, a patella-like structure was obtained when the hydrostatic stress was averaged considering all the angles. A different predominant angle for each case was evaluated: weighting high flexion, weighting low flexion angles and heavily weighting high flexion. If the predominant angle was large, a big patella was obtained, whereas if the predominant angle was small, a short patella was obtained (Fig. 4-12).

The last evaluated theory was based on the application of TO, which is also feasible to explain the onset of sesamoid bones such as the patella. In this case, we assume that the tissue can adapt to its mechanical environment in a way that its strain energy is reduced. Different angles were also evaluated. However, the outcome was not as

expected for smaller angles since no patella-like structure was obtained. Nevertheless, a patella-like structure was achieved with angles of 90° and 110°. The shape of the obtained patella is remarkably similar, especially with an angle of 90°. The results of this model imply that the patella might allow reducing the strain energy and, consequently, the displacements and deformations of the tendon. These results also imply that the patella and the femur articular surface have a low relative movement. This is due to the low deformation of the tendon, protecting somehow the femur articular surface from wear.

A patella-like structure was obtained for most of the knee flexion angles in all the theories we have evaluated. Our results show that tissue remodeling and adaptation, based on Carter's theory or on TO, could be responsible for the patella onset. The shape, position and size of the patella would depend on the flexion angle of the leg, and the time that the leg spends on each position, obtaining a larger-sized patella compared to the biochemical approach. However, there is not much evidence in the literature that can support the second and third theories. Some studies have shown that while limitation of movement (through drugs) on embryos affects the formation of the patella, it develops anyway, although small in size [138]. Therefore, the mechanical load may not be necessary for the appearance of the patella, but it may be necessary for its morphogenesis and maintenance. Hence, molecular factors and their interactions trigger the formation of the patella, as evidenced by molecular expression analyzed in histological slides [117]. These factors, applied through a computational model, were consistent with the results we obtained. However, since only the

limitation of the movement does not guarantee that there are no hydrostatic stresses on the tendon, more tests should be run in which only biochemical factors influence the development of the tendon and the patella. It is also possible that these mechanisms are redundant and that both influence the patella onset

This study proposes a simplified mathematical model of the regulatory mechanisms that might influence the formation of the patella bone. Each theory was evaluated separately to observe its outcome and the likelihood of its influence on the patella onset. The results obtained were consistent, and patella-like structures were obtained in most cases. Nevertheless, the literature suggests that the patella onset could be triggered by biochemical factors during tendon development [117]; according to our results, this approach does lead to a patella-like structure. Also, it is certain that the mechanical environment must affect the patella development. However, this environment might affect it mostly after the tendon is formed by helping the patella to obtain its final shape and maintain its structure.

This work is a first approximation on understanding the process of the development of the patella. It should be considered that these models had several simplifications, such as that they were all two-dimensional models, that the geometry was a simplified knee joint, that all the materials were modeled as linear elastic, and that the molecular concentrations, since they are difficult to measure and there are no reports in literature, were established through an iterative process. Even though of the simplifications, we obtained results that might explain the onset of the patella and would help in the proposition of new points of

view that might explain the patella onset. Furthermore, these models could provide new insight and guidelines of experimentation, and of course, new mathematical models as well. However, a combination of the theories evaluated in this study is suggested for future works, so that the patella onset is determined due to biochemical factors, and thereafter the mechanical loads may regulate its shape and maintenance. The exact instant and way that mechanical loads affect the patella development should be an issue to evaluate in further models, as well as the dynamic movement of the knee during the development.

Chapter 5. CARTILAGE

REGENERATION

5.1. INTRODUCTION

Articular cartilage has a limited ability to repair itself, therefore, it is common to find pathologies related to articular cartilage injuries or aging. This may be since the articular cartilage is an avascular tissue and has a low capacity to regenerate itself. Hence, in a lesion of the articular cartilage, a scar composed mainly of fibrocartilage is frequently generated, which is a tissue with mechanical properties inferior to hyaline cartilage that degrades over time [1,147].

Lesions in the articular cartilage have different causes such as intra-articular fracture, progressive degradation of OA, or osteochondritis dissecans, among others [3,148,149]. Lately, the damage that suffers the subchondral bone has received increasing interest for its role in joint injury, since changes of properties of the subchondral bone seems to mediate changes observed in OA, *e.g.* sclerosis reduces the shock-absorbing capability of the subchondral bone and increases the risk of shear-induced tensile failure of the articular cartilage [29]. Moreover, due to the rich vascularization and innervation of the subchondral bone, it is a source of inflammatory mediators, which are associated with the degradation of deeper layers of articular cartilage [29]. On the architectural level, can be observed

the emerging of microcracks within the subchondral bone, encourage the rapid bone remodeling as an excessive bone formation, which may result in bone sclerosis.

Proposed treatments for OA range from symptomatic, with analgesics and anti-inflammatory, to more invasive ones that not always can be used or have no good results, *e.g.*, microfracture, endochondral transplantation, periosteum or perichondrium, cellular transplantation (chondrocytes or stem cells); being the last resort arthrodesis treatments, or total replacement of the joint [150]. In any case, it is preferable not to reach the last resort and to preserve the original function of the joint through the regeneration of the articular cartilage rather than the replacement of the joint or an arthrodesis, especially in young patients.

The osteochondral grafts is the most effective of the articular cartilage regeneration treatments [1,2]. Being an autologous implant, this treatment avoids the immunity response [1]. However, these grafts have disadvantages: patients must go through two surgeries, new defects are created, they are not appropriate to treat large articular defects, they do not fuse with the adjacent articular cartilage therefore they become unstable with time, and normally the new tissue is fibrocartilage and not hyaline cartilage [1]. In the end, 10-20% of cases need to be re-operated in the short term, and the percentage increases in the long term [2].

The articular cartilage degenerative problem is part of the scope of tissue engineering. It is necessary to search for clinical advances in cartilage regeneration, which are less invasive, in both mild and acute

joint injuries. In tissues such as bone or skin, repair techniques have been based on the use of implants obtaining good results [3]. In cartilage, based on the same techniques, they have used scaffolds, which have gained attention in the last two decades [3]. The scaffolds allow rapid filling of joint defects, providing a substrate where cells can anchor, while maintaining mechanical integrity.

More recently, the scaffold technic involves three mayor components: scaffold materials, cell proliferation or differentiation factors, and cellular sources [3]. Scaffolds can be made of both natural (*e.g.*, collagen) and synthetic materials [1,4,147,151–157]. Concerning the chondro-inductive growth factors, members of the TGF- β , insulin-like growth factor-1 (IGF-1) and specific members FGF family are considered. [1,3,157]. Regarding cellular sources, they include isolated autologous chondrocytes, multipotent stem cells, pluripotent stem cells and induced pluripotent stem cells [1,3,157]; however, scaffolds can also be used without cellular sources [4,147,158–160].

The use of scaffolds has the advantage that it facilitates the implant process being a less invasive process than the autologous osteochondral grafts [147]. However, it is difficult to replicate in a scaffold the specific conditions of the ECM [1,161]. Moreover, manufacture scaffolds with biophysical, biochemical, and structural characteristics similar to those of articular cartilage is a challenging problem [1,162]. Nevertheless, great steps have been taken in the development of biomaterials allowing them to maintain their integrity and support the mechanical loads to which the cartilage is subjected, in

this way, these biomaterials are capable of imitating the characteristics of healthy tissues [147,160,163,164].

Since 2010, researchers have increased the use of scaffolds without a cellular source [160]. The latter method has shown results similar to the scaffold/cell method, avoiding risks associated with cell manipulation (contamination of bacteria and phenotype loss during handling), and reduced costs [158–160,165,166].

Previous work in our group showed that when scaffolds/cell-free implants were used in a rabbit experimental model, hyaline cartilage was generated in the upper part of the scaffold by the third month after implantation [4,158,167]. The rapid growth of the superficial layer of the cartilage covered the scaffold while it was displaced to the subchondral bone [4]. The role of scaffolds is to ensure a propitious mechanical environment, which is an important factor to activate mechanisms of cellular proliferation and differentiation to chondrocytes [158,163]; mechanical feedback determines the behavior of cells on its shape, migration, division, differentiation and death [168]. It is in this mechanical relationship that computational models contribute to the study of the biomechanical environment of chondrocytes, evaluating difficult-to-reach aspects for experimental models [5]. In this way, computational models can provide a quantitative and qualitative evaluation of mechanobiological interactions while being fed with clinical or experimental parameters [6].

The biological computational models have been very useful to simulate pathologies, repair and recovery of tissues and organs, *e.g.*,

bone regeneration [7], bone growth [8], pattern formation [9–15], embryonic development [16], among others. For cartilage, various computational models have been developed for the articular cartilage of the knee [17–19] and the mechanobiology of articular cartilage under compression in confinement conditions [5]. Likewise, computational models have been evaluated to simulate the behavior of chondrocytes in 3D constructs [169–171], and the variables that should include the computational models of articular cartilage [18,116,163,172–175].

Taking into account the above, our interest is to propose and develop a simulation tool to predict the results of implanting polymer scaffolds within a defect in the articular cartilage, in order to evaluate their weaknesses and advantages. In this way, a deeper understanding of the processes involved in the regeneration of articular cartilage could be achieved. This computational model would provide insights into how this process develops and determine the appropriate mechanical conditions for cartilage regeneration, that can be difficult to obtain through experimental techniques.

5.2. MATERIALS AND METHODS

5.2.1. GEOMETRY AND MESH

A plain strain axisymmetric 2D geometry was developed to represent a simplify cartilage/bone/scaffold structure (Fig. 5-1). The total width of the domain was considered as 36 *mm*, large enough to prevent that the effect of the boundary conditions would not affect the

Cartilage regeneration

zone of the defect. The height of the structure was established at 8.3 mm, high enough in order to avoid that the boundary conditions at the bottom affects the zone of the defect. Due to the symmetry, only half of the geometry was considered, thus an 18 mm wide structure was modeled. Cartilage thickness was set to 1.0 mm, with a subchondral cortical bone layer of 0.3 mm (Fig. 5-1). A defect was modeled in the symmetry axis as a full depth cartilage defect and filled with an implant of 3.0 mm diameter. A perfect fit of the implant into the defect was assumed.

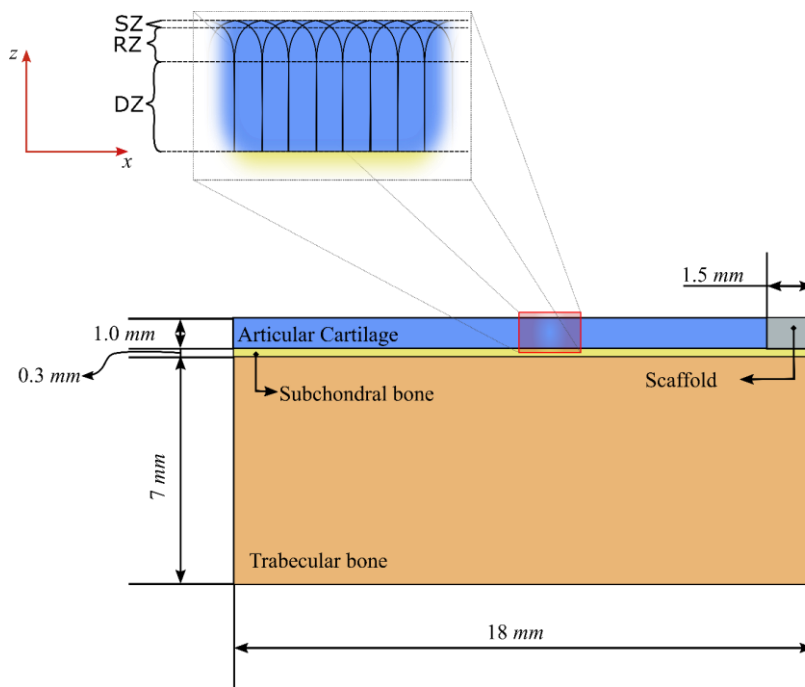


Fig. 5-1 Schematic representation of the 2D finite element geometry of the articular surface and subchondral bone, with the scaffold implanted.

The zoomed area shows a representation of the modeled collagen fibers. The Articular collagen zones are: Deep Zone (DZ), Radial Zone (RZ) and Superficial Zone (SZ).

The model was meshed using 4-node pore pressure plain strain elements with size ranging from 0.1mm to 0.4mm. All the equations were solved with FEM and implemented in a user element Subroutine in Fortran and solved with ABAQUS v6.10 (Dassault Systèmes). Both mesh and time-step were refined until further refinement no longer yielded noticeable improvements in all models.

5.2.2. BOUNDARY CONDITIONS

The normal stress and strain conditions for the subchondral and trabecular bone were established by applying load prior to the scaffold implantation. The nodes in the symmetry axis were fixed in the horizontal direction (Fig. 5-2), whereas the nodes on the lower part of the model were only allowed to move on the horizontal direction. Free fluid flow was applied by prescribed zero pore pressure at the free edges of the cartilage (top) and the implant (top) (Fig. 5-2).

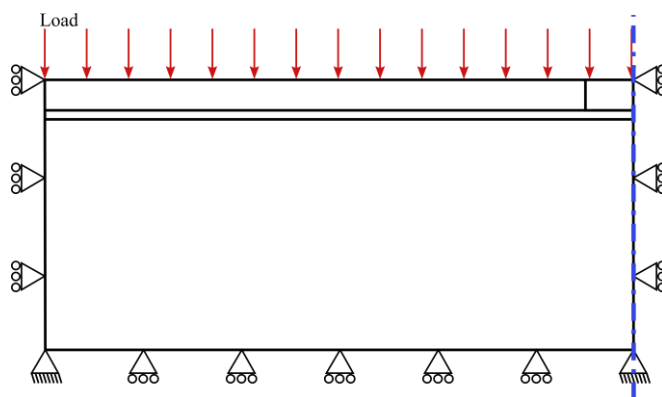


Fig. 5-2 Boundary conditions applied to the finite element model.

The right side (which is on the symmetry axis) was allowed to move on the vertical direction, the same was considered for the left side. The bottom was only allowed to move horizontally, and the cyclic load was applied at the top.

A unitary load was uniformly applied on the top of the cartilage. The load was applied as an oscillatory load with 1 Hz frequency until the values of fluid velocity (FV), stress and strain stabilize. It was assumed that the cartilage experiences this load each day of simulation.

5.2.3. MATERIAL MODELS

5.2.3.1. Cartilage Model

Articular cartilage consists of ECM divided into two phases: solid and fluid. The solid part contains mainly the ground substance that includes glycoprotein and proteoglycans (PGs) anchored to hyaluronic acid, and a fibrillar network made of collagen (type II) [176].

The mechanical response of the cartilage is highly influenced by its tissue composition and structure [177,178]. The collagen fibrillar network stabilizes the matrix expansion [177], and supports tension loads, but it has low resistance for compression due to its skinniness [176].

The collagen network is composed by a combination of large primary collagen fibrils and smaller ad disorganized secondary fibrils. For simplicity and computational savings, only the primary fibers were considered. As Benninghoff described (1925) [179], bundles of primary fibrils extend perpendicular from the subchondral bone, curving up close to the surface and gradually taking a horizontal course, leveling with the articular surface, and merging into the superficial layer [175,177,179,180] (Fig. 5-1). In the Deep Zone (DZ) (Fig. 5-1 & Fig. 5-3), the angle of the fibrils with respect to the x -axis was considered as

$\pi/2$ (90°). In the Radial Zone (RZ) and Superficial Zone (SZ) this angle of the fiber was decreased until it became zero (Fig. 5-1& Fig. 5-3) (Eq. 5-1). The approximate thickness of each zone was obtained from literature [175,181].

The collagen fibers were modeled as linear elastic for the sake of the simplicity of the model. The fibrils supported only tension loads.

The non-fibrillar part of the solid part of the cartilage, was assumed as linear poroelastic with a Young's modulus E_{n-f} , a Poisson's ratio ν_{n-f} and a permeability k (for the fibrillar a Young's modulus E_f was used) (see Appendix C).

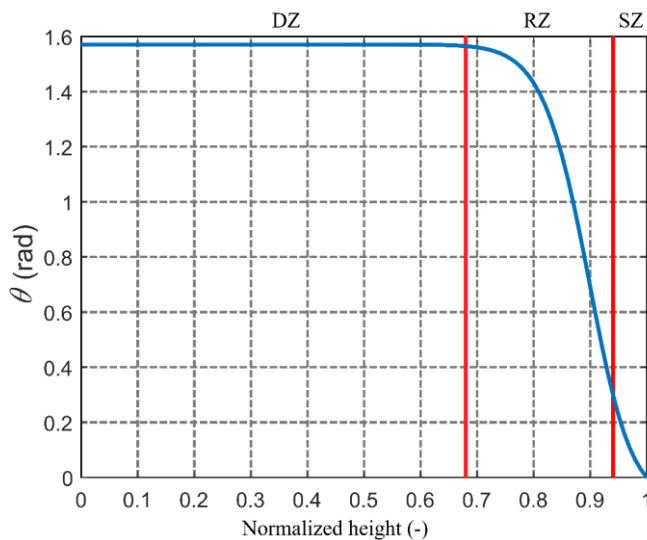


Fig. 5-3 Graphic of the angle of the fibers at each zone. Angle θ of the primary collagen fibers present in the articular cartilage matrix, with respect to the normalize height.

$$\theta = -0.079 + \frac{\frac{\pi}{2} + 0.079}{\left(1 + \left(\frac{z}{0.93}\right)^{19.87}\right)^{1.86}} \quad \text{Eq. 5-1}$$

At each integration point, the total stress in the solid matrix is given by the sum of the stresses of the fibrillar and non-fibrillar parts (Eq. 5-2).

$$\sigma_{tot} = \sigma_{n-f} + \sum_{i=1}^{fib} \sigma_f \quad \text{Eq. 5-2}$$

where σ_{n-f} and σ_f are the stresses in the non-fibrillar matrix and in each individual fibril, both with respect to the global coordinate system. To determine the local fibril stress at each integration point, the initial orientation of each fibril is given by a unit vector \mathbf{v}_0 , then, after deformation a new unit fibril vector is given as \mathbf{v}_{new} (Eq. 5-3)

$$\mathbf{v}_{new} = \frac{\mathbf{F} \cdot \mathbf{v}_0}{\|\mathbf{F} \cdot \mathbf{v}_0\|} \quad \text{Eq. 5-3}$$

with \mathbf{F} being the deformation gradient tensor. The logarithmic fibril strain was calculated as in Eq. 5-4.

$$\varepsilon_f = \log(\|\mathbf{F} \cdot \mathbf{v}_0\|) \quad \text{Eq. 5-4}$$

5.2.3.2. Bone Remodeling Model

Wolff was the first to suggest that there is a relationship between the bone structure and the applied loads [182,183]. It is believed that the mechanical stress influences the action of bone remodeling cells

(osteoblasts and osteoclasts) through the osteocytes. It seems that mechanosensitive osteocytes are capable of transducing changes in mechanical stimuli into biochemical signals that regulate cellular (osteoblasts and osteoclasts) responses [184]. Also, osteocytes may detect matrix micro damage and signal for micro damage removal to prevent accumulation of damage within the bone tissue [185,186]. Evidence shows that the formation of micro cracks through fatigue damage may be the stimulus for bone remodeling, which begins with bone resorption followed by bone formation [187]. Then, bones, especially subchondral bone, can be adapted to loads on trajectories of stress, through mineral apposition, *i.e.*, more material is deposited in the lines of high stress [188]. Furthermore, low stresses (low loads) are commonly regarded as a reason for bone resorption since there is no need to maintain the strength of the structure [189]. However, if the bone stresses are so high (overloads) due to an abnormal load condition, such as the implantation of a scaffold, the self-repair mechanism cannot follow the increasing damage, and thus overload resorption will occur [187]. For convenience, stress or strain can usually be considered as the mechanical stimulus for bone remodeling [184,187].

Several computational models partly answer the mechano-regulation of bone mass in response to strain and micro damage [184,185,187,188,190–194]. One characteristic of most of those models is the presence of a lazy zone (also known as equilibrium zone or originally termed as dead zone), a range of mechanical stimulus (around a value that the bone detects as normal) within which no change in bone density is evident [195]. Therefore, net bone formation (or resorption)

is produced, if the mechanical stimulus is well over or below those reference values.

Some studies have debated the likeliness of the presence of a lazy zone [196], suggesting that bone remodeling is correlated with the tissue loads following a linear relationship without a lazy zone. Actually, the lazy zone seems more like a mathematical approximation than a mechanobiological fact [195]. In fact, the inclusion of the lazy zone has a serious drawback: the final bone density distribution depends on the starting density, so the solution of the density distribution is not unique nor guaranteed [195]. Hence, it can be said that the remodeling response of the bone has a mechanobiological basis and governs the behavior of the bone in every aspect.

It is believed that this mechanobiological response (bone density redistribution or bone remodeling) is more complex than it seems; a more complete model, as in Klika *et al.*, [197], should include variables like load frequency, hormonal response, cellular interactions pathology, etc. [195]. Then, simplistic bone redistribution models should be applied once the distribution of density is correctly established, for example, to predict variations of bone density due to changes in the normal activity [195]. In light of the aforementioned, and for simplicity's sake, we employed a basic bone remodeling model which considers the response to strain, and the basal conditions as initial conditions.

In our remodeling model, we considered the basal maximum deformation (ε_{max}^b) of the bone tissues. Before the scaffold was implanted, the basal maximum deformation was calculated as an

average of the daily maximal deformation of the tissue (subchondral and trabecular bone). The number of days to calculate the basal conditions were defined until ε_{max}^b had little variation. Then, abnormal loading conditions were generated after the scaffold was implanted, hence the maximum strain patterns within the tissue changed. This variation in strain conditions was considered to affect the bone density distribution, and therefore the Young's modulus of the subchondral and trabecular bone [184,187]. The Young's modulus for a time-step ($i + 1$) was computed following a simple isotropic damage theory equation (Eq. 5-5), where the 'damage' was based on the difference between the actual maximum strain ε_{max}^{act} and ε_{max}^b (Eq. 5-6).

$$E_{i+1} = \begin{cases} E_i(1 - D * \alpha), & \text{if } D > D_{th} \\ E_i(1 + D * \alpha), & \text{if } D < D_{th} \end{cases} \quad \text{Eq. 5-5}$$

$$D = |\varepsilon_{max}^b| - |\varepsilon_{max}^{act}| \quad \text{Eq. 5-6}$$

where α was calculated through an iterative process being different for each type of bone (subchondral and trabecular) (see Appendix C). With these conditions, the bones (subchondral and trabecular) would go under resorption when subjected to underload and overload, and under apposition when D is between zero and D_{th} . A maximum and minimum Young's modulus was set for each bone tissue.

It was established that the bone tissue under the scaffold would fail if the average Young's modulus of the line of elements under the scaffold was smaller than a E_{fail} ; a different E_{fail} value was given to

each bone tissue. If the bone failed, the scaffold was able to move downwards within the bone.

5.2.3.3.Potential vascularity factor

A hypothetic potential vascularity factor (PVF) was also considered. This factor was assumed to diffuse from the bottom of the domain, where it had a unitary concentration, towards the top of the domain. This molecule had a low diffusion rate and determined if a mesenchymal tissue might be vascularized or not.

5.2.3.4. Tissue regeneration model

In our model, we were dealing with the regeneration of two types of tissue, cartilage and bone. The osteogenesis process might be regulated by the mechanical environment, and it has been studied from computational and experimental approaches. It is possible that the sequential differentiation of precursor cells during bone healing is highly influenced by the local mechanical stimuli [198]. Several mechanoregulation algorithms have been proposed to analyze the possible relationship between cell differentiation and mechanical stimulation [7,199–201]. Also, these algorithms have been used to simulate different aspects of tissue regeneration [202–210], and the results have been compared to experimental outcomes. The tissue regeneration algorithms regulated by deviatoric strain and FV were the most accurate to predict healing as observed in vivo [211].

Cellular processes are another important aspect considered for bone healing mechanoregulatory algorithms. Additionally, cell-

phenotype specific actions influence on other cell mediated aspects of bone healing, such as matrix production [204].

For bone regeneration, we proposed a model based Isaksson *et al.*, [204]. They developed a mechanistic model of tissue differentiation which couples the cellular mechanisms to mechanical stimuli during bone healing. They hypothesized that cells act as sensors of mechanical stimuli. Therefore, cell proliferation, migration, differentiation or de-differentiation, and production of cellular matrix are based on the mechanical stimuli they are experiencing [204].

For the cartilage tissue, to our knowledge, there are not deep computational models in literature to explain how this tissue is regenerated. Hence, we consider three factors for its regeneration. First, it was considered a positive relationship between cyclic hydrostatic stress and cartilage growth [113]. Second, cartilage could only regenerate in elements with mesenchymal tissue. Third, for cartilage to regenerate it must have low concentration of PVF (hypothetic molecule used as an indicator of the potential vascularity of the tissue).

Once there was any displacement of the scaffold due to failure of the bone under it, the void on top of the scaffold was then filled with mesenchymal tissue, which later would differentiate into other tissue (bone or cartilage). This newly-formed tissue would initiate with a concentration of mesenchymal cells.

If an element had mesenchymal tissue, only two paths could be taken, either differentiates into cartilage, or follows the osteogenesis model. For a mesenchymal element to differentiate into cartilage, the

element must have low concentration of PVF and a neighbor element which was cartilage. Additionally, this neighbor must have high hydrostatic stress.

Moreover, if none of the above conditions were achieved, then the osteogenesis model came into action. In this case the mesenchymal tissue could differentiate into fibrous, cartilage or bone tissue depending on the mechanical stimuli. The tissue production and degradation matrices were considered. Matrix production rates were proportional to the mechanical stimuli, if the mechanical environment was convenient for that type of tissue [204]. Also, for matrix degradation, it was assumed that the extra cellular matrix degrades if the mechanical environment was not favorable for that type of tissue [204].

The concentration of the tissue type was calculated as a function of the mechanical stimuli ψ . The tissue matrix production was defined as (Eq. 5-7):

$$\frac{\partial m_j}{\partial t} = \overbrace{f_j^{PM}(\psi) \left(1 - \frac{m_j}{m_{space}}\right)}^{\text{Matrix production}} - \overbrace{f_j^{DM}(\psi)m_j}^{\text{Matrix degradation}} \quad \text{Eq. 5-7}$$

where m_j is the concentration of the matrix type j , being $j = 5$ -fibrous tissue, 6 - cartilage and 7 -bone. Also, f_j^{PM} is the rate of matrix production and f_j^{DM} is the rate of matrix degradation (see Appendix C). These rates also depend on the mechanical stimuli ψ , f_j^{PM} and f_j^{DM} are turned “on” when ψ is equal to $j - 3$ (see sub-section

Mechanoregulation algorithm). m_{space} is the space available in the element for more tissue matrix and is calculated as follows [204]:

$$m_{space} = m_{max} - \sum_{j=5}^7 m_j \quad \text{Eq. 5-8}$$

where m_{max} is the maximal matrix concentration (see Appendix C). The kind of tissue with higher matrix concentration defines the new tissue for the element.

5.2.3.5. Mechanoregulation algorithm

As in previous studies [204], the combined effect of the deviatoric shear strain (DSS) and FV was used to regulate cell and tissue differentiation [199], which has shown to be versatile on predicting bone healing [202,204,208,212]. Then, the DSS and the FV were used to determine the value of ψ . For which, the mechanical stimulation (MS) is calculated as follows:

$$MS = \frac{DSS}{3.75} + \frac{FV}{3.0} \quad \text{Eq. 5-9}$$

According to the mechanoregulation algorithm proposed by Prendergast *et al.*, 1997 [199]:

$MS > 3$	$\psi = 2$	Fibroblast cells and fibrous tissue stimulation
$3 \geq MS > 1$	$\psi = 3$	Chondrocyte cells and cartilage tissue stimulation
$1 \geq MS > 0.01$	$\psi = 4$	Osteoblast cells and bone tissue stimulation

5.2.3.6. New Tissue

Some theories have been proposed on how the collagen fibers within the cartilage get oriented in such unique way. It is hypothesized that the particular collagen structure is consequence of the mechanical conditions detected by the cartilage cells, which modify their ECM accordingly [174]. Orientation of collagen fibers have been studied in the aortic heart valve in which the collagen fibers (collagen type I) align following the direction of the principal strain [213]. For cartilage, whose fiber are collagen type II, it has been proposed that the fibers are also oriented following the tensile strain direction, at least in the surface [174].

In our model, the new tissue (mesenchymal) tissue has differentiated into cartilage or any other (bone or fibrous tissue). If the mesenchymal tissue differentiates into cartilage (new cartilage), fibrils were placed within the new cartilage tissue oriented $\pm 45^\circ$, as in *Wilson et al.*, [174]. Then, a collagen remodeling algorithm based on the one proposed by *Wilson et al.*, [174] was implemented. For each day (time-step), the average direction of the maximal deformation was computed and used to reorient the fibers direction. Conversely, if the mesenchymal tissue differentiated into bone, it started with a small Young's modulus, which increased accordingly to the deformation of the bone until the maximum limit was achieved.

5.2.4. GENERAL ALGORITHM

Fig. 5-4 shows a flowchart of the employed algorithm. The model started, at $n = 1$, with an initial mechanical analysis of the model

where cyclic load was applied to the tissue for a number k_{stop} of steps. From this analysis, stress, strain, and FV were calculated. These calculations were averaged through each n until little variation on the average values was obtained (until $n = n_{scaff}$); these values were used as the basal values. At $n = n_{scaff}$, a defect was introduced in the articular cartilage and a scaffold was implanted within it. Thereafter, for each time-step n , the mechanical analysis was conducted again and stress, strain and FV average values are calculated, and tissue remodeling, and regeneration were also conducted.

In the tissue remodeling and regeneration part of the algorithm every element was analyzed. The path of the algorithm depended on the type of tissue of the element j . If it was mesenchymal tissue, then it was analyzed if it could differentiate into neo-cartilage or go through the osteogenesis process. If the element was bone tissue, then it was remodeled (resorption or apposition) according to its strain. If the element had neo-cartilage tissue, then the collagen fibers within it would reorient accordingly to the principal strain. Lastly, if the element had new bone tissue, then its Young's modulus would increase depending on the strain of the element.

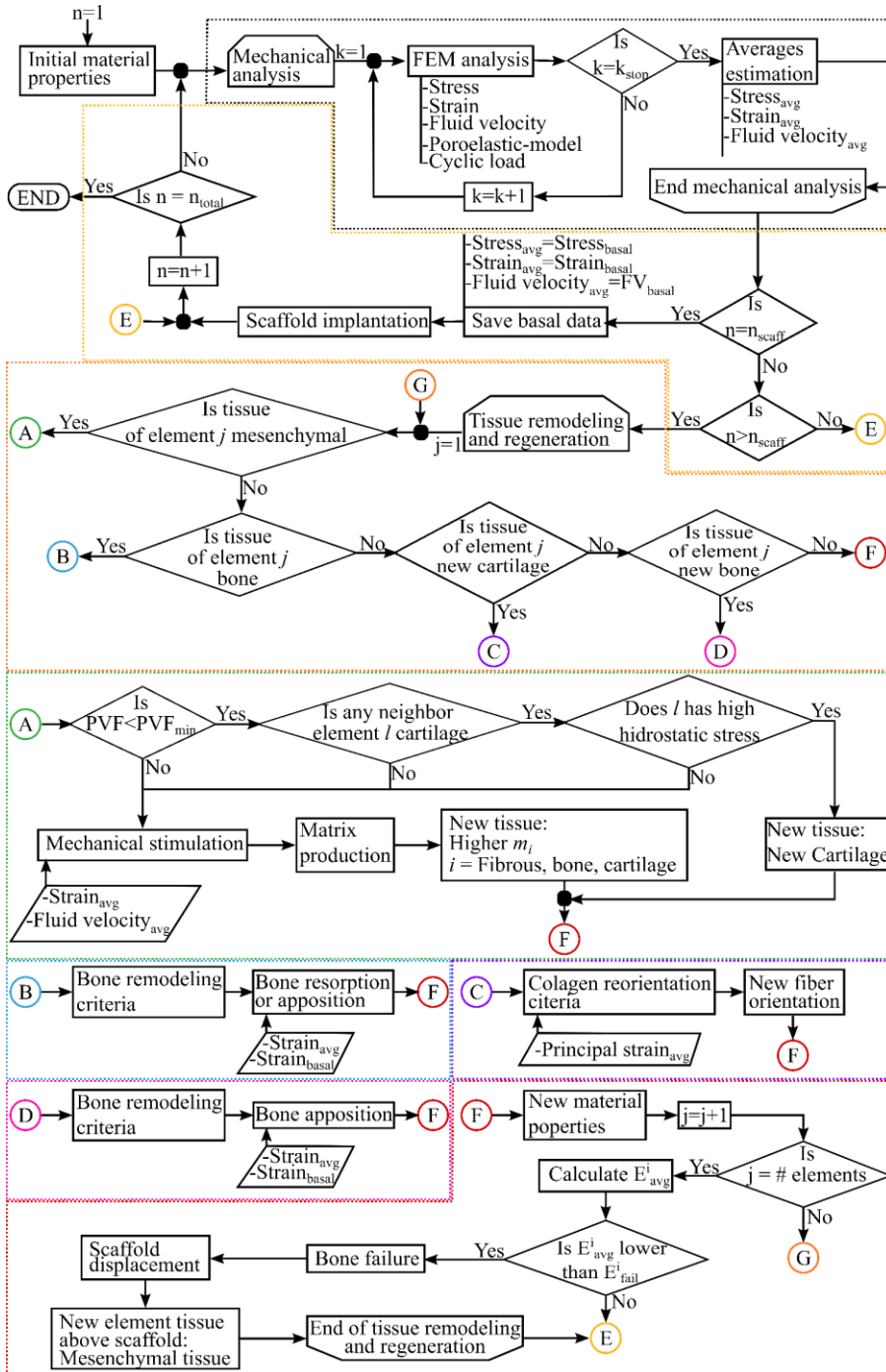


Fig. 5-4 Flow chart of the employed algorithm for cartilage or bone regeneration.

Afterwards, the material properties of the element j was updated, and then, the next element was analyzed. Subsequently, after all the elements were analyzed, the line of elements under the scaffold was inspected. If the average of their Young's modulus E_{avg}^i was smaller than a E_{fail}^i , then it was considered that the bone tissue under the scaffold would fail and the scaffold could displace one line of elements downwards. The void left above the scaffold was considered mesenchymal tissue. Then, n increased one unit and the process continued until $n = n_{total}$.

5.3. RESULTS

The developed model considers the mechanism to regenerate bone and cartilage. It was assumed that there are three factors that influence the cartilage regeneration. First, a factor related to the potential vascularity of the tissue (hypothetic molecule). Secondly, cartilage tissue induces its chondrocyte inducers that promote the differentiation of mesenchymal cells into cartilage. Lastly, high hydrostatic stresses promote cartilage growth.

When a polymeric scaffold was placed within a defect in the articular cartilage, the load, stress, and strain conditions of the surrounding tissues changed. These changes and the new loading conditions provoked the tissue under the scaffold to remodel. Therefore, a bone remodeling model was implemented for the subchondral and trabecular bones after the implantation of the scaffold.

The model simulates the changes that occurred during one year after the implantation of the scaffold. Tissues evolution was obtained at different times of the year (Fig. 5-5). The scaffold started to descend after the first week when a line of neocartilage tissue covered the superficial surface of the scaffold. After 3 months the scaffold moved had more inside the subchondral and trabecular bone and cartilage grew on the upper part of the scaffold due to the favorable mechanical conditions of the surrounding cartilage. In the sixth month, it seemed that the influence of the PVF was not high enough in the upper limit of the scaffold, therefore, the differentiation of the mesenchymal tissue generated after the scaffold moved downwards, followed the mechanoregulation algorithm. Moreover, at this stage the mechanical stimulus at the top part of the scaffold, seemed to promote bone formation. By the end of the year, the scaffold was displaced deeply within the bone, whereas the cartilage in the zone of the defect has regenerated.

When the articular cartilage on the defect started to regenerate, it formed a neocartilage with the collagen fibers initially placed at $\pm 45^\circ$. Then, these fibers reoriented following the direction of the principal strain (Fig. 5-6). By the end of the year the fibers tended to orient with an inclination close to $\pm 60^\circ$ (Fig. 5-6).

Due to the presence of the scaffold, the bones' Young's modulus, and therefore its density, changed (Fig. 5-7). These alterations allowed the bones to remodel in order to bear the variations in loading conditions provoked by the scaffold, however, the Young's modulus stabilized by the end of the simulation.

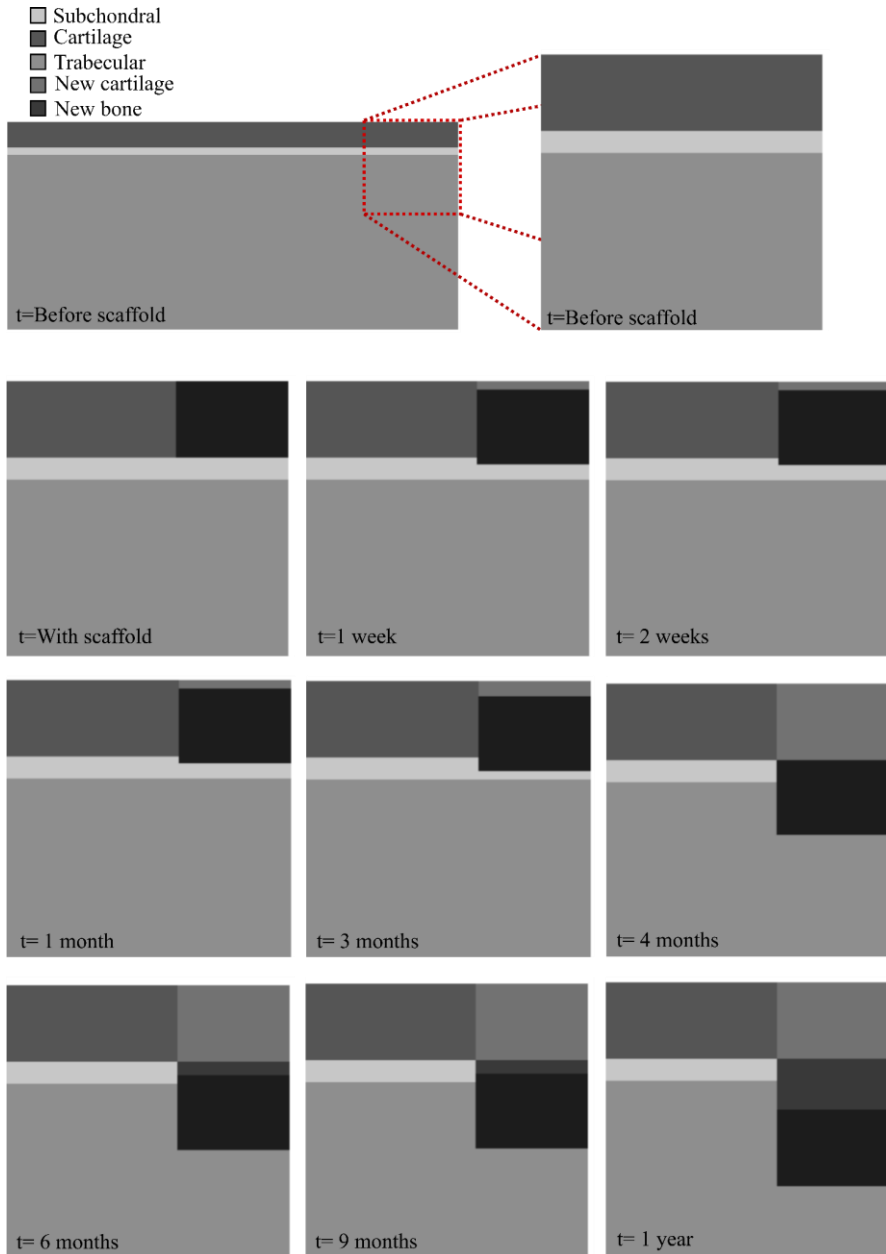


Fig. 5-5 Simulation of tissue differentiation after scaffold implantation throughout the simulation. From the first week to the third month the scaffold displaced downwards just a small distance. By the fourth month, the top end of the scaffold is almost aligning with the top part of subchondral bone, and cartilage is generated on the upper part of the scaffold. Then, between the fourth and ninth month, the scaffold moved slowly downwards inside the bone, and new bone started to be generated on the top of the scaffold, under the cartilage. At the end of the year, the tissue is almost stabilized, and cartilage and bone had formed on the scaffold.

Cartilage regeneration

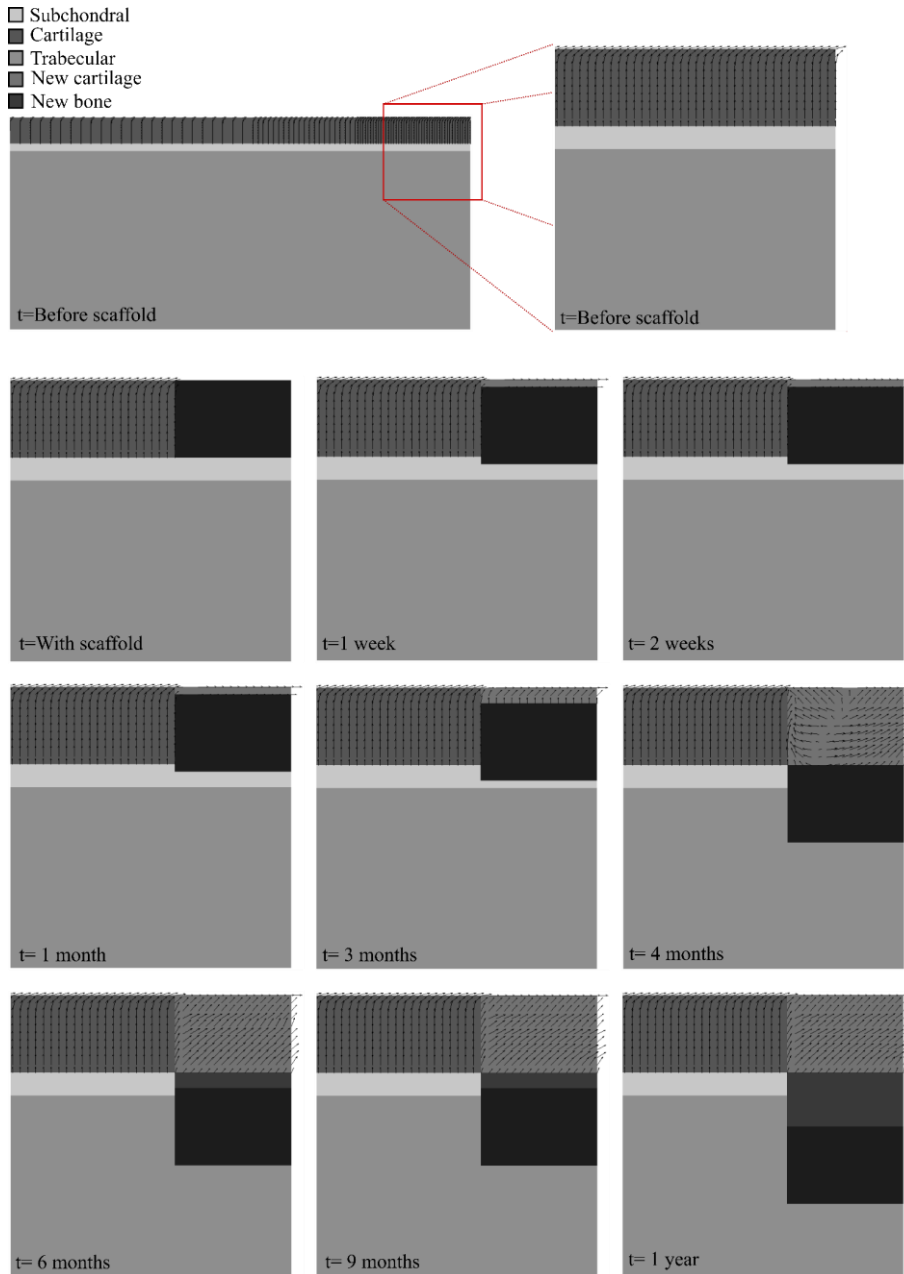


Fig. 5-6 Simulation of collagen fiber orientation after implantation. Only one set of fibers is shown in the figure. The model also included the mirror fibers of the ones shown in the image. By the fourth month, when the cartilage is formed, the fibers are disorganized. By the end of the simulation (1 year), the fibers get reoriented at nearly 60°

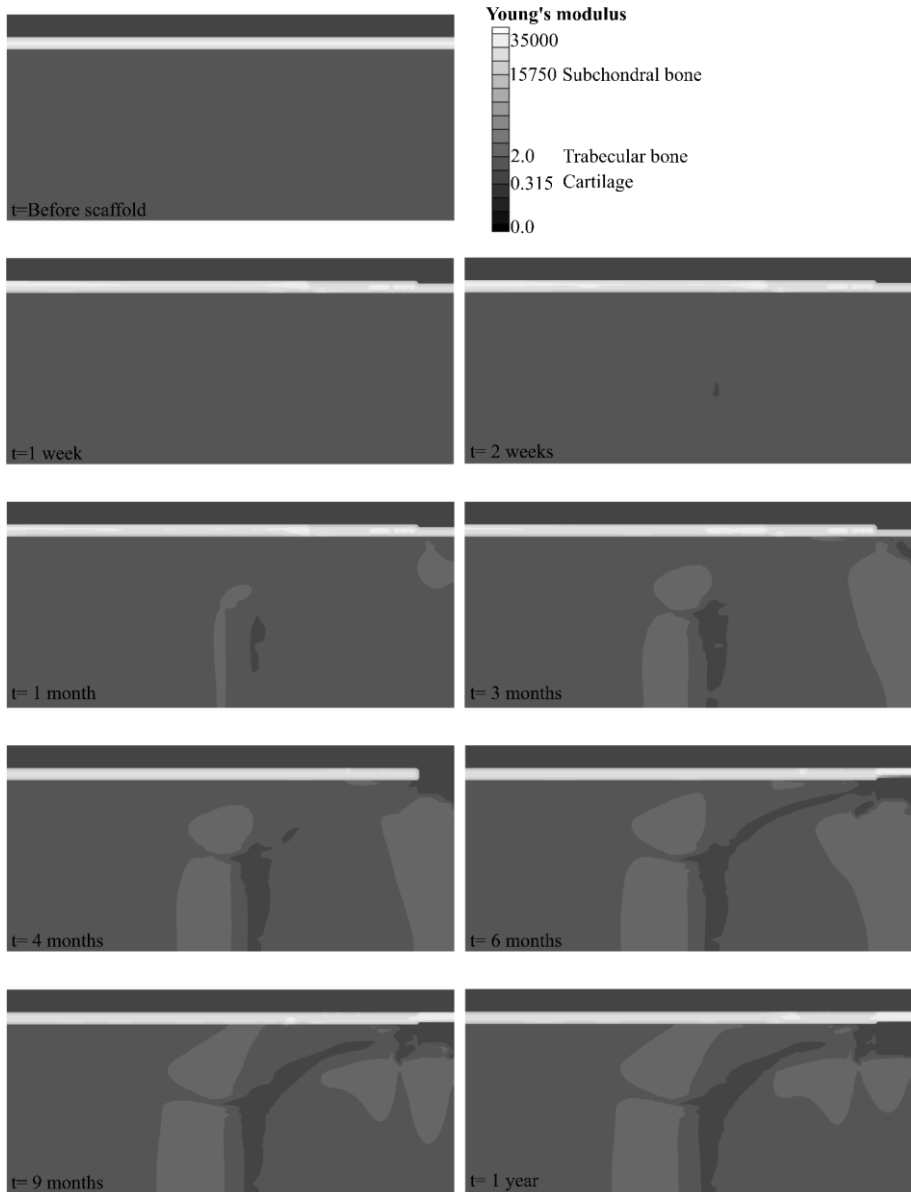


Fig. 5-7 Simulation of bones' Young's modulus after scaffold implantation.
The Young's modulus of the subchondral and trabecular bones: the tissues get more or less, rigid according to the bone remodeling algorithm.

5.4. DISCUSSION

We developed a model to explain some of the processes that influence cartilage regeneration when implanting a polymeric scaffold in the site of an articular cartilage the defect. The subchondral bone, trabecular bone, cartilage and scaffold were considered in the model as poroelastic materials. The cartilage's collagen fibers were modeled as a linear elastic, tension only, material.

The model considers the basal conditions of the system, that means, the stress and strain conditions when the scaffold is not yet implanted. These data were then compared to the ones obtained when the scaffold is implanted. The differences between both states, allowed to determine the remodeling behavior of the bones, which helped to decide whether the bone should either reabsorb or densify by apposition at specific zones. This meant that a reduction of bones' strain (low loads) would translate into bone resorption [189]; a small increase of strain ('medium' loads) translated to bone apposition (bone resorption followed by a quick bone formation) [187]; and finally, a high increase of bones' strain (overload) was also assumed as bone resorption [187]. This simulated the normal behavior of a bone tissue that goes under a remodeling process [187,189].

Bone resorption and appositions processes, bone remodeling, was modeled as a change in the Young's modulus of the bone. An increase and a reduction of the Young's modulus was assumed when the apposition or resorption processes took place, respectively (Fig. 5-7). Trabecular bone had to remodel in order to bare the abnormal load

brought by the scaffold (Fig. 5-7). Moreover, the Young's modulus of the trabecular bone increases at the zone under the scaffold once is implanted; but decreases, due to overload, on line right under the scaffold (Fig. 5-7). However, by the end of the simulation time (a year), the trabecular bone's Young's modulus had the tendency to return to basal conditions, which can be considered as if the system is stabilizing (Fig. 5-7).

The scaffold was displaced inside the bone if the Young's modulus of the bone under the scaffold was small. This displacement left a void on the top of the scaffold, which was assumed to be filled with mesenchymal tissue. This mesenchymal tissue, as soon as it was generated, had two options, either differentiate into cartilage or follow an osteogenesis process algorithm; within which it could differentiate into fibrous tissue, cartilage or bone, depending on the mechanical stimuli. To differentiate into cartilage, the mesenchymal tissue must fulfill three conditions: First, the concentration of PVF had to be low enough so that differentiation into tissue with low vascularity were promoted. Secondly, the tissue that surrounds the mesenchymal one had to be cartilage, this way, the influence of the chondro-inductive molecules that might diffuse from the cartilage tissue is simulated. Third and lastly, it was assumed that cartilage growth is induced under high hydrostatic conditions, therefore, not only the surrounding tissue needed to be cartilage, but it also needed to bear high hydrostatic loads. In the results, cartilage started forming on the top part of the scaffold until the fourth and sixth month, where the concentration of the PVF was high enough to avoid the formation of cartilage (Fig. 5-5).

Initially, the new formed cartilage had collagen fibers in a ‘disorganized’ way, later it aligned following the direction of the principal strain. After the simulation time, the final direction of the fibers was about 60°. In this model, the new fibers did not align entirely as the fibers of a native articular cartilage (Fig. 5-6); factors that we did not consider could be influencing the reorientation of the new collagen fibers, which should be addressed in future models.

If the conditions for a mesenchymal tissue to differentiate into cartilage were not fulfilled, the osteogenesis process algorithm happened. We calculated a mechanical stimulus for the osteogenesis algorithm, and it defined whether the mesenchymal tissue should differentiate into cartilage, bone, or fibrous tissue. In our model, the calculated mechanical stimulus was ideal to stimulate the mesenchymal tissue to differentiate only into bone (Fig. 5-5).

A previous experiment from our group implanted polymeric scaffold as treatment to repair a chondral defect [4]. In that study, a full-depth chondral defect was made in the knee joint in a rabbit experimental model, where a biostable, poly (ethyl acrylate-co-hydroxyethyl acrylate) copolymer, porous scaffold was implanted. We studied the evolution of the cartilage repair process through histological techniques. Histological images for 1 and 2 weeks, and for 1, 3, and 12 months after implantation [4]. At early stages (first months), we observed a thin layer of tissue covering the scaffold surface (Fig. 5-8). In the results of our model, it can also be observed that for the first months, there was also a thin layer of new cartilage tissue that was formed on the upper part of the scaffold, which agrees with our findings

[4] (Fig. 5-8). At 3 months, the scaffold was completely covered by a thicker layer of new cartilage [4]. In our computational model, the results at three months also agree with the ones observed in the experiment (Fig. 5-8). A year after the implantation of the scaffold, the cartilage in the experimental model was completely repaired, and the scaffold was displaced towards the inside of the bone; in our computational model it is also observed that the scaffold was displaced inside the bone, whereas the defect in the articular cartilage was already covered (Fig. 5-8).

It should be considered that our model assumed some simplifications for computational savings. For example, the cartilage was modeled as poroelastic, when it is well known that the cartilage is composed by a more complex material. Moreover, the fibers within the cartilage were modeled as linear elastic but their real behavior might imply more variables and a more complex model. Also, the model employs a 2D geometry, and the fibers of the cartilage were only modeled in this 2D-plane, but in reality, they align in a 3D direction. However, despite all the simplifications made, when comparing the results of our computational model, with those of the experimental model developed by Sancho-Tello *et al.*, [4], it can be seen that our model is able to predict various results: the tissue evolution of the cartilage repair process phenomenon, the time of repairing, and the final results of the treatment. Our computational model could be useful when a comparison on the effect of using different scaffold materials is wanted, or when different loading conditions or tissue degeneration is required and compared with an idealized treatment condition. We

conclude that the proposed model is promising and might be helpful when planning treatments for articular cartilage regeneration. Moreover, this model might be useful as an analysis tool prior experimental *in vivo* studies, allowing to discard approaches that might not bring good results which at the end translates to a reduction on the need of animal use.

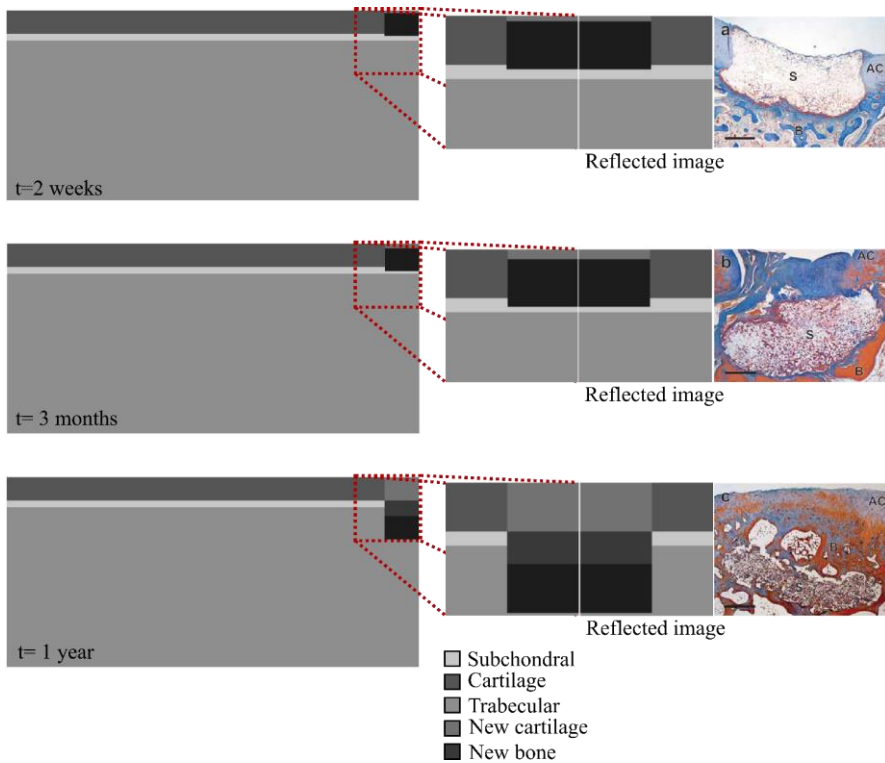


Fig. 5-8 Comparison of our results with the histological findings of a previous experimental study. At the left, tissue evolution obtained with our simulation model where the zone near the scaffold is zoomed-in and mirrored. At the right the histological images obtained by the experimental model developed in Sancho-Tello *et al.*, [4]. Histological images modified from [4].

Chapter 6. GENERAL CONCLUSIONS AND RECOMMENDATIONS

6.1. GENERAL CONCLUSIONS

The principal aim of this thesis was to computationally model the mechanical and biochemical aspects involved in the development of synovial joints. Therefore, this work portrays two models to explain the joint development from the interzone onset to morphogenesis (Joint Onset and Joint Morphogenesis). Additionally, it was also proposed an extra computational study, related to joint development, in which three different theories for patella development were explored through computational models (Patella Onset). Moreover, another model was developed to explain some phenomena related to the articular cartilage regeneration (Cartilage regeneration).

All the computational models developed in this study employed theories about tissue behavior under mechanical and biochemical stimuli. The obtained results, when compared to experimental works found in the literature, showed promising outcomes. Hence the procedures and considerations taken for each proposed computational model are not far from what is really happening on the analyzed biological phenomena.

From the outcomes of this work we can say that the interphalangeal joint development can be explained through the

interaction of only six (generic) molecules, each of which played an important role in the joint onset. These proposed generic molecules can be related to real molecules that have been shown that might influence joint development. It should be pointed out that the human body is a redundant system (there are groups of molecules which might do the same task in case the principal molecule fails), which is the reason why we did not tie to specific molecules. Moreover, it was found a good correlation when the results of the joint onset model were compared to the histological observations found in literature, which is an indicator that the proposed interaction of the molecules is a reliable approximation of what is happening in the joint onset process.

Once the joint begins its development, after the interzone appearance and the cavitation processes, comes the morphogenesis: a stage in which the joint gets its final shape. In the computational model that we proposed for this stage, we believed that both, mechanical loads and molecular factors, have an influence on how the shape of the joint evolves. A remarkable similitude was found when the obtained results were compared to anatomical observations of an interphalangeal joint. Moreover, we obtained better results than those of previous computational model describe by other authors, in which only the mechanical load was considered. Then, the outcomes of our computational model suggest that, in fact, both stimuli (mechanical and biochemical) are necessary for the joint morphogenesis process.

Within some synovial joints, there are some small bones called sesamoid bones, the largest being the patella. However, there is a lot of debate regarding why and how these bones develop. Some theories have

been proposed to explain the formation and function of the patella, but still there is not a unified theory that clarifies the development of these bones. In order to explore this issue, we developed a computational model for each one of the theories found in the literature, as a tool to evaluate their likelihood. Three theories were evaluated, two of them with a mechanical approach and the other with a biochemical one. With our computational models we were able to predict the patella onset with all three theories, being the “biochemical theory” the one that showed better results, *i.e.*, a better resemblance with the anatomical and histological observations. However, since there are studies that have found that mechanical loads influence joint development (studies where the limb was immobilized and the patella developed but smaller than control), we propose that the molecular interaction triggers the patella onset and that mechanical loads are necessary for the patella growth and maintenance.

Once the synovial joint and all the related structures have developed, there are some pathologies that might affect the internal structures of the joint, compromising its functionality. It was of our interest to evaluate a treatment employed for one of these pathologies, thus we focused on a novel therapy used to repair injuries in the articular cartilage. So, we developed a computational model in which we intend to characterize aspects that might influence cartilage regeneration when a polymeric implant is used. We based the model on experimental outcomes of previous works, and we obtained coherent results. In our model, we observed that not only the cartilage has to adapt during the regeneration process but also the surrounding tissue, *e.g.*, subchondral

and trabecular bone. The developed computational model could be helpful to compare different scaffold materials and load conditions and evaluate which approach results in a better outcome.

With the developed computational models of this thesis we were able to evaluate mechanical and biochemical conditions of some biological phenomena, that would be difficult to test through experimental approaches. This work explored several aspects of the joints (synovial) from its development to its mature state. We hope that these models become useful for medical and biological researches, helping in the design of prevention and therapy strategies for joint related pathologies.

6.2. RECOMMENDATIONS

- The developed computational models could be improved by employing more complex material models for the tissues. However, it should be considered the computational cost that this would imply.
- For future work, it is suggested to apply the methodologies proposed for interphalangeal joint onset and morphogenesis to other joints, such as the hip joint, to evaluate the happenings of developmental pathologies like the DDH. Moreover, our model can be extended by adding the effect of load prior to the cavitation process (since it is believed that loading starts affecting the development of large joints prior to the cavitation process).
- For the patella development, it is suggested that a general model should be developed, in which the biochemical theory is combined with

the mechanical one. It is advised that the biochemical theory triggers the formation of the patella, and once the tendon is fully developed, the mechanical loading shapes and maintain the patella.

- Cartilage regeneration model can be widened by considering the effect of other tissues, scaffold structures, types of biomaterials and molecules that could influence the cartilage regeneration.
- Although the developed models were proposed in 2D and show good results in the task of explaining the biological processes studied, it must be evaluated if it is worthwhile to translate some of these models into a 3D environment.

SUMMARY

Joints connect the skeletal components of the body and enable a relative movement between them. Among the different kind of joints, the synovial ones offer the widest range of motion between the bones. Most synovial joints are in the appendicular skeleton (limbs). Depending on the joint, they can have different internal structures. However, they all have four common features: the enclosed articular capsule containing synovial fluid (lubricant); the articulating cartilaginous surfaces at each end of the bone, which slide against each other; the synovial membrane, which covers the inner surface of the capsule; and the ligaments, tendon and muscles, which provide stability and mobility to the joint.

How is this kind of joint formed? Studies have shown that onset and development of synovial joints are regulated by different genetic, biochemical and mechanical factors. The synovial joints development is a multipart process that starts in the fetal stages of prenatal development. Around five weeks of development, limb buds start growing and become noticeable. At the beginning, these limb buds have an uninterrupted mass of mesenchymal cells within its core. This bulk of cells is known as skeletal blastema and it is covered by a layer of ectoderm. Then, most of these blastemal cells differentiate into chondrocytes, although, some of them remain undifferentiated at the interzone, where the future joint will form. The separation of the joint occurs during the cavitation process, in which interzone cells are likely

suffer apoptosis, leaving a space between the chondrocyte bone rudiments.

After the joint cleavage (cavitation), joint morphogenesis occurs as cells proliferate on both sides of the joint, allowing the head of the bones to take their final shape. Studies have shown that the shaping of the joints is influenced by movements and muscle contractions that are present during limb development, although local and systemic biochemical factors could also have some effects. If there are abnormal conditions during fetal development, joints can develop incomplete or abnormal, or even they might not develop at all.

Once the embryonic period has finished, the synovial joint and its internal structures (like the articular cartilage, ligaments and synovial capsule) are completely developed. Moreover, POC and SOC of the bone appear. These structures help the bone grow and ossify until the adulthood is reached.

However, once the synovial joints are formed, they might suffer several pathologies that impair their movement and probably affect the lifestyle of the individual who is suffering from it. These pathologies, such as the OA, which is a degenerative joint disease, can occur due to repeated trauma, aging, surgery, obesity, hormonal disorders, injuries on the joint surfaces and overloading due to abnormal shape of the joint, among others.

In the OA, the wear and degeneration of the articular cartilage can eventually cause the loss of a portion of it. This condition is worsened by the poor ability of the cartilage to regenerate itself. The

worn cartilage is generally replaced by an unsuitable tissue, fibrous cartilage. This new tissue produces an uneven articular surface that causes friction, which can trigger joint pain and stiffness, aggravating the pathology.

Several treatments have been proposed to repair the articular cartilage and they range from symptomatic to more invasive ones, being the last resort a total replacement of the affected joint or joint arthrodesis treatments, i.e. fusion of all or some of the bones that are part of the synovial joint. Of course, it is preferable to preserve the original structure and function of the joint rather than a joint replacement or an arthrodesis, especially in the case of young patients.

Tissue engineering has been trying to find definitive treatments for degenerative pathologies of articular cartilage by proposing less invasive approaches to these injuries. In the last two decades, the use of scaffolds has been proposed as an alternative treatment to the osteochondral graft. The scaffolds allow a rapid filling of the joint defects and provide cells a substrate for anchoring. The use of scaffolds in tissue engineering involves three main components: scaffolds' materials, cell differentiation factors and cellular sources. In addition, scaffolds without cellular sources have also been used showing excellent results, avoiding the risks associated with cell manipulation (e.g., contamination of bacteria and phenotype loss during handling), as well as reducing costs.

It is vital to understand the processes through which the joint tissue goes from its development to its maturity stage in order to

develop new direct and effective therapeutic strategies for pathologies related to the joints. However, to achieve it entirely through experimental analyses could lead to a great consumption of resources and time. Therefore, computational models appear as a convenient tool to complement the study of the joint processes. Computational models provide a quantitative and qualitative evaluation of mechanical and biological interactions while feeding on clinical or experimental observations. Therefore, computational models contribute to these studies since they evaluate difficult-to-reach aspects for experimental models.

This thesis studies, through computational models, the controlled biochemical interaction that occurs at the onset of the interzone and the cavitation process during the synovial joint development. In the case of the morphogenesis process, besides the biochemical interaction, the possible effect of the mechanical load that could be present during the shaping process of the epiphyses of the bones is also considered.

As part of the development, we also analyzed, computationally, different theories that have been proposed to explain the existence of the sesamoid bones; bones which are superficially embedded within tendons and are usually around joints. This study is focused on the patella (kneecap), which is the largest, most recognized and studied sesamoid bone in the human body.

Moreover, we also analyzed through a computational model the processes that occur when a defect in the articular cartilage is treated with the implantation of a polymeric scaffold. This may be useful to

compare different scaffold materials, shapes, and conditions of the scaffold that could influence the outcome of the treatment.

To summarize, the objectives of this thesis are:

Principal aim:

To model, computationally, the mechanical and biological aspects that occur during the development of synovial joints.

Specific aims:

- To formulate the mathematical description of the mechanobiological phenomena that govern the development of the synovial joints.
- To computationally evaluate the behavior of the model during the interzone onset of synovial joints.
- To computationally evaluate the behavior of the model during the cavitation process and morphogenesis of synovial joints.

1- Joint Onset

1.1. Methodology for the joint onset model

A computational model was developed based on two generic molecular actions and two molecular self-regulatory loops, expressed as reaction-diffusion equations. The aim was to predict the molecular patterns associated with the joint formation process. The model was solved in a finite elements' framework. Mathematical equations predicted patterns that represent molecular mechanisms that model the structures and shapes during joint development, such as interzone formation, cavitation, and condylar shape of the bone ends.

Reaction-diffusion equations and the formation of Turing patterns were used to simulate the location of joint cleavage, the number of joints formed, the sides of the joints that would form the epiphyses, and the initial condylar shape of the joint.

Based on the molecules that have been reported in the literature to have a role on joint development, six generic molecular factors involved in joint onset were modeled. Note that each factor may represent multiple molecules achieving the same action. The process in the model was organized in two stages. The first one marked the interzone onset, factor (G), which was located at the cleavage position while its antagonist, and was also considered a factor (N), located everywhere else. Factor (G), which was related to GDF-5, prevented the differentiation of the mesenchymal tissue into cartilage, whereas factor (N) was associated to the BMP antagonist Noggin. In the second stage, the zones that differentiate into cartilage secreted *Ihh*, factor (I), and PTHrP, factor (P), both establishing a regulatory loop that governs cell proliferation and hypertrophy. Factor (I) regulated chondrocyte proliferation, maturation, and hypertrophy, whereas factor (P) inhibited chondrocyte hypertrophy.

Meanwhile, the domain kept growing and two other factors, (H) and (W), regulated the joint separation and related structures. (H) controls the differential amount of tissue growth from proximal to distal. Mathematically, there was a gradient in (H) that affected the growth rate by promoting the longitudinal growth of the limb and bones anlagen. (W), expressed in the interzone, induced cell death and allowed the generation of a joint space. Factors (H) and (W) led to

separation of the rudiments and was also observed in parts of the fibrous capsule in later stages of development.

The finite element model included a PDE integrated with a CA-like system (PDE+CA-like). The PDE part described the molecular diffusion and established the biochemical concentrations, which enable the CA-like part to determine whether the tissue differentiated or not. Each element started with a tissue state (mesenchymal, pre-cartilaginous, cartilaginous, or interzone) and the CA-like system allowed the element to differentiate from one tissue state to another. This process loops until the stop criteria is reached (joint cleavage and its initial shaping).

Four different cases were explored. In *Case I*, the conditions for the development of an interphalangeal joint were established. The following three cases were modifications of the first one. In *Case II* and *Case III*, the effect of changing the dimensions of the initial domain in the joint development was tested. In *Case IV*, we analyzed how the growth rates of the domain modified the outcome. Besides, a parallel experimental procedure was replicated, in which GDF-5 beads were implanted in the side and tip of a developing chick autopod.

1.2. Results and discussion from the joint onset model

In *Case I*, the comparison of the obtained results for factor (G) with expression of GDF-5 in experimental studies demonstrated similar distributions. Additionally, the loop (I-P) results in a distribution where (P) was near the distal ends and (I) was at the proximal ends of the rudiment, as seen for Ihh and PTHrP in the literature.

The factor (W) established the formation of the articular cartilage in each articular surface and was consistent with the distribution of Wnt in the literature. The shape of the joint was comparable with the histologic findings: both sides of the joint have articular cartilage, but on one side there is an epiphysis-like structure. This led to the formation of a larger epiphysis-like at the distal end and another not so wide at the proximal end. From this point on, the morphology of the joint is likely influenced by mechanical conditions.

The obtained results suggest that the size of the initial domain during development may have an influence on the number of joints formed. In the simulation, one and three joints were acquired when the length/width ratio was established in 3 (*Case I*) and 5 (*Case II*), respectively. It is known that Turing patterns depend on the domain ratio, therefore the number of joints must depend on the initial geometry. Nevertheless, the literature shows that one joint is formed at a time and that is why, we propose that a joint might formed each time the distal anlage within a limb bud reach a ratio of approximately 3.

In *Case III* (faster growth velocity), a single joint was obtained with two growing regions located at both ends of the rudiments with high concentrations of (I). In *Case IV*, the goal was to simulate the onset of a joint located between a large bone and a shorter one (e.g. between a metatarsal or a metacarpal and a phalanx). Therefore, the length/width ratio of its initial domain was set to 2.5.

Case V and *Case VI* simulate the experimental study performed by Merino *et al.*, which analyzed the effects of placing GDF-5 beads in the developing autopod of embryonic chicks, specifically at the tip of

the digits. Comparing the results from *Case V* and *Case VI* with those reported in Merino *et al.*, three similarities were found: a very similar morphology was achieved, the resulting rudiment was curved when the molecule is implanted on one side of the mesenchymal condensation, and a bulb was formed when (G) was implanted at the tip of the mold. These effects might be explained since high concentration of (G) which, after the cavitation process, implied high concentration of (W) encouraging the differentiation of the tissue into articular cartilage. This abnormal location of articular cartilage impacts on the Turing pattern between (I) and (P), hence abnormal growth of the tissue was obtained.

In this thesis, a simplified model to study the development of joints was proposed. A good agreement was found between the results obtained with the simulation model and those reported in the literature for experimental works where histological analyses were performed. Although multiple molecules often influence the same biological process, it was shown, by modeling generic molecules, how the pattern formation of simple patterns between enzyme-substrate molecules predicts many events present in joint formation. The model shows a good response with interphalangeal and metacarpal/metatarsal-phalangeal joints. The results obtained in the study of this chapter will be useful for researchers focused on pathologies associated with embryo and joints development. Furthermore, this model could provide new insights and guidelines of experimentation and, of course, new mathematical and computational models of the following phases of joint development.

2- Joint Morphogenesis

2.1. *Methodology for the joint morphogenesis model*

After the interzone onset and cavitation process, takes place the last step of joint development, its morphogenesis. Experimental and computational studies have shown that there is a relationship between mechanical stress and skeletal morphogenesis. From a computational perspective, two models have been developed to evaluate the relationship between joint morphogenesis and mechanical stresses. Heegaard *et al.* and Giorgi *et al.*, both computational studies, used the hydrostatic stress distribution for describing the growth and joint morphogenesis. Although those studies obtained relevant results on the morphogenesis process, the final shapes of the two opposing rudiments do not match to with the actual interphalangeal morphology, indicating that biochemical interactions during bone morphogenesis might be necessary to achieve congruent joint shapes. Nevertheless, to date, there is still no experimental or computational model able to accurately explain how a synovial joint is shaped. Thus, the aim of this section is to develop a computational model that might bring us closer to understanding the process of joint morphogenesis.

A 2D finite element model of the interphalangeal joint that includes the synovial capsule was developed. This model considered the biochemical and mechanical effects on the joint morphogenesis, from the cavitation stage to the appearance of POC and SOC.

The model initiated with the last obtained geometry of the previous section model. This geometry was the first reference geometry. Then, the distal bone anlage of the reference geometry was

rotated to simulate the movement of the finger; only four steps of the movement were evaluated: 90°, 60°, 30° and 0°. The calculations were made on each position and then translated into the reference geometry (0°) and averaged in each element. Then, the average cartilage growth and ossification parameters were computed and used to update the reference geometry. Afterwards, the distal phalanx was rotated again to the positions analyzed. This process continued until the shape of the joint agreed with the shape of an interphalangeal joint.

Regarding the mechanical part of the model, an axial displacement of $1\mu\text{m}$ was applied to the upper boundary of the distal phalanx. The proximal phalanx was fixed at its bottom on the central node so that the other nodes of the lower end could move in the lateral direction. The cartilage of the anlagen bones was assumed to be almost incompressible.

The effect of the PTHrP and Ihh molecules was also considered. Ihh controls chondrocyte proliferation, maturation, and hypertrophy, whereas PTHrP inhibits chondrocyte hypertrophy. Additionally, a remaining part of the molecule Wnt was considered because of its action on the morphogenesis process. The initial distribution of these molecules was taken from the last step of the simulation performed in the previous section.

For tissue growth, it was assumed that the tissue response to mechanical stimuli had a positive relationship between cartilage growth and cyclic hydrostatic stress, and it was inhibited by octahedral shear stress. Additionally, it was considered that high concentrations of

PTHrP and Wnt promoted chondrocyte proliferation and, consequently, cartilage growth.

For the bone ossification, the OI was used to predict the appearance of the POC and SOC within the anlagen. It was considered that the cartilage in the diaphysis ossified under high OI and low PTHrP and Wnt, whereas for the SOC appearance, only the OI is considered.

2.2. Results and discussion from the joint morphogenesis model

Four different positions of the interphalangeal joint were analyzed. The same weight was given to each position, since there are no reports in the literature about how the fingers of the fetus move during the morphogenesis stage. The obtained final shapes of the bones' diaphysis were coherent with those seen in literature.

The appearances of SOC and POC were also simulated. SOC emerges in the top head of the proximal phalanx and in the lower head of the distal phalanx. In the proximal phalanx, it is formed as a circular shaped structure. In the distal anlage, the SOC took an elliptical shape, most likely due to the way in which the convex surface distributed the octahedral shear stress and hydrostatic stress (used to calculate the OI).

In places of low concentrations of PTHrP and high concentrations of Ihh, the chondrocytes became hypertrophic and the tissue eventually ossified forming the POC. The model showed how the OI predicts areas of high ossification on the diaphysis, and how the PTHrP and hydrostatic stresses helped with the cartilage growth and maintenance. The obtained results are comparable with those from

former studies where only the endochondral ossification and OI distribution was analyzed.

The obtained joint shape agrees remarkably with those observed in *x-rays*. Therefore, this work sheds some light on how the mechanical environment, combined with biochemical factors, influences the morphogenesis of a synovial joint. It is worth mentioning that dynamic hydrostatic stress, since it promotes cartilage growth, is key to joint morphogenesis. However, for a joint to achieve complex shapes, it is necessary to include cell/tissue responses to biochemical and mechanical stimuli.

The presented model offers an excellent approximation of what is happening during joint development and morphogenesis and provides a new understanding of these processes which, eventually, may lead to the development of new treatments for developmental pathologies, or even prevent malformations of the fetus.

3- Patella Onset

There is still a lack of understanding about the development of the patella. The most accepted theory is that it develops inside the tendon in response to mechanical stimuli. While the tendon is immature, a zone of the tendon is subjected to high hydrostatic stress and low tensile strain. This leads to the differentiation of the fibrous tissue precursor into cartilage and then to the ossification of the cartilage to form the patella.

Currently, according to the best of our knowledge, there is no accepted nor unified mechanism in the literature that explains the

formation of sesamoid bones. The aim of this part of the document was to evaluate, separately, the outcome of three conceptual computational models for the development of the kneecap. The first model considered the biochemical aspects present at the onset of the quadriceps tendon and the patella. The second model examined the cellular behavior under the mechanical stimuli present during the formation of this sesamoid bone. And the third model optimized the mechanical environment of the tissues through topological optimization (TO) based on the minimizing the strain energy.

3.1. *Biochemical theory*

This biochemical theory was first proposed by Eyal *et al.* According to this theory, the patella develops as a bone eminence attached to the distal femur end, where new sox9-positive chondrogenic cells attach to the mentioned femoral end. This new aggregation of chondrogenic cells is separated from the preexisting cartilage because of the effect of a remaining joint inducer on the articular surface of the femur.

The model started with the initial conditions given by the concentrations of the molecules and a domain of Scx-cells. Then, TGF- β and BMP diffused from muscle and bone and, consequently, the Scx-cells were attracted towards high concentrations of TGF- β . Once the muscle detected the presence of Scx-cells, it expressed FGF. The differentiation process involved the Scx-cells and the concentrations of FGF and BMP. If there was enough concentration of Scx-cells and BMP, the cells differentiated into chondrocytes, whereas if there was enough concentration of Scx-cells and FGF, the cells differentiated into

tenocytes (tendon tissue). At the same time, the remaining interzone marker (named GDF-5) diffused inside the newly formed cartilage structure, which later will induce the joint formation between the patella and the femur.

This theory was evaluated with different flexion angles of the leg (30°, 45°, 60° and 90°), without modifying any other parameter. The range of the angle changed the coinciding area between the zone where the tendon will form and the distal end of the femur. No patella-like structure was achieved with 30° and 45°, only a small incipient patella at 60°, and a complete patella-like structure with 90°. This outcome was possible since the coinciding area is much smaller and proximal with 30°, 45° and 60°.

The obtained results with this theory for the 90° model were coherent with the histological observations made by Eyal *et al.* A patella-like structure embedded superficially within the tendon was obtained only considering the biochemical factors involved in the development of the tendon and the eminence. Hence, it might be possible that the patella onset is a consequence of a biochemical process, without any mechanical influence.

3.2. *Mechanical theory:*

The mechanical stimuli play a crucial role in tissue differentiation. The mechanical conditions of the tendons in formation generate a favorable environment for the development of the patella. The tendon is a fibrous tissue (dense connective tissue) composed by bundles of parallel type I collagen fibers. According to the theory

proposed by Carter *et al.*, if the fibrous tissue (tendon) is subjected to high compressive hydrostatic stress (with a low principal tensile strain), it may differentiate from fibrous tissue to cartilage and eventually become the patella (sesamoid bone).

This theory posits that the patella bone is formed due to high hydrostatic stress and low tensile strain in specific regions of a fibrous tissue, such as the tendon. Leg flexion angles of 30°, 45°, 60°, 90° and 110° were analyzed in this thesis. The results of all flexion angles of the leg were projected in the domain at 90° to facilitate comparison of the stress distributions.

Considering that the understanding of the embryo movement is limited, three different scenarios were modeled in which the effect of each leg angle was averaged. The weightings for the angles of 30°, 45°, 60°, 90° and 110° for the three scenarios were as follows: for *Scenario 1* (soft weighting of high flexion angles), 5%, 10%, 15%, 25% and 45%; for *Scenario 2* (heavily weighting low flexion angles), 60%, 25%, 9%, 5%, and 1%; and for *Scenario 3* (heavily weighting high flexion angles), 1%, 5%, 9%, 25% and 60%.

The results obtained with this model show the development of a patella-like structure embedded within the tendon, the same as with the biochemical theory. The size of the structure depended on the flexion angle. This might indicate that the wrapping (mechanical environment) of the tendon on the distal femoral end generates the mechanical conditions necessary for the patella onset.

3.3. *Topological optimization TO*

This theory is also based on mechanical stimuli and its influence on tissue differentiation, which might also be explained through TO. TO can be applied in tissue remodeling, as it iteratively redistributes the material in a design domain determining an optimal material arrangement or tissue type. This adaptation process can be characterized as a self-enhancing system with the objective of minimizing tendon strain.

As an initial condition, this thesis considered that the tendon was already formed and loaded. A two-dimensional FEA is performed based on the algorithm proposed on Sigmund. The algorithm is founded on the “power-law approach”, also known as SIMP approach. This approach assumes that properties of the materials are constant within each element of the design domain, whereas the relative material densities of the elements are the variables.

The same flexion angles that in the mechanical theory are tested in this case, but no weighting is considered. However, coherent results (formed patella) are obtained only with 90° and 110°. For these angles, a high-density zone close to the usual patella position was observed. Specifically, for the 90° case, the shape of the high-density zone was more consistent with reality. This suggested that the mechanical environment that surrounds the tendon may affect the patella and its development.

3.4. *Discussion of the patella development theories*

In the three evaluated theories, a patella-like structure was obtained for the highest tested flexion angles of the leg. The results show that tissue remodeling and adaptation, based on Carter's theory or on TO, could answer the patella onset. The shape, position and size of the patella would depend on the flexion angle of the leg and on the time that the leg spends in each position, obtaining a larger patella compared to the biochemical approach. However, there is not much evidence in the literature that can support the second and third theories. Therefore, mechanical loading may not be necessary for the appearance of the patella, but it may be necessary for its morphogenesis and maintenance.

Arguably, molecular factors and their interactions trigger the formation of the patella, as evidenced by the molecular expression of the cells analyzed in histological slides. These factors, applied to a computational model, are consistent with the obtained results. However, since the limitation of the movement alone does not guarantee that there are no hydrostatic stresses in the tendon, more tests should be performed in which only biochemical factors influence the development of the tendon and the patella. It is also possible that these mechanisms are redundant and that both influence the patella onset

Also, it is certain that the mechanical environment must affect patella development. However, this environment might affect it mainly after the tendon is formed by helping the patella to obtain its final shape and maintain its structure. This work is a first approximation on the understanding of the process of the development of the patella. Furthermore, these models could provide new insights and guidelines

of experimentation and mathematical models. A combination of the evaluated theories in this study is suggested as future work, so that the patella onset is determined due to biochemical factors and, subsequently, the mechanical loads may regulate its shape and maintenance.

4- Cartilage Regeneration

4.1. *Methodology for the cartilage regeneration model*

A plain strain axisymmetric 2D geometry was developed in this thesis to represent a simplified cartilage-bone-scaffold structure. The normal stress and strain conditions for the subchondral and trabecular bone were established by applying load prior to the scaffold implantation. An oscillatory load of 1 Hz frequency is applied until the values of FV, stress and strain stabilize. It is assumed that the cartilage undergoes this load every day of simulation.

Articular cartilage consists of an ECM divided into two phases: solid and fluid. The solid phase contains mainly proteoglycans (PGs) and a type-II collagen fibrillar network. The bundles of primary fibrils extend perpendicular from the subchondral bone, which near the surface gradually curve to a horizontal course, parallel to the articular surface. The collagen fibrils were modeled as linear elastic tension-only materials. The non-fibrillar part of the solid part was assumed as linear poroelastic.

For the bone, it was employed a basic bone remodeling model that considered the response to strain, and the basal conditions as initial conditions. Before the scaffold was implanted, the maximum basal

deformation was calculated as an average of the maximum daily deformation of the tissue. After the implantation of the scaffold, abnormal loading conditions were generated, hence the patterns of maximum strain within the tissue changed. This variation in strain conditions was considered to affect the bone density distribution, and therefore the Young's modulus of the subchondral and trabecular bone.

It was established that the bone tissue under the scaffold failed if the average Young's modulus of the line of elements under the scaffold was smaller than a threshold. If the bone failed, the scaffold was able to move down into the bone.

A PVF was also considered (hypothetic molecule, with low diffusion rate, that determined if a mesenchymal tissue might be vascularized or not). It is assumed that this factor is diffuses from the bottom of the domain to the upper part of the domain.

The developed model dealt with the regeneration of two types of tissue: cartilage and bone. The osteogenesis process was regulated by the mechanical environment. For bone regeneration, a mechanistic model of tissue differentiation was used that couples the cellular mechanisms to mechanical stimuli during bone healing.

As far as the author know, there are not many computational models in the literature to explain how this tissue is regenerated. Hence, a positive relationship between cyclic hydrostatic stress and cartilage growth was considered. Besides, the model is configured so that the cartilage can only regenerate in elements with mesenchymal tissue and only with low concentrations of PVF.

Once there was any displacement of the scaffold due to the failure of the bone under it, the void remaining at the top of the scaffold was then filled with mesenchymal tissue, which later differentiated into other tissue (bone, cartilage, or fibrous tissue). For a mesenchymal element to differentiate into cartilage, two conditions must be accomplished: the element must have had low concentration of PVF, and it must have a cartilage neighbor element subjected to high hydrostatic stress. If none of the above conditions were achieved, the osteogenesis model activates. In this case the mesenchymal tissue could differentiate into fibrous, cartilage or bone tissue depending on the mechanical stimuli, which was the combined effect of the deviatoric strain and FV.

4.2. Results and discussion from the cartilage regeneration model

The bone resorption and apposition processes were modeled as changes in the Young's modulus of bone. In the results, the trabecular bone must remodel in order to bear the abnormal load brought by the scaffold. Moreover, the Young's modulus of the trabecular bone increased in the zone under the scaffold once it was implanted; but decreases, due to the overload, in the element line just under the scaffold. On the other hand, cartilage forms on top of the scaffold until the fourth and sixth month, when the concentration of the PVF is high enough to avoid the formation of cartilage.

When the osteogenesis process was activated, the calculated mechanical stimulus was ideal to stimulate bone tissue, so it differentiates only into bone.

One year after the implantation of the scaffold, the model revealed a cartilage completely recovered and the scaffold displaced into the bone. These results were in concordance with those obtained by Sancho-Tello *et al.*, who implanted a copolymer porous scaffold in the knee joint of a rabbit to repair a full-depth chondral defect.

The computational model developed in this thesis can be used to compare the effect of using different scaffold materials, different loading conditions, or tissue degeneration (pathology) with respect to ideal treatment conditions. It can also be helpful when planning treatments for the regeneration of articular cartilage.

5- General Conclusions of the thesis

In this thesis, several aspects of the synovial joints are explored from its onset to its mature state. In particular, four different computational models are proposed to reproduce the development of the synovial joints and the regeneration of the articular cartilage based on mechanical and biochemical factors. In general, the obtained results from the simulations show a great concordance with the histological studies experiments reported in the literature.

The developed model for the joint onset was able to explain the interphalangeal joint development through the interaction of only six generic molecular factors. Therefore, it can be concluded that the interzone formation and the cavitation processes are regulated by the concentrations of six molecules related to: GDF-5, Noggin, Ihh, PTHrP, Hox genes, and Wnt.

As opposed to previous computational models, the morphogenesis model proposed in this thesis includes biochemical factors in addition to the mechanical ones, which led to a notably higher degree of agreement between the final shape of the simulated interphalangeal joint and the shapes reported in histological studies. It is therefore demonstrated that both mechanical and biochemical stimuli are needed for synovial joints to achieve their final shapes.

In addition, we were able to predict the appearance of this sesamoid with the three evaluated theories, being the "biochemical theory" the one that showed the best results and is supported by recent histological studies found in the literature. We propose that the molecular interaction triggers the beginning of the patella and that the mechanical loads are necessary for the growth and maintenance of the patella.

According to the results obtained by the cartilage regeneration model, not only the cartilage has to adapt during the regeneration process but also the surrounding tissue. The developed computational model can be helpful to compare different scaffold materials and load conditions and evaluate which treatment approach might result in a better outcome.

The computational models developed in this thesis allow to evaluate many different mechanical and biochemical conditions of some biological phenomena, that would be hard to test through experimental set-up. We hope that these models have the potential to

Summary

become useful tools in medical and biological research, helping in the design of therapeutic strategies for joint related pathologies.

SUMMARY IN VALENCIAN

Les articulacions connecten els components esquelètics i habiliten el moviment relatiu entre ells. Entre els diferents tipus d'articulacions, les sinovials ofereixen el rang de moviment més ampli entre ossos. La majoria de les articulacions sinovials es troben a l'esquelet apendicular (extremitats) i, encara que poden presentar diferents estructures internes, quatre trets comuns les caracteritzen: la càpsula articular tancada que conté el líquid sinovial (lubricant); les superfícies del cartílag articular, situades sobre cada os de l'articulació, llisquen entre elles; la membrana sinovial, que proporciona el tancament de la càpsula; i els lligaments, el tendó i els músculs, que proporcionen estabilitat i mobilitat a l'articulació.

Com es formen aquestes articulacions? Alguns estudis han mostrat que l'inici i el desenvolupament de les articulacions sinovials estan regulats per diferents factors genètics, bioquímics i mecànics al llarg del temps. El seu desenvolupament comença durant les etapes fetals del desenvolupament prenatal. Després d'unes cinc setmanes de desenvolupament, els brots de les extremitats comencen a créixer i es fan notables. Al principi, aquests brots tenen una massa ininterrompuda de cèl·lules mesenquimàtiques dins del seu nucli. Aquest gruix de cèl·lules mesenquimàtiques s'anomena blastema esquelètic i està cobert per una capa d'ectoderma. Llavors, la majoria de les cèl·lules blastemàtiques diferencien en condròcits. No obstant això, algunes romanen a la interzona, on es formarà la futura articulació. La separació

de l'articulació es produeix durant el procés de cavitació: les cèl·lules de la interzona tendeixen a patir apoptosi deixant un espai entre els rudiments d'os condròcit.

Després de l'escissió articular (cavitació), es produeix la morfogènesi: les cèl·lules proliferen a ambdues bandes de l'articulació permetent que el cap de l'os prenga la seua forma final. Alguns estudis han demostrat que els moviments i les contraccions musculars durant el desenvolupament de les extremitats afecten la forma que prenen les articulacions, encara que els factors bioquímics locals i sistèmics també hi podrien afectar. Si es donen condicions anormals durant el desenvolupament fetal, les articulacions poden desenvolupar-se incompletament o anormal o ni tan sols desenvolupar-se.

Una vegada finalitzat el període embrionari, les articulacions sinovials i la seua estructura interna (cartílag articular, lligaments i càpsula sinovial) ja estan completament desenvolupades. A més, apareixen els centres d'ossificació primari (*primary ossification center*, POC) i secundari (*secondary ossification center*, SOC). Aquestes estructures ajuden a que l'os creixca i s'ossifique fins que assoleix l'edat adulta.

No obstant, una vegada formades, les articulacions poden patir diverses patologies que afecten el seu moviment i, potencialment, també l'estil de vida de l'individu que les pateix. Entre les possibles causes d'aquestes patologies es troben, entre altres, els traumatismes reiterats, l'envelliment, la cirurgia, l'obesitat, els desordres hormonals, les lesions en les superfícies de les articulacions o sobrecàrrega deguda a la malformació de l'articulació.

Per exemple, en una malaltia degenerativa de les articulacions com l'artrosi, el desgast i la degeneració del cartílag articular poden arribar a causar-ne la pèrdua d'una porció en la superfície articular. A més, el cartílag no es pot regenerar, només és capaç de reemplaçar la part desgastada per un teixit més dur, el cartílag fibrós. Aquest nou teixit produeix una superfície articular irregular que pot causar dolor i rigidesa, agreujant així la patologia.

Des de simptomàtics fins a d'altres més invasius, diversos tractaments s'han proposat per a la reparació del cartílag articular. Com a últim recurs s'utilitzen el reemplaçament total de l'articulació afectada o l'artròdesi, *i.e.* la fusió de tots o alguns dels ossos que formen l'articulació sinovial. Òbviament, es prefereix preservar l'estructura i la funció originals de l'articulació, especialment en pacients joves.

L'enginyeria de teixits proposa accions no invasives per a trobar un tractament definitiu per a la degeneració del cartílag. Durant les últimes dues dècades, a més de l'empelt osteocondral, s'han proposat els implants, que permeten omplir ràpidament els defectes de l'articulació i aporten un substrat per al fixament de les cèl·lules. La tècnica de l'implant involucra tres aspectes fonamentals: el material de l'implant, els factors de diferenciació cel·lular i les fonts cel·lulars. Però també s'han obtingut bons resultats amb implants sense fonts cel·lulars. D'aquesta manera s'eviten riscos associats amb la manipulació de les cèl·lules (*e.g.* contaminació bacteriana, pèrdua de fenotips) i es redueix el cost econòmic.

Per a desenvolupar noves estratègies terapèutiques que siguen efectives, és imprescindible comprendre els processos que afecten el teixit articular des del seu desenvolupament fins a la seua maduresa. No obstant, aconseguir-ho únicament mitjançant anàlisis experimentals pot resultar molt costós en termes de recursos i temps. Per tant, els models computacionals es presenten com una ferramenta convenient per a complementar l'estudi dels processos articulars. Aquests models utilitzen informació resultant d'anàlisis clíniques i observacions experimentals per a avaluar quantitativament i qualitativa les interaccions mecàniques i bioquímiques que es donen en els processos abans mencionats. Així, els models computacionals contribueixen a aquests estudis, ja que avaluen les condicions difícils d'implementar experimentalment.

En aquesta tesis s'estudien, mitjançant models computacionals, la interacció bioquímica de la formació de la interzona i el procés de cavitació durant el desenvolupament de les articulacions sinovials. En el cas del procés de morfogènesi, a més de la interacció bioquímica, també es considera el possible efecte de la possible càrrega mecànica durant la formació de les epífisis.

També s'analitzen computacionalment diferents teories proposades per a explicar l'existència dels ossos sesamoides, *i.e.* xicotets ossos o cartílags medul·lars envoltats de tendons normalment situats al voltant de les articulacions. L'estudi se centra en la ròtula, el major i més estudiat os sesamoide present en el cos humà.

A més, també s'analitzen, mitjançant un model computacional, els processos que ocorren quan s'utilitza un implant polimèric per a

tractar un defecte en el cartílag articular. D'aquesta manera es pot comparar com influeixen el material, la forma i les condicions de l'implant en el resultat del tractament.

En resum, els objectius d'aquesta tesi són:

Objectiu principal:

La modelització computacional dels processos mecànics i biològics que ocorren Durant el desenvolupament de les articulacions sinovials.

Objectius específics:

- La formulació matemàtica dels fenòmens mecanobiològics que controlen el desenvolupament de les articulacions sinovials.
- L'avaluació computacional del comportament del model durant la formació de la interzona de les articulacions sinovials.
- L'avaluació computacional del comportament del model durant el procés de cavitació i la morfogènesi de les articulacions sinovials.

1. Aparició de l'articulació

1.1. *Metodologia per al model d'aparició d'articulacions:*

Es desenvolupa un model computacional basat en dues accions moleculars genèriques i dos bucles d'autorregulació expressats com a equacions de reacció-difusió. L'objectiu és predir els patrons moleculars associats al procés de formació de l'articulació. El model es resol mitjançant l'anàlisi d'elements finits. Les equacions matemàtiques prediuen patrons que representen mecanismes moleculars que modelitzen les estructures i les formes durant el

desenvolupament de les articulacions, com ara la formació de la interzona, la cavitació i la forma condílica dels extrems de les articulacions.

Les equacions de reacció-difusió i la formació de patrons de Turing s'utilitzen per simular la localització del clivatge articular, el nombre d'articulacions formades, les superfícies de les articulacions que formaran les epífisis i la forma condílica inicial de l'articulació.

En base a les molècules que, segons la literatura, intervenen en el desenvolupament de les articulacions, es modelitzen sis factors moleculars genèrics involucrats en l'aparició de les articulacions. Cada factor pot representar diferents molècules realitzant la mateixa acció. El procés del model s'organitza en dues etapes. La primera marca l'inici de la interzona, el factor (G), que es troba a la posició d'escissió, mentre que el seu antagonista, factor (N), està per tot arreu. El factor (G), que està relacionat amb el GDF-5, evita la diferenciació del teixit mesenquimàtic en cartílag, mentre que el factor (N) és controlat per l'antagonista de BMP, Noggin. En la segona etapa, les zones que es diferencien en cartílag secreten Ihh, factor (I), i PTHrP, factor (P), que estableixen un bucle regulador que regeix la proliferació cel·lular i la hipertròfia. El factor (I) regula la proliferació de condrocits, la maduració i la hipertròfia, mentre que el factor (P) inhibeix la hipertròfia de condrocits.

Mentrestant, el domini segueix creixent i dos altres factors, (H) i (W), regulen la separació de l'articulació i en relacionen les estructures. (H) controla la quantitat diferencial de creixement del teixit de proximal a distal. Matemàticament, hi ha un gradient en (H) que

afecta el ritme de creixement promovent el creixement longitudinal de les extremitats i dels primordis dels ossos. (W), secretat en la interzona, indueix la mort cel·lular i permet la generació d'un espai articular. Els factors (H) i (W), associats respectivament als gens Hox i el senyal Wnt, condueixen a la separació dels rudiments i també s'observen en parts de la càpsula fibrosa en etapes posteriors de desenvolupament.

El model d'elements finits inclou equacions diferencials parcials (*partial differential equations*, PDE) integrades amb un sistema del tipus *Cellular Automaton* (CA). La part de les PDE descriu la difusió molecular i estableix les concentracions bioquímiques, que permeten a la part de la CA determinar si el teixit es diferencia o no. Cada element comença amb un estat de teixit (mesenquimàtic, pre-cartilaginós, cartilaginós o interzonal) i el sistema CA permet que l'element es diferencie d'un estat de teixit a un altre. Aquest procés es repeteix fins que s'arriba al criteri de parada.

S'exploren quatre casos diferents. En el *Cas I*, s'estableixen les condicions per al desenvolupament d'una articulació interfalàngica. Els tres casos següents són modificacions de la primera. En el *Cas II* i el *Cas III*, s'analitza l'efecte de canviar les dimensions del domini inicial en el desenvolupament de l'articulació. En el *Cas IV*, s'analitza com les taxes de creixement del domini modifiquen el resultat. A més, es replica un procediment experimental paral·lel en el qual s'implanta GDF-5 al costat i a la punta d'un dit de la pota en desenvolupament d'un pollet.

1.2. *Resultats i discussió del model d'inici de l'articulació*

En el *Cas I*, la comparació dels resultats obtinguts per al factor (G) amb la secreció de GDF-5 en estudis experimentals demostra distribucions similars. A més, el bucle (I)-(P) resulta en una distribució on (P) és a prop dels extrems distals i (I) es troba als extrems proximals del rudiment, tal com es veu a la literatura per a Ihh i PTHrP.

El factor (W) estableix la formació del cartílag articular a cada superfície articular i és coherent amb la distribució de Wnt a la literatura. La forma de l'articulació és comparable amb les troballes histològiques: els dos costats de l'articulació tenen un cartílag articular, però en un costat hi ha una estructura semblant a una epífisi. Això condueix a la formació d'una epífisi més gran a l'extrem distal i un altre de menor grandària a l'extrem proximal. A partir d'aquest moment, és probable que les condicions mecàniques afecten en la morfologia de l'articulació.

Els resultats obtinguts suggereixen que la mida del domini inicial durant el desenvolupament pot influir en el nombre d'articulacions sinovials formades. En la simulació, s'adquireixen una i tres articulacions quan la ràtio longitud/amplada es fixa en 3 (*Cas I*) i en 5 (*Cas II*), respectivament. Els patrons de Turing depenen de la ràtio longitud/amplada del domini, per tant, el nombre d'articles ha de dependre de la geometria inicial. No obstant això, la literatura mostra que només es pot formar una articulació simultàniament i per això, en el model proposat, es forma una articulació cada vegada que el primordi distal dins d'un brot de les extremitats assoleix una ratio longitud/amplada aproximada de 3.

En el *Cas III* (velocitat de creixement més ràpida), s'obté una única articulació amb dues regions ràpid creixement situades en ambdós extrems dels rudiments amb altes concentracions de (I). En el *Cas IV*, l'objectiu és simular l'aparició d'una articulació situada entre un os gran i un altre més curt (*e.g.* entre un metatarsià o un metacarpà i una falange). Per tant, la ràtio longitud/amplada del seu domini inicial es fixa en 2.5.

El *Cas V* i el *Cas VI* simulen l'estudi experimental realitzat per Merino *et al.* (1999), que analitza els efectes de la implantació de GDF-5 en les potes en desenvolupament de pollets embrionaris, concretament a la punta dels dits. En comparar els resultats del *Cas V* i del *Cas VI* amb els obtinguts per Merino *et al.* (1999), es troben tres similituds: s'aconsegueix una morfologia molt similar, el rudiment resultant es corba quan la molècula s'implanta en una de les cares de la condensació mesenquimàtica, i el bulb es forma quan (G) s'implanta a la punta del primordi. Aquests efectes poden ser deguts a l'alta concentració de (G) que, després del procés de cavitació, implica una alta concentració de (W) fomentant la diferenciació del teixit en cartílag articular. Aquesta ubicació anormal del cartílag articular afecta el patró de Turing entre (I) i (P), per la qual cosa s'obté un creixement anormal del teixit.

En aquesta tesi es proposa un model simplificat per estudiar el desenvolupament de les articulacions. Es troba un bon acord entre els resultats obtinguts amb el model de simulació i els d'estudis experimentals trobats a la literatura que inclouen anàlisis histològiques. Encara que moltes molècules sovint influeixen en el mateix procés biològic, es mostra, mitjançant la modelització de molècules

genèriques, com la formació de patrons simples entre molècules enzim-substrat prediu molts esdeveniments presents en la formació de les articulacions. El model mostra una bona resposta amb articulacions interfalàngiques i metacarpianes/metatarsianes-falàngiques. Els resultats obtinguts en aquest capítol seran útils per als investigadors centrats en patologies associades al desenvolupament d'embrions i articulacions. A més, aquest model podria proporcionar noves idees i pautes d'experimentació i, per descomptat, nous models matemàtics i computacionals de les següents fases del desenvolupament de les articulacions.

2. Morfogènesi d'articulació

2.1. Metodologia per al model de morfogènesi d'articulació

Després de l'inici de l'interzona i el procés de cavitació, es produeix l'últim pas del desenvolupament de les articulacions, la seva morfogènesi. Els estudis experimentals i computacionals han demostrat que hi ha una relació entre l'esforç mecànic i la morfogènesi de l'esquelet. Des de la perspectiva computacional, s'han desenvolupat dos models per avaluar la relació entre la morfogènesi de les articulacions i els esforços mecànics. Heegaard *et al.*(1999) i Giorgi *et al.* (2014), tots dos estudis computacionals, van utilitzar la distribució d'estrès hidrostàtic per descriure el creixement i la morfogènesi articular. Tot i que aquests estudis han obtingut resultats rellevants en el procés de morfogènesi, les formes finals dels dos rudiments oposats no coincideixen amb la morfologia real interfalàngica, la qual cosa indica que les interaccions bioquímiques durant la morfogènesi òssia podrien ser necessàries per aconseguir formes articulars congruents. No obstant

això, fins a la data, encara no hi ha cap model experimental ni computacional capaç d'explicar amb precisió com es forma la junta sinovial. Així, l'objectiu d'aquesta secció és desenvolupar un model computacional que ens permeti apropar-nos a la comprensió del procés de morfogènesi de les articulacions.

Es va desenvolupar un model d'elements finits en 2D de l'articulació interfalàngica que inclou la càpsula sinovial. Aquest model va considerar els efectes bioquímics i mecànics sobre la morfogènesi de les articulacions, des de l'etapa de cavitació fins a l'aparició de POC i SOC.

El model iniciat amb una geometria aproximada d'una articulació sinovial. Aquesta geometria va ser la primera geometria de referència. A continuació, es va fer girar l'os distal de la geometria de referència per simular el moviment del dit; només es van avaluar quatre passos del moviment: 90°, 60°, 30° i 0°. Els càlculs es van fer a cada posició i després es van traduir a la geometria de referència (0°) i es van fer mitjanes en cada element, i es van calcular els paràmetres mitjans de creixement i ossificació del cartílag i es van utilitzar per actualitzar la geometria de referència. Aleshores, la falange distal es va girar de nou a les posicions analitzades. Aquest procés va continuar fins que la forma de l'art va coincidir amb la forma d'una articulació interfalàngica.

Pel que fa a la part mecànica del model, s'aplica un desplaçament axial d'1µm al límit superior de la falange distal. La falange proximal es va fixar al fons del node central de manera que els

altres nodes de l'extrem inferior poguessin moure's en la direcció lateral. Se suposava que el cartílag dels primordi d'os era gairebé incompressible.

També es va considerar l'efecte de les molècules PTHrP i Ihh. Ihh controla la proliferació de condrocits, la maduració i la hipertròfia, mentre que el PTHrP inhibeix la hipertròfia de condrocits. A més, es va considerar una part restant de la molècula Wnt per la seva acció en el procés de morfogènesi. La distribució inicial d'aquestes molècules s'ha extret de l'últim pas de la simulació realitzada al capítol anterior.

Per al creixement dels teixits, es va assumir que la resposta dels teixits als estímuls mecànics tenia una relació positiva entre el creixement del cartílag i l'estrès hidrostàtic cíclic i que va ser inhibida per una tensió de tall corticològica. A més, es va considerar que altes concentracions de PTHrP i Wnt van promoure la proliferació de condrocits i, per tant, el creixement del cartílag.

Per a l'ossificació òssia, s'ha utilitzat l'OI per predir l'aparició del POC i el SOC dins de els primordi d'os. Es va considerar que el cartílag en la diàfisi es va ossificar sota un alt OI i PTHrP i Wnt baix, mentre que per a SOC es considera només l'OI.

2.2. Resultats i discussió per al model de morfogènesi d'articulació:

Es van analitzar quatre posicions diferents de l'articulació interfalàngica. Es va donar el mateix pes a cada posició, ja que no hi ha informes a la literatura sobre com es mouen els dits del fetus durant la

fase morfogènica. Les formes finals obtingudes de la diàfisi dels ossos són coherents amb les observades a la literatura.

També es van simular les aparences de SOC i POC. El SOC emergeix al capçal superior de la falange proximal i al capçal inferior de la falange distal. A la falange proximal, es forma com una estructura de forma circular. A l'anàlisi distal, el SOC va prendre una forma el·líptica, probablement a causa de la forma en què la superfície convexa va distribuir l'estrès octaèdrica de tall i l'estrès hidrostàtic (que s'utilitza per calcular l'OI).

En llocs de baixes concentracions de PTHrP i altes concentracions de Ihh, els condrocits es van convertir en hipertròfia i el teixit va ossificar-se eventualment formant el POC. El model va mostrar com l'OI prediu àrees d'ossificació elevades en la diàfisi, i com el PTHrP i les tensions hidrostàtiques ajuden amb el creixement i el manteniment del cartílag. Els resultats obtinguts són comparables amb els dels estudis anteriors on només es va analitzar l'ossificació endocondral i la distribució OI.

La forma de l'articulació obtinguda coincideix notablement amb les observades a les radiografies. Per tant, aquest treball ens explica com l'entorn mecànic, combinat amb factors bioquímics, influeix en la morfogènesi d'una articulació sinovial. Val la pena esmentar que l'estrès dinàmic hidrostàtic, ja que promou el creixement del cartílag, és clau per a la morfogènesi de les articulacions. No obstant això, per tal que una articulació aconseguixi formes complexes, cal incloure respostes cel·lulars/tissulars a estímuls bioquímics i mecànics.

El model presentat ofereix una excel·lent aproximació al que passa durant el desenvolupament i la morfogènesi de les articulacions i proporciona una nova comprensió d'aquests processos que, eventualment, poden conduir al desenvolupament de nous tractaments per a patologies del desenvolupament, o fins i tot prevenir malformacions del fetus.

3. Aparició de la ròtula

Encara existeix una manca de comprensió sobre el desenvolupament de la ròtula. La teoria més acceptada és que es desenvolupa dins del tendó en resposta a estímuls mecànics. Mentre el tendó és immadur, una zona del tendó està sotmesa a una elevada tensió hidrostàtica i una baixa deformació de tensió. Això condueix a la diferenciació del teixit fibrós en cartílag i després a l'ossificació del cartílag per a formar la ròtula.

Actualment, segons el coneixement dels autors, no hi ha cap mecanisme acceptat ni unificat en la literatura que explique la formació d'ossos sesamoides. L'objectiu d'aquesta part del document és avaluar, per separat, el resultat de tres models computacionals conceptuals per al desenvolupament de la ròtula. El primer model considera els aspectes bioquímics presents en l'aparició del tendó del quàdriceps i la ròtula. El segon model examina el comportament de les cèl·lules sota els estímuls mecànics presents durant la formació de la ròtula. I el tercer model optimitza l'entorn mecànic dels teixits mitjançant l'optimització topològica (topological optimization, TO) basant-se en la minimització de l'energia de deformació.

3.1. *Teoria bioquímica:*

Aquesta teoria bioquímica va ser proposada per primera vegada per Eyal *et al.* (2015). Segons aquesta teoria, la ròtula es desenvolupa com una eminència òssia adherida a l'extrem distal del fèmur, on les noves cèl·lules cartilaginoses de *sox9* s'uneixen a l'esmentat extrem femoral. Aquesta nova agregació de cèl·lules cartilaginoses se separa del cartílag preexistent a causa de l'efecte d'un inductor de l'articulació restant a la superfície articular del fèmur.

El model comença amb les condicions inicials donades per les concentracions de les molècules i un domini de les cèl·lules Scx. Després, el TGF- β i el BMP es difonen a partir del múscul i l'os i, en conseqüència, les cèl·lules Scx són atretes cap a altes concentracions de TGF- β . Una vegada que el múscul detecta la presència de cèl·lules Scx, secreta FGF. El procés de diferenciació implica les cèl·lules Scx i les concentracions de FGF i BMP. Si hi ha suficient concentració de cèl·lules Scx i BMP, les cèl·lules es diferencien en condròcits, mentre que si hi ha prou concentració de cèl·lules Scx i FGF, les cèl·lules es diferencien en tenòcits (teixit del tendó). Al mateix temps, el marcador interzona restant (anomenat GDF-5 en aquest model) es difon dins de l'estructura del cartílag de recent formació, que posteriorment induirà la formació de les articulacions entre la ròtula i el fèmur.

En aquesta tesi, s'avalua la teoria amb diferents angles de flexió de la cama (30°, 45°, 60° i 90°) sense modificar cap altre paràmetre. El rang de l'angle canvia l'àrea coincident entre la zona on es formarà el tendó i l'extrem distal del fèmur. Amb 30° i 45°, no s'aconsegueix cap

estructura de tipus ròtula. Amb 60°, només s'observa una xicoteta ròtula incipient. I amb 90°, es forma una estructura completa de tipus ròtula. Aquest resultat és possible ja que la zona de coincidència és molt més menuda i proximal amb 30°, 45° i 60°.

Els resultats obtinguts amb aquesta teoria i una flexió de 90° són coherents amb les observacions histològiques realitzades per Eyal *et al.* (2015). S'obté una estructura de tipus ròtula incrustada superficialment dins del tendó només tenint en compte els factors bioquímics implicats en el desenvolupament del tendó i de l'eminència. Per tant, és possible que l'aparició de la ròtula siga conseqüència d'un procés bioquímic, sense cap influència mecànica.

3.2. Teoria mecànica:

Els estímuls mecànics tenen un paper crucial en la diferenciació de teixits. Les condicions mecàniques dels tendons en formació generen un entorn favorable per al desenvolupament de la ròtula. El tendó és un teixit fibrós (teixit connectiu dens) compost per feixos de fibres de col·lagen de tipus I paral·leles. Segons la teoria proposada per Carter *et al.* (1987), si el teixit fibrós (tendó) està sotmès a una elevada tensió hidrostàtica compressiva (amb una baixa deformació de tensió en la direcció principal), pot diferenciar-se en cartílag i, finalment, convertir-se en la ròtula (os sesamoide).

Aquesta teoria postula que l'os de la ròtula es forma a causa d'una elevada tensió hidrostàtica i de baixa deformació de tensió en regions específiques d'un teixit fibrós com el tendó. En aquesta tesi s'analitzen angles de flexió de les cames de 30°, 45°, 60°, 90° i 110°. Els

resultats de tots els angles de flexió de la cama es projecten al domini a 90° per facilitar la comparació de les distribucions de tensió.

Tenint en compte que la comprensió del moviment embrionari és limitada, es modelen tres escenaris diferents en els que es mitjana l'efecte de cada angle de la cama. Els pesos per als angles de 30° , 45° , 60° , 90° i 110° per als tres escenaris són els següents: per a l'*Escenari 1* (afavorint lleugerament els angles de flexió grans), 5%, 10%, 15%, 25% i 45%; per a l'*Escenari 2* (afavorint fortament els angles de flexió menuts), 60%, 25%, 9%, 5% i 1%; i per a l'*Escenari 3* (afavorint fortament els angles de flexió grans), l'1%, el 5%, el 9%, el 25% i el 60%.

Els resultats obtinguts amb aquest model mostren el desenvolupament d'una estructura de tipus ròtula incrustada dins del tendó, igual que la teoria bioquímica. La mida de l'estructura depèn de l'angle de flexió. Això pot indicar que l'embolcall (entorn mecànic) del tendó sobre l'extrem femoral distal genera les condicions mecàniques necessàries per a l'aparició de la ròtula.

3.3. *Optimització topològica TO*

Aquesta teoria també es basa en estímuls mecànics i la seua influència en la diferenciació de teixits, que també es pot explicar a través de TO. La TO es pot aplicar en la remodelació de teixits, ja que redistribueix iterativament el material en un domini de disseny determinant una disposició òptima del material o tipus de teixit. Aquest procés d'adaptació es pot caracteritzar com un sistema d'automillora amb l'objectiu de minimitzar la deformació del tendó.

Com a condició inicial, aquesta tesi considera que el tendó ja està format i suportant càrrega. Es realitza un FEA bidimensional basat en l'algorisme proposat per Sigmund (2001). L'algorisme es basa en l'enfocament de la "lleï exponencial", també conegut com a enfocament SIMP (*solid isotropic material with penalization*). Aquest enfocament suposa que les propietats dels materials són constants dins de cada element del domini de disseny, mentre que les densitats de material relatives dels elements són variables.

Per a aquest model s'analitzen diferents angles de flexió (igual que en l'escenari anterior). No obstant això, només s'obtenen resultats coherents (ròtula formada) amb 90° i 110°. Per a aquests angles, s'observa una zona d'alta densitat propera a la posició habitual de la ròtula. Concretament, per al cas de 90°, la forma de la zona d'alta densitat és més coherent amb la realitat. Açò suggereix que l'entorn mecànic que envolta el tendó pot afectar la ròtula i el seu desenvolupament.

3.4. *Discussió de les teories del desenvolupament de la ròtula:*

En les tres teories avaluades s'obté una estructura de tipus ròtula per als majors angles de flexió analitzats. Els resultats mostren que la remodelació i l'adaptació dels teixits, basades en la teoria de Carter *et al.* (1987) o en la TO, podrien respondre a l'aparició de la ròtula. La forma, la posició i la mida de la ròtula dependrien de l'angle de flexió de la cama i del temps que la cama passa en cada posició, obtenint una ròtula més gran en comparació amb l'enfocament bioquímic. No obstant això, no hi ha molta evidència en la literatura que pugui donar

suport a la segona i la tercera teoria. Per tant, pot ser que la càrrega mecànica no siga necessària per a l'aparició de la ròtula, però pot ser necessària per a la seua morfogènesi i el seu manteniment.

Els factors moleculars i les seues interaccions desencadenen la formació de la ròtula, com ho demostra la secreció molecular de les cèl·lules analitzades en imatges histològiques. Aquests factors, aplicats a un model computacional, són coherents amb els resultats obtinguts. No obstant això, atès que la limitació del moviment en solitari no garanteix que no hi haja tensions hidrostàtiques al tendó, s'haurien de realitzar més proves en les que només els factors bioquímics influeixen en el desenvolupament del tendó i la ròtula. També és possible que aquests mecanismes siguen redundants i que tots dos influeixen l'aparició de la ròtula.

A més, és cert que l'entorn mecànic ha d'afectar el desenvolupament de la ròtula. Tanmateix, aquest entorn el pot afectar sobretot després que el tendó estiga format, ajudant la ròtula a obtenir la seua forma final i mantenir la seua estructura. Aquest treball és una primera aproximació a la comprensió del procés del desenvolupament de la ròtula. A més, aquests models podrien proporcionar noves idees i pautes d'experimentació i models matemàtics. Com a treball futur es suggereix una combinació de les teories avaluades en aquest estudi, de manera que es determine l'aparició de la ròtula a causa de factors bioquímics i, posteriorment, les càrregues mecàniques puguen regular la seua forma i el seu manteniment.

4. Regeneració del cartílag

4.1. *Metodologia per al model de regeneració del cartílag*

Es desenvolupa una geometria 2D axisimètrica de tensió simple per representar una estructura cartílag-os-implant simplificada. La distribució normal d'esforç i deformació en els ossos subcondral i trabecular s'estableix aplicant càrrega al sistema abans de la col·locació de l'implant. S'aplica una càrrega oscil·lant d'1 Hz fins a estabilitzar els valors de la velocitat del fluid, l'esforç i la deformació. Se suposa que el cartílag suporta aquesta càrrega cada dia de simulació.

El cartílag articular consisteix en una matriu extracel·lular dividida en dues fases: sòlida i fluida. La part sòlida conté principalment proteoglicans i una xarxa fibril·lar de col·lagen tipus II. Els feixos de fibril·les primàries s'estenen perpendicularment des de l'os subcondral i divergeixen prop de la superfície en fibril·les que es corben gradualment fins a situar-se paral·lelament a la superfície articular. Les fibril·les de col·lagen es modelitzen com a materials de tensió elàstica lineal. La part no fibril·lar de la part sòlida del cartílag se suposa lineal poroelàstica.

Per a l'os s'utilitza un model bàsic de remodelació dels ossos que considera la resposta a la deformació i les condicions basals com a condicions inicials. Abans de la col·locació de l'implant, es calcula la deformació màxima basal com a mitjana de la deformació màxima diària del teixit. Després de la col·locació de l'implant, es generen condicions de càrrega anormals i, per tant, es canvien els patrons de deformació màxims dins del teixit. Es considera que aquesta variació

en les condicions de la deformació afecta la distribució de la densitat òssia i, per tant, el mòdul de Young dels ossos subcondral i trabecular.

S'estableix que el teixit ossi sota l'implant falla si el mòdul de Young mitjà de la línia d'elements sota l'implant és menor que un llinar. Si l'os falla, l'implant es pot desplaçar descendentment dins de l'os.

També es considera un factor de potencial vascular (*potencial vascularity factor*, PVF). Se suposa que aquest factor es difon des del fons del domini fins a la part superior del domini. Es fixa una taxa de difusió baixa per a aquesta molècula de manera que determine si un teixit mesenquimàtic pot ser vascularitzat o no.

El model desenvolupat s'ocupa de la regeneració de dos tipus de teixits: cartílag i os. El procés d'osteogènesi es regula mitjançant l'entorn mecànic. Per a la regeneració òssia s'utilitza un model mecànic de diferenciació de teixits que acobla els mecanismes cel·lulars als estímuls mecànics durant la curació òssia.

Durant la realització d'aquesta tesi no s'han trobat a la literatura models computacionals capaços d'explicar com es regenera aquest teixit. Per tant, es considera una relació positiva entre la tensió hidrostàtica cíclica i el creixement del cartílag. A més, el cartílag només és capaç de regenerar-se en elements amb teixit mesenquimàtic i baixa concentració de PVF.

Si l'os sota l'implant falla i es produeix un desplaçament de l'implant, el buit que queda a la part superior de l'implant s'ompli amb

teixit mesenquimàtic que, posteriorment, es diferencia en altres teixits (os, cartílag o teixit fibrós). Per a que un element mesenquimàtic es diferencie en cartílag, l'element ha d'haver tingut una baixa concentració de PVF i tindre un element veí cartilaginós amb alta tensió hidrostàtica. Si no es compleixen les condicions anteriors, s'activa el model d'osteogènesi. En aquest cas, el teixit mesenquimàtic pot diferenciar-se en teixits fibrosos, cartílags o ossis en funció dels estímuls mecànics (efecte combinat de la deformació deviatòrica i la velocitat del fluid).

4.2. Resultats i discussió del model de regeneració del cartílag:

Els processos de resorció i aposició òssies es modelitzen com a canvis en el mòdul de Young de l'os. Segons els resultats, l'os trabecular s'ha de remodelitzar per suportar la càrrega anormal causada per l'implant. A més, el mòdul de Young de l'os trabecular augmenta a la zona sota l'implant un cop s'ha col·locat; però disminueix, a causa de la sobrecàrrega, a la línia elemental situada just sota l'implant. D'altra banda, el cartílag es forma a la part superior de l'implant fins al quart i el sisè mes, quan la concentració del PVF és suficientment alta per evitar la formació del cartílag.

Quan s'activa el procés d'osteogènesi, l'estímul mecànic calculat pel model és ideal per estimular el teixit ossi, de manera que només es diferencia en l'os.

Un any després de la col·locació de l'implant, el model mostra el cartílag completament recuperat i l'implant desplaçat cap a l'interior de l'os. Aquests resultats concorden amb els obtinguts per Sancho-Tello

et al. (2015), qui van col·locar un implant porós de copolímer en l'articulació del genoll d'un conill per a reparar un defecte condral de profunditat.

El model computacional desenvolupat en aquesta tesi es pot utilitzar per a comparar l'efecte d'utilitzar implants de diferents materials, diferents condicions de càrrega o degeneració (patologia) de teixits respecte a condicions de tractament ideals. També pot ser útil en la planificació de tractaments per a la regeneració del cartílag articular.

5. General Conclusions

En aquesta tesi s'exploren diferents aspectes de les articulacions sinovials des de la seua aparició fins la seua maduresa. Concretament, es proposen quatre models computacionals basats en factors mecànics i bioquímics per a reproduir el desenvolupament de les articulacions sinovials i la regeneració del cartílag articular. En general, els resultats obtinguts de les simulacions mostren una gran concordança amb els estudis histològics trobats a la literatura. Les conclusions específiques extretes de cada model s'exposen a continuació.

El model per a l'aparició d'articulacions es capaç d'explicar el desenvolupament de l'articulació interfalàngica a través de la interacció de només sis factors moleculars genèrics. Per tant, es pot concloure que la concentració de sis molècules relacionades amb GDF-5, Noggin, Ihh, PTHrP, gens *How* i *Wnt* regula la formació de la interzona i el procés de cavitació.

El model de morfogènesi d'articulacions proposat en aquesta tesi, a diferència d'altres models computacionals anteriors, inclou

factors bioquímics a més de factors mecànics. Açò resulta en un grau d'acord entre la forma final de l'articulació sinovial interfalàngica simulada i les formes mostrades en estudis histològics notablement major. Per tant, es demostra que tant els estímuls mecànics com els bioquímics són necessaris per a que les articulacions sinovials assolisquen la seua forma final.

Pel que fa a l'aparició de la ròtula, s'avaluen tres teories, cadascuna implementada mitjançant un model computacional diferent. Els tres models són capaços de predir l'aparició d'aquest os sesamoide i, comparant amb els estudis histològics més recents trobats a la literatura, els millors resultats s'obtenen amb la teoria bioquímica. En aquesta tesi es proposa que la interacció molecular desencadena l'aparició de la ròtula, però les càrregues mecàniques són necessàries per al seu creixement i el seu manteniment.

Segons els resultats del model de regeneració del cartílag, no només el cartílag s'ha d'adaptar durant el procés de regeneració, sinó també el teixit que l'envolta. El model computacional desenvolupat pot resultar útil per a comparar l'efecte d'implants de diferents materials i de diferents condicions de càrrega i així avaluar quina alternativa és la més convenient en cada cas.

Els models computacionals desenvolupats en aquesta tesis permeten avaluar moltes condicions mecàniques i bioquímiques diferents en diversos fenòmens biològics sense la necessitat de cap muntatge experimental (amb les dificultats tècniques, costos materials i econòmics i temps que implicarien). A més, tenen el potencial de convertir-se en ferramentes útils per a la recerca mèdica i biològica,

ajudant en el disseny d'estratègies terapèutiques per a les patologies relacionades amb les articulacions.

REFERENCES

- [1] D. Correa, S.A. Lietman, Articular cartilage repair: Current needs, methods and research directions, *Semin. Cell Dev. Biol.* 62 (2017) 67–77. doi:10.1016/j.semcdb.2016.07.013.
- [2] E. Hohmann, K. Tetsworth, Large osteochondral lesions of the femoral condyles: Treatment with fresh frozen and irradiated allograft using the Mega OATS technique, *Knee.* 23 (2016) 436–441. doi:10.1016/j.knee.2016.01.020.
- [3] K.L. Caldwell, J. Wang, Cell-based articular cartilage repair: The link between development and regeneration, *Osteoarthr. Cartil.* 23 (2015) 351–362. doi:10.1016/j.joca.2014.11.004.
- [4] M. Sancho-Tello, F. Forriol, P. Gastaldi, A. Ruiz-Saurí, J.J. Martín de Llano, E. Novella-Maestre, C.M. Antolinos-Turpín, J.A. Gómez-Tejedor, J.L. Gómez Ribelles, C. Carda, Time evolution of in vivo articular cartilage repair induced by bone marrow stimulation and scaffold implantation in rabbits, *Int. J. Artif. Organs.* 38 (2015) 210–223. doi:10.5301/ijao.5000404.
- [5] H. Guo, S.A. Maher, P.A. Torzilli, A biphasic multiscale study of the mechanical microenvironment of chondrocytes within articular cartilage under unconfined compression, *J. Biomech.* 47 (2014) 2721–2729. doi:10.1016/j.jbiomech.2014.05.001.
- [6] S.R. Moore, G.M. Saidel, U. Knothe, M.L. Knothe Tate, Mechanistic, Mathematical Model to Predict the Dynamics of Tissue Genesis in Bone Defects via Mechanical Feedback and Mediation of Biochemical Factors, *PLoS Comput. Biol.* 10 (2014). doi:10.1371/journal.pcbi.1003604.
- [7] D.R. Carter, G.S. Beaupré, N.J. Giori, J.A. Helms, Mechanobiology of skeletal regeneration, *Clin. Orthop. Relat. Res.* (1998) S41–S55. <http://eutils.ncbi.nlm.nih.gov/entrez/eutils/elink.fcgi?dbfrom=pubmed&id=9917625&retmode=ref&cmd=prlinks%5Cnpapers3://publication/uuid/A49B3192-CFAA-4EE2-86BA-95563B2811A4>.
- [8] J.M. Guevara, M.A. Moncayo, J.J. Vaca-González, M.L. Gutierrez, L.A. Barrera, D.A. Garzón-Alvarado, Growth plate stress distribution implications during bone development: A simple framework computational approach, *Comput. Methods Programs Biomed.* 118 (2015) 59–68. doi:10.1016/j.cmpb.2014.10.007.
- [9] D.A. Garzón-Alvarado, J.M. García-Aznar, M. Doblaré, A reaction-diffusion model for long bones growth, *Biomech. Model. Mechanobiol.* 8 (2009) 381–95. doi:10.1007/s10237-008-0144-z.

References

- [10] T. Miura, P.K. Maini, Periodic pattern formation in reaction–diffusion systems: An introduction for numerical simulation Introduction: Periodic pattern formation in biological systems and the Turing reaction–diffusion model, *Anat. Sci. Int.* 79 (2004) 112–123. doi:10.1111/j.1447-073x.2004.00079.x.
- [11] A. Madzvamuse, Time-stepping schemes for moving grid finite elements applied to reaction-diffusion systems on fixed and growing domains, *J. Comput. Phys.* 214 (2006) 239–263. doi:10.1016/j.jcp.2005.09.012.
- [12] A. Madzvamuse, P.K. Maini, Velocity-induced numerical solutions of reaction-diffusion systems on continuously growing domains, *J. Comput. Phys.* 225 (2007) 100–119. doi:10.1016/j.jcp.2006.11.022.
- [13] D.A. Garzón-Alvarado, J.M. García-Aznar, M. Doblaré, Appearance and location of secondary ossification centres may be explained by a reaction-diffusion mechanism, *Comput. Biol. Med.* 39 (2009) 554–561. doi:10.1016/j.combiomed.2009.03.012.
- [14] D.A. Garzón-Alvarado, A.M.R. Martínez, D.L.L. Segrera, A model of cerebral cortex formation during fetal development using reaction-diffusion-convection equations with Turing space parameters, *Comput. Methods Programs Biomed.* 104 (2011) 489–497. doi:10.1016/j.cmpb.2011.07.001.
- [15] K. Kristiansen, *Reaction-Diffusion Models in Mathematical Biology*, Technical University of Denmark, 2008.
- [16] S.A. Newman, S. Christley, T. Glimm, H.G.E. Hentschel, B. Kazmierczak, Y.-T. Zhang, J. Zhu, M.S. Alber, Multiscale Models for Vertebrate Limb Development, *Curr. Top. Dev. Biol.* 90 (2008) 979–990. doi:10.1016/S0070-2153(07)81011-8.
- [17] L.P. Räsänen, M.E. Mononen, M.T. Nieminen, E. Lammentausta, J.S. Jurvelin, R.K. Korhonen, Implementation of subject-specific collagen architecture of cartilage into a 2D computational model of a knee joint-data from the osteoarthritis initiative (OAI), *J. Orthop. Res.* 31 (2013) 10–22. doi:10.1002/jor.22175.
- [18] T.A.M. Heck, W. Wilson, J. Foolen, A.C. Cilingir, K. Ito, C.C. van Donkelaar, A tissue adaptation model based on strain-dependent collagen degradation and contact-guided cell traction, *J. Biomech.* 48 (2015) 823–831. doi:10.1016/j.jbiomech.2014.12.023.
- [19] J.M.P. Quiroga, K. Ito, C.C. van Donkelaar, Meniscus replacement: Influence of geometrical mismatches on chondroprotective capabilities, *J. Biomech.* 48 (2015) 1371–1376. doi:10.1016/j.jbiomech.2015.02.063.
- [20] J.H. Heegaard, G.S. Beaupre, D.R. Carter, G.S. Beaupré, D.R. Carter, Mechanically modulated cartilage growth may regulate joint surface morphogenesis, *J. Orthop. Res.* 17 (1999) 509–517. doi:10.1002/jor.1100170408.

-
- [21] M. Giorgi, A. Carriero, S.J. Shefelbine, N.C. Nowlan, Mechanobiological simulations of prenatal joint morphogenesis., *J. Biomech.* 47 (2014) 989–95. doi:10.1016/j.jbiomech.2014.01.002.
- [22] L.R. Cochard, *Netter's Atlas Embryology of Human*, Updated Ed, Elsevier Health Sciences, Chicago, Illinois, 2012.
- [23] Th.W. Sadler, *Langman's Medical Embryology*, 12th ed., Lippincott Williams & Wilkins, Cambridge, 2012.
- [24] OpenStax, *Anatomy and Physiology*, OpenStax CNX, 2016. <http://cnx.org/contents/14fb4ad7-39a1-4eee-ab6e-3ef2482e3e22@8.24>.
- [25] F. Geneser, *Atlas de Histología*, 8th ed., Editorial Medical Panamericana S.A., Madrid, 1998.
- [26] P. Pustejovsk, *Biochemical and mechanical processes in synovial fluid – modeling, analysis and computational simulations Mathematical*, Charles University in Prague; Heidelberg University, 2012.
- [27] L.R. Gale, *Biotribological Assessment for Artificial Synovial Joints: The Role of Boundary Lubrication*, Queensland University of Technology, 2007.
- [28] D.E. Marcinko, M.D. Dollard, Physical and mechanical properties of joints (the pathomechanics of articular cartilage degeneration), *J. Foot Surg.* 25 (1986) 3–13. <http://www.ncbi.nlm.nih.gov/pubmed/3512683>.
- [29] H.L. Stewart, C.E. Kawcak, The Importance of Subchondral Bone in the Pathophysiology of Osteoarthritis, *Front. Vet. Sci.* 5 (2018) 1–9. doi:10.3389/fvets.2018.00178.
- [30] A.M. Säämänen, J.P.A. Arokoski, J.S. Jurvelin, I. Kiviranta, The structure and regenerative capacity of synovial joint tissues, *Regen. Med. Biomater. Repair Connect. Tissues.* (2010) 1–38. doi:10.1533/9781845697792.1.
- [31] J.G. Skedros, S.L. Baucom, Mathematical analysis of trabecular “trajectories” in apparent trajectorial structures: the unfortunate historical emphasis on the human proximal femur, *J. Theor. Biol.* 244 (2007) 15–45. doi:10.1016/j.jtbi.2006.06.029.
- [32] T. Aigner, N. Schmitz, S. Söder, Understanding osteoarthritis and other cartilage diseases, *Regen. Med. Biomater. Repair Connect. Tissues.* (2010) 155–177. doi:10.1533/9781845697792.1.155.
- [33] J. Fish, T. Belytschko, *A First Course in Finite Elements*, John Wiley & Sons, Ltd, Chichester, UK, 2007. doi:10.1002/9780470510858.
- [34] M. Pacifici, E. Koyama, M. Iwamoto, Mechanisms of synovial joint and articular cartilage formation: Recent advances, but many lingering mysteries, *Birth Defects Res. Part C - Embryo Today Rev.* 75 (2005) 237–248. doi:10.1002/bdrc.20050.
-

References

- [35] H. Yasuda, B. de Crombrughe, Joint Formation Requires Muscle Formation and Contraction, *Dev. Cell.* 16 (2009) 625–626. doi:10.1016/j.devcel.2009.05.003.
- [36] A.M. Nalin, T.K. Greenlee, L.J. Sandell, Collagen gene expression during development of avian synovial joints: transient expression of types II and XI collagen genes in the joint capsule., *Dev. Dyn.* 203 (1995) 352–362. doi:10.1002/aja.1002030307.
- [37] S. Kimura, K. Shiota, Sequential changes of programmed cell death in developing fetal mouse limbs and its possible roles in limb morphogenesis, *J. Morphol.* 229 (1996) 337–346. doi:10.1002/(SICI)1097-4687(199609)229:3<337::AID-JMOR8>3.0.CO;2-V.
- [38] G. Abu-Hijleh, O. Reid, R.J. Scothorne, Cell death in the developing chick knee joint: I. Spatial and temporal patterns, *Clin. Anat.* 10 (1997) 183–200. doi:10.1002/(SICI)1098-2353(1997)10:3<183::AID-CA4>3.0.CO;2-V.
- [39] R. Bellairs, M. Osmond, *Atlas of Chick Development*, 2nd ed., Elsevier Science, 2005.
- [40] N.C. Nowlan, C. Bourdon, G. Dumas, S. Tajbakhsh, P.J. Prendergast, P. Murphy, Developing bones are differentially affected by compromised skeletal muscle formation., *Bone.* 46 (2010) 1275–85. doi:10.1016/j.bone.2009.11.026.
- [41] F. Accio, C. Bari, F.P. Luyten, Molecular basis of joint development, *Japanese J. Rheumatol.* 9 (1999) 17–29. doi:10.1007/BF03041256.
- [42] S.E. Stasko, G.F. Wagner, Possible roles for stanniocalcin during early patterning and joint formation in the mouse, *J. Endocrinol.* 171 (2001) 237–248. doi:10.1677/joe.0.1710237.
- [43] G. Lizarraga, A. Lichtler, W.B. Upholt, R.A. Kosher, Studies on the role of *Cux1* in regulation of the onset of joint formation in the developing limb, *Dev. Biol.* 243 (2002) 44–54. doi:10.1006/dbio.2001.0559.
- [44] M. Pacifici, M. Liu, E. Koyama, Joint formation: new findings shed more light on this critical process in skeletogenesis, *Curr. Opin. Orthop.* 13 (2002) 339–344. doi:10.1097/00001433-200210000-00003.
- [45] C.W. Archer, G.P. Dowthwaite, P. Francis-West, Development of synovial joints, *Birth Defects Res. Part C - Embryo Today Rev.* 69 (2003) 144–155. doi:10.1002/bdrc.10015.
- [46] I.M. Khan, S.N. Redman, R. Williams, G.P. Dowthwaite, S.F. Oldfield, C.W. Archer, The Development of Synovial Joints, *Curr. Top. Dev. Biol.* 79 (2007) 1–36. doi:10.1016/S0070-2153(06)79001-9.
- [47] N.C. Nowlan, J. Sharpe, K.A. Roddy, P.J. Prendergast, P. Murphy, Mechanobiology of embryonic skeletal development: Insights from animal models, *Birth Defects Res. Part C Embryo Today Rev.* 90 (2010) 203–213.

doi:10.1002/bdrc.20184.

- [48] F. Witte, J. Dokas, F. Neuendorf, S. Mundlos, S. Stricker, Comprehensive expression analysis of all Wnt genes and their major secreted antagonists during mouse limb development and cartilage differentiation, *Gene Expr. Patterns*. 9 (2009) 215–223. doi:10.1016/j.gep.2008.12.009.
- [49] K.L. Cooper, Self-organization in the limb: a Turing mechanism for digit development, *Curr. Opin. Genet. Dev.* 32 (2015) 92–97. doi:10.1016/j.gde.2015.02.001.
- [50] W. Schlegel, C. Albrecht, P. Eckl, H. Freudenthaler, A. Berger, V. Vécsei, S. Marlovits, Dedifferentiation of human articular chondrocytes is associated with alterations in expression patterns of GDF-5 and its receptors, *J. Cell. Mol. Med.* 13 (2009) 3398–3404. doi:10.1111/j.1582-4934.2009.00953.x.
- [51] E.E. Storm, D.M. Kingsley, GDF5 coordinates bone and joint formation during digit development, *Dev. Biol.* 209 (1999) 11–27. doi:10.1006/dbio.1999.9241.
- [52] E. Kavanagh, V.L. Church, A.C. Osborne, K.J. Lamb, C.W. Archer, P.H. Francis-West, A.A. Pitsillides, Differential regulation of GDF-5 and FGF-2/4 by immobilisation in ovo exposes distinct roles in joint formation, *Dev. Dyn.* 235 (2006) 826–834. doi:10.1002/dvdy.20679.
- [53] S. Provot, E. Schipani, Molecular mechanisms of endochondral bone development, *Biochem. Biophys. Res. Commun.* 328 (2005) 658–665. doi:10.1016/j.bbrc.2004.11.068.
- [54] J.E.M. Brouwers, C.C. van Donkelaar, B.G. Sengers, R. Huiskes, Can the growth factors PTHrP, Ihh and VEGF, together regulate the development of a long bone?, *J. Biomech.* 39 (2006) 2774–2782. doi:10.1016/j.jbiomech.2005.10.004.
- [55] D.A. Garzón-Alvarado, L.M. Peinado Cortés, R.P. Cárdenas Sandoval, A mathematical model of epiphyseal development: hypothesis of growth pattern of the secondary ossification centre., *Comput. Methods Biomech. Biomed. Engin.* 14 (2011) 23–32. doi:10.1080/10255842.2010.484810.
- [56] L.M. Peinado Cortés, J.C. Vanegas Acosta, D.A. Garzón Alvarado, A mechanobiological model of epiphysis structures formation., *J. Theor. Biol.* 287 (2011) 13–25. doi:10.1016/j.jtbi.2011.07.011.
- [57] F.P. Luyten, P. Tylzanowski, R.J. Lories, Wnt signaling and osteoarthritis, *Bone*. 44 (2009) 522–527. doi:10.1016/j.bone.2008.12.006.
- [58] A.M. Turing, The Chemical Basis of Morphogenesis, *Philos. Trans. R. Soc. Lond. B. Biol. Sci.* 237 (1952) 37–72. doi:10.1098/rstb.1952.0012.
- [59] J.D. Murray, A Pre-pattern formation mechanism for animal coat markings, *J. Theor. Biol.* 88 (1981) 161–199. doi:10.1016/0022-5193(81)90334-9.

References

- [60] A. Madzvamuse, *A Numerical Approach to the Study of Spatial Pattern Formation*, Oxford University, 2000.
- [61] D.M. Wellik, M.R. Capecchi, Hox10 and Hox11 genes are required to globally pattern the mammalian skeleton., *Science*. 301 (2003) 363–367. doi:10.1126/science.1085672.
- [62] P. Dollé, E. Ruberte, P. Kastner, M. Petkovich, C.M. Stoner, L.J. Gudas, P. Chambon, Differential expression of genes encoding α , β and γ retinoic acid receptors and CRABP in the developing limbs of the mouse, *Nature*. 342 (1989) 702–705. doi:10.1038/342702a0.
- [63] Y. Yokouchi, H. Sasaki, A. Kuroiwa, Homeobox gene expression correlated with the bifurcation process of limb cartilage development, *Nature*. 353 (1991) 443–445. doi:10.1038/353443a0.
- [64] C.E. Nelson, B.A. Morgan, A.C. Burke, E. Laufer, E. DiMambro, L.C. Murtaugh, E. Gonzales, L. Tessarollo, L.F. Parada, C. Tabin, Analysis of Hox gene expression in the chick limb bud., *Development*. 122 (1996) 1449–1466.
- [65] A. Badugu, C. Kraemer, P. Germann, D. Menshykau, D. Iber, Digit patterning during limb development as a result of the BMP-receptor interaction, *Sci. Rep.* 2 (2012) 991. doi:10.1038/srep00991.
- [66] J.M. Kindblom, O. Nilsson, T. Hurme, C. Ohlsson, L. Savendahl, Expression and localization of Indian hedgehog (Ihh) and parathyroid hormone-related protein (PTHrP) in the human growth plate during pubertal development, *J. Endocrinol.* 174 (2002) 1–6. doi:10.1677/joe.0.174R001.
- [67] B. St-Jacques, M. Hammerschmidt, A.P. McMahon, Indian hedgehog signaling regulates proliferation and differentiation of chondrocytes and is essential for bone formation., *Genes Dev.* 13 (1999) 2072–2086. doi:10.1101/gad.13.16.2072.
- [68] E. Zelzer, B.R. Olsen, The genetic basis for skeletal diseases., *Nature*. 423 (2003) 343–348. doi:10.1038/nature01659.
- [69] E. KOYAMA, T. OCHIAI, R.B. ROUNTREE, D.M. KINGSLEY, M. ENOMOTO-IWAMOTO, M. IWAMOTO, M. PACIFICI, Synovial Joint Formation during Mouse Limb Skeletogenesis: Roles of Indian Hedgehog Signaling, *Ann. N. Y. Acad. Sci.* 1116 (2007) 100–112. doi:10.1196/annals.1402.063.
- [70] D. Mitrovic, Development of the diarthrodial joints in the rat embryo, *Am. J. Anat.* 151 (1978) 475–485. doi:10.1002/aja.1001510403.
- [71] Y.-T. Zhang, M.S. Alber, S.A. Newman, R.H. Dillon, Mathematical modeling of vertebrate limb development., *Math. Biosci.* 243 (2013) 1–17. doi:10.1016/j.mbs.2012.11.003.
- [72] S.A. Newman, R. Bhat, Activator-inhibitor dynamics of vertebrate limb pattern formation, *Birth Defects Res. Part C - Embryo Today Rev.* 81 (2007)

- 305–319. doi:10.1002/bdrc.20112.
- [73] R. Chaturvedi, C. Huang, B. Kazmierczak, T. Schneider, J.A. Izaguirre, T. Glimm, H.G.E. Hentschel, J.A. Glazier, S.A. Newman, M.S. Alber, On multiscale approaches to three-dimensional modelling of morphogenesis, *J. R. Soc. Interface.* 2 (2005) 237–253. doi:10.1098/rsif.2005.0033.
- [74] J.D. Murray, *Mathematical Biology II: Spatial Models and Biomedical Applications*, Springer-Verlag, New York, 1993. doi:10.1007/b98869.
- [75] B. Boehm, H. Westerberg, G. Lesnicar-Pucko, S. Raja, M. Rautschka, J. Cotterell, J. Swoger, J. Sharpe, The Role of Spatially Controlled Cell Proliferation in Limb Bud Morphogenesis, *PLoS Biol.* 8 (2010) e1000420. doi:10.1371/journal.pbio.1000420.
- [76] A. Goriely, *The Mathematics and Mechanics of Biological Growth*, Springer New York, New York, NY, 2017. doi:10.1007/978-0-387-87710-5.
- [77] R. Merino, D. Macias, Y. Gañan, A.N. Economides, X. Wang, Q. Wu, N. Stahl, K.T. Sampath, P. Varona, J.M. Hurler, Expression and function of Gdf-5 during digit skeletogenesis in the embryonic chick leg bud, *Dev. Biol.* 206 (1999) 33–45. doi:10.1006/dbio.1998.9129.
- [78] E. Koyama, Y. Shibukawa, M. Nagayama, H. Sugito, B. Young, T. Yuasa, T. Okabe, T. Ochiai, N. Kamiya, R.B. Rountree, D.M. Kingsley, M. Iwamoto, M. Enomoto-Iwamoto, M. Pacifici, A distinct cohort of progenitor cells participates in synovial joint and articular cartilage formation during mouse limb skeletogenesis, *Dev. Biol.* 316 (2008) 62–73. doi:10.1016/j.ydbio.2008.01.012.
- [79] F.R. Bailey, A.M. Miller, *Embryology*, William Wood and Co., New York, 1921.
- [80] J. Raspopovic, L. Marcon, L. Russo, J. Sharpe, Digit patterning is controlled by a Bmp-Sox9-Wnt Turing network modulated by morphogen gradients, *Science* (80-.). 345 (2014) 566–570. doi:10.1126/science.1252960.
- [81] B. Gao, J. Hu, S. Stricker, M. Cheung, G. Ma, K.F. Law, F. Witte, J. Briscoe, S. Mundlos, L. He, K.S.E. Cheah, D. Chan, A mutation in *Ihh* that causes digit abnormalities alters its signalling capacity and range., *Nature.* 458 (2009) 1196–1200. doi:10.1038/nature07862.
- [82] C. Hartmann, C.J. Tabin, Wnt-14 plays a pivotal role in inducing synovial joint formation in the developing appendicular skeleton, *Cell.* 104 (2001) 341–351. doi:10.1016/S0092-8674(01)00222-7.
- [83] R.S. Decker, E. Koyama, M. Enomoto-Iwamoto, P. Maye, D. Rowe, S. Zhu, P.G. Schultz, M. Pacifici, Mouse limb skeletal growth and synovial joint development are coordinately enhanced by Kartogenin, *Dev. Biol.* 395 (2014) 255–267. doi:10.1016/j.ydbio.2014.09.011.

References

- [84] K.D. Kavanagh, O. Shoval, B.B. Winslow, U. Alon, B.P. Leary, A. Kan, C.J. Tabin, Developmental bias in the evolution of phalanges, *Proc. Natl. Acad. Sci.* 110 (2013) 18190–18195. doi:10.1073/pnas.1315213110.
- [85] P.H. Francis-West, J. Parish, K. Lee, C.W. Archer, BMP/GDF-signalling interactions during synovial joint development, *Cell Tissue Res.* 296 (1999) 111–119. doi:10.1007/s004410051272.
- [86] N.C. Nowlan, J. Sharpe, Joint shape morphogenesis precedes cavitation of the developing hip joint, *J. Anat.* 224 (2014) 482–489. doi:10.1111/joa.12143.
- [87] V. Bialik, G.M. Bialik, S. Blazer, P. Sujov, F. Wiener, M. Berant, Developmental Dysplasia of the Hip: A New Approach to Incidence, *Pediatrics.* 103 (1999) 93–99. doi:10.1542/peds.103.1.93.
- [88] A. Fassier, P. Wicart, J. Dubousset, R. Seringe, Arthrogyrosis multiplex congenita. Long-term follow-up from birth until skeletal maturity, *J. Child. Orthop.* 3 (2009) 383–390. doi:10.1007/s11832-009-0187-4.
- [89] D.J. Gray, E. Gardner, Prenatal development of the human knee and superior tibiofibular joints, *Am. J. Anat.* 86 (1950) 235–287. doi:10.1002/aja.1000860204.
- [90] E. Gardner, R. O’Rahilly, The early development of the knee joint in staged human embryos, *J. Anat.* 102 (1968) 289–299. <http://www.ncbi.nlm.nih.gov/pubmed/5643844>.
- [91] D.R. Carter, Mechanical loading history and skeletal biology, *J. Biomech.* 20 (1987) 1095–1109. doi:10.1016/0021-9290(87)90027-3.
- [92] D.R. Carter, P.R. Blenman, G.S. Beauprk, Correlations between Mechanical Stress History and Tissue Differentiation in Initial Fracture Healing, *J. Orthop. Res.* 6 (1988) 736–748. doi:10.1002/jor.1100060517.
- [93] D.R. Carter, M. Wong, The role of mechanical loading histories in the development of diarthrodial joints, *J. Orthop. Res.* 6 (1988) 804–816. doi:10.1002/jor.1100060604.
- [94] E.L. Radin, D.B. Burr, B. Caterson, D. Fyhrie, T.D. Brown, R.D. Boyd, Mechanical Determinants of Osteoarthritis, *Semin. Arthritis Rheum.* 21 (1991) 12–21. doi:10.1016/0049-0172(91)90036-Y.
- [95] P.N.P. Singh, C.A. Shea, S.K. Sonker, R.A. Rolfe, A. Ray, S. Kumar, P. Gupta, P. Murphy, A. Bandyopadhyay, Precise spatial restriction of BMP signaling in developing joints is perturbed upon loss of embryo movement, *Development.* 145 (2018) dev153460. doi:10.1242/dev.153460.
- [96] K.M. Márquez-Flórez, J.R. Monaghan, S.J. Shefelbine, A. Ramirez-Martínez, D.A. Garzón-Alvarado, A computational model for the joint onset and development, *J. Theor. Biol.* 454 (2018) 345–356. doi:10.1016/j.jtbi.2018.04.015.

- [97] K.M. Márquez-Flórez, O. Silva, C.A. Narváez-Tovar, D.A. Garzón-alvarado, A Comparison of the Contact Force Distributions on the Acetabular Surface Due to Orthopedic Treatments for Developmental Hip Dysplasia, *J. Biomech. Eng.* 138 (2016) 074501-1-074501–7. doi:10.1115/1.4033547.
- [98] K.A. Roddy, P.J. Prendergast, P. Murphy, Mechanical influences on morphogenesis of the knee joint revealed through morphological, molecular and computational analysis of immobilised embryos, *PLoS One.* 6 (2011). doi:10.1371/journal.pone.0017526.
- [99] A.C. Osborne, K.J. Lamb, J.C. Lewthwaite, G.P. Dowthwaite, A.A. Pitsillides, Short-term rigid and flaccid paralyses diminish growth of embryonic chick limbs and abrogate joint cavity formation but differentially preserve pre-cavitated joints., *J. Musculoskelet. Neuronal Interact.* 2 (2002) 448–456. <http://www.ncbi.nlm.nih.gov/pubmed/15758413>.
- [100] B. Mikic, T.L. Johnson, A.B. Chhabra, B.J. Schalet, M. Wong, E.B. Hunziker, Differential effects of embryonic immobilization on the development of fibrocartilaginous skeletal elements., *J. Rehabil. Res. Dev.* 37 (2000) 127–33. <http://www.ncbi.nlm.nih.gov/pubmed/10850818>.
- [101] J. Kahn, Y. Shwartz, E. Blitz, S. Krief, A. Sharir, D.A. Breitel, R. Rattenbach, F. Relaix, P. Maire, R.B. Rountree, D.M. Kingsley, E. Zelzer, Muscle Contraction Is Necessary to Maintain Joint Progenitor Cell Fate, *Dev. Cell.* 16 (2009) 734–743. doi:10.1016/j.devcel.2009.04.013.
- [102] N.C. Nowlan, J. Sharpe, K. a. Roddy, P.J. Prendergast, P. Murphy, Mechanobiology of embryonic skeletal development: Insights from animal models., *Birth Defects Res. C. Embryo Today.* 90 (2010) 203–13. doi:10.1002/bdrc.20184.
- [103] D.R. Carter, T.E. Orr, D.P. Fyhrie, D.J. Schurman, Influences of mechanical stress on prenatal and postnatal skeletal development., *Clin. Orthop. Relat. Res. No. 219* (1987) 237–50. <http://www.ncbi.nlm.nih.gov/pubmed/3581576>.
- [104] N. Burton-Wurster, M. Vernier-Singer, T. Farquhar, G. Lust, Effect of compressive loading and unloading on the synthesis of total protein, proteoglycan, and fibronectin by canine cartilage explants, *J. Orthop. Res.* 11 (1993) 717–729. doi:10.1002/jor.1100110514.
- [105] F. Guilak, B. Meyer, A. Ratcliffe, V. Mow, The effects of matrix compression on proteoglycan metabolism in articular cartilage explants, *Osteoarthr. Cartil.* 2 (1994) 91–101. doi:10.1016/S1063-4584(05)80059-7.
- [106] Y.J. Kim, R.L.Y. Sah, A.J. Grodzinsky, A.H.K. Plaas, J.D. Sandy, Mechanical Regulation of Cartilage Biosynthetic Behavior: Physical Stimuli, *Arch. Biochem. Biophys.* 311 (1994) 1–12. doi:10.1006/abbi.1994.1201.
- [107] T.H. Korver, R.J. van de Stadt, E. Kiljan, G.P. van Kampen, J.K. van der Korst, Effects of loading on the synthesis of proteoglycans in different layers

References

- of anatomically intact articular cartilage in vitro., *J. Rheumatol.* 19 (1992) 905–12. <http://www.ncbi.nlm.nih.gov/pubmed/1404127>.
- [108] J.J. Parkkinen, M.J. Lammi, H.J. Helminen, M. Tammi, Local stimulation of proteoglycan synthesis in articular cartilage explants by dynamic compression in vitro, *J. Orthop. Res.* 10 (1992) 610–620. doi:10.1002/jor.1100100503.
- [109] P.H. Francis-West, A. Abdelfattah, P. Chen, C. Allen, J. Parish, R. Ladher, S. Allen, S. MacPherson, F.P. Luyten, C.W. Archer, Mechanisms of GDF-5 action during skeletal development., *Development.* 126 (1999) 1305–15. <http://www.ncbi.nlm.nih.gov/pubmed/10021348>.
- [110] Y.Q. Yang, Y.Y. Tan, R. Wong, A. Wenden, L.K. Zhang, A.B.M. Rabie, The role of vascular endothelial growth factor in ossification, *Int. J. Oral Sci.* 4 (2012) 64–68. doi:10.1038/ijos.2012.33.
- [111] S.E. Usmani, M.A. Pest, G. Kim, S.N. Ohora, L. Qin, F. Beier, Transforming growth factor alpha controls the transition from hypertrophic cartilage to bone during endochondral bone growth, *Bone.* 51 (2012) 131–141. doi:10.1016/j.bone.2012.04.012.
- [112] X. Guo, K.K. Mak, M.M. Taketo, Y. Yang, The Wnt/ β -catenin pathway interacts differentially with PTHrP signaling to control chondrocyte hypertrophy and final maturation, *PLoS One.* 4 (2009). doi:10.1371/journal.pone.0006067.
- [113] D.R. Carter, G.S. Beaupré, M. Wong, R.L. Smith, T.P. Andriacchi, D.J. Schurman, The mechanobiology of articular cartilage development and degeneration., *Clin. Orthop. Relat. Res.* 427 (2004) S69-77. doi:10.1097/01.blo.0000144970.05107.7e.
- [114] V. Sarin, D. Carter, Mechanobiology and joint conformity regulate endochondral ossification of sesamoids., *J. Orthop. Res.* 18 (2000) 706–712. doi:10.1002/jor.1100180505.
- [115] J.C.V. Acosta, D.A. Garzón-Alvarado, L.M.P. Corte, A mechanobiological model of epiphysis structures formation, *J. Theor. Biol.* 287 (2011) 13–25. doi:10.1016/j.jtbi.2011.07.011.
- [116] D.R. Carter, M. Wong, Modelling cartilage mechanobiology, *Philos. Trans. R. Soc. Lond. B. Biol. Sci.* 358 (2003) 1461–1471. doi:10.1098/rstb.2003.1346.
- [117] S. Eyal, E. Blitz, Y. Shwartz, H. Akiyama, S. Ronen, E. Zelzer, On the development of the patella, *Development.* (2015) 1–9. doi:10.1242/dev.121970.
- [118] F.S. Sutton, C.H. Thompson, J. Lipke, D.B. Kettelkamp, The effect of patellectomy on knee function., *J. Bone Joint Surg. Am.* 58 (1976) 537–540. <http://www.ncbi.nlm.nih.gov/pubmed/1270472>.
- [119] O.S. Schindler, W.N. Scott, Basic kinematics and biomechanics of the patello-

- femoral joint. Part 1: The native patella., *Acta Orthop. Belg.* 77 (2011) 421–31. <http://www.ncbi.nlm.nih.gov/pubmed/21954748>.
- [120] S. Mottershead, Sesamoid bones and cartilages: An enquiry into their function, *Clin. Anat.* 1 (1988) 59–62. doi:10.1002/ca.980010110.
- [121] D.S. Howale, Z.K. Patel, Hypothesis : Morphology & Development of Patella, *Int. J. Sci. Res. Publ.* 3 (2013) 1–5.
- [122] I.G. Jang, I.Y. Kim, Application of design space optimization to bone remodeling simulation of trabecular architecture in human proximal femur for higher computational efficiency, *Finite Elem. Anal. Des.* 46 (2010) 311–319. doi:10.1016/j.finel.2009.11.003.
- [123] K. Cai, Z. Luo, Y. Wang, Topology optimization for human proximal femur considering bi-modulus behavior of cortical bones, *Springer Proc. Math. Stat.* 95 (2015) 263–270. doi:10.1007/978-3-319-08377-3_26.
- [124] P.G. Coelho, P.R. Fernandes, H.C. Rodrigues, J.B. Cardoso, J.M. Guedes, Numerical modeling of bone tissue adaptation-A hierarchical approach for bone apparent density and trabecular structure, *J. Biomech.* 42 (2009) 830–837. doi:10.1016/j.jbiomech.2009.01.020.
- [125] I.G. Jang, I.Y. Kim, Computational study of Wolff’s law with trabecular architecture in the human proximal femur using topology optimization, *J. Biomech.* 41 (2008) 2353–2361. doi:10.1016/j.jbiomech.2008.05.037.
- [126] C. Boyle, I.Y. Kim, Three-dimensional micro-level computational study of Wolff’s law via trabecular bone remodeling in the human proximal femur using design space topology optimization, *J. Biomech.* 44 (2011) 935–942. doi:10.1016/j.jbiomech.2010.11.029.
- [127] C.L. Chang, C.S. Chen, C.H. Huang, M.L. Hsu, Finite element analysis of the dental implant using a topology optimization method, *Med. Eng. Phys.* 34 (2012) 999–1008. doi:10.1016/j.medengphy.2012.06.004.
- [128] H. Kang, C.Y. Lin, S.J. Hollister, Topology optimization of three dimensional tissue engineering scaffold architectures for prescribed bulk modulus and diffusivity, *Struct. Multidiscip. Optim.* 42 (2010) 633–644. doi:10.1007/s00158-010-0508-8.
- [129] A. Sutradhar, G.H. Paulino, M.J. Miller, T.H. Nguyen, Topological optimization for designing patient-specific large craniofacial segmental bone replacements, *Proc. Natl. Acad. Sci.* 107 (2010) 13222–13227. doi:10.1073/pnas.1001208107.
- [130] M. Fraldi, L. Esposito, G. Perrella, A. Cutolo, S.C. Cowin, Topological optimization in hip prosthesis design, *Biomech. Model. Mechanobiol.* 9 (2010) 389–402. doi:10.1007/s10237-009-0183-0.
- [131] R. Schweitzer, E. Zelzer, T. Volk, Connecting muscles to tendons: tendons

References

- and musculoskeletal development in flies and vertebrates., *Development*. 137 (2010) 2807–2817. doi:10.1242/dev.047498.
- [132] F. Edom-Vovard, B. Schuler, M.-A. Bonnin, M.-A. Teillet, D. Duprez, Fgf4 positively regulates scleraxis and tenascin expression in chick limb tendons., *Dev. Biol.* 247 (2002) 351–366. doi:10.1006/dbio.2002.0707.
- [133] S. Eloy-Trinquet, H. Wang, F. Edom-Vovard, D. Duprez, Fgf signaling components are associated with muscles and tendons during limb development, *Dev. Dyn.* 238 (2009) 1195–1206. doi:10.1002/dvdy.21946.
- [134] E. Blitz, A. Sharir, H. Akiyama, E. Zelzer, Tendon-bone attachment unit is formed modularly by a distinct pool of Scx- and Sox9-positive progenitors, *Development*. 140 (2013) 2680–2690. doi:10.1242/dev.093906.
- [135] N.J. Giori, G.S. Beaupré, D.R. Carter, Cellular shape and pressure may mediate mechanical control of tissue composition in tendons, *J. Orthop. Res.* 11 (1993) 581–591. doi:10.1002/jor.1100110413.
- [136] J. Wilkinson, Fracture of the patella treated by total excision. A long-term follow-up, *J. Bone Joint Surg. Br.* 59 (1977) 352–354. <http://www.ncbi.nlm.nih.gov/pubmed/893514>.
- [137] D.R. Carter, P.R. Blenman, G.S. Beaupre, G.S. Beaupré, Correlations between mechanical-stress history and tissue differentiation in initial fracture-healing, *J. Orthop. Res.* 6 (1988) 736–748. doi:10.1002/jor.1100060517.
- [138] D.B. Drachman, L. Sokoloff, The role of movement in embryonic joint development, *Dev. Biol.* 14 (1966) 401–420. doi:10.1016/0012-1606(66)90022-4.
- [139] T.A. Wren, G.S. Beaupré, D.R. Carter, Mechanobiology of tendon adaptation to compressive loading through fibrocartilaginous metaplasia, *J. Rehabil. Res. Dev.* 37 (2000) 135–143.
- [140] H. Aslan, N. Kimelman-Bleich, G. Pelled, D. Gazit, Molecular targets for tendon neof ormation, *J. Clin. Invest.* 118 (2008) 439–444. doi:10.1172/JCI33944.
- [141] L. Geris, J. Vander Sloten, H. Van Oosterwyck, In silico biology of bone modelling and remodelling: regeneration, *Philos. Trans. R. Soc. A Math. Phys. Eng. Sci.* 367 (2009) 2031–2053. doi:10.1098/rsta.2008.0293.
- [142] S. Piszczatowski, Material aspects of growth plate modelling using Carter’s and Stokes’s approaches., *Acta Bioeng. Biomech.* 13 (2011) 3–14. <http://www.ncbi.nlm.nih.gov/pubmed/22097913>.
- [143] W.R. MacAusland, Total excision of the patella for fracture, *Am. J. Surg.* 72 (1946) 510–516. doi:10.1016/0002-9610(46)90385-6.
- [144] J. Bruce, R. Walmsley, Exision of the patella: Some Experimental and Anatomical Observations, *JBJS.* 24 (1942) 311–325.

- https://journals.lww.com/jbjsjournal/Fulltext/1942/24020/EXCISION_OF_THE_PATELLA__Some_Experimental_and.8.aspx.
- [145] O. Sigmund, A 99 line topology optimization code written in matlab, *Struct. Multidiscip. Optim.* 21 (2001) 120–127. doi:10.1007/s001580050176.
- [146] A. Sutradhar, J. Park, D. Carrau, T.H. Nguyen, M.J. Miller, G.H. Paulino, Designing patient-specific 3D printed craniofacial implants using a novel topology optimization method, *Med. Biol. Eng. Comput.* 54 (2016) 1123–1135. doi:10.1007/s11517-015-1418-0.
- [147] T.A.E. Ahmed, M.T. Hincke, Strategies for Articular Cartilage Lesion Repair and Functional Restoration, *Tissue Eng. Part B Rev.* 16 (2010) 305–329. doi:10.1089/ten.teb.2009.0590.
- [148] J.E.J. Bekkers, M. Inklaar, D.B.F. Saris, Treatment Selection in Articular Cartilage Lesions of the Knee, *Am. J. Sports Med.* 37 (2009) 148–155. doi:10.1177/0363546509351143.
- [149] N.L. Grimm, J.M. Weiss, J.I. Kessler, S.K. Aoki, Osteochondritis dissecans of the knee: Pathoanatomy, epidemiology, and diagnosis, *Clin. Sports Med.* 33 (2014) 181–188. doi:10.1016/j.csm.2013.11.006.
- [150] T.M. Simon, D.W. Jackson, Articular Cartilage: Injury Pathways and Treatment Options, *Sports Med. Arthrosc.* 26 (2018) 31–39. doi:10.1097/JSA.000000000000182.
- [151] C.M. Agrawal, R.B. Ray, Biodegradable polymeric scaffolds for musculoskeletal tissue engineering, *J. Biomed. Mater. Res.* 55 (2001) 141–150. doi:10.1002/1097-4636(200105)55:2<141::AID-JBM1000>3.0.CO;2-J.
- [152] M. Pérez Olmedilla, N. Garcia-Giralt, M.M. Pradas, P.B. Ruiz, J.L. Gómez Ribelles, E.C. Palou, J.C.M. García, Response of human chondrocytes to a non-uniform distribution of hydrophilic domains on poly (ethyl acrylate-co-hydroxyethyl methacrylate) copolymers, *Biomaterials.* 27 (2006) 1003–1012. doi:10.1016/j.biomaterials.2005.07.030.
- [153] W.-J. Li, K.G. Danielson, P.G. Alexander, R.S. Tuan, Biological response of chondrocytes cultured in three-dimensional nanofibrous poly(ϵ -caprolactone) scaffolds, *J. Biomed. Mater. Res.* 67A (2003) 1105–1114. doi:10.1002/jbm.a.10101.
- [154] G. Luca, M. Calvitti, C. Nastruzzi, L. Bilancetti, E. Becchetti, G. Angeletti, F. Mancuso, R. Calafiore, Encapsulation, *In Vitro* Characterization, and *In Vivo* Biocompatibility of Sertoli Cells in Alginate-Based Microcapsules, *Tissue Eng.* 13 (2007) 641–648. doi:10.1089/ten.2006.0137.
- [155] M. Wong, M. Siegrist, X. Wang, E. Hunziker, Development of mechanically stable alginate/chondrocyte constructs: effects of guluronic acid content and matrix synthesis, *J. Orthop. Res.* 19 (2001) 493–499. doi:10.1016/S0736-0266(00)90023-8.

References

- [156] S.R. Frenkel, P.E. Dicesare, Scaffolds for articular cartilage repair, *J. Long. Term. Eff. Med. Implants.* 22 (2004) 26–34. doi:10.1023/B:ABME.0000007788.41804.0d.
- [157] B.J. Huang, J.C. Hu, K.A. Athanasiou, Cell-based tissue engineering strategies used in the clinical repair of articular cartilage, *Biomaterials.* 98 (2016) 1–22. doi:10.1016/j.biomaterials.2016.04.018.
- [158] M. Sancho-Tello, F. Forriol, J.J. Martín de Llano, C. Antolinos-Turpin, J.A. Gómez-Tejedor, J.L. Gómez Ribelles, C. Carda, Biostable scaffolds of polyacrylate polymers implanted in the articular cartilage induce hyaline-like cartilage regeneration in rabbits, *Int. J. Artif. Organs.* 40 (2017) 350–357. doi:10.5301/ijao.5000598.
- [159] L. Vikingsson, M. Sancho-Tello, A. Ruiz-Saurí, S.M. Díaz, J.A. Gómez-Tejedor, G.G. Ferrer, C. Carda, J.C. Monllau, J.L. Gómez Ribelles, Implantation of a polycaprolactone scaffold with subchondral bone anchoring ameliorates nodules formation and other tissue alterations, *Int. J. Artif. Organs.* 38 (2015) 659–666. doi:10.5301/ijao.5000457.
- [160] E. Kon, A. Roffi, G. Filardo, G. Tesei, M. Marcacci, Scaffold-based cartilage treatments: with or without cells? A systematic review of preclinical and clinical evidence, *Arthroscopy.* 31 (2015) 767–775. doi:10.1016/j.arthro.2014.11.017.
- [161] M. Cucchiari, H. Madry, F. Guilak, D. Saris, M. Stoddart, M. Koon Wong, P. Roughley, A vision on the future of articular cartilage repair, *Eur. Cells Mater.* 27s (2014) 12–16. doi:10.22203/eCM.v027sa03.
- [162] I. Gadjanski, K. Spiller, G. Vunjak-Novakovic, Time-Dependent Processes in Stem Cell-Based Tissue Engineering of Articular Cartilage, *Stem Cell Rev. Reports.* 8 (2012) 863–881. doi:10.1007/s12015-011-9328-5.
- [163] C.J. Little, N.K. Bawolin, X. Chen, Mechanical Properties of Natural Cartilage and Tissue-Engineered Constructs, *Tissue Eng. Part B Rev.* 17 (2011) 213–227. doi:10.1089/ten.teb.2010.0572.
- [164] L. Vikingsson, G. Gallego Ferrer, J.A. Gómez-Tejedor, J.L. Gómez Ribelles, An “in vitro” experimental model to predict the mechanical behavior of macroporous scaffolds implanted in articular cartilage, *J. Mech. Behav. Biomed. Mater.* 32 (2014) 125–131. doi:10.1016/j.jmbbm.2013.12.024.
- [165] G. Filardo, E. Kon, A. Roffi, A. Di Martino, M. Marcacci, Scaffold-based repair for cartilage healing: A systematic review and technical note, *Arthrosc. J. Arthrosc. Relat. Surg.* 29 (2013) 174–186. doi:10.1016/j.arthro.2012.05.891.
- [166] E. Kon, G. Filardo, A. Roffi, L. Andriolo, M. Marcacci, New trends for knee cartilage regeneration: From cell-free scaffolds to mesenchymal stem cells, *Curr. Rev. Musculoskelet. Med.* 5 (2012) 236–243. doi:10.1007/s12178-012-9135-x.

-
- [167] S. Martinez-Diaz, N. Garcia-Giralt, M. Lebourg, J.A. Gómez-Tejedor, G. Vila, E. Caceres, P. Benito, M. Monleón Pradas, X. Nogues, J.L. Gómez Ribelles, J.C. Monllau, In Vivo Evaluation of 3-Dimensional Polycaprolactone Scaffolds for Cartilage Repair in Rabbits, *Am. J. Sports Med.* 38 (2010) 509–519. doi:10.1177/0363546509352448.
- [168] H. Van Oosterwyck, Computational mechanobiology: may the force be with you, *J. Math. Biol.* 70 (2015) 1323–1326. doi:10.1007/s00285-014-0795-6.
- [169] T.-H. Lin, H.-Y. Jhang, F.-C. Chu, C.A. Chung, Computational modeling of nutrient utilization in engineered cartilage, *Biotechnol. Prog.* 29 (2013) 452–462. doi:10.1002/btpr.1687.
- [170] M.S. Hossain, D.J. Bergstrom, X.B. Chen, Modelling and simulation of the chondrocyte cell growth, glucose consumption and lactate production within a porous tissue scaffold inside a perfusion bioreactor, *Biotechnol. Reports.* 5 (2015) 55–62. doi:10.1016/j.btre.2014.12.002.
- [171] M. Shakhawath Hossain, D.J. Bergstrom, X.B. Chen, A mathematical model and computational framework for three-dimensional chondrocyte cell growth in a porous tissue scaffold placed inside a bi-directional flow perfusion bioreactor, *Biotechnol. Bioeng.* 112 (2015) 2601–2610. doi:10.1002/bit.25678.
- [172] H. Mohammadi, K. Mequanint, W. Herzog, Computational aspects in mechanical modeling of the articular cartilage tissue, *Proc. Inst. Mech. Eng. Part H J. Eng. Med.* 227 (2013) 402–420. doi:10.1177/0954411912470239.
- [173] A. Erdemir, C. Bennetts, S. Davis, A. Reddy, S. Sibole, Multiscale cartilage biomechanics: technical challenges in realizing a high-throughput modelling and simulation workflow., *Interface Focus.* 5 (2015) 20140081. doi:10.1098/rsfs.2014.0081.
- [174] W. Wilson, N.J.B. Driessen, C.C. van Donkelaar, K. Ito, Prediction of collagen orientation in articular cartilage by a collagen remodeling algorithm, *Osteoarthr. Cartil.* 14 (2006) 1196–1202. doi:10.1016/j.joca.2006.05.006.
- [175] W. Wilson, C.C. Van Donkelaar, B. Van Rietbergen, K. Ito, R. Huiskes, Stresses in the local collagen network of articular cartilage: A poroviscoelastic fibril-reinforced finite element study, *J. Biomech.* 37 (2004) 357–366. doi:10.1016/S0021-9290(03)00267-7.
- [176] L.P. Li, J. Soulhat, M.D. Buschmann, A. Shirazi-Adl, Nonlinear analysis of cartilage in unconfined ramp compression using a fibril reinforced poroelastic model, *Clin. Biomech.* 14 (1999) 673–682. doi:10.1016/S0268-0033(99)00013-3.
- [177] P. Julkunen, W. Wilson, H. Isaksson, J.S. Jurvelin, W. Herzog, R.K. Korhonen, A Review of the Combination of Experimental Measurements and Fibril-Reinforced Modeling for Investigation of Articular Cartilage and
-

References

- Chondrocyte Response to Loading, *Comput. Math. Methods Med.* 2013 (2013) 1–23. doi:10.1155/2013/326150.
- [178] R.K. Korhonen, M.S. Laasanen, J. Töyräs, R. Lappalainen, H.J. Helminen, J.S. Jurvelin, A.I.N. Press, Fibril reinforced poroelastic model predicts specifically mechanical behavior of normal, proteoglycan depleted and collagen degraded articular cartilage, *J. Biomech.* 36 (2003) 1373–1379. doi:10.1016/S0021-9290(03)00069-1.
- [179] A. Benninghoff, Form und Bau der Gelenkknorpel in ihren Beziehungen zur Funktion, *Zeitschrift Für Zellforsch. Und Mikroskopische Anat.* 2 (1925) 783–862. doi:10.1007/BF00583443.
- [180] W. Wilson, C.C. van Donkelaar, J.M. Huyghe, A comparison between mechano-electrochemical and biphasic swelling theories for soft hydrated tissues., *J. Biomech. Eng.* 127 (2005) 158–165. doi:10.1115/1.1835361.
- [181] E.B. Hunziker, K.E. Kuettner, R. Schleyerbach, J.G. Peyron, V.C. Hascall, Articular cartilage structure in human and experimental animals, *Articul. Cartil. Osteoarthr.* (1992) 183–199. <https://ci.nii.ac.jp/naid/10017097116/en/> (accessed March 13, 2019).
- [182] Z. Xinghua, G. He, G. Bingzhao, The application of topology optimization on the quantitative description of the external shape of bone structure, *J. Biomech.* 38 (2005) 1612–1620. doi:10.1016/j.jbiomech.2004.06.029.
- [183] J. Wolff, *The Law of Bone Remodelling*, Springer Berlin Heidelberg, Berlin, Heidelberg, 1986. doi:10.1007/978-3-642-71031-5.
- [184] L.M. McNamara, P.J. Prendergast, Bone remodelling algorithms incorporating both strain and microdamage stimuli, *J. Biomech.* 40 (2007) 1381–1391. doi:10.1016/j.jbiomech.2006.05.007.
- [185] P.J. Prendergast, D. Taylor, Prediction of bone adaptation using damage accumulation, *J. Biomech.* 27 (1994) 1067–1076. doi:10.1016/0021-9290(94)90223-2.
- [186] P.J. Prendergast, R. Huiskes, Microdamage and osteocyte-lacuna strain in bone: a microstructural finite element analysis, *J. Biomech. Eng.* 118 (1996) 240–246. doi:10.1115/1.2795966.
- [187] J. Li, H. Li, L. Shi, A.S.L. Fok, C. Ucer, H. Devlin, K. Horner, N. Silikas, A mathematical model for simulating the bone remodeling process under mechanical stimulus, *Dent. Mater.* 23 (2007) 1073–1078. doi:10.1016/j.dental.2006.10.004.
- [188] D.A. Garzón-Alvarado, A.M. Ramírez-Martínez, C.A. Cardozo De Martínez, C. Alicia, C. De Martínez, Numerical test concerning bone mass apposition under electrical and mechanical stimulus, *Theor. Biol. Med. Model.* 9 (2012). doi:10.1186/1742-4682-9-14.
- [189] S.C. Cowin, *Bone Mechanics Handbook*, Second Edition, CRC Press, Boca

- Raton, 2001. doi:10.1201/b14263.
- [190] S.C. Cowin, Bone stress adaptation models, *J. Biomech. Eng.* 115 (1993) 528–533. doi:10.1115/1.2895535.
- [191] D.H. Hegedus, S.C. Cowin, N. Orleans, Bone remodeling II: small strain adaptive elasticity, *J. Elast.* 6 (1976) 337–352. doi:10.1007/BF00040896.
- [192] S.C. Cowin, D.H. Hegedus, Bone remodeling I: theory of adaptive elasticity, *J. Elast.* 6 (1976) 313–326. doi:10.1007/BF00041724.
- [193] R. Huiskes, R. Ruimerman, G.H. van Lenthe, J.D. Janssen, Effects of mechanical forces on maintenance and adaptation of form in trabecular bone, *Nature.* 405 (2000) 704–706. doi:10.1038/35015116.
- [194] H. Weinans, R. Huiskes, H.J. Grootenboer, Effects of material properties of femoral hip components on bone remodeling, *J. Orthop. Res.* 10 (1992) 845–853. doi:10.1002/jor.1100100614.
- [195] J. Martínez-Reina, J. Ojeda, J. Mayo, On the Use of Bone Remodelling Models to Estimate the Density Distribution of Bones. Uniqueness of the Solution, *PLoS One.* 11 (2016) e0148603. doi:10.1371/journal.pone.0148603.
- [196] P. Christen, K. Ito, R. Ellouz, S. Boutroy, E. Sornay-Rendu, R.D. Chapurlat, B. Van Rietbergen, Bone remodelling in humans is load-driven but not lazy, *Nat. Commun.* 5 (2014) 1–5. doi:10.1038/ncomms5855.
- [197] V. Klika, M.A. Pérez, J.M. García-Aznar, F. Maršík, M. Doblaré, A coupled mechano-biochemical model for bone adaptation, *J. Math. Biol.* 69 (2013) 1383–1429. doi:10.1007/s00285-013-0736-9.
- [198] H. Isaksson, Recent advances in mechanobiological modeling of bone regeneration, *Mech. Res. Commun.* 42 (2012) 22–31. doi:10.1016/j.mechrescom.2011.11.006.
- [199] P.J. Prendergast, R. Huiskes, K. Søballe, Biophysical stimuli on cells during tissue differentiation at implant interfaces, *J. Biomech.* 30 (1997) 539–548. doi:10.1016/S0021-9290(96)00140-6.
- [200] L.E. Claes, C.A. Heigele, Magnitudes of local stress and strain along bony surfaces predict the course and type of fracture healing, *J. Biomech.* 32 (1999) 255–266. doi:10.1016/S0021-9290(98)00153-5.
- [201] F. Pauwels, Eine neue Theorie über den Einfluß mechanischer Reize auf die Differenzierung der Stützgewebe, *Z. Anat. Entwicklungsgesch.* 121 (1960) 478–515. doi:10.1007/BF00523401.
- [202] D.J. Kelly, P.J. Prendergast, Mechano-regulation of stem cell differentiation and tissue regeneration in osteochondral defects, *J. Biomech.* 38 (2005) 1413–1422. doi:10.1016/j.jbiomech.2004.06.026.

References

- [203] H. Isaksson, O. Comas, C.C. van Donkelaar, J. Mediavilla, W. Wilson, R. Huiskes, K. Ito, Bone regeneration during distraction osteogenesis: Mechano-regulation by shear strain and fluid velocity, *J. Biomech.* 40 (2007) 2002–2011. doi:10.1016/j.jbiomech.2006.09.028.
- [204] H. Isaksson, C.C. van Donkelaar, R. Huiskes, K. Ito, A mechano-regulatory bone-healing model incorporating cell-phenotype specific activity, *J. Theor. Biol.* 252 (2008) 230–246. doi:10.1016/j.jtbi.2008.01.030.
- [205] H. Isaksson, C.C. van Donkelaar, K. Ito, C.C. Van Donkelaar, K. Ito, Sensitivity of tissue differentiation and bone healing predictions to tissue properties, *J. Biomech.* 42 (2009) 555–564. doi:10.1016/j.jbiomech.2009.01.001.
- [206] S.J. Shefelbine, P. Augat, L. Claes, U. Simon, S.J. Shefelbine, P. Augat, L. Claes, U. Simon, Trabecular bone fracture healing simulation with finite element analysis and fuzzy logic, *J. Biomech.* 38 (2005) 2440–2450. doi:10.1016/j.jbiomech.2004.10.019.
- [207] D.P. Byrne, D. Lacroix, P.J. Prendergast, Simulation of fracture healing in the tibia: Mechanoregulation of cell activity using a lattice modeling approach, *J. Orthop. Res.* 29 (2011) 1496–1503. doi:10.1002/jor.21362.
- [208] D. Lacroix, P.J. Prendergast, A mechano-regulation model for tissue differentiation during fracture healing: Analysis of gap size and loading, *J. Biomech.* 35 (2002) 1163–1171. doi:10.1016/S0021-9290(02)00086-6.
- [209] D. Lacroix, P.J.I. Prendergast, G. Li, D. Marsh, Biomechanical model to simulate tissue differentiation and bone regeneration: Application to fracture healing, *Med. Biol. Eng. Comput.* 40 (2002) 14–21. doi:10.1007/BF02347690.
- [210] D. Lacroix, P.J. Prendergast, Three-dimensional simulation of fracture repair in the human tibia, *Comput. Methods Biomech. Biomed. Engin.* 5 (2002) 369–376. doi:10.1080/1025584021000025014.
- [211] H. Isaksson, C.C. van Donkelaar, R. Huiskes, K. Ito, C.C. Van Donkelaar, R. Huiskes, K. Ito, Corroboration of Mechano-regulatory Algorithms for Tissue Differentiation during Fracture Healing: Comparison with In Vivo Results, *J. Orthop. Res.* 65 (2006) 354–359. doi:10.1002/jor.
- [212] H. Isaksson, W. Wilson, C.C. Van Donkelaar, C.C. van Donkelaar, R. Huiskes, K. Ito, Comparison of biophysical stimuli for mechano-regulation of tissue differentiation during fracture healing, *J. Biomech.* 39 (2006) 1507–1516. doi:10.1016/j.jbiomech.2005.01.037.
- [213] N.J.B. Driessen, W. Wilson, C.V.C. Bouten, F.P.T. Baaijens, A computational model for collagen fibre remodelling in the arterial wall, 226 (2004) 53–64. doi:10.1016/j.jtbi.2003.08.004.
- [214] W. Wilson, C.C. van Donkelaar, B. van Rietbergen, R. Huiskes, A fibril-

reinforced poroviscoelastic swelling model for articular cartilage, *J. Biomech.* 38 (2005) 1195–1204. doi:10.1016/j.jbiomech.2004.07.003.

APPENDIXES

APPENDIX A – VALUE OF THE PARAMETERS USED ON CHAPTER 2 (JOINT ONSET)

Values of the coefficients employed on the model that describes the joint development from the interzone onset to the cavitation process.

Parameter	Value	Equation	Description	Cases	Molecules
a	0.1	Eq. 2-3 and Eq. 2-4	Constant rate value for u -expression	All	(G), (N), (P), (I)
b	0.9	Eq. 2-3 and Eq. 2-4	Constant rate value for v -expression	All	(G), (N), (P), (I)
γ	10.0	Eq. 2-3 and Eq. 2-4	Rate value for the reaction term	All	(G), (N), (P), (I)
D_u	1.0	Eq. 2-3 and Eq. 2-4	Diffusion constant for u	All	(G), (N), (P), (I)
D_v	29.0	Eq. 2-3 and Eq. 2-4	Diffusion constant for v	All	(G), (N), (P), (I)
D_w	2E-2	Eq. 2-8	Diffusion constant for w	All	(W)
	5E-5		Diffusion constant for w		
D_H	2E2	Eq. 2-10	Diffusion constant for H	All	(H)
ϑ	1.E-2	Eq. 2-9	Rate value for the reaction term for W	All	(W)
S_G^{Th}	1.42	Table 2-1	Differentiation Mesenchyme to Interzone	All	(G)
S_I^{Th}	1.35	Table 2-1	Differentiation Mesenchyme to Chondrogenic tissue	All	(I)
$^1S_W^{Th}$	5.E-2	Table 2-1	Differentiation from Chondrogenic tissue to articular cartilage	All	(W)
$^2S_W^{Th}$	1.E-2	Table 2-1	Differentiation from Mesenchyme tissue to Joint Capsule and ligament	All	(W)
α_{iso}	0	Eq. 2-11	Growth by concentration of (I): MSc	All	(I)
	5.E-4		Chondrogenic tissue		
	5.E-2		Articular Cartilage		
	0		Other tissues		
β_{iso}	0	Eq. 2-11	Growth by concentration of (P): MSc	All	(P)
	5.E-4		Chondrogenic tissue		
	5.E-2		Articular Cartilage		
	0		Other tissues		

Appendixes

Parameter	Value	Equation	Description	Cases	Molecules
μ_{iso}	1.E-3	Eq. 2-11	Growth by concentration of (H): MSc	All	(H)
	1.E-3		Chondrogenic tissue	All	
	3.E-3		Chondrogenic tissue	Case III	
	0		Other tissues	All	
α_i	0	Eq. 2-11	Growth by gradient of (I): MSc	All	(I)
	5.E-4		Chondrogenic tissue		
	0		Articular Cartilage		
	0		Other tissues		
β_i	0	Eq. 2-11	Growth by gradient of (P): MSc	All	(P)
	5.E-4		Chondrogenic tissue		
	0		Articular Cartilage		
	0		Other tissues		
μ_i	1.E-2	Eq. 2-11	Growth by gradient of (H): MSc	All	(H)
	1.E-2		Chondrogenic tissue	All	
	3.E-3		Chondrogenic tissue	Case III	
	0		Other tissues	All	

APPENDIX B – VALUE OF THE PARAMETERS USED ON CHAPTER 4 (PATELLA ONSET)

Values of the coefficients employed on the model of theory I and theory II.

Variable	Value				
	Mesenchymal	Cartilage	Tendon	Interzone	theory
σ_{hyd}^{cart}		-0.013			II
$D_{TGF-\beta}$	1.0	1.0/10	1.0/10	1.0/10	I
D_{BMP}	0.05	0.05/10	0.05/10	0.05/10	I
$\mu(s_{at}(x, t))$	$0.1 + 0.1 * S_{TGF-\beta}$	$0.1 * S_{TGF-\beta}$	0.0001	0.0001	I
$\chi(s_{at}(x, t))$	0.5	0.0005	0.0005	0.0005	I
D_{FGF}	7.0/1000	7.0/1000	7.0	7.0/1000	I
D_{GDF-5}	0.05	0.05/1000	0.05/10	0.05/10	I
b_c^{Th}		0.65			I
S_{BMP}^{Th}		0.03			I
S_{FGF}^{Th}		0.1			I
S_{GDF-5}^{Th}		0.038			I

APPENDIX C – VALUE OF THE PARAMETERS USED ON CHAPTER 5 (CARTILAGE REGENERATION)

Variable	Value	Reference	Description
E_f	2.737 [MPa]	[214]	Fiber Young's modulus
E_{n-f}	0.315 [MPa]	[214]	Cartilage Young's modulus
ν_{n-f}	0.42	[178]	Cartilage Poisson's modulus
k_{n-f}	$0.1 \left[\frac{m^4}{Ns} \times 10^{-14} \right]$		Cartilage permeability
E_{trab}	2.0 [MPa]	[204]	Trabecular bone Young's modulus
ν_{trab}	0.3	[204]	Trabecular bone Poisson's modulus
k_{trab}	$0.02 \left[\frac{m^4}{Ns} \times 10^{-14} \right]$		Trabecular bone porosity
E_{subch}	15750 [MPa]	[204]	Subchondral bone Young's modulus
ν_{subch}	0.3	[204]	Subchondral bone Poisson's modulus
k_{subch}	$0.01 \left[\frac{m^4}{Ns} \times 10^{-14} \right]$		Subchondral bone permeability
E_{scaff}	0.48 [MPa]	Averaged [4]	Scaffold Young's modulus
ν_{scaff}	0.3	Proposed	Scaffold Poisson's modulus
k_{scaff}	$0.2 \left[\frac{m^4}{Ns} \times 10^{-14} \right]$	Proposed	Scaffold permeability
$E_{fail-trab}$	7500 [MPa]	Iteratively	Minimum Young's modulus for the trabecular bone (Minimum Young's modulus)
$E_{fail-subch}$	0.5 [MPa]	Iteratively	Minimum Young's modulus for the subchondral bone (Minimum Young's modulus)
α_{trab}	0.05	Iteratively	Parameter for trabecular bone damage
α_{subch}	1.0	Iteratively	Parameter for subchondral bone damage
f_{FT}^{PM}	0.2 [day^{-1}]	[204]	Fibrous tissue production rate
f_{FT}^{DM}	0.05 [day^{-1}]	[204]	Fibrous tissue degradation rate
f_C^{PM}	0.05 [day^{-1}]	[204]	Cartilage production rate
f_C^{DM}	0.05 [day^{-1}]	[204]	Cartilage degradation rate
f_B^{PM}	0.10 [day^{-1}]	[204]	Bone production rate
f_B^{DM}	0.05 [day^{-1}]	[204]	Bone degradation rate
m_{max}	1	Proposed	Maximal matrix concentration

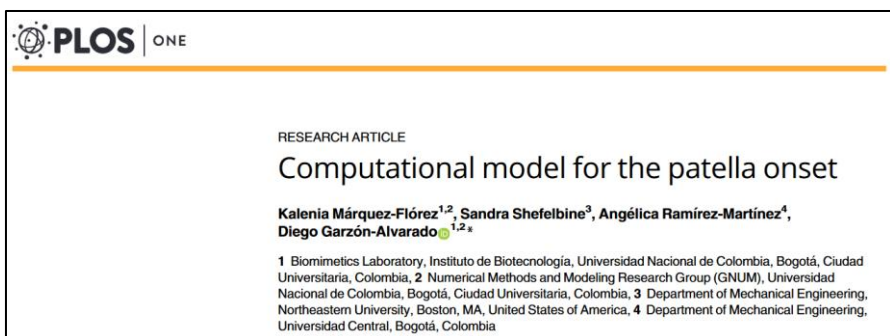
APPENDIX D – PUBLISHED AND SUBMITTED WORKS

Published works:

→ K.M. Márquez-Flórez, J.R. Monaghan, S.J. Shefelbine, A. Ramirez-Martínez, D.A. Garzón-Alvarado, A computational model for the joint onset and development, *J. Theor. Biol.* 454 (2018) 345–356. doi:10.1016/j.jtbi.2018.04.015.



→ K. Márquez-Flórez, S. Shefelbine, A. Ramirez-Martínez, D. Garzón-Alvarado, Computational model for the patella onset, *PLoS One.* 13 (2018) e0207770. doi:10.1371/journal.pone.0207770.



Submitted works:

Carrera-Pinzón A.F., Márquez-Flórez K., Kraft R., Garzón-Alvarado D.A., *Computational Model of a Synovial Joint Morphogenesis*, PLoS One. 2019- PONE-S-19-08473

Congresses:

K. Márquez-Flórez, S.J. Shefelbine, D.A. Garzón-Alvarado (June 2017). *A computational approach on patella development*. VII International Conference on Computational Methods for Coupled Problems in Science and Engineering. Coupled problems 2017, CIMNE. Rhodes, Greece.


Posters:

K. Márquez-Flórez, D. Garzón-Alvarado, C. Carda, M. Sancho-Tello (May 2019). *Computational model for the cartilage regeneration process induced by scaffold implantation*. Tissue Engineering and Regenerative Medicine International Society (TERMIS) EU 2019. Rhodes, Greece.


APPENDIX E – JOURNALS’ PERMISSIONS


For Márquez-Flórez KM, Monaghan JR, Shefelbine SJ, Ramirez-Martínez A, Garzón-Alvarado DA. *A computational model for the joint onset and development*. J Theor Biol. 2018; 454:345–356. doi: 10.1016/j.jtbi.2018.04.015

3/12/2019 Rightslink® by Copyright Clearance Center



RightsLink®

[Home](#)
[Create Account](#)
[Help](#)




Title: A computational model for the joint onset and development

Author: Kalenia M. Márquez-Flórez, James R. Monaghan, Sandra J. Shefelbine, Angélica Ramirez-Martínez, Diego A. Garzón-Alvarado

Publication: Journal of Theoretical Biology

Publisher: Elsevier

Date: 7 October 2018

© 2018 Elsevier Ltd. All rights reserved.

LOGIN

If you're a **copyright.com** user, you can login to RightsLink using your copyright.com credentials. Already a **RightsLink** user or want to [learn more?](#)

Please note that, as the author of this Elsevier article, you retain the right to include it in a thesis or dissertation, provided it is not published commercially. Permission is not required, but please ensure that you reference the journal as the original source. For more information on this and on your other retained rights, please visit: <https://www.elsevier.com/about/our-business/policies/copyright#Author-rights>

BACK

CLOSE WINDOW

Copyright © 2019 [Copyright Clearance Center, Inc.](#) All Rights Reserved. [Privacy statement](#). [Terms and Conditions](#). Comments? We would like to hear from you. E-mail us at customer-care@copyright.com

For Márquez-Flórez K, Shefelbine S, Ramírez-Martínez A, Garzon-Alvarado DA. *Computational model for the patella onset* PLoS One. 2018;1–22.

From PLOS webpage: <https://journals.plos.org/plosone/s/licenses-and-copyright>

“PLOS applies the [Creative Commons Attribution \(CC BY\) license](#) to articles and other works we publish. If you submit your paper for publication by PLOS, you agree to have the CC BY license applied to your work. Under this Open Access license, you as the author agree that anyone can reuse your article in whole or part for any purpose, for free, even for commercial purposes. Anyone may copy, distribute, or reuse the content as long as the author and original source are properly cited. This facilitates freedom in re-use and also ensures that PLOS content can be mined without barriers for the needs of research.”